KOMMUNIKATIONSSYSTEME ALS TARGETS ZUR ÜBERWINDUNG VON RESISTENZEN TUMORALER UND BAKTERIELLER ERKRANKUNGEN: 17β-HSD1-HEMMSTOFFE UND *QUORUM SENSING INHIBITOREN*

DISSERTATION

zur Erlangung des Grades des Doktors der Naturwissenschaften
der Naturwissenschaftlich-Technischen Fakultät III
Chemie, Pharmazie, Bio- und Werkstoffwissenschaften
der Universität des Saarlandes

von

Claudia Henn

Saarbrücken
2012

Tag des Kolloquiums:	31. August 2012
Dekan:	Prof. Dr. W.F. Maier
Berichterstatter:	Prof. Dr. Rolf W. Hartmann Prof. Dr. Elmar Heinzle
Vorsitz:	Prof. Dr. Dr. h.c. Hans H. Maurer
Akad. Mitarbeiter:	Dr. Eva-Maria Collnot

Die vorliegende Arbeit wurde von Oktober 2008 bis April 2012 unter Anleitung von Herrn Prof. Dr. Rolf W. Hartmann in der Fachrichtung 8.2 Pharmazeutische und Medizinische Chemie der Naturwissenschaftlich-Technischen Fakultät III der Universität des Saarlandes und am Helmholtz-Institut für Pharmazeutische Forschung Saarland (HIPS) angefertigt.

WENN DU LIEBST, WAS DU TUST,

WIRST DU NIE WIEDER ARBEITEN.

KONFUZIUS

FÜR MEINE FAMILIE

ABSTRACT

The communication systems of eukaryotes and prokaryotes display targets for innovative therapeutic interventions to overcome resistance in the treatment of cancer and infectious diseases. As 17β-HSD1 inhibitors are promising compounds for the treatment of estrogen-dependent diseases, the endometriosis model in *C. jacchus* has been identified to adduce the *in vivo proof of concept*. A series of potent 17β-HSD1 inhibitors has been evaluated *in vitro* in this species and the class of the (hydroxyphenyl)naphthols with good pharmacokinetic properties has been optimized concerning their species-specific activity. The resulting 17β-HSD1 inhibitors are highly potent toward human 17β-HSD1 and at least one highly active and selective candidate toward 17β-HSD1 of *C. jacchus* was identified. After further pharmacological evaluation this compound might be able to be a candidate for the *in vivo* evaluation in *C. jacchus*.

To interfere via PqsD and PqsR with the *pqs QS*-System of *P. aeruginosa* is a promising strategy to overwhelm antibiotic resistance. In the current work two SPR-biosensor assays have been developed to investigate these target proteins. The kinetic mechanism of PqsD was elucidated by SPR-based results. Moreover, by combination of rational design and biophysical methods the first drug-like PqsR-antagonists have been identified. The best compound showed good activity in *P. aeruginosa* and is a candidate for further optimization.

ZUSAMMENFASSUNG

Die Kommunikationssysteme von Eukaryoten und Prokaryoten bieten zahlreiche Ansatzpunkte zur Entwicklung innovativer Strategien zur Überwindung von Resistenzen bei der Behandlung von Krebs- und Infektionserkrankungen. Für 17β-HSD1-Inhibitoren als vielversprechender Ansatz zur Therapie von estrogen-abhängigen Erkrankungen wurde das Endometriosemodell in *C. jacchus* zur Durchführung eines *in vivo Proof of Concepts* identifiziert. Eine Reihe hochpotenter 17β-HSD1-Hemmstoffe wurde *in vitro* an Enzymen dieser Spezies untersucht und die Klasse der (Hydroxyphenyl)naphthole mit sehr gutem pharmakokinetischen Profil hinsichtlich ihrer speziesspezifischen Aktivität weiter optimiert. Die entwickelten 17β-HSD1-Inhibitoren zeigen eine hohe Aktivität an der humanen 17β-HSD1 und ein hochpotenter und selektiver Kandidat an *C. jacchus* 17β-HSD1 konnte identifiziert werden. Nach pharmakologischen Untersuchungen soll dieser Hemmstoff als Kandidat für Untersuchungen im Endometriosemodell dienen.

Der Eingriff in das *pqs-QS*- System von *P. aeruginosa* über PqsD und PqsR bietet einen aussichtsreichen Angriffspunkt zur Überwindung von Antibiotikaresistenzen. In dieser Arbeit wurden SPR-Biosensorassays zur Untersuchung dieser beiden Targetproteine entwickelt. Der kinetische Mechanismus von PqsD wurde durch SPR-spektroskopisch-gestützte Ergebnisse geklärt. Die Kombination aus rationalem Design und biophysikalischen Methoden resultierte in den ersten „drug-like“ PqsR-Antagonisten. Die Hitverbindung dieser Studie zeigt darüber hinaus gute Aktivität in *P. aeruginosa* und hat sehr gutes Potential für eine weitere Optimierung.

EINGEFLOSSENE PUBLIKATIONEN

Die vorgelegte Arbeit gliedert sich in fünf Publikationen, welche durch römische Zahlengekennzeichnet sind:

I Structural Basis for Species Specific Inhibition of 17β-Hydroxysteroid Dehydrogenase Type 1 (17β-HSD1): Computational Study and Biological Validation
Tobias Klein[#], Claudia Henn[#], Matthias Negri, Martin Frotscher

PLoS ONE **2011**, 6, e22990.

II New drug-like hydroxyphenylnaphthol steroidomimetics successfully developed as potent and selective 17β-HSD1 inhibitors for the treatment of estrogen-dependent diseases
Sandrine Marchais-Oberwinkler, Marie Wetzel, Erika Ziegler, Patrizia Kruchten, Ruth Werth, Claudia Henn, Rolf W. Hartmann, Martin Frotscher,
Journal of Medicinal Chemistry **2011,** 54, (2), 534-547

III Lead optimization of 17β-HSD1 inhibitors of the (hydroxyphenyl)naphthol sulfonamide type for the treatment of endometriosis
Claudia Henn, Almuth Einspanier, Sandrine Marchais-Oberwinkler, Martin Frotscher, Rolf W. Hartmann

Journal of Medicinal Chemistry **2012,** 55, (7), 3307-3318

IV Catalytic enzyme activity on a biosensor chip: Combination of Surface Plasmon Resonance and Mass Spectrometry
Claudia Henn, Stefan Boettcher, Anke Steinbach, Rolf W. Hartmann

Analytical Biochemistry **2012,** 428, (1), 28-30

V Identification of Small-Molecule Antagonists of the *Pseudomonas aeruginosa* Transcriptional Regulator PqsR: Biophysically Guided Hit Discovery and Optimization
Tobias Klein[#], Claudia Henn[#], Johannes C. de Jong, Christina Zimmer, Benjamin Kirsch, Christine K. Maurer, Dominik Pistorius, Rolf Müller, Anke Steinbach, Rolf W. Hartmann

ACS Chemical Biology **2012**

[#] These authors contributed equalliy to this work

STELLUNGNAHME ÜBER DIE BEITRÄGE DER AUTORIN

Die Autorin möchte zu ihren Beiträgen zu den Veröffentlichungen **I**–**V** in der Dissertation Stellung nehmen.

I Contribution

Die Autorin etablierte und validierte den *in vitro* Assay zur Untersuchung der Inhibitoren. Sie war zuständig für die Interpretation der erhaltenen Ergebnisse, konzipierte und verfasste das Manuskript.

II Contribution

Die Autorin war für die Durchführung der Routinetests und für die Interpretation der erhaltenen Ergebnisse verantwortlich. Sie trug zur Evaluierung der Verbindungen sowie zur Erstellung des Manuskripts bei.

III Contribution

Die Autorin plante, synthetisierte und charakterisierte alle neuen Substanzen. Sie evaluierte die Verbindung im biochemischen Assay und war zuständig für die Interpretation der erhaltenen Ergebnisse. Sie konzipierte und verfasste das Manuskript.

IV Contribution

Die Autorin etablierte und validierte den Biosensorassay. Sie war zuständig für massenspektrometrischen Analysen und die Interpretation der erhaltenen Ergebnisse. Sie konzipierte und verfasste das Manuskript.

V Contribution

Die Autorin etablierte und validierte den Biosensorassay, war zuständig für die Auswahl sowie die Evaluierung der Substanzbibliothek und allen SPR-spektroskopischen Messungen. Sie interpretierte die Ergebnisse, konzipierte und verfasste das Manuskript.

WEITERE PUBLIKATIONEN DES AUTORS, DIE NICHT GEGENSTAND DER DISSERTATION SIND

I **Bicyclic Substituted Hydroxyphenylmethanone Type Inhibitors of 17 β-Hydroxysteroid Dehydrogenase Type 1 (17 β-HSD1): The Role of the Bicyclic Moiety.**
Alexander Oster, Tobias Klein, Claudia Henn, Ruth Werth, Sandrine Marchais-Oberwinkler, Martin Frotscher, Rolf W. Hartmann
ChemMedChem **2011,** 6, (3), 476-487.

II **17[beta]-Hydroxysteroid dehydrogenases (17βHSDs) as therapeutic targets: Protein structures, functions, and recent progress in inhibitor development.**
Sandrine Marchais-Oberwinkler, Claudia Henn, Gabriele Möller, Tobias Klein, Matthias Negri, Alexander Oster, Alessandro Spadaro, Ruth Werth, Marie Wetzel, Kuiying Xu, Martin Frotscher, Rolf W. Hartmann, Jerzy Adamski,
Journal of Steroid Biochemistry and Molecular Biology, **2011,** 125, (1-2), 66-82.

III **Discovery of Antagonists of PqsR, a Key Player in 2-Alkyl-4-quinolone-dependent *Quorum Sensing* in *Pseudomonas aeruginosa*.**
Cen Bin Lu, Benjamin Kirsch, Christina Zimmer, Johannes C. de Jong, Claudia Henn, Christine Maurer, Matthias Müsken, Susanne Häussler, Anke Steinbach, Rolf W. Hartmann
Chemistry & Biology **2012**,*19 (3), 381-390.*

INHALTSVERZEICHNIS

ABKÜRZUNGSVERZEICHNIS

µCI	MikroCurie
µM	mikromolar
17β-HSD1	17β-Hydroxysteroiddehydrogenase Typ 1
17β-HSD2	17β-Hydroxysteroiddehydrogenase Typ 2
17β-HSD4	17β-Hydroxysteroiddehydrogenase Typ 4
17β-HSD7	17β-Hydroxysteroiddehydrogenase Typ 7
A	Androstendion
Å	Ångström
ACoA	Anthraniloyl Coenzym A
ADMET	Absorption Distribution Metabolismus Exkretion Toxikologie
AGP	α1-saures-Glykoprotein
AHL	Acyl-homoserin-Lactone
AHQ	2-Alkyl-4-Chinolone
AI	Autoinducer
AI	Aromataseinhibitor
AS	Aminosäure
AUC	Area under the curve
βF	β-Faltblatt
β-K	β-Ketodecanoat
BPH	Benigne Prostatahyperplasie
C. jacchus	*Callithrix jacchus*
cAMP	zyklisches Adenosinmonophosphat
CD_3OD	Deuteriertes Methanol
CD_3ODCD_3	Deuteriertes Aceton
$CDCl_3$	Deuteriertes Chloroform
CF	Cystische Fibrose
CID	Collision induced decay
*cj*17β-HSD1	*Callithrix jacchus* 17β-Hydroxysteroiddehydrogenase Typ 1
*cj*17β-HSD2	*Callithrix jacchus* 17β-Hydroxysteroiddehydrogenase Typ 2
CoA	Coenzym A
COX2	Cyclooxygenase
CTRF	Cystic fibrosis transmembrame conductance regulator
CYP	Cytochrom P450
CYP19	Aromatase

DMSO	Dimethylsulfoxid
DNA	Desoxyribonukleinsäure
E2	Estradiol
EDC	N-ethyl-N´-(dimethylaminopropyl)carbodiimid
EDD	Estrogen abhängige Erkrankungen
ELISA	Enzyme-linked Immunosorbent Assay
EPS	Extrazelluläre Polymermatrix
eq	Äquivalent
ER	Estrogen Rezeptor
ESI	Elektrospray Ionisation
F	Phenylalanin
G	Freie Bindungsenergie
GnRH	Gonadotropin Releasing Hormon
GST	Glutathion-S-Transferase
H	Enthalpie
*h*17β-HSD1	humane 17β-Hydroxysteroiddehydrogenase Typ 1
HCN	Wasserstoffcyanid
HHQ	2-Heptyl-4-Chinolon
HPLC	High Performance Liquid Chromatography
HSA	Humanes Serumalbumin
HSL	Homoserinlacton
HTS	Highthroughput Screening
IC_{50}	Mittlere inhibitorische Konzentration
IL-6	Interleukin 6
IL-6-SR	Interleukin 6 soluble receptor
ITC	Isothermale Titrationskalorimetrie
k_a	Assoziationsgeschwindigkeit
K_D	Dissoziationskonstante
k_d	Dissoziationsgeschwindigkeit
kDa	Kilodalton
k_{off}	Dissoziationsgeschwindigkeit
k_{on}	Assoziationsgeschwindigkeit
LE	Ligandeneffizienz
MD	Moleküldynamik
MEP	Molekular elektrostatisches Potential
mM	millimolar
mRNA	messenger Ribonukleinsäure

MS	Massenspektrometrie
MS2	Tandem-Massenspektrometrie
MW	Molekulargewicht
NAD^+	Nicotinamid Adenin Dinukleotid
NADH	Nicotinamid Adenin Dinukleotid (reduzierte Form)
$NADP^+$	Nicotinsäureamid-Adenin-Dinucleotidphosphat
NADPH	Nicotinsäureamid-Adenin-Dinucleotidphosphat (reduzierte Form)
NHS	2-(N-hydroxysuccinimid)
nM	nanomolar
NMR	Nuklearmagnetische Resonanzspektroskopie
ns	Nanosekunde
OH	Hydroxy
PCNA	proliferating cell nuclear antigen
PDB	Proteindatenbank
PGE2	Prostaglandin E2
pI	Isoelektrischer Punkt
PK	Pharmakokinetik
PQS	Pseudomonas Quinolone Signal
ps	Pikosekunde
QS	*Quorum Sensing*
QSI	*Quorum Sensing Inhibitoren*
RBA	Relative Bindungsaffinität
RMSD	root-mean-square deviation
R-Protein	Signalrezeptor
rt	Raumtemperatur
RU	Response Unit
S	Entropie
SAR	Struktur-Wirkungs-Beziehung
SDRs	Side-chain-Dehydrogenasen/Reduktasen
SERM	selektive Estrogen Rezeptor Modulatoren
SF	Selektivitätsfaktor
SPR	Oberflächenplasmonresonanz
SUMO	Small Ubiquitin-like Modifier
T	Temperatur
TFA	Trifluoressigsäure
TIR	Totale interne Reflektion
TRIS	2-Amino-2-hydroxymethyl-propane-1,3-diol

UHPLC	Ultra High Performance Liquid Chromatography
WHO	Weltgesundheitsorganisation

1 Einleitung

Neben Herzkreislauferkrankungen gehören Krebs und Infektionskrankheiten zu den weltweit häufigsten Todesursachen. (WHO, 2008). Die Sterberate der weltweit an Krebs erkrankten Patienten liegt bei 80 %. Laut WHO liegt die Häufigkeit von tödlichen Infektionen bei 11.6 Mio. jährlich (WHO, 2002b). Die hohe Sterberate für diese Erkrankungen ist zum Großteil auf die Entwicklung von Resistenzen gegenüber Chemotherapeutika und Antibiotika zurückzuführen (WHO, 2002a; Siddik and Mehta, 2009). Deshalb ist es dringend notwendig die entsprechenden Resistenzmechanismen zu überwinden und neue Medikamente gegen diese Erkrankungen zu entwickeln.

1.1 17β-Hydroxysteroiddehydrogenase 1

1.1.1 Estrogenabhängige Erkrankungen

1.1.1.1 Brustkrebs

Krebs ist das unkontrollierte Zellwachstum, was durch ein gestörtes Gleichgewicht zwischen Zellzyklus und Apoptose entsteht. Brustkrebs ist die häufigste Krebsart bei Frauen und macht mehr als ein Viertel aller Krebserkrankungen von weiblichen Patienten aus. Die Ursachen der meisten Brustkrebserkrankungen sind hormonellen Ursprungs. Estrogene, insbesondere Estradiol (E2), spielen für das Fortschreiten der Erkrankung eine große Rolle (Key *et al.*, 2003). Brustkrebs wird in zwei Klassen eingeteilt; estrogenrezeptor-positiver (ER+) und estrogenrezeptor-negativer (ER-) Brustkrebs. Ungefähr 57 % der Brustkrebserkrankungen bei prämenopausalen Frauen sind ER^+, bei postmenopausalen Frauen sind es 72% (Lower *et al.*, 1999). Die Häufigkeit der auftretenden Brustkrebserkrankungen bei postmenopausalen Frauen ist auf die Einstellung der Estrogen-Biosynthese der Ovarien zurückzuführen, wodurch E2 lokal in den peripheren Zielgeweben, wie beispielsweise der Brust, gebildet wird (Simpson *et al.*, 1999)

1.1.1.2 Endometriose

Endometriose sind gutartige Wucherungen des Gebärmutterschleimhautgewebes (Endometrium), die sich außerhalb der Gebärmutter vermehrt in den Ovarien, den Eileitern und auch in der Bauchhöhle ansiedeln. Die Prävalenz liegt bei 10 – 15 % bei Frauen im fruchtbaren Alter (Allaire, 2006), bei 25 - 40 % bei infertilen Frauen. Die Ursachen einer Endometriose sind eine Kombination aus retrograder Menstruation in die Bauchhöhle und ektoper Endometriumanomalien, denen eine veränderte Proteinbiosynthese und deren Sekretion und ein verändertes Genexpressionsmuster zugrunde liegen (Stilley *et al*, 2012.). Das potente, weibliche Geschlechtshormon E2 ist in sehr hohen Konzentrationen im ektopen Gewebe vorzufinden und ist für die Implantation und Proliferation verantwortlich (Bulun *et al.*, 2000). E2 induziert die Cyclooxygenase 2 (COX 2), wodurch dann indirekt die Produktion von Prostaglandin E2 (PGE2) stimuliert wird, welches wiederum die E2-Biosynthese fördert (Bulun,

2009). In endometrischen Läsionen spielt sich ständig ein circulus vituosus aus den beschriebenen Stimulationen ab, wodurch das Wachstum des Gewebes weiter gefördert wird.

1.1.2 Therapieoptionen für estrogenabhängige Erkrankungen

Eine Möglichkeit der Behandlung stellt die operative Entfernung des erkrankten Gewebes dar, wobei dies im Fall von Brustkrebs - um Rezidive zu verhindern - meistens in Kombination mit Chemo- oder Strahlentherapie Anwendung findet. Bei der Laparoskopie ist die Entstehung von Rezidiven per se sehr hoch. Häufig werden zur Endometriosebehandlung auch COX2-Hemmer eingesetzt, die in die entzündlichen Prozesse der Endometriose eingreifen und gleichzeitig auch für Schmerzlinderung sorgen (Laschke *et al.*, 2007).

Ein weiterer Ansatz zur Behandlung von Brustkrebs und Endometriose ist auf endokriner Ebene angesiedelt (Adamo *et al.*, 2007; Miller *et al.*, 2007), wobei man versucht mit der Estrogenwirkung zu interferieren (Miller *et al.*, 2007). Dies ist einerseits durch das Eingreifen in die Estrogenbiosynthese und andererseits durch eine Unterdrückung der Estrogenwirkung möglich.

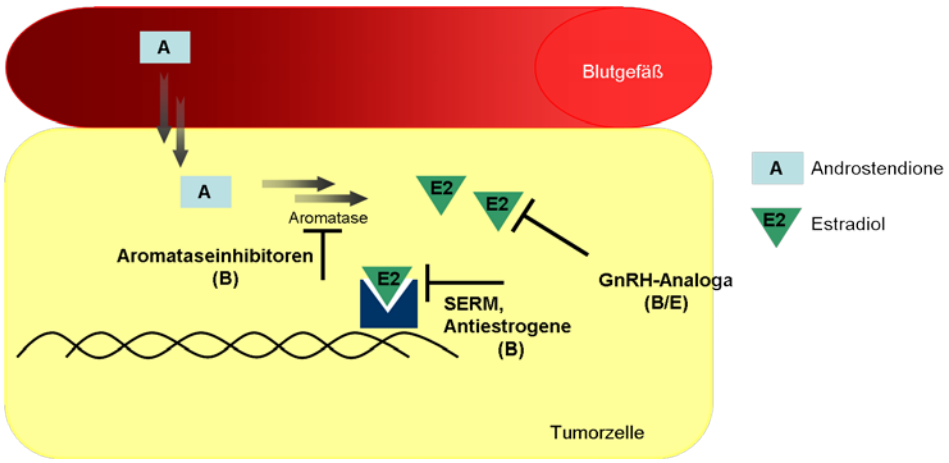

Abbildung 1: Endokrine Therapie bei estrogenabhängigen Erkrankungen; B: Brustkrebstherapie; E: Endometriosetherapie

Ein möglicher Eingriff zur Unterdrückung der Estrogenbiosynthese ist die Gabe von GnRH-Analoga (Gonadotropin-Releasing-Hormon-Analoga, Abbildung 1). Diese unterbrechen den zentralen Feedback-Mechanismus, der die Biosynthese steuert. Damit wird die Estrogenbildung im ganzen Körper reduziert (Emons *et al.*, 2003).

Peripher lässt sich die Estrogenbiosynthese durch Aromataseinhibitoren, die den letzten Schritt der Estronbiosynthese hemmen, unterdrücken. Zur Endometriosebehandlung werden Aromataseinhibitoren momentan noch nicht eingesetzt, es gibt jedoch vielversprechende Studien zum Therapieeinsatz (Bulun *et al.*, 2001; Racine *et al.*, 2012). Durch die Behandlung mit Antiestrogenen oder SERMs (Selektive-Estrogenrezeptormodulatoren) lässt sich eine Verhinderung der

Estrogenwirkung auf Rezeptorebene erzielen. Hier unterscheiden sich Antiestrogene und SERMs in ihrem Wirkort. Während Antiestrogene im ganzen Organismus wirken, wirken SERMs gewebsspezifisch als Agonisten oder Antagonisten. Diese Therapien finden momentan nur Anwendung bei Brustkrebserkrankungen. In einer Mausmodellstudie hat man jedoch gefunden, dass Bazedoxifen (ein sehr starker ER-Antagonist) in der Lage ist, sowohl die Größe von Endometrioseläsionen zu verringern, als auch die Marker der endometrischen Proliferation herabzusetzen (Kulak *et al.*, 2011).

1.1.3 Nachteile und Resistenzen bestehender Therapien

Generell führt eine systemische Absenkung der Estrogenkonzentration zu einem Missverhältnis der natürlichen Hormonbilanz und kann dadurch bedingt zahlreiche bekannte und unbekannte, unerwünschte Wirkungen nach sich ziehen. GnRH-Analoga stellen durch die Unterdrückung der Estrogenbiosynthese in den Ovarien und damit auch im ganzen Körper ein großes Risiko für Nebenwirkungen dar. Auch bei Aromataseinhibitoren, die zwar fokussierter ihre Wirkung zeigen, kommt es durch die vollständige Unterdrückung des Estrogenbiosynthese zu starken Nebenwirkungen wie Osteoporose, Hitzewallungen oder Depressionen (Perez, 2007; Abdulhaq und Geyer, 2008). Hinzu kommt, dass solche Inhibitoren nur bei postmenopausalen Frauen eingesetzt werden können, da bei prämenopausalen Frauen durch einen hypothalämisch/hypophysären Feedback-Mechanismus die Ovarien stark stimuliert würden (Ortmann *et al.*, 2009). Des Weiteren führt auch die längerfristige Anwendung zu Resistenzen und damit zu zahlreichen Problemen bei der Behandlung von erkrankten Frauen (Urruticoechea, 2007). Auch im Falle von Estrogenrezeptorantagonisten ist eine Resistenzentwicklung zu beobachten (Gradishar, 2004; Jordan und O'Malley, 2007; Hurvitz und Pietras, 2008). Durch verstärktes Wachstum von Uterusgewebe kann es zusätzlich noch zum Endometriosekarzinom kommen (Saadat *et al.*, 2007; DeMichele *et al.*, 2008).
Zusammenfassend kann man sagen, dass effiziente Therapieoptionen zur Verfügung stehen, welche jedoch eine Reihe von Nachteilen aufweisen, insbesondere durch die Resistenzentwicklung. Deshalb ist es notwendig, neue Ansätze zur Therapie von estrogenabhängigen Erkrankungen zu finden.

1.1.4 17β-HSD1 als neues Target zur Behandlung von estrogenabhängigen Erkrankungen

1.1.4.1 Allgemeines

E2 ist das potenteste weibliche Sexualhormon und ist verantwortlich für die Differenzierung und Progression von estrogensensitiven Geweben wie der Brust und der Gebärmutterschleimhaut. Hauptsächlich produziert wird E2 in den Granulosazellen der Ovarien. In einem ersten Schritt wird es

durch Aromatisierung von Androstendion gebildet, worauf die lokale Konversion von Estron (E1) zu E2 durch die 17β-Hydroxysteroiddehydrogenase Typ 1 (17β-HSD1) erfolgt (Abbildung 2).

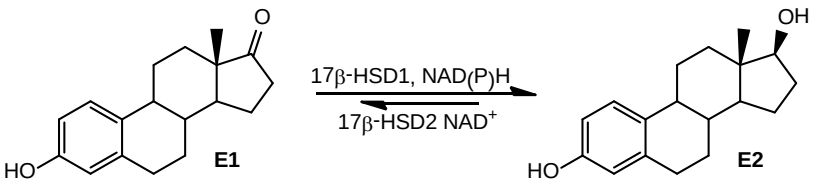

Abbildung 2: Katalyse von E1 zu E2

Das Verhältnis von E2 gegenüber E1 ist sowohl in Brusttumoren als auch in endometriotischen Läsionen erhöht (Smuc *et al.*, 2007; Jansson, 2009) und zusätzlich liegen hohe Level an17β-HSD1-mRNA vor. Durch dieses Missverhältnis und die Überexpression ist die E2-Biosynthese lokal im erkrankten Gewebe verstärkt, wodurch die Proliferation des Gewebes direkt stimuliert wird. Die Hemmung von 17β-HSD1 stellt einen interessanten Ansatz dar, um direkt im Zielgewebe die E2-Konzentration zu verringern und dadurch das Fortschreiten der Erkrankung zu unterdrücken. Dieses intrakrine Konzept bringt den Vorteil mit sich, dass durch die Hemmung der E2-Biosynthese in ihrem letzten Schritt, E1 weiterhin seine schwach estrogene Wirkung im Organismus entfalten kann. Dadurch könnte den typischen Nebenwirkungen wie Osteoporose, Hitzewallungen und Depressionen vorgebeugt werden. 17β-HSD1 stellt also ein interessantes, vielversprechendes Target zur Therapie von estrogen-abhängigen Erkrankungen dar.

1.1.4.2 Struktur und Funktion

17β-HSD1 ist ein cytosolisches Enzym, das zur Klasse der side-chain-Dehydrogenasen/Reduktasen (SDRs) gehört (Joernvall *et al.*, 1995). Es liegt in der aktiven Form als lösliches, cytosolisches Homodimer vor, von welchem die Untereinheiten jeweils aus 327 Aminosäuren (34.9 kDa) bestehen (Peltoketo *et al.*, 1988). Ein Monomer besteht aus sieben parallel angeordneten β-Faltblättern und 11 α-Helices (Ghosh *et al.*, 1995).

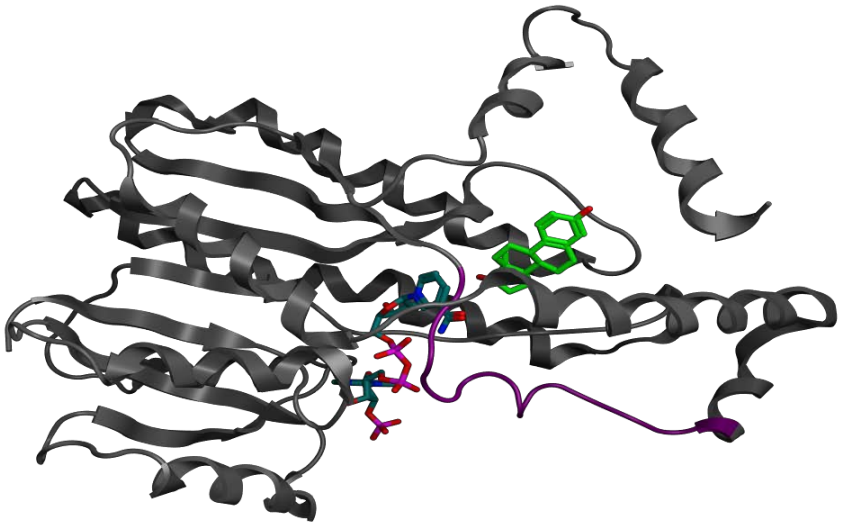

Abbildung 3: Röntgenkristallstruktur der humanen 17β-HSD1 als Kokristallisat mit E2 (grün) und NADP+ (Türkis), PDB Code 1a27. a-Helices und β-Faltblätter in grau dargestellt, flexibler Loop in violett.

Strukturell lässt sich die 17β-HSD1 in Rossmanfold, Substratbindetasche und Cofaktorbindetasche unterteilen. Die Cofaktorbindetasche kann man sich als hydrophoben Tunnel mit polaren Funktionen an beiden Enden vorstellen. Auf der C-terminalen Seite wird der Tunnel durch die polaren Aminosäuren His221 und Glu282 begrenzt und durch Ser142 und Tyr155 auf der N-terminalen Seite. Letztere Aminosäuren bilden zusammen mit Asn114 und Lys159 die katalytische Tetrade, die man in den meisten der charakterisierten SDRs findet (Azzi *et al.*, 1996; Filling *et al.*, 2002). Im aktiven Zentrum bindet das Produkt der katalytischen Reaktion E2. Es wird über drei bis vier Wasserstoffbrücken und durch hydrophobe Wechselwirkungen mit den apolaren Aminosäuren der Bindetasche im aktiven Zentrum stabilisiert (Abbildung 4). Die Hydroxygruppe am C17 von E2 bildet zwei Wasserstoffbrücken zu Ser142 und Tyr155 auf der einen Seite des katalytischen Zentrums und die phenolische Hydroxygruppe am C3 interagiert mit His221 auf der gegenüberliegenden Seite. Obwohl Mutagenesestudien ergaben, dass Glu282 zur Substratbindung nicht notwendig sein sollen, fand man in Kristallstrukturen Wasserstoffbrückenbindungen zwischen der phenolischen Hydroxyfunktion von E2 und Glu282 (Sawicki *et al.*, 1999). Durch Ausbildung einer Salzbrücke zum His221 soll der Glutamatrest auch zur Stabilität des Enzyms beitragen (Ghosh *et al.*, 1995).

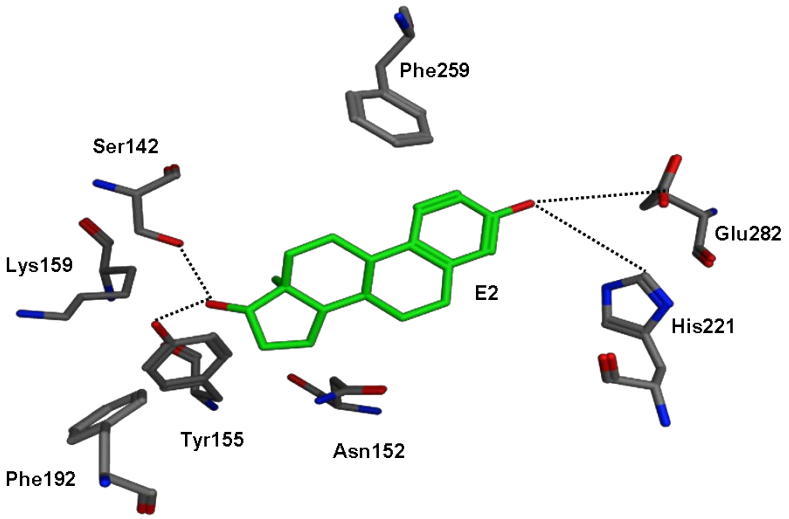

Abbildung 4: Bindungsmodus von E2 (grün) in der Substratbindetasche der humanen 17β-HSD1 (PDB ID: 1A27), Wasserstoffbrücken in schwarz (gestrichelt)

Zurzeit sind 22 Kristallstrukturen der humanen 17β-HSD1 in der Proteindatenbank veröffentlicht, als Apoform, als binärer oder ternärer Komplex (http://www.pdb.org, Mazumdar *et al.*, 2009a ; Mazumdar *et al.*, 2009b; Marchais-Oberwinkler *et al.*, 2011) Alle Kristallstrukturen zeigen eine fast identische Tertiärstruktur mit großen Unterschieden im hochflexiblen βFαG´-loop. In 10 der Kristallstrukturen ist dieser Loop nicht aufgelöst und in den verbleibenden 12 Kristallstrukturen fand man hohe B-Faktoren für diese Region, was ein weiterer Hinweis auf die hohe Flexibilität ist. Dieser Proteinabschnitt stellt die Grenze von Substrat- und Cofaktorbindetasche dar, und definiert somit Volumen und Form dieser Kavitäten. Abhängig von Anwesenheit des Cofaktors und Ligand kann der Loop drei verschiedene Positionen einnehmen: eine geöffnete, eine halb-geöffnete und eine geschlossene Enzymkonformation (Negri *et al.*, 2010).

1.1.4.3 Propagierter Katalysemechanismus

Obwohl eine Vielzahl struktureller Informationen zur 17β-HSD1 verfügbar sind, konnte bis dato noch nicht genau geklärt werden, wie der katalytische Mechanismus abläuft. Drei unterschiedliche Mechanismen werden in der Literatur postuliert, ein konzertierter (Ghosh und Vihko, 2001) und zwei schrittweise Mechanismen (Penning, 1997). Allen gemeinsam ist, das ein reversibler Hydrid- oder Protonentransfer von NADPH oder Hydroxysteroid zum Ketosteroid bzw. zum NAD^+ stattfindet.

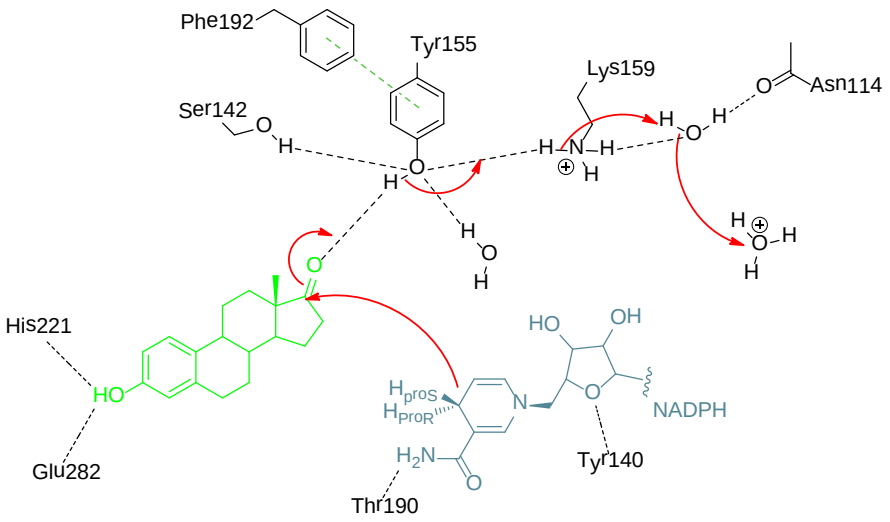

Abbildung 5: Postulierter schrittweiser Katalysemechanismus (Substrat in grün, Cofaktor in türkis, Aminosäuren in schwarz, Elektronentransferpfeile in rot, Wasserstoffbrücken in schwarz-gestrichelt und π-stacking in dunkelgrün-gestrichelt dargestellt.)

Am plausibelsten erscheint der schrittweise Mechanismus, da das Sauerstoffanion des tetrahedralen Kohlenstoffs am C17 besser die Protonen vom Tyr155 aufzunehmen kann als der Sauerstoff des planaren C17-Kohlenstoffs am E1.

In einem ersten Schritt wir das pro S-Hydrid von NADPH auf die α-Seite des planaren C17 Kohlenstoffs von E1 übertragen, woraus das energetisch favorisierte aromatische System des Nicotinamidrest von NADP resultiert. Anschließend wird das entstandene Oxyanion von der aziden Hydroxygruppe des Tyr155 protoniert. Diese Protonenübertragung wird einmal durch das Wasserstoffbrückennetzwerk zwischen Tyr155, Lys159 dem Rückgrat von Asn114 und zwei Wassermolekülen begünstigt, sowie durch das π-stacking der beiden Phenylringe von Tyr155 und Phe192 (Negri *et al.*, 2010).

1.1.4.4 Interspeziesanalyse

Interspeziesunterschiede sind für die Auswahl einer geeigneten Spezies für *in-vivo*-Studien zur Evaluierung der Hemmstoffe *in vivo* von großer Bedeutung. Die Aminosäuresequenz-Identitäten zwischen humaner 17β-HSD1 und 17β-HSD1 von anderen Spezies reichen von 68 % bei der Maus bis hin zu 99 % beim Schimpansen, während die vergleichbaren Similaritäten von 77 % bis 100% reichen.

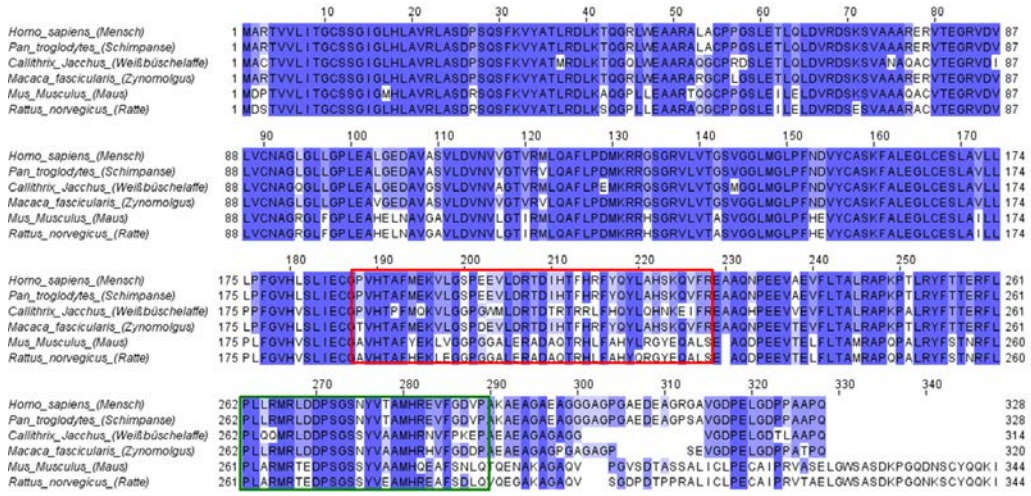

Abbildung 6: Multiples Sequenzalignment von 17β-HSD1 verschiedener Spezies. Die rote Box repräsentiert das F/G-Segment, die grüne Box die C-terminale Region. Die Nummerierungen der Aminosäuren beziehen sich auf die humane Sequenz. Das Alignment wurde mit Jalview 2.5.1 als MAFFT muliple sequence alignment webserver erstellt.

Die größten Unterschiede im Vergleich der humanen Sequenz mit verschiedenen Spezies in der Primärstruktur und auch in der Tertiärstruktur findet man in den beiden Bereichen, die die polare Substratbindetasche darstellen: das F/G-Segment (AS 191 – 230) und der C-terminale Bereich (AS 262 - 287). Diese nur moderaten Similaritäten können zu Schwierigkeiten bei der Identifizierung einer geeigneten Spezies für ein *in vivo Proof of Concept* führen. Für Ratte und Maus liegen die Similaritäten beispielsweise bei 78 % und 77% (Identitäten: 69 % [Ratte] und 68 % [Maus]) in den ersten 287 Aminosäuren. Dadurch erklären sich auch die verschiedenen Substrataffinitäten und die Tatsache, dass die murine 17β-HSD1 im Gegensatz zu den anderen Spezies auch Androgene umsetzen kann (Akinola *et al.*, 1996; Nokelainen *et al.*, 1996; Mindnich *et al.*, 2005). Verschiedene Ansätze zur Evaluierung von 17β-HSD1- Inhibitoren an verschiedenen Spezies sind in der Literatur beschrieben. So wurden verschiedene nicht-steroidale Hemmstoffe (hoch aktiv und selektiv am humanen Enzym) an Rattenleberpreparationen getestet (Kruchten *et al.*, 2009c) und dabei nur moderate Aktivitäten und geringe Selektivitäten gegenüber 17β-HSD2 der Ratte festgestellt wurden. Ein ähnlicher Ansatz war der von Möller *et al.*, in dem die Inhibitorpotenz von E2/E1-Derivaten gegenüber 17β-HSD1 von verschiedenen Spezies (rekombinant aus *E.coli*) getestet wurden. Auch hier fand man Inaktivität gegenüber den murinen Enzymen. Vergleichbare Aktivitäten mit dem humanen Enzym für die oben genannten Derivate wurden gegenüber 17β-HSD1 von *Callithrix jacchus (C. jacchus,* 80 % Identität) gefunden (Möller *et al., 2010*).

1.1.4.5 Tiermodelle

Tiermodelle werden in der Regel verwendet um weitere Einblicke in die physiologische Rolle des Targets zu bekommen und auch um zu testen, wie sich die Behandlung mit einem potentiellen Arzneimittelkandidaten auf den Organismus einer Spezies auswirkt. Je näher der Organismus eines Modells dem menschlichen Organismus kommt, desto besser ist dieser als Tiermodell geeignet, da man dadurch mehr über eventuelle off-target-Effekte am Menschen erfahren kann. Für die Inhibitor-Evaluierung von 17β-HSD1 sind verschiedene Tiermodelle in verschiedenen Spezies beschrieben. Durch die großen Speziesunterschiede zwischen der humanen 17β-HSD1 (*h*17β-HSD1) und den murinen Enzymen (siehe Kapitel 1.1.4.4) besteht eine hohe Wahrscheinlichkeit, dass die humanen Hemmstoffe keine Effekte in einem murinen Modell auslösen. Hinzu kommt das veränderte Expressionsmuster des Targetenzyms in den verschiedenen Geweben. Um diese Probleme zu umgehen, verwendet man Xenograft- oder Nacktmausmodelle. Eine weitere Möglichkeit ist die Verwendung von transgenen Mäusen, die das Gen für humane 17β-HSD1 aufweisen und dadurch das Enzym exprimieren. Lamminen *et al.* beschreiben ein solches Modell, bei dem sie sowohl eine erhöhte 17β-HSD1 Aktivität in verschiedenen Geweben, als auch die Hemmung der E1/E2-Konversion gezeigt haben (Lamminen *et al.*, 2009).

1.1.4.6 Tiermodelle für estrogenabhängige Erkrankungen

1.1.4.6.1 Brustkrebs

Es gibt zwei beschriebene Krankheitsmodelle für Brustkrebs, bei denen immundefizienten Mäusen Brustkrebs induziert wird, indem man humane Mammakarzinomzellen einpflanzt. Eines dieser Modelle verwendet MCF-7-Zellen (Husen *et al.*, 2006a; Husen *et al.*, 2006b). Diese Zelllinie exprimiert 17β-HSD1 nur im geringen Ausmaß (Day *et al.*, 2006; Smuc and Rizner, 2009), weshalb die Zellen vor der Inokulation in die Flanke von ovarektomierten Mäusen stabil mit 17β-HSD1 transfiziert werden. Zur Ausbildung der Tumore wird das Wachstum zunächst mit E2 stimuliert. Während der Experimente wird E1 zugeführt, damit man die enzymatische Konversion zu E2 der im Tumor exprimierten 17β-HSD1 messen kann. Als Marker, wird die Tumorgröße verwendet. In diesem Modell hat man bereits steroidale 17β-HSD1-Inhibitoren untersucht (Messinger *et al.*, 2006).
In einem zweiten Xenograft-Modell werden T47D-Zellen (Day *et al.*, 2008b) verwendet, welche von sich aus genügend 17β-HSD1 exprimieren. (Day *et al.*, 2006). Hier erfolgt die Tumorstimulation über E1. Als Marker dienen Tumorgröße, E2-Spiegel im Plasma und 17β-HSD1-Aktivität im Tumorgewebe. Ein verringertes Tumorwachstum konnte hier mit dem steroidalen Inhibitor STX1040 demonstriert werden (Day *et al.*, 2008a).
Durch die Verwendung von Xenograft-Modellen kann man zusätzlich zu den Informationen über das Verhalten potenzieller Hemmstoffe in den Zelllinien auch pharmakokinetische Parameter evaluieren.

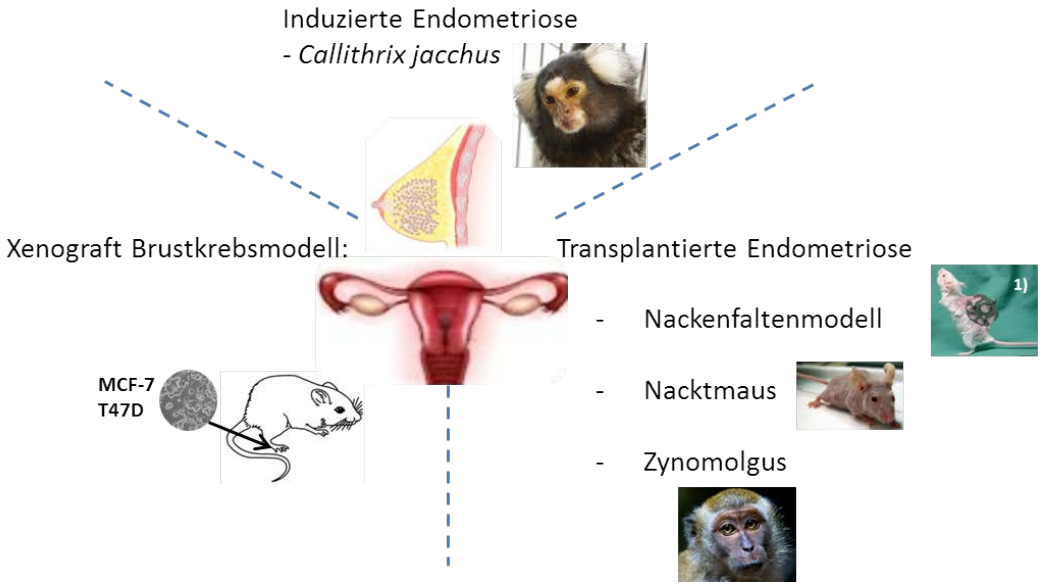

Abbildung 7: Tiermodelle für Brustkrebs und Endometriose [1) (Laschke et al., 2005)]

1.1.4.6.2 Endometriose

Auch für Endometriose gibt es einige interessante Tiermodelle. Zusätzlich zu den Nagermodellen sind hier auch Primatenmodelle beschrieben. Nur eines der Modelle arbeitet jedoch mit humaner 17β-HSD1, deshalb müssen hier auch die beschriebenen Speziesunterschiede dementsprechend berücksichtigt werden. Für das von Laschke *et al*. beschriebene Skinfoldchamber-Modell können verschiedene Nager eingesetzt werden. Den Tieren werden autologe Endometriumfragmente in die Nackenfalte transplantiert (Menger *et al.*, 2002; Laschke *et al*., 2005). Als Parameter gelten hier erreichte Größe des Transplantats, VEGF und PCNA (proliferating cell nuclear antigen) als Marker für das Wachstum. Potentielle Hemmstoffe wurden an diesem Modell bisher nicht getestet. Das Modell von Grümmer *et al*. arbeitet mit humanen Endometriosefragmenten, die am Peritoneum von ovariektomiereten Nacktmäusen vernäht werden (Scotti *et al.*, 2000; Grümmer *et al.*, 2001). Es werden Expressionsänderungen E2-sensitiver Gene, von 17β-HSD1 und Aromatase untersucht und der Blutestradiolspiegel kontrolliert. Eine Reihe von 17β-HSD1-Inhibitoren zeigten an diesem Modell veränderte Genexpressionsmuster (Firnhaber, 2006).

Zwei Primatenmodelle sind für das Krankheitsbild der Endometriose beschrieben, eines an Zynomolgen (*Macaca fascicularis*, 92 % Aminosäuresequenzidentität) und eines an Weißbüschelohraffen (*C. jacchus*). Diese sind weniger artifiziell, jedoch auch deutlich aufwändiger. Am Zynomolgenmodell werden autologe Endometriumfragmente in das Abdomen transplantiert. Als Marker werden die Größe der entstandenen Läsionen, IL-6 (Interleukin 6), IL-6-SR (Interleukin 6 soluble receptor) und die Plasmaestradiolspiegel untersucht (Sillem *et al.*, 1996; Yang *et al.*, 2000). Am Modell des Weißbüschelohraffen wird Endometriose induziert, indem man Endometriumzellen durch den Bauchraum in den Uterus einspült, wo sie sich zu Endometrioseherden entwickeln. Es

werden die Größe der entstandenen Läsionen und der Blutfluss innerhalb dieser Läsionen, die Protein- und mRNA-Expression von CYP19, 17β-HSD1 und ER untersucht (Einspanier *et al.*, 2006).
Die Ergebnisse, die man in der Anwendung von 17β-HSD1-Inhibitoren an verschiedenen Tiermodellen für estrogen-abhängige Erkrankungen erzielt hat, stellen einen interessanten Ansatzpunkt dar. Die weitere Entwicklung von 17β-HSD1-Inhibitoren ist somit ein vielversprechender Ansatz zur Therapiemöglichkeit.

1.1.4.7 17β-HSD1-Inhibitoren

In den letzten Jahren sind eine Reihe von 17β-HSD1-Inhibitoren entwickelt und beschrieben worden, was das enorme Potential dieser Hemmstoffe und das Interesse, auch seitens der pharmazeutischen Industrie, widerspiegelt. Es sind verschiedene Übersichtsartikel in der Literatur veröffentlich, die sich mit steroidalen und nicht-steroidalen 17β-HSD1 Inhibitoren befassen (Poirier, 2003; Brozic *et al.*, 2008; Day et al., 2008a; Poirier, 2009; Day *et al.*, 2010; Marchais-Oberwinkler *et al.*, 2011). Bis auf die von Michiels *et al.* beschriebenen Phytoestrogene (Michiels *et al.*, 2009) binden alle bekannten Hemmstoffe in der Substratbindetasche und/oder in der Cofaktorbindetasche. Für die Phytoestrogene wurden durch kompetitive NMR-Experimente weder Wechselwirkungen mit der Substratbindetasche noch mit der Cofaktorbindetasche gefunden, sondern das Dimerinterface von 17β-HSD1 wurde als mögliche Bindestelle postuliert (Michiels et al., 2009).
Die steroidalen Inhibitoren leiten sich im Wesentlichem vom E1 oder E2-Grundgerüst ab (Allan *et al.*, 2006a; Allan *et al.*, 2006b; Vicker *et al.*, 2006). Es wurden Variationen an C17 durchgeführt (Deluca *et al.*, 2006) und auch weitere Seitenketten an C2 (Cushman *et al.*, 1995; Leese *et al.*, 2005), C5, C6, C15 (Messinger *et al.*, 2008b; Messinger *et al.*, 2008a; Messinger *et al.*, 2009) und C16 (Sam *et al.*, 1998; Rouillard *et al.*, 2008) am Steroidgrundgerüst eingeführt. Mit dem steroidalen Inhibitor STX1040 (Abbildung 8 **A**, (Lawrence *et al.*, 2005)) wurde das erste *Proof of Concept* für 17β-HSD1-Inhibitoren erstellt (Day et al., 2008b). Mit E2B, einem weiteren steroidalen Hemmstoff (Abbildung 8 **B**) hat man durch Co-Kristallisation eine zusätzliche, kleine lipophile Bindetasche unterhalb des katalytischen Zentrums identifiziert (Mazumdar *et al.*, 2009c).
Von dem ersten sogenannten Dual-site-Inhibitor (Abbildung 8 **C**), eine Kombination aus Estradiol-Grundgerüst, das über einen Alkylspacer mit einem Adenosinrest verbunden ist, erwartete man, dass sowohl die Substratbindetasche, als auch die Cofaktorbindetasche besetzt würden (Qiu *et al.*, 2002).
Als erste nicht-steroidale Hemmstoffe mit vergleichsweise geringer Aktivität wurden Coumestrol- und Gossypolderviate beschrieben (Mäkelä *et al.*, 1995; Brown *et al.*, 2003). Bei einem computergestützten Ansatz wurden mit Hilfe eines Pharmakophormodells die relativ schwach aktiven Glycyrrhetinsäurederivate gefunden (Schuster *et al.*, 2008). Ähnlich geringe Aktivitäten fand man für die Phenylketone (Lota *et al.*, 2007) und die Phenylalkylimidazole (Olusjano *et al.*, 2004). Mit dem Ziel den natürlichen Liganden E1 zu imitieren, entwickelte Allan *et al.* die Biphenylethanone und die

Indanon/Tetralon-Derivate, welche mittlere Aktivitäten zeigten (z.B. Abbildung 8 **D**, Allan *et al.*, 2008).

Eine weitere Verbindungsklasse, zu denen zwei der aktivsten nicht-steroidalen Hemmstoffe gehören, sind die Thiophenpyridiminone (Abbildung 8**E**, Messinger *et al.*, 2006; Karkola *et al.*, 2009; Lilienkampf *et al.*, 2009).

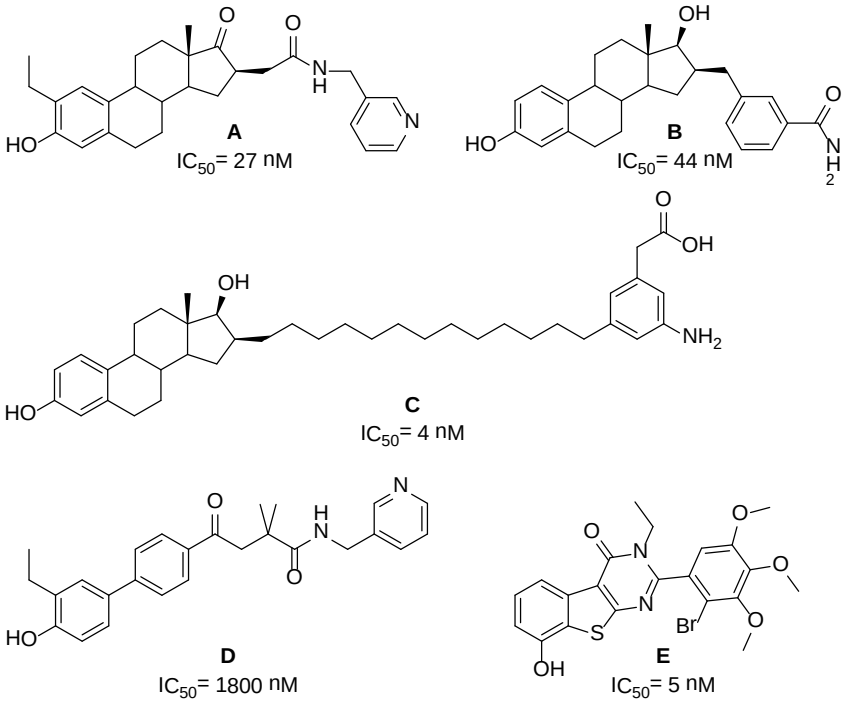

Abbildung 8: Beispiele für steroidale und nicht-steroidale Hemmstoffe verschiedener Substanzklassen und deren biologische Aktivität gegenüber 17β-HSD1

In unserem Arbeitskreis wurden bis dato vier unterschiedliche hoch aktive Substanzklassen von nicht-steroidalen Hemmstoffen entwickelt, die allesamt sehr gute Selektivitäten gegenüber 17β-HSD2 zeigen.

In der Klasse der Bis(hydroxyphenyl)arene (Bey *et al.*, 2008a; Bey *et al.*, 2008b; Al-Soud *et al.*, 2009; Bey *et al.*, 2009, Abbildung 9 **A**) wurden ausführliche SAR-Studien durchgeführt, in denen gezeigt wurde, dass der Austausch des mittleren Rings einer inaktiven Verbindung zu hochaktiven und selektiven Verbindungen führen kann. Eine mögliche Erklärung für diese scharfe SAR, konnte durch die unterschiedlichen MEP-(Molekular-Elektrostatisches Potential)Verteilungen dieser Verbindungen identifiziert werden. Durch das Erstellen eines Pharmakophor-Modells, das auf den zwei steroidalen Sauerstoffen des E2 basiert (Abstand 12 Å) konnte eine weitere Substanzklasse identifiziert werden, die (Hydroxphenyl)naphthalene (Frotscher *et al.*, 2008; Marchais-Oberwinkler *et al.*, 2008; Marchais-Oberwinkler *et al.*, 2009), Abbildung 9**B**). Durch die Kombination von liganden- und strukturbasiertem Ansatz wurden heterozyklische, substituierte Estronmimetika unter Einbeziehung

eines Pharmakophormodells zu bizyklischen, substituierten Hydroxyphenylmethanonen weiterentwickelt (Oster *et al.*, 2010a; Oster *et al.*, 2010b; Oster *et al.*, 2010c); Abbildung 9 **C**). Die Hydroxybenzothiazole (Spadaro *et al.*, 2012a; Spadaro *et al.*, 2012b), Abbildung 9 **D**) wurden unter Einsatz eines kristallstrukturbasierten Pharmakophormodells und einem anschließenden virtuellen Screening einer kleinen Substanzbibliothek identifiziert.

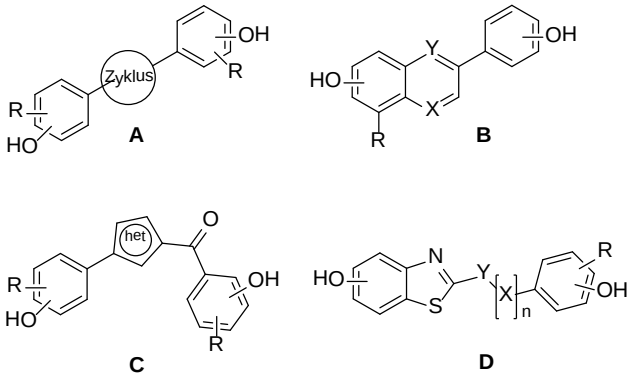

Abbildung 9: Nicht-steroidale 17β-HSD1 Inhibitorklassen aus unserem Arbeitskreis

Alle entwickelten Verbindungen werden in einem biologischen Screeningsystem, das aus zehn unterschiedlichen Assays besteht, evaluiert. Die Verbindungen werden hinsichtlich ihrer Aktivität (zellfrei und zellulär) und ihrer Selektivität (17β-HSD2, ERα, ERβ und hepatischer CYPs) genau untersucht (Kruchten *et al.*, 2009a). Auch hinsichtlich ihrer spezies-spezifischen Aktivität werden die Verbindungen evaluiert (Kruchten *et al*., 2009c). Ein *in vitro Proof of Concep*t wurde für ausgesuchte Verbindungen aus der Substanzklasse der Bis(hydroxyphenyl)arene und der Hydroxphenyl)naphthalene an einem zellulären System (T47D) erbracht. Die Verbindungen waren in der Lage, eine E1-induzierte Zellproliferation zu hemmen (Kruchten *et al.*, 2009b).

1.2 Quorum Sensing

1.2.1 Pseudomonas aeruginosa

Pseudomonas aeruginosa (*P. aeruginosa*) sind gram-negative, opportunistische Stäbchenbakterien, die sehr anpassungsfähig sind und in relativ anspruchsloser Umgebung überleben. Sie verursachen eine Reihe von Infektionen, hauptsächlich der Atem- und Harnwege, Brandwunden oder auch Sepsi. Circa 10 % aller nosokomialen Infektionen werden durch dieses Pathogen verursacht (de Bentzmann and Plésiat, 2011), mitunter ist es verantwortlich für die chronische Lungeninfektion von mehr als 80 % der Patienten mit cystischer Fibrose (van Delden and Iglewski, 1998).

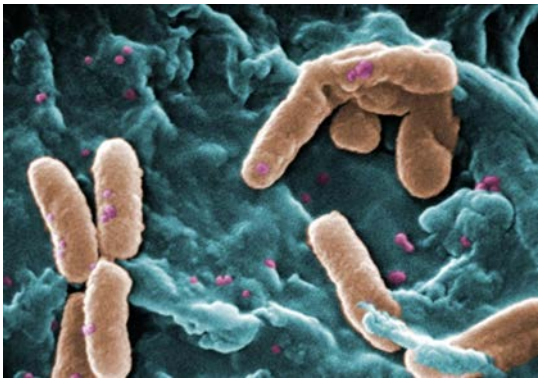

Abbildung 10: Pseudomonas aeruginosa (www.pseudomonas-aeruginosa.de)

Cystische Fibrose (CF), oder auch Mukoviszidose, ist eine autosomal, rezessiv vererbte Stoffwechselerkrankung, die durch Mukusübersektretion aufgrund einer Fehlfunktion in Chloridionenkanälen, charakterisiert ist. CF ist die am häufigsten auftretende, tödlich verlaufende genetische Erkrankung bei Menschen weißer Hautfarbe (Donaldson und Boucher, 2006). 1989 wurde das Gene, das verantwortlich für diesen Defekt ist, identifiziert und kloniert, seitdem kennt man die Ursache dieser Fehlfunktion (Kerem *et al.*, 1989; Riordan *et al.*, 1989). Es sind Mutationen am langen Arm des Chromosoms 7 des Gens, das für CTRF (cystic fibrosis transmembrane conductance regulator) codiert (Rommens *et al.*, 1989). Die häufigste Mutation ist die Δ508F, was für das Fehlen des Phenylalanins an Position 508 steht. Das CTRF-Protein besteht aus 1480 Aminosäuren und ist in der apikalen Membran von Epithelzellen lokalisiert. Es ist ein cAMP-sensitiver Chloridkanal, der mit für den Ionenaustausch verantwortlich ist und zur Familie der ABC-Transporter gehört. Durch die Mutation des CTRF-Gens kommt es zu einem gestörten Transport von Chloridionen und dadurch zu einem Missverhältnis der Chlorid-Konzentration von intra- zu extrazellulär. Die Rolle des CTRF-Gens beschränkt sich jedoch nicht nur auf die Funktion Chloridkanäle, sondern es wirkt auch aus bisher ungeklärten Mechanismen insbesondere hemmend auf die epithelialen Natriumkanäle (Stutts *et al.*, 1995; Stutts *et al.*, 1997). Das CTRF-Gen gilt daher als zentraler Regulator des Salz-und Wassertransports und die Mutation dieses Gens hat organspezifische Störungen zur Folge. Es kommt

zur verringerten, zähflüssigen Schleimbildung bei CF-Patienten. Insbesondere die Atemwege sind davon betroffen, da es dort durch den zähen Mucus zur Störung des natürlichen Abwehrmechanismus der Atemwege kommt und Pseudomonaden sich dort gut am Epithel kolonisieren können (Matsui *et al.*, 2005). Die Kolonialisierung ist der erste Schritt zur Biofilmformation. Die Entstehung eines manifesten Biofilms lässt sich in drei Phasen einteilen; Induktions-, Wachstums- und Plateauphase (Reisner *et al.*, 2005), Abbildung 11).

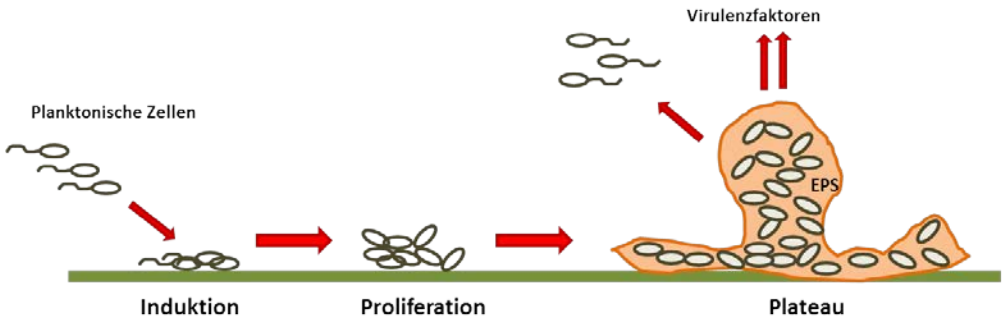

Abbildung 11: Phasen der Biofilmentstehung

In der Induktionsphase heften sich die Bakterien an der Oberfläche an, im Fall von CF bevorzugt in der Lunge oder den Atemwegen, zuerst geschieht dies reversibel, worauf nach längerer Aufenthaltsphase die irreversible Phase folgt. In der zweiten Phase, kommt es zur Adaption des Stoffwechsels, die Bakterien gehen in die sessile Lebensform über (Reisner *et al.*, 2005). Es werden biofilmspezifische Gene induziert und die Bildung einer extrazellulären Polymermatrix (EPS) wird eingeleitet (Costerton *et al.*, 1995), zusätzlich akkumulieren weiterhin auch noch planktonische Zellen. Die Plateauphase ist gekennzeichnet durch ein Gleichgewicht zwischen Wachstum und Ablösung von Zellen (Molin und Tolker-Nielsen, 2003). Ein Biofilm besteht hauptsächlich aus Wasser, den Bakterien und einer extrazellulären Polymermatrix (EPS). Diese besteht aus Polysaccariden, extrazellulärer DNA und anderen Makromolekülen wie Proteinen und Nukleinsäuren. Die hohe Persistenz von *P. aeruginosa* in CF-Patienten ist mitunter darauf zurückzuführen, dass diese Mikroorganismen in der Lage sind einen Biofilm auszubilden, der sie von Angriffen des Immunsystems und auch vor Antibiotika schützt (Costerton *et al.*, 1995; Costerton *et al.*, 1999). Hierbei schirmt die EPS-Matrix die Bakterien vor den Phagozyten des Immunsystems ab (Hoiby *et al.*, 2001) und wirkt gleichzeitig auch als Barriere für Antibiotika, die regelrecht durch die EPS adsorbiert werden können, wodurch das Durchdringen zu den Bakterien und somit auch ihre Wirkung verringert ist. Durch die Kolonialisierung verändert sich auch das Expressionsmuster der Bakterien, es werden spezifische Schutzfaktoren (Multidrug-Efflux-Pumpen oder Stressreaktionsregulatoren), die mitunter für die erhöhte Resistenz verantwortlich sind, und extrazelluläre Virulenzfaktoren gebildet (van Delden und Iglewski, 1998; Stoodley *et al.*, 2002). Die Regulation all dieser Faktoren und die

Biofilmformation werden über ein komplexes zelldichte-abhängiges Kommunikationssystem gesteuert, das als *Quorum-Sensing* bezeichnet wird (Swift *et al.*, 2001).

1.2.2 Quorum Sensing

1.2.2.1 Allgemeines

Quorum Sensing bezeichnet man das Phänomen, das es Bakterien erlaubt über kleine, hormonartige Signalmoleküle, die man als Autoinducer bezeichnet, miteinander zu kommunizieren (Fuqua *et al.*, 1994). Bei geringer Zelldichte liegt die Konzentration der Autoinducer auf einem Basallevel, die sich jedoch mit ansteigender Zelldichte erhöht.

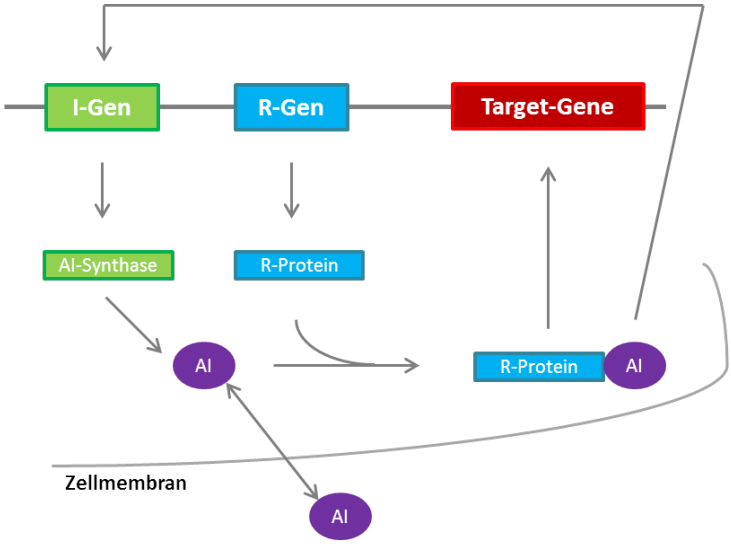

Abbildung 12: Das Zell-Zell-Kommunikationssystem besteht aus mindestens 2 Genen, Das I-Gen codiert für die Autodinducersynthase und das R-Gen für den Transkriptionsregulator (R-Protein). Die Autoinducer-Synthase ist für die Synthese des Autoinducers (AI) verantwortlich, der die Zellmembran passieren kann. Der R-Protein-AI-Komplex aktiviert die Expression der spezifischen Target-Gene (modifiziert von Van Delden 1998)

Erreicht die Konzentration einen Schwellenwert, wird über spezifische Rezeptoren (R-Protein) die Autoinduktion vermittelt, es entsteht ein Rezeptor/Autoinducer-Komplex, welcher an die spezifische DNA binden kann und so die Gentranskription und die anschließende Expression von verschiedenen Genen aktiviert. Unter anderem werden auch die Gene exprimiert, die für die Expression der Autoinducer selbst verantwortlich sind. Diese positive Rückkopplung führt zur vollständigen Aktivierung des Rezeptors, was wiederum die Regulation von weiteren Genen zur Folge hat (Abbildung 12, (van Delden und Iglewski, 1998; Waters und Bassler, 2005).

Das erste beschriebene *Quorum Sensing* System ist das lux-System der gram-negativen *Vibrio fischeri* (Fuqua et al., 1996). Das lux-System kontrolliert die Expression der Gene, die die Biolumineszenz dieser Bakterien auslösen. Bei *Vibrio fischeri* stellt LuxR das R-Protein und LuxI die Autoinducer-Synthase dar. Die meisten der gramnegativen Bakterien besitzen Kommunikationssysteme des LuxIR-

Typs und kommunizieren über Acyl-homoserin-Lactone (AHL) als Signalmoleküle (Fuqua *et al*., 1996; Manefield und Turner, 2002), weshalb man diese Kommunikationssysteme auch als AHL-Systeme bezeichnet.

1.2.2.2 Quorum Sensing in Pseudomonas aeruginosa

In *P. aeruginosa* gibt es zwei AHL-Systeme, das Las-und das Rhl-System (Abbildung 13). Das Las-System besteht aus *lasI*, dem Autoinducer-Synthase Gen für die Synthese von 3-oxo-C12-HSL (N-[3-oxododecanoyl]-L-homoserinlacton) und *lasR*, dem Gen, das die Transkription reguliert. Das Las-System kontrolliert die Produktion verschiedenster Virulenzfaktoren, die bei der akuten Infektion und bei der Zerstörung der Wirtszellen involviert sind, wie LasA, LasB, Elastase und Exotoxin A. Das Rhl-System produziert über die RhlI-Synthase seinen Autoinducer C4HSL (N-butanoyl-homoserin-Lacton) als Autoinducer, welcher über den Transkriptionsregulator RhlR erkannt wird. Dieses System ist unter anderem für die Regulation der Rhamnolipid-Expression verantwortlich. Trotz der Ähnlichkeit ihrer Autoinducer sind diese beiden Systeme sehr spezifisch, d.h. weder 3-oxo-C12-HSL ist in der Lage RhlR zu aktivieren, noch ist C4-HSL in der Lage LasR zu aktivieren (Latifi *et al.*, 1995; Pearson *et al.*, 1997). Dennoch stehen sie in einer Hierarchie zueinander, das Las-System kontrolliert das Rhl-System, dadurch, dass der 3-oxo-C12-HSL/LasR-Komplex direkt die *rhlR*-Transkription positiv reguliert (Latifi *et al.*, 1996). Ein drittes Kommunikationssystem hat man mit der Entdeckung von 2-heptyl-3-hydroxy-4-Chinolon, dem *Pseudomonas Quinolone Signal* (PQS), identifiziert (Pesci *et al.*, 1999). Dieses Signal kontrolliert eine Vielzahl von Virulenzfaktoren und greift in die *Quorum Sensing* Kaskade ein, indem es den regulatorischen Link zwischen dem Las- und dem Rhl-System darstellt (McKnight *et al.*, 2000; Diggle *et al.*, 2003). Das PQS-System wird positiv von LasR und negativ von RhlR reguliert. Die *pqs*ABCD Genprodukte katalysieren die Umsetzung von Anthranilat und einer α-Ketofettsäure zu 2-Heptyl-4-Chinolon (HHQ), der Vorstufe von PQS. PqsA wurde als Benzoat Coenzym A Ligase identifiziert, während PqsB, PqsC und PqsD Ähnlichkeit zu β-Keto-Acyl-Acyl Carrier Protein Synthetasen zeigen (Lépine *et al.*, 2004). PqsD katalysiert den letzten Schritt der HHQ-Biosynthese (Pistorius *et al.*, 2011). HHQ wird dann intrazellulär durch PqsH zu PQS umgesetzt (Gallagher *et al.*, 2002; Lépine *et al*., 2004), ist ein bestimmter Schwellenwert an PQS erreicht, bindet PQS an PqsR. Dieser PQS/PqsR-Komplex aktiviert wiederum die Expression des *pqsABCD*- und *phnA*-Operons, woraus gesteigerte PQS- und Pyocyanin-Produktion resultiert (Cao *et al.*, 2001; Diggle et al., 2003; Déziel *et al.*, 2005).

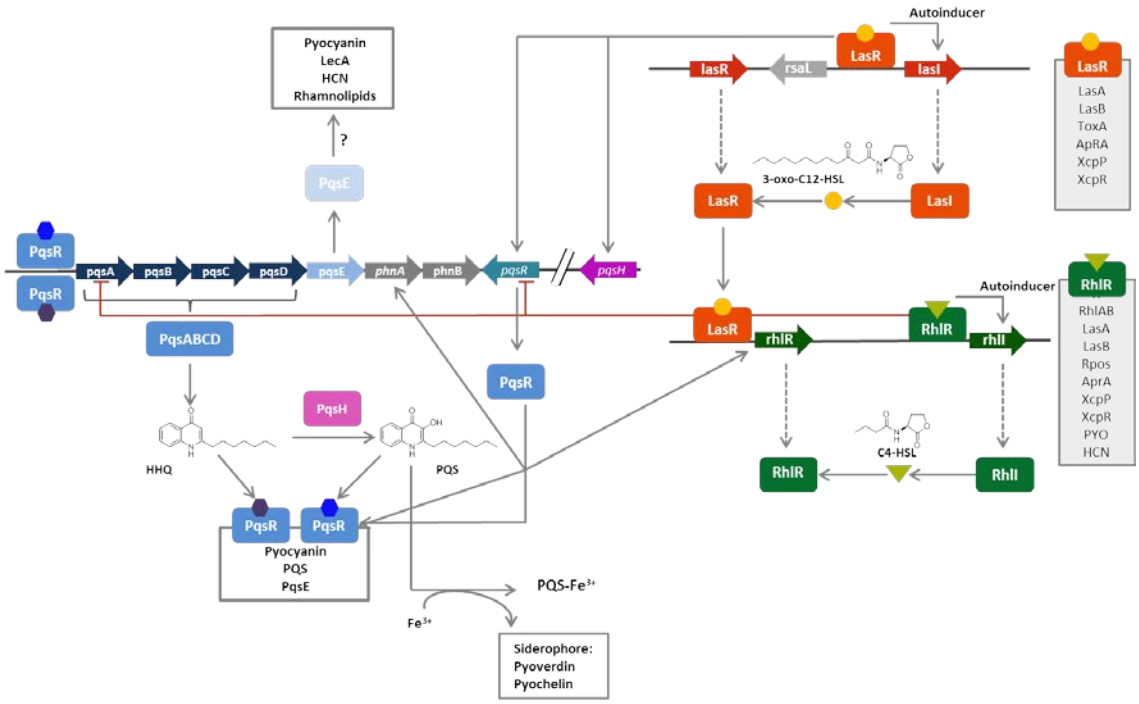

Abbildung 13. Biosynthese, Autoinduktion und Virulenzregulation der P. aeruginosa cell-to-cell-Signalübertragung. AHQ und AHL-abhängiges Quorum sensing sind eng miteinander verknüpft. LasR/3-oxo-C12-HSL reguliert die Expression von pqsH. pqsR ist positiv unter der Kontrolle von lasR. pqsA und pqsR werden durch RhlR unterdrückt. HHQ wird über pqsA produziert, was sich selbst über pqsR reguliert. PQS und HHQ induzieren PqsR- abhängig die Expression von pqsA. Für die Expression von Lectin und Pyocyanin ist PqsE notwendig. PQS aus der Zelle bildet einen PQS-Fe^{3+}-Komplex. Entfernung des Eisens aus der extrazellulären Umgebung durch PQS induziert die Genexpression für die Siderophorproduktion unabhängig von der cell-to-cell-Signalübertragung. Graue Pfeile repräsentieren die positive Regulation, rote Linien die negative Regulation (modifiziert von (nach Dubern und Diggle, 2008; Nadal Jimenez et al., 2012).

Das *pqsABCDE*-Operon beinhaltet ein fünftes Gen, *pqsE*, das für ein Protein mit Metallo-β-Lactamase-Region codiert. PqsE ist für die PQS-Synthese nicht notwendig und bisher ist über die Funktion von PqsE und seine Substrate wenig bekannt. Sicher ist jedoch, dass es sich um den Hauptvirulenzeffektor bei den 4-Alkylchinolonen handelt, welcher die Produktion von Pyocyanin, Lectin, den Rhamnolipiden und HCN kontrolliert und somit eine große Rolle in der akuten Infektion spielt (Gallagher *et al*., 2002; Diggle *et al*., 2003). Eine Vielzahl von strukturverwandten 4-Chinolonen werden durch die PqsABCD-Proteine produziert, die meisten jedoch in solch geringen Konzentrationen, dass sie keine Rolle in der Zellkommunikation spielen. Eine Ausnahme bildet HHQ, der Vorläufer von PQS, für den man gezeigt hat, dass dieser auch als Signalmolekül wirken kann (Lépine *et al.*, 2004). HHQ kann ins extrazelluläre Medium abgegeben und von den benachbarten Zellen aufgenommen werden, wo es entweder durch PqsH umgesetzt wird oder aber auch direkt an PqsR binden kann. In beiden Fällen wird die PQS-regulierte Genexpression in Gang gesetzt, entweder durch die Bindung von HHQ an den Rezeptor (PqsR) oder durch das entstandene PQS. Über diese HHQ-Aktivierung kommt es jedoch nicht zur Pyocyanin-Biosynthese (Xiao *et al.*, 2006).

1.2.3 Quorum Sensing als neues Target zur Überwindung von Resistenzmechanismen

1.2.3.1 Quorum Sensing Inhibitoren

Quorum Sensing Inhibitoren (*QSI*s), die ganz spezifisch mit dem bakteriellen Zellkommunikationssystem interferieren, sind eine alternative Behandlungsmöglichkeit zur herkömmlichen Antibiotikatherapie (Rasmussen und Givskov, 2006; Bjarnsholt und Givskov, 2007). Der selektive Eingriff in die Pathogenität, ohne das Bakterienwachstum zu beeinflussen, reduziert den natürlichen Selektionsdruck und somit eventuell auch die Entwicklung von Resistenzen. Die Autoinducer-Synthase (AI-Synthase, Abbildung 12) und der Signalrezeptor (R-Protein, Abbildung 12) bieten verschiedene Angriffspunkte im *QS*-System von *P. aeruginosa* für die Entwicklung von *QSIs*.

Eines der wenigen Antibiotika, das das klinische Resultat von CF Patienten, die mit P. *aeruginosa* infiziert sind, verbessert, ist Azithromycin. Skindersoe *et al.* haben gezeigt, dass sowohl Azithromycin, als auch Ceftazidim und Ciprofloxacin das *QS*-System von *P. aeruginosa* beeinflussen, indem sie möglicherweise die Membranpermeabilität verändern und dadurch den 3-oxo-C12-HSL-Fluss beeinflussen (Skindersoe *et al.*, 2008). Sie wirken jedoch bakteriostatisch und führen somit auch zu Selektionsdruck und Resistenzentwicklung (Tramper-Stranders *et al.*, 2007). Suga *et al*. identifizierten 2003 die ersten LasR-Antagonisten, unter denen 2-Amino-Cyclopentanon und 2-Amino-Cyclohexanon (Abbildung 14, **A** und **B**) die potentesten sind. Für Letzeres hat man zusätzlich einen geringen RhlR-Antagonismus nachgewiesen (Smith *et al.*, 2003b, 2003a; Suga und Smith, 2003). Strukturelle Ähnlichkeit mit dem natürlichen Substrat haben auch die von Geske *et al*. synthetisierten LasR-Antagonisten; PHL und Indol-AHL (Abbildung 14 **C** und **D**; (Geske *et al.*, 2005). Als besonders potent haben sich die zwei halogenierten Furanone, C30 und C56, herausgestellt (Abbildung 14 **E** und **F,** Hentzer *et al.*, 2003). Für C30 hat man über einen funktionalen Assay hinaus in Versuchen mit *P. aeruginosa* Biofilmen eine erhöhte Anfälligkeit bei der Behandlung mit Antibiotika und Detergenzien festgestellt (Manefield and Turner, 2002; Hentzer *et al*., 2003). In einem Ultra-Highthroughput-Screening hat man zwei weitere Verbindungen identifiziert, die generell das *QS*-System inhibieren und als Grundstrukturen für weitere Entwicklungen dienen können (Abbildung 14 **G** und **H**, Müh *et al.*, 2006). Ein weiterer Ansatz zu Identifizierung von *QSI*s, war das strukturbasierte, virtuelle Screening von Yang *et al*., bei dem drei bereits bekannte Arzneistoffe als potentielle LasR-Antagonisten gefunden wurden (Salicylsäure, Nifuroxazid, Chloroxazon; (Yang *et al.*, 2009).

Für die von Amara *et al*. gefundenen Acetamide (Abbildung 14 **I**; Amara *et al.*, 2009) hat man eine kovalente Bindung an Cys79 von LasR nachgewiesen und so auch den partiellen Agonismus dieser Verbindungen erklärt.

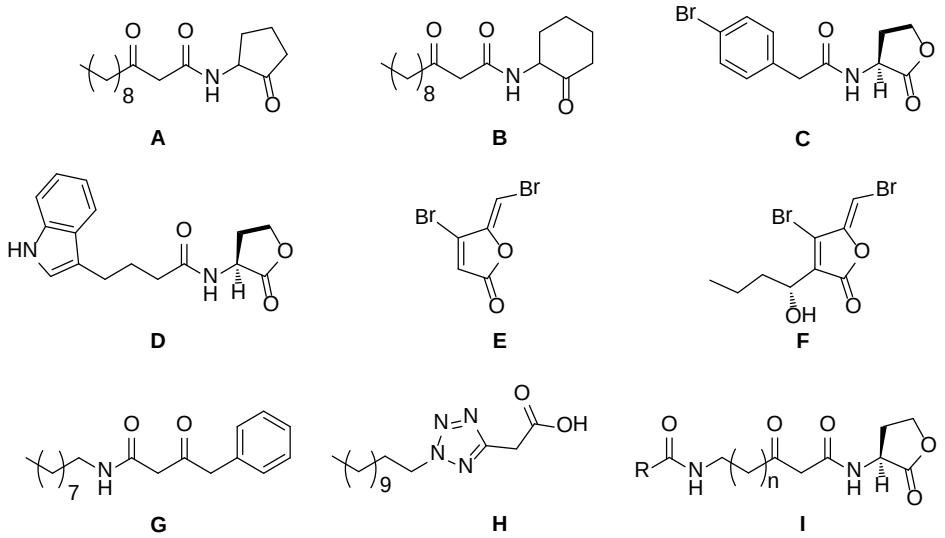

Abbildung 14: Quorum Sensing Inhibitoren (QSIs)

Verbindungen, die mit dem *pqs*-System interferieren, hat man bisher nur in einer Strukturklasse identifiziert. Die Substrat-Analoga von Lu *et al*. (Abbildung 15; Lu *et al*., 2011) antagonisieren den PqsR. Bei diesen hochpotenten Verbindungen handelt es sich um am Chinolongerüst substituierte HHQ-Analoga, die Aktivität im unteren nanomolaren Bereich zeigen (Abbildung 15 **A**, **B**, **C**). Da das *pqs* System eine entscheidende Rolle in der Pathogenität spielt, ist dieses System ein attraktives Target für die Entwicklung von *QSI*s, um die *pqs*-abhängige Genexpression zu stören. Auch die Tatsache, dass man PQS in großen Mengen im Sputum von CF-Patienten gefunden hat (Collier *et al.*, 2002), verdeutlicht die Annahme, dass die Blockade des *pqs QS* Systems die durch *P. aeruginosa* verursachten Lungeninfektionen in CF-Patienten zur besseren Behandlung führt. In diesem System gibt es über den Pqs-Rezeptor hinaus noch ein weiteres, vielversprechendes Target; die Hemmung von PqsD und somit die Hemmung des letzten Schritts der HHQ-Biosynthese. Beiden Strategien gemeinsam ist die Limitierung der Pathogenität von *P. aeruginosa*, ohne dabei die Viabilität der Bakterien zu beeinflussen und so den Selektionsdruck und auch die Resistenzmechanismusentwicklung zu unterbinden.

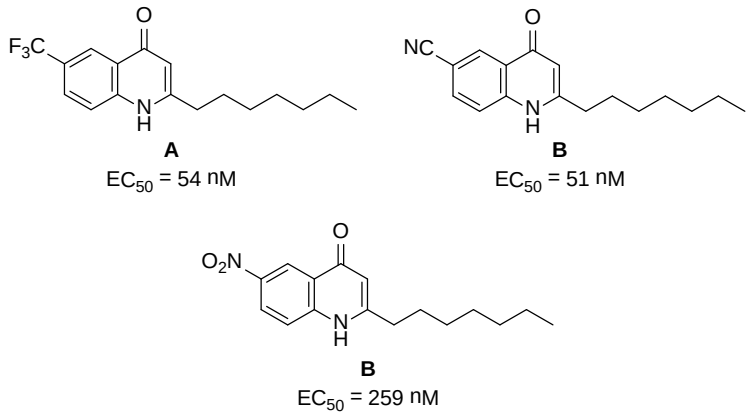

Abbildung 15: HHQ-Analoga

1.2.3.2 Tiermodelle.

Verschiedene Tiermodelle bestätigen den Einfluss der *QS*-regulierten Virulenzfaktoren auf die Pathogenität von *P. aeruginosa*. Das einfachste Infektionsmodel wurde in *C. elegans* (*Caernorhabditis elegans*) etabliert. Werden Nematoden mit *P. aeruginosa* gefüttert, so sterben sie innerhalb kürzester Zeit durch die von *P. aeruginosa* sekretierten Cyanide und Phenazine. Füttert man sie jedoch mit *P. aeruginosa*, die Mutationen im *QS*-System aufweisen, so wird das Sterben der Nematoden verhindert (Darby *et al.*, 1999; Mahajan-Miklos *et al.*, 1999; Rasmussen *et al.*, 2005). Für PqsD- und PqsR-Mutanten wurde im Nematodenmodell eine herabgesetzte Mortaliät gezeigt (Gallagher et al., 2002).

In einem Verbrennungsmodell an Mäusen hat man hat gezeigt, dass *QS* eine signifikante Rolle bei Wundinfektionen spielt (Rahme *et al.*, 1995). PqsR-Mutanten setzen in diesem Mausmodell die Mortalität herab (Cao et al., 2001; Déziel et al., 2005; Xiao et al., 2006).

In einem weiteren Mausmodell werden die initialen Stadien einer chronischen Lungeninfektion durch das Einsetzten von mit *P. aeruginosa* behafteten Beads in die Lunge von Mäusen und Ratten, modelliert (Pedersen *et al.*, 1990). Sind diese Mäuse mit *QS*-Mutanten infiziert, so ist ihre Immunantwort und auch die Akkumulation der Antikörper in der infizierten Lunge schneller (Wu *et al.*, 2001; Smith *et al.*, 2002; Bjarnsholt *et al.*, 2005).

1.3 Oberflächenplasmonresonanz-Spektroskopie

1.3.1 Allgemeines

Oberflächenplasmonresonanz (SPR) ist ein physikalischer Prozess, der eintritt wenn linear, polarisiertes Licht bei totaler interner Reflektion auf einen Metallfilm trifft (Biacore, 2005).

An der Grenzfläche zweier transparenter Medien mit verschiedenen Refraktionsindices (bspw. Wasser und Glas) wird einfallendes Licht von der Seite des höheren Brechungsindex teilweise reflektiert und teilweise gebrochen. Oberhalb eines kritischen Einfallswinkels (θ) wird kein Licht über die Grenzfläche hinweg gebrochen, sondern es kommt zur totalen internen Reflexion (TIR). Obwohl das einfallende Licht komplett reflektiert wird, kann jedoch ein elektromagnetisches Feld über eine kurze Distanz hinweg in das Medium des geringeren Brechungsindex penetrieren, man nennt dieses elektromagnetische Feld eine *evaneszente* Welle.

Wenn polarisiertes Licht nun durch ein Prisma hindurch auf einen Sensorchip, der mit einem dünnen Metallfilm beschichtet ist, fällt, wird bei einem spezifischen Einfallswinkel die Intensität des reflektierten Lichtes deutlich reduziert (Abbildung 15). Genau bei diesem Einfallswinkel sind die Photonen des einstrahlenden Lichtes in der Lage mit den freien Elektronen der Metallbeschichtung wechselzuwirken, sie werden absorbiert und ihre Energie wird auf die Elektronen transferiert, wodurch Oberflächenplasmone entstehen. Dadurch wird die Energie des reflektieren Lichtes reduziert (Abbildung 15). Dieses Phänomen bezeichnet man als Oberflächenplasmonresonanz und der spezifische Einfallswinkel nennt man Resonanzwinkel oder SPR-Winkel θ (Schaasfort and Tudos, 2008).

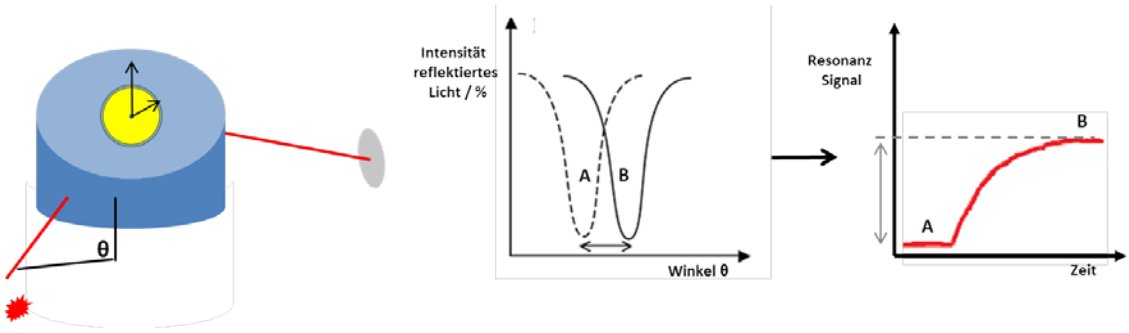

Abbildung 15: Schematisches Setup-Up der Oberflächenplasmonresonanz. Ein mit Gold beschichteter Sensorchip ist auf einem Prisma fixiert. Polarisiertes Licht scheint von der Lichtquelle (Stern) auf den Chip. Das reflektierte Licht wird vom Detektor gemessen (Disk). In einem bestimmten Einfallswinkel, werden Oberflächenplasmone angeregt, woraus ein Minimum in der Intensität des reflektierten Lichtes resultiert (A). Eine Änderung des Brechungsindex auf der Goldoberfläche verändert den Einfallswinkel von A nach B. Diese Änderung wird in einem Sensorgramm aufgezeichnet (Modifiziert aus Handbook of Surface Plasmon Resonance).

Dieser Winkel ist abhängig von der optischen Charakteristik des Systems, wie beispielsweise dem Brechungsindex der beiden Medien und auch des verwendeten Metalls auf der Oberfläche des

Sensorchips. Für die Beschichtung wird hauptsächlich Gold verwendet, da es inert gegenüber den meisten wässrigen Lösungen ist. Bei der Oberflächenplasmon Resonanz Spektroskopie ändert sich der Brechungsindex auf der Prismenseite nicht, in der unmittelbaren Nähe der Metalloberfläche ändert sich dieser jedoch durch Massenänderungen, beispielsweise durch adsorbierende Proteine. Infolgedessen ändern sich die Oberflächenplasmonresonanz Bedingungen und durch die damit einhergehende Verschiebung des SPR-Winkels θ kann man Aussagen über die Proteinadsorption auf der Oberfläche treffen. Die Änderung des SPR-Winkels wird in ein Response Signal umgewandelt (Abbildung 16), dessen Einheit die Response Unit (RU) ist, was einem Winkel von 10^{-4}° entspricht (Johnsson *et al.*, 1991). Die Korrelation zwischen Massenänderung und Resonanzsignal wurde experimentell bestimmt und lässt sich folgendermaßen darstellen (Stenberg *et al.*, 1991):

$$1\ RU = 1pg/mm^2$$

In einem typischen SPR-Experiment ist ein Bindungspartner (Ligand) an der Oberfläche des Sensorschips immobilisiert und der zweite Bindungspartner wird in Lösung injiziert (Abbildung 16). Die Sensorchips besitzen eine spezielle Oberfläche, die eine biologisch aktive Immobilisierung des Liganden erlaubt.

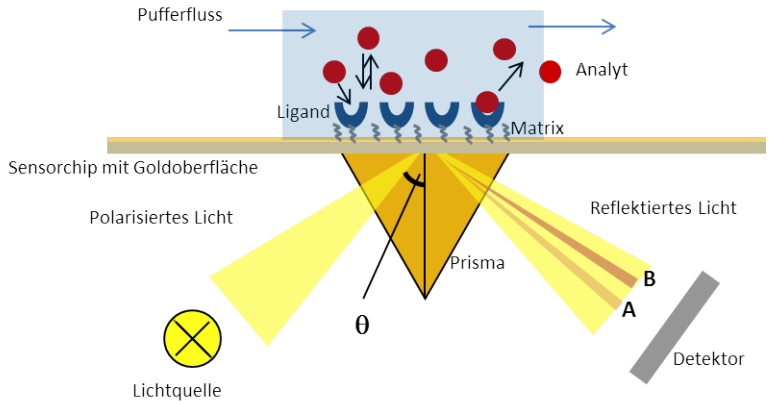

Abbildung 16: Schematischer Aufbau eines SPR-Experimentes. Ein Ligand ist in einem polymeren Hydrogel auf der Goldoberfläche immobilisiert. Detektion der Bindung eines Analyten in Lösung ist durch Oberflächenplasmonresonanz möglich.

Man kann sich diese Oberfläche als polymere Matrix aus thiolierten Carboxymethyl-Dextran-Ketten vorstellen, die über eine Adhäsionslinkerschicht direkt mit der Goldoberfläche verbunden sind. Die freien Carboxylgruppen dieser Ketten ermöglichen eine Immobilisierung in diese Matrix über eine Vielzahl von verschiedenen Methoden (siehe Kapitel 1.3.2 Immobilisierungsmethoden). Die Änderung des SPR-Winkels θ wird in Echtzeit gemessen und in Abhängigkeit der Zeit gezeigt. Ein solches Diagramm nennt man Sensorgramm, das die verschiedenen Stadien einer Bindung aufzeigt und die Evaluierung dieser erlaubt (Abbildung 17).

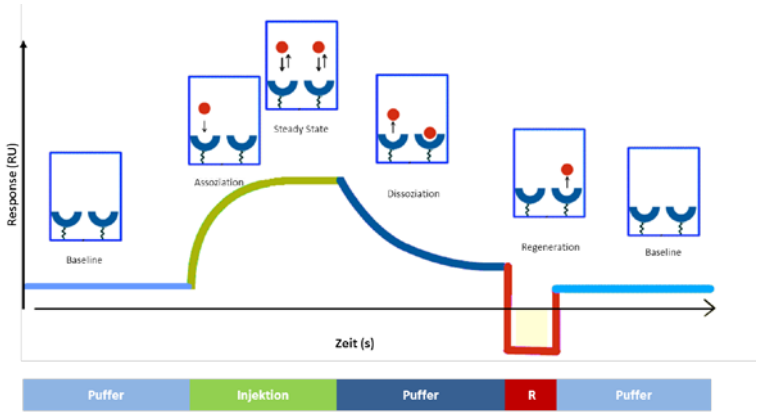

Abbildung 17: Schematisches Sensorgram als zeitliche Ansicht des Bindungsevents. R (Regeneration).

Fließt lediglich Puffer durch das System erreicht das Signal eine stabile Basislinie. Wird nun ein Analyt in Lösung injiziert, kann man die Bindung des Analyten an das immobilisierte Targetmolekül (Ligand) durch das ansteigende Signal beobachten - die *Assoziation*. Nach einer gewissen Zeit erreicht das Signal den *Steady-State*, was bedeutet, dass sich ein Equilibrium zwischen freiem Analyt und Target-Analyt-Komplex eingestellt hat. Sobald die Injektion stoppt, fließt nur noch Puffer über den Liganden und der Target-Analyt-Komplex löst sich auf – die *Dissoziation*. Ist die Interaktion zwischen Analyt und Ligand sehr stark, kann eine *Regeneration* des Komplexes notwendig sein um wieder eine stabile Basislinie zu erhalten. Anhand der Form der entstandenen Kurve können kinetische Parameter, wie die Assoziation- und Dissoziationsgeschwindigkeit k_a (k_{on}) und k_d (k_{off}) bestimmt werden. Die Dissoziationskonstante K_D kann entweder aus den kinetischen Geschwindigkeiten (k_a und k_d) berechnet werden oder aber konzentrationsabhängig über die Signale am Equilibrium.

1.3.2 Immobilisierung

Die Immobilisierung ist die Kupplung eines Liganden in die Matrix des Sensorchips. Dies ist der kritische Schritt wenn man biomolekulare Interaktionen messen möchte, weil hierzu gewährleistet sein muss, dass der Ligand nach der Immobilisierung aktiv und auch sterisch noch zugänglich ist. Es gibt verschiedene Immobilisierungsstrategien: die der adsorptiven, der kovalenten, der ionischen und der adaptiven Kupplung.

Die am häufigsten verwendeten Kupplungsstrategien sind die der kovalenten und der adaptiven Immobilisierung (Abbildung 18). Stellvertretend für diese beiden Methoden, werden die Aminkupplung sowie die Immobilisierung über Biotin näher erläutert.

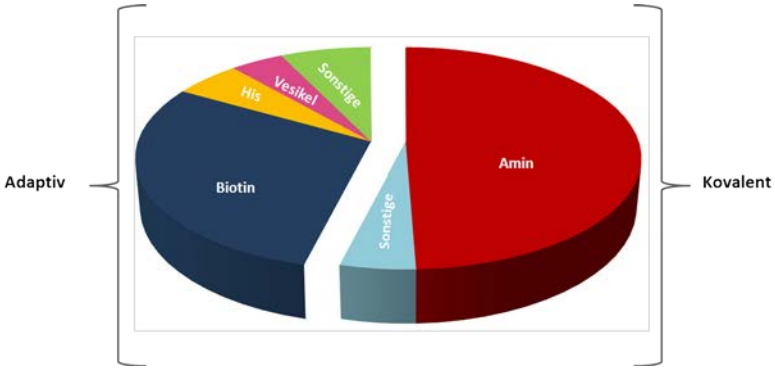

Abbildung 18: Hauptsächlich verwendete Immobilisationsmethoden. Kovalent sonstige: Thiol- oder Aldehydkupplung; Adaptiv Sonstige: Antikörper, GST (Glutation-S-transferase), Protein A (modifiziert von (Rich und Myszka, 2005))

1.3.2.1 Aminkupplung

Bei der Aminkupplung (Abbildung 19) werden die freien Carboxylgruppen der Matrix durch Carbodiimid aktiviert und dann in Aktivester umgewandelt. Diese chemische Modifikation erfolgt meistens durch die Zugabe von einem EDC/NHS-Gemisch (EDC = N-ethyl-N´-(dimethylaminopropyl)carbodiimid; NHS = 2-(N-hydroxysuccinimid). Die Aktivester formen mit Lysinen oder freien NH_2-Gruppen des Liganden eine Amidbindung. Bei dieser Immobilisierungsmethode spielt der pH-Wert eine große Rolle, denn für die Kupplung von Aktivester und Aminogruppe (Abbildung 19) muss der Ligand möglichst nah an die Chip-Oberfläche gebracht werden. Dies erreicht man, in dem man den pH-Wert des Immobilisierungspuffers unterhalb des isoelektrischen Punktes (pI) des Liganden einstellt, wodurch eine *Präkonzentrierung* erreicht wird. Der positiv geladene Ligand kann so über elektrostatische Wechselwirkungen mit den negativ geladenen Carboxylgruppen der Matrix interagieren (Johnsson *et al.*, 1991). Da die Reaktion zwischen Aktivester und Aminogruppen jedoch nur mit ungeladenen Aminogruppen funktioniert, sollte der pH-Wert nicht zu niedrig gewählt werden (Johnsson *et al.*, 1991). Die unreagierten Aktivester werden anschließend durch die Zugabe von Ethanolaminhydrochlorid (1M, pH 8.5) inaktiviert (2-Hydroxyethanamide entstehen), zusätzlich erfolgt durch die hohe Salzkonzentration dieser Lösung gleichzeitig das Abschwächen der elektrostatischen Wechselwirkung, so dass auch unreagierte Proteine mit dem Pufferfluss abtransportiert werden können (Johnsson *et al.*, 1991). Große Vorteile dieser Immobilisierungsmethode sind die Effizienz dieser Reaktion, die schnelle Durchführbarkeit und ihre universelle Einsetzbarkeit, da die meisten Proteine freie Aminogruppen bzw. Lysine an ihrer Oberfläche tragen. Andererseits können auch ungerichtete Immobilisierungen und Crosslinking auftreten, wodurch die Aktivität des Liganden deutlich verringert sein kann (Schaasfort und Tudos, 2008).

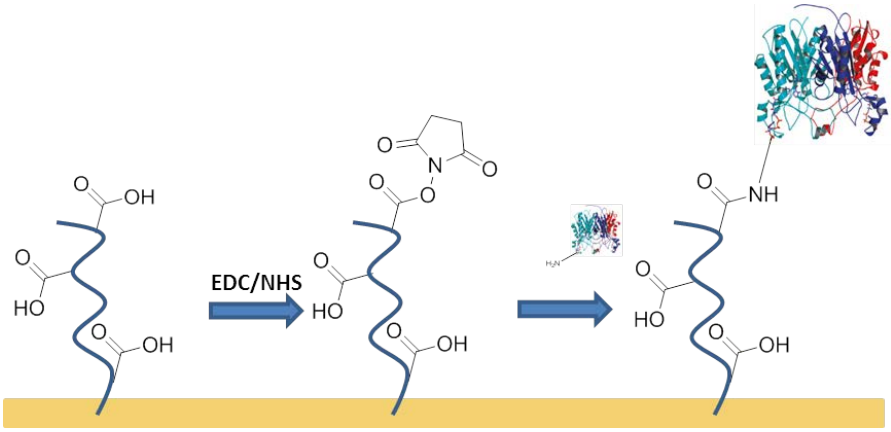

Abbildung 19: Kovalente Immobilisierung über Aminkupplung

1.3.2.2 Biotinkupplung

Die Biotin-Kupplung ist eine indirekte Immobilisierungsmethode, bei der die Liganden über die sehr starke Affinität von Biotin zu Streptavidin (10^{-15} M, (Haun und Wasi, 1990) auf dem Sensorchip verankert werden. Es gibt kommerziell erhältliche Sensorchips, die eine Streptavidin behandelte Oberfläche besitzen, auf der man den biotinylierten Liganden direkt immobilisieren kann (Abbildung 20). Eine Biotinylierung kann direkt mit der Expression des gewünschten Proteins erreicht werden, indem ein Expressionsvektor verwendet wird, der gleichzeitig auch für eine Biotinligase codiert (Beckett *et al.*, 1999). Oder es erfolgt eine synthetische Biotinylierung nach der Expression durch Sulfo-NHS-aktiviertes Biotin, das mit primären Aminen eine Amidbindung eingeht. Die synthetische Biotinylierung kann bei geringen Temperaturen und in Puffer durchgeführt werden (Papalia und Myszka, 2010), was sehr schonend für die Proteine ist. Durch das Einführen eines Spacers in verschiedenen Längen hat man die Möglichkeit den Liganden möglichst flexibel auf der Oberfläche zu immobilisieren.

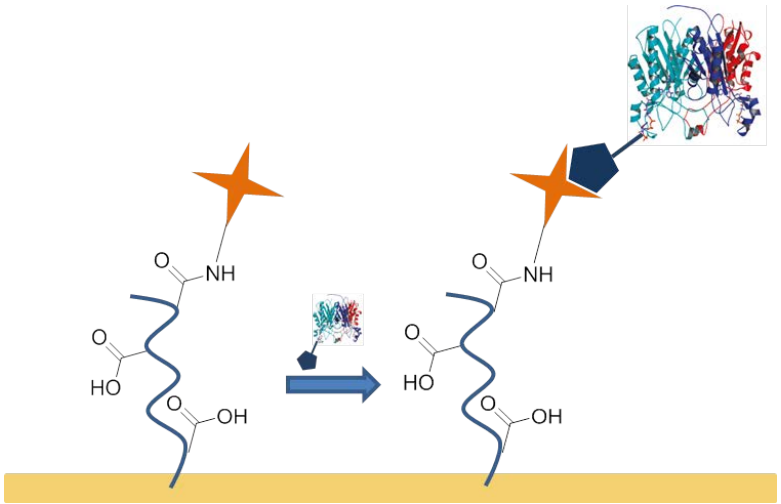

Abbildung 20: Adaptive Immobilisierung über Streptavidin-Biotin Kupplung (Stern: Streptavidin kovalent am Sensorchip immobilisiert, Fünfring: Biotin über Linker mit dem Liganden verbunden

Ein wichtiger Punkt bei der synthetischen Methode ist jedoch die Minimalbiotinylierung (Papalia und Myszka, 2010). So kann Crosslinking komplett vermieden werden, was den großen Vorteil dieser Methode ausmacht.

1.3.3 SPR–Spektroskopie im Drug Discovery Prozess

Oberflächenplasmonresonanz Biosensoren sind mittlerweile ein Standardtool in der pharmazeutischen und biotechnologischen Forschung. Der große Vorteil ergibt sich aus der label-freien Echtzeit-Messung, bei der Interaktionen von molekularen Systemen aller Art aufgezeichnet werden können. Angefangen bei der Targetidentifizierung und Hitfindung über Leadoptimierung bis hin zu klinischen Studien und der Produktion von Arzneistoffen findet man beschriebene SPR-Biosensorassays für die jeweilige Anwendung (Abbildung 21, (Myszka und Rich, 2000).

Eine Methode zur Targetidentifizierung ist die von Graffinity Pharmaceuticals entwickelte Methode (www.graffinity.com). Es werden gleichzeitig eine Vielzahl an Fragmenten auf einem Biosensor kovalent gebunden. Statt eines Screenings mit unzähligen Verbindungen gegen ein immobilisiertes Target, können unbekannte Proteine gegen bekannte Verbindungen getestet und so neue Targets identifiziert werden. Ist ein neues Target identifiziert, können spezifische Assays entwickelt und weitere Screenings durchgeführt werden. Hierbei ist der hohe Durchsatz von großem Vorteil. In einem Primärscreening werden Bindungspartner gefunden und dann in einem sekundären Screening validiert und näher charakterisiert. So kann man „falsch-positive“ Hits identifizieren und direkt am Anfang der Arzneistoffentwicklung eliminieren (Karlsson *et al.*, 2000). Im weiteren Prozess der Leadfindung können kinetische und thermodynamische Parameter bestimmt und erste SAR-Studien mittels dieser Daten durchgeführt werden. Makren *et al.* beschreiben hierzu einen Assay, bei dem die „Binder“ aufgrund ihrer Assoziations- und Dissoziationsraten gerankt und Lead-SAR-Studien durchgeführt werden *(Markgren et al., 2002)*.

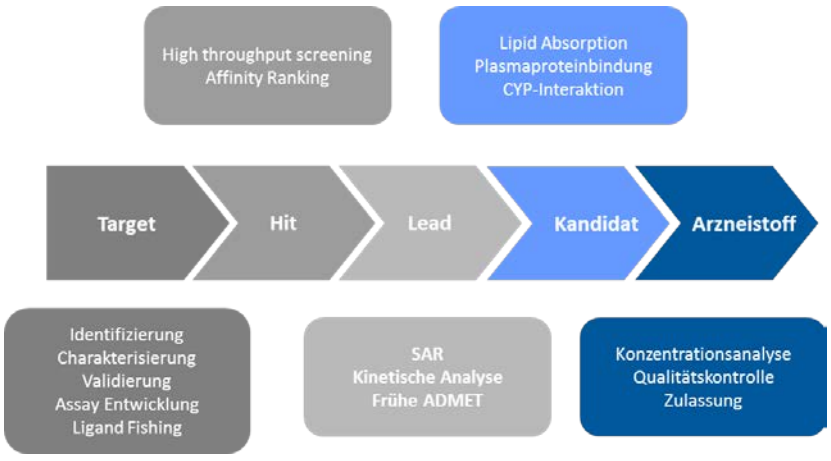

Abbildung 21: Übersicht der Anwendungsmöglichkeiten der SPR-Spektroskopie im Drug Discovery Prozess (modifiziert von Cooper 2002).

Das Erstellen pharmakokinetischer Profile ist ein wichtiges Kriterium im Prozess der Arzneistoffentwicklung. Viele Substanzen binden reversibel an humanes Serumalbumin (HSA), α_1-saures-Glykoprotein (AGP) und andere Serumkomponenten, wie Immunglobuline. Eine starke Proteinbindung reduziert die Konzentration an freiem Arzneistoff und dadurch auch dessen physiologische Aktivität. Deshalb ist die Plasmaproteinbindung ein wichtiger Faktor für die Balance zwischen physiologischer Aktivität, Langzeiteffizienz und potentieller Nebenwirkungen (Frostell-Karlsson *et al.*, 2000). Studien zur Plasmaproteinbindung wurden von verschiedenen Gruppen mit bekannten Arzneistoffen an HSA und auch an AGP durchgeführt und die bereits bekannten Daten für Plasmaproteinbindung durch einen Biosensorassay bestätigt (Frostell-Karlsson *et al.*, 2000; Day und Myszka, 2003; Cimitan *et al.*, 2005; Gustafsson *et al.*, 2011). Ein weiterer wichtiger ADME-Faktor ist die passive und aktive Arzneistoffaufnahme über den Gastrointestinaltrakt oder auch die Blut-Hirn-Schranke. Zur Bestimmung der Permeabilität können verschiedene Lipidschichten auf einem Biosensor immobilisiert und die Substanzen hinsichtlich ihrer Permeabilität evaluiert werden (Danelian *et al.*, 2000; Baird *et al.*, 2002; Ahmad *et al.*, 2003; Abdiche und Myszka, 2004).

Am Ende der Pipeline der Arzneistoffentwicklung stehen die Qualitätskontrolle und die Konzentrationsanalyse. Auch in diesem Bereich finden Biosensorstudien ihre Anwendung (Swanson und Mytych, 2011), insbesondere in der Analyse von serologischen Proben hinsichtlich der Antikörper-Titer (Ritter *et al.*, 2001; Hale *et al.*, 2010).

SPR-Spektroskopie bietet den besonderen Vorteil, dass es sich um ein label-freies System handelt, geringe Mengen Protein benötigt werden und eine enorme Flexibilität, was das Assaydesign betrifft, vorhanden ist (Cooper, 2002). Im Allgemeinen unterscheiden sich die Daten, die mittels SPR Biosensoren generiert werden nicht von denen der Experimente in Lösung, dies bestätigen zahlreiche Studien (Day *et al.*, 2002; Myszka D. G. *et al.*, 2003; Navratilova *et al.*, 2007; Heinrich *et al.*, 2010). SPR-Daten sollten jedoch mit anderen Methoden generierte Daten mit komplementären Methoden (ITC, NMR, ELISA, Fluoreszenz-Assays) validiert und nicht als reine Alternative angesehen werden. Unter Berücksichtigung dieser Argumente können SPR-Biosensorexperimente eine wichtige Rolle spielen und auch zu einer deutlichen Kostenerleichterung im Drug Discovery Prozess führen.

2 Ziel der Arbeit

Aufgrund der hohen Resistenzentwicklung gegenüber herkömmlichen Arzneistoffen zur Behandlung von Krebs- und Infektionserkrankungen ist es dringend notwendig neue Ansätze zur Überwindung dieser Mechanismen zu erforschen. Die vorliegende Arbeit befasst sich mit der Entwicklung von neuen Substanzen zur Überwindung dieser Resistenzen und gliedert sich in zwei Teile.

E2 ist in die Entstehung und Progression von estrogen-abhängigen Erkrankungen wie Brustkrebs und Endometriose involviert. Den letzten Schritt der E2-Biosynthese katalysiert die Steroiddehydrogenase 17β-HSD1, deren mRNA in den erkrankten Geweben überexprimiert vorliegt (Gunnarsson *et al.*, 2005; Smuc *et al.*, 2007). Deshalb ist die Entwicklung von 17β-HSD1-Inhibitoren ein vielversprechender Ansatz um die intrazellulären E2-Konzentrationen zu reduzieren und estrogenabhängige Erkrankungen zu therapieren. Das schwach aktive E1 bleibt im gesamten Organismus erhalten und die bekannten Nebenwirkungen herkömmlicher Therapien, die auf einem vollkommenen Estrogenentzug beruhen, bleiben aus.
Im Arbeitskreis gibt es bereits eine Reihe von hochpotenten nicht-steroidalen 17β-HSD1 Hemmstoffen, die sich für den Eintritt in die präklinische Phase eignen. Für einige Verbindungen wurde bereits ein *in vitro Proof of Concept* erbracht (Kruchten et al., 2009b). Ein nächster Schritt in Richtung präklinischer Phase ist das *in vivo Proof of Concept* in einem geeigneten Tiermodell. Es soll zunächst eine geeignete Spezies identifiziert werden, in der nach Möglichkeit bereits ein Krankheitsmodell etabliert ist. Danach soll ein biochemischer Assay mit 17β-HSD1 der geeigneten Spezies etabliert werden, um die ausgewählten Spitzenverbindungen jeder Substanzklasse zu untersuchen. Zusätzlich sollen hier auch Aussagen über die Selektivität gegenüber 17β-HSD2 getroffen werden können. Da unterschiedliche Spezies Variationen in der Aminosäuresequenz der 17β-HSD1 aufweisen, ist es durchaus möglich, dass die evaluierten Verbindungen veränderte Aktivitäten an 17β-HSD1 der jeweiligen Spezies zeigen. In diesem Fall soll eine speziesspezifische Optimierung der ausgewählten Hemmstoffe erfolgen, um einen geeigneten Kandidaten für das *in vivo Proof of Concept* zu identifizieren.

P. aeruginosa ist ein adaptives opportunistisches Pathogen, das für eine Vielzahl nosokomialer Infektionen und auch für die chronische Lungeninfektion der meisten CF Patienten verantwortlich ist. Diese Bakterien koordinieren sich über ein zelldichte-abhängiges *pqs QS*- System, das charakteristisch für *P. aeruginosa* ist. Es wirkt über die beiden Signalmoleküle PQS und dessen Vorläufer HHQ, die mit PqsR interagieren und so Transkription von Virulenzfaktoren und die Biofilmformation kontrollieren. Eine vielversprechende Strategie zur Überwindung von Antibiotikaresistenzen insbesondere in *P. aeruginosa* ist es deren Pathogenität zu schwächen ohne ihre Viabiliät zu beeinflussen. Geeignete Angriffspunkte im *pqs*-System von *P. aeruginosa* sind hierfür die Hemmung von PqsD und auch die Antagonisierung des Rezeptors PqsR. Die vielseitige Anwendbarkeit der

Oberflächenplasmonresonanz-Spektroskopie im Drug Discovery Prozess (Kapitel 1.3.3) soll anhand der beiden Targetproteine PqsD und PqsR demonstriert werden.

PqsD gehört zu den Bi-Substrat-Enzymen und katalysiert die Bildung von HHQ aus Anthraniloyl-CoA und β-Ketodecansäure. Sowohl die katalytischen als auch die kinetischen Parameter für PqsD sind unbekannt. Da diese Faktoren eine Rolle für die Hemmstoffentwicklung spielen, sollen sie im Folgenden genauer untersucht werden. Es soll ein SPR-Assay entwickelt werden, der es ermöglicht Untersuchungen zum katalytischen und kinetischen Mechanismus von PqsD anzustellen und für spätere Substanztests anwendbar sein.

Für PqsR wurden im Arbeitskreis bereits hochpotente Antagonisten gefunden. Diese sind vom natürlichen Substrat HHQ abgeleitet und zeigen dadurch jedoch ungenügende physikochemische Eigenschaften, was sie für einen Einsatz als Arzneistoffe ungeeignet macht. Aufgabe war es deshalb neue Leitstrukturen für die Entwicklung von PqsR-Antagonisten zu identifizieren. Hierzu sollte ein SPR-Assay aufgebaut werden, der es ermöglicht Verbindungen im High-Throughput zu analysieren. Anschließend sollte eine geeignete Methode entwickelt werden, die es erlaubt, die untersuchten Verbindungen möglichst effizient zu klassifizieren und dadurch die Lead-Findung zu erleichtern.

3 Ergebnisse

3.1 Structural Basis for Species Specific Inhibition of 17β-Hydroxysteroid Dehydrogenase Type 1 (17β-HSD1): Computational Study and Biological Validation

Tobias Klein[#], **Claudia Henn**[#], Matthias Negri, Martin Frotscher

[#] These authors contributed equalliy to this work

PLoS ONE **2011**, *6*, e22990.

Publication I

Abstract: 17β-Hydroxysteroid dehydrogenase type 1 (17β-HSD1) catalyzes the reduction of estrone to estradiol, which is the most potent estrogen in humans. Inhibition of 17β-HSD1 and thereby reducing the intracellular estradiol concentration is thus a promising approach for the treatment of estrogen dependent diseases. In the past, several steroidal and non-steroidal inhibitors of 17β-HSD1 have been described but so far there is no cocrystal structure of the latter in complex with 17β-HSD1. However, a distinct knowledge of active site topologies and protein-ligand interactions is a prerequisite for structure-based drug design and optimization. An elegant strategy to enhance this knowledge is to compare inhibition values obtained for one compound toward ortholog proteins from various species, which are highly conserved in sequence and differ only in few residues. In this study the inhibitory potencies of selected members of different non-steroidal inhibitor classes toward marmoset 17β-HSD1 were determined and the data were compared with the values obtained for the human enzyme. A species specific inhibition profile was observed in the class of the (hydroxyphenyl)naphthols. Using a combination of computational methods, including homology modelling, molecular docking, MD simulation, and binding energy calculation, a reasonable model of the three-dimensional structure of marmoset 17β-HSD1 was developed and inhibition data were rationalized on the structural basis. In marmoset 17β-HSD1, residues 190 to 196 form a small α-helix, which induces conformational changes compared to the human enzyme. The docking poses suggest these conformational changes as determinants for species specificity and energy decomposition analysis highlighted the outstanding role of Asn152 as interaction partner for inhibitor binding. In summary, this strategy of comparing the biological activities of inhibitors toward highly conserved ortholog proteins might be an alternative to laborious x-ray or site-directed mutagenesis experiments

in certain cases. Additionally, it facilitates inhibitor design and optimization by offering new information on protein-ligand interactions.

Introduction

Human 17β-hydroxysteroid dehydrogenase type 1 (17β-HSD1) catalyzes the NAD(P)H dependent reduction of the weak estrogen estrone (E1) to the biologically most active estrogen estradiol (E2; Fig. 1) [1].

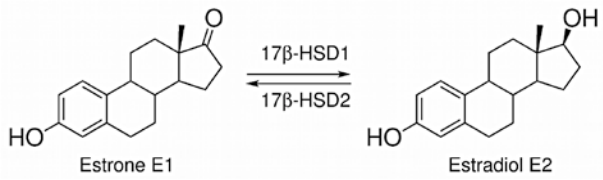

Figure 1. *Interconversion of estrone (E1) and estradiol (E2).*

This reaction, which represents the last step in E2 biosynthesis, takes place in target cells where the estrogens exert their effects via the estrogen receptors α and β. Besides their physiological effects, estrogens are involved in the development and the progression of estrogen dependent diseases (EDDs) like breast cancer, endometriosis and endometrial hyperplasia [2-4]. In the past few years, aromatase inhibitors have been intensively investigated for the treatment of EDDs [5-7] but they lead to unwanted side effects due to their strong reduction of estrogen levels in the whole body. Therefore reducing local E2 levels by inhibition of 17β-HSD1 is a promising therapeutic approach for the treatment of EDDs. An analogous intracrine concept has already been proved successful for the treatment of androgen dependent diseases such as benign prostatic hyperplasia and alopecia by using 5α-reductase inhibitors [8-11]. 17β-HSD2 catalyzes the reverse reaction (oxidation of E2 to E1; Fig. 1) and inhibition of this enzyme must be avoided for the therapeutic concept to work. However, specific inhibition of 17β-HSD2 in bone cells may provide a novel approach to prevent osteoporosis [12].

17β-HSD1 is a cytosolic enzyme that belongs to the superfamiliy of short-chain dehydrogenases/reductases (SDRs) [13]. It consists of 327 amino acid residues (34.9 kDa) and the active form exists as homodimer [14]. 17β-HSD1 comprises a Rossmann fold, associated with cofactor binding, and a steroid-binding cleft [15]. The latter is described as a hydrophobic tunnel with polar residues at each end: His221/Glu282 on the C-terminal side, and Ser142/Tyr155, belonging to the catalytic tetrad, which is present in the majority of characterized SDRs [16], on the other side [17]. To date 22 crystal structures of 17β-HSD1 are available as apoform, binary or ternary complexes [18-20]. All crystal structures show an overall identical tertiary structure, while major differences have been identified only for the highly flexible βFαG'-loop. It is not resolved in ten crystal structures, while the remaining twelve showed high b-factor values for this area, which is an additional hint for the flexibility of the βFαG'-loop. In some crystal structures a short α-helix was observed in the loop region but its occurrence seems not to be dependent on the presence of steroidal ligands, cofactor or

inhibitor. However, the position and length of the α-helix changes: in the apoform (PDB entry 1bhs) the helix is limited to the beginning of the loop while in presence of steroidal ligands and/or cofactor it is shifted to the end (PDB entries 1dht, 1equ, and 1iol). Further, dependent on the presence of cofactor and ligands, the βFαG'-loop can occupy three possible orientations: an opened, semi-opened, and closed enzyme conformation [21].

Several steroidal and non-steroidal inhibitors of 17β-HSD1 have been described [18,22-37], but only for the former cocrystal structures exist. While several computational studies have been performed in order to elucidate the interactions of non-steroidal inhibitors with 17β-HSD1 [26,27,33,37,38], structural data confirming the results are still missing.

However, a distinct knowledge of active site topologies and protein-ligand interactions is a prerequisite for structure-based drug design and optimization. To further increase this knowledge, inhibition values obtained for one compound toward proteins, differing only in few residues might be advantageous. For this purpose, wild type proteins and their mutants carrying a set of point mutations can be used. As alternative, proteins from various species, which are highly conserved in sequence and differ only in few residues, might be considered.

This latter approach was applied in the present study employing human and marmoset monkey (*callithrix jacchus*) 17β-HSD1. Selected human 17β-HSD1 inhibitors, representative of our structurally diverse inhibitor classes, were tested toward the marmoset 17β-HSD1. The resulting inhibitory potencies were compared with those obtained for the human enzyme and remarkable differences were only observed in the class of the (hydroxyphenyl)naphthols. In order to rationalize the species-specific inhibition profiles at the structural basis, a homology model of the marmoset enzyme was built using a human 17β-HSD1 x-ray structure as template. Further, the docking poses of selected compounds into both the human crystal structure and the modelled marmoset 17β-HSD1 were considered. Notably, the marmoset homology model and the docking poses of the inhibitors presented herein were validated by their ability to explain inhibition data. Subsequently, the complexes of two representative inhibitors, docked into the marmoset model and the human crystal structure, respectively, were subjected to MD simulations to investigate their conformational equilibrium. In addition, binding energy calculations as well as energy decomposition analysis were performed, with the aim to investigate the influence of the marmoset amino acid variations on the inhibitory potencies. The current work provides new insights into the marmoset 17β-HSD1 active site topology, reveals probable inhibitor binding modes in human and marmoset 17β-HSD1, and identifies amino acids responsible for species specificity in 17β-HSD1 inhibition.

Results

Comparison of 17β-HSD type 1 and type 2 sequences

To identify regions that are conserved through several species, the sequences of rodent, cynomolgus, marmoset and human 17β-HSDs 1 were aligned (Fig. 2A). The N-terminal region (residues 1-190), which constitutes the common Rossmann fold as well as the catalytic tetrad, is highly conserved for

the analyzed species. Remarkable differences were observed in the F/G segment (residues 191-230), which is lining the steroid-binding site, and the C-terminal region (residues 231-285). Sequence alignment of human and marmoset 17β-HSD1 revealed that they share 80 % sequence identity and 85 % similarity (Fig. 2A). Focusing on the steroid-binding site (residues 94 to 196 and 214 to 284), the identity increases to 87 %, with five major amino acid variations observed in the marmoset enzyme: A191P, E194Q, S222N, V225I and E282N. In contrast, comparing cynomolgus and human 17β-HSD1, which show even 91% identity, only one of the aforementioned amino acid variations can be found (E282H; Fig. 2A). With the exception of marmoset 17β-HSD1, Ala191 and Glu194 are conserved through the analyzed species (Fig. 2A) indicating the significance of the observed variations between human and marmoset. 17β-HSDs 1 of mouse and rat are 83 % similar to the human enzyme in the first 287 amino acids. In both analyzed rodent enzymes His221, which is involved in steroid binding [17], is mutated into a glycine (H221G). Moreover, several other amino acids of the substrate-binding site are replaced by more bulky residues (L96F, N152H, M193Y/H, S222Y). Interestingly, rat and mouse 17β-HSDs 1 are significantly less sensitive to inhibition by steroidal inhibitors compared to the human ortholog [39] and different classes of non-steroidal potent human 17β-HSD1 inhibitors turned out to be only weak inhibitors of E2 formation in rat liver preparations [40]. This might be partially explained by the absence of His221 as interaction partner as well as by the reduced volume of the active site (M193Y/H, S222Y).

Sequence identities between human 17β-HSD2 and 17β-HSD2 of the selected species range from 61 % (mouse) to 93 % (cynomolgus) while the F/G segment and the C-terminal region show the most pronounced variability (Fig. 2B). The comparison of 17β-HSD1 with the correspondent type 2 enzymes of the analyzed species revealed, that the type 2 enzymes have about 80 additional N-terminal residues relative to the type 1 enzymes. Sequence comparison showed that they share a very low overall sequence identity (≤ 25 %) with major differences in the F/G segment and the C-terminal domain, which constitute the active site. However, some amino acid motifs, characteristic for SDR enzymes [18], are highly conserved: the T-G-xxx-G-x-G motif, the Y-xxx-K sequence and the N-A-G motif (Fig. 2B). For marmoset 17β-HSD2 only a fragment of the primary sequence is available, which is 143 amino acids in length and constitutes the Rossman fold whereas the F/G segment and the C-terminal region are missing (Fig. 2B). This segment is 29 % identical to marmoset 17β-HSD1.

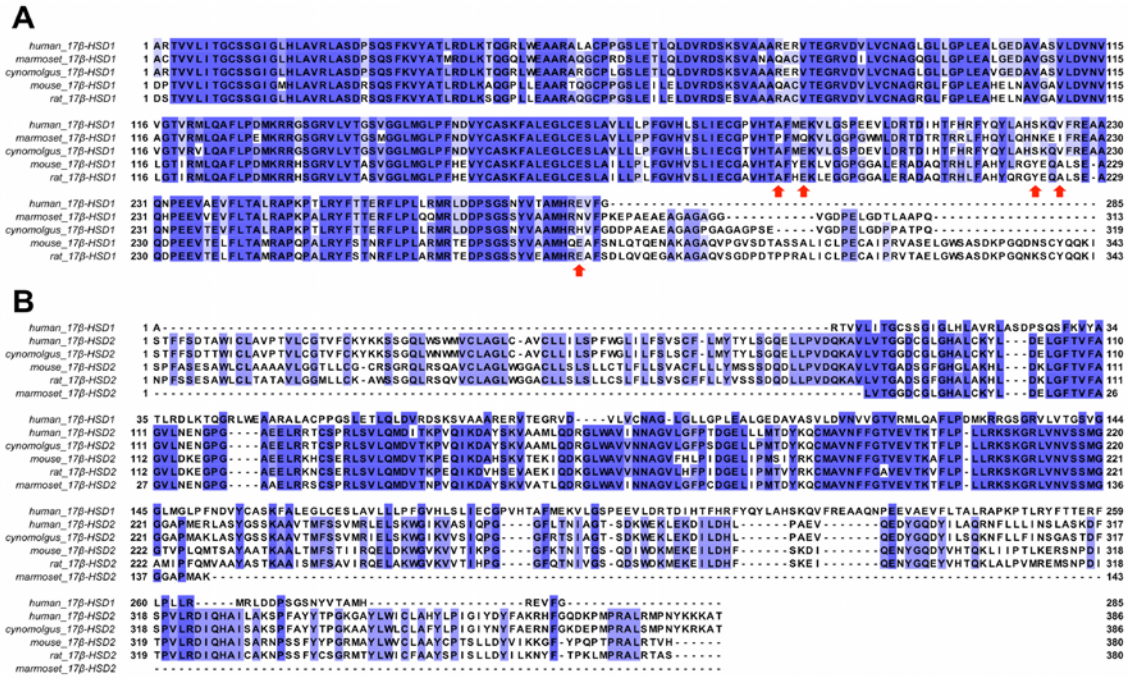

Figure 2. *Multiple sequence alignment of 17β-HSD type 1 and type 2 from selected species. Species and subtype are indicated on the left, followed by residue numbering. Residues are colored by percentage identity and red arrows indicate major amino acid variations in marmoset compared to the other species. A) Multiple sequence alignment of 17β-HSD1 from selected species. B) Multiple sequence alignment of human 17β-HSD1 with 17β-HSD2 from selected species.*

As human and marmoset 17β-HSD1 differ in few residues of the active site, comparison of the inhibitory potencies of selected inhibitors, observed toward both enzymes, is suitable to further increase the knowledge of active site topologies and protein-ligand interactions. In particular, the amino acid variations in the flexible βFαG'-loop, which is suggested to play a crucial role in ligand binding, will be used to elucidate the function of the loop in more detail.

Inhibition of marmoset 17β-HSD1 and 17β-HSD2

Marmoset placental tissue was used as enzyme source and the proteins were partially purified following a described procedure [41]. Tritiated E1 was incubated with 17β-HSD1, cofactor and inhibitor. The separation of substrate and product was performed by HPLC. In an assay similar to the 17β-HSD1 test, marmoset placental microsomes containing 17β-HSD2 were incubated with tritiated E2 in the presence of NAD^+ and inhibitor. Labelled product was quantified after HPLC separation.

The inhibition values of compounds **1**-**20** (Fig. 3) are shown in Table 1. The bis(hydroxyphenyl) substituted arenes **1**-**11** showed comparable or even higher inhibitory potencies toward marmoset 17β-HSD1 compared to the human enzyme. For example, compound **8**, which is a potent inhibitor of human 17β-HSD1 (IC_{50} = 151 nM), showed a stronger inhibitory potency toward marmoset 17β-HSD1 (IC_{50} = 4 nM). Comparable inhibition data for human and marmoset 17β-HSD1 were also measured for the bicyclic substituted hydroxyphenylmethanones **12** and **13**. This indicates that the

binding of the two aforementioned inhibitor classes is reinforced or at least not affected by the amino acid variations in marmoset 17β-HSD1. In the class of the (hydroxyphenyl)naphthols, the human 17β-HSD1 inhibitor **14** (IC_{50} = 116 nM) showed also a good inhibitory potency toward marmoset 17β-HSD1 (IC_{50} > 50 nM). The introduction of space filling substituents in position 1 of the naphthol core of **14** is beneficial for the inhibition of the human enzyme (**16**, IC_{50} = 26 nM), but for marmoset 17β-HSD1 no increase in inhibitory potency was observed (**16**, IC_{50} > 50 nM) compared to the unsubstituted **14**. Interestingly, further enlargement of the substituents in 1-position of **14** led to highly active human 17β-HSD1 inhibitors (**19**, IC_{50} = 15 nM) while a reduced potency toward marmoset 17β-HSD1 (**19**, IC_{50} > 50 nM) was found.

The inhibitory potencies of compounds **1**-**20** toward marmoset 17β-HSD2 were also determined to prove whether marmoset monkey is a suitable species for *in vivo* evaluation of 17β-HSD1 inhibitors (Table 1). Remarkably, lower selectivity of compounds toward non-target marmoset 17β-HSD2 was observed, when comparing to human 17β-HSD2.

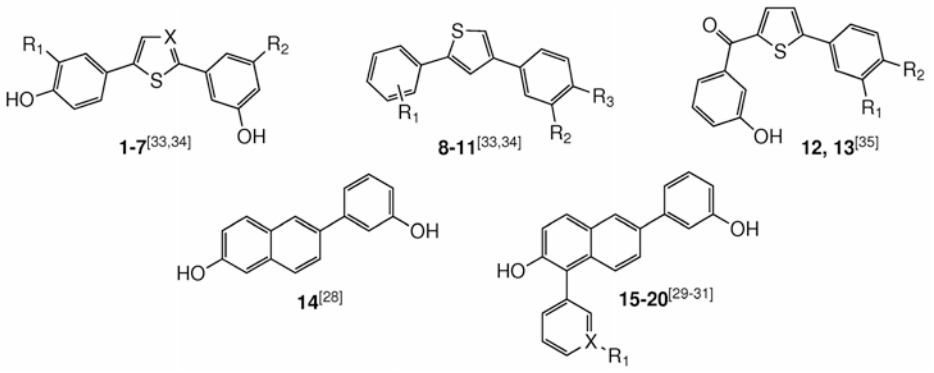

Figure 3. *Chemical structures of selected human 17β-HSD1 inhibitors. Representative structures of our three inhibitor classes: the bis(hydroxyphenyl) substituted arenes (**1**-**11**), the bicyclic substituted hydroxyphenylmethanones (**12**, **13**) and the (hydroxyphenyl)naphthols (**14**-**20**).*

Table 1. Inhibition of human and marmoset 17β-HSD1 and 17β-HSD2 by compounds **1**-**20**.

					Human IC_{50} [nM]		Marmoset IC_{50} [nM][c]	
compd	X	R_1	R_2	R_3	17β-HSD1[a]	17β-HSD2[b]	17β-HSD1[d]	17β-HSD2[e]
1	CH	F	H		8	940	< 5[f]	> 50
2	N	H	H		50	4004	102	> 50
3	CH	H	H		69	1953	31	> 50
4	CH	CH_3	H		46	1971	< 50	> 50
5	N	CH_3	H		143	2023	< 50	> 50
6	CH	H	F		42	463	< 5[f]	85
7	CH	F	F		17	218	< 5[f]	43
8		4-OH	OH	H	151	1690	4[f]	> 50
9		3-OH	H	OH	77	1271	2[f]	> 50
10		3-OH	CH_3	OH	64	869	3[f]	> 50
11		3-OH	F	OH	64	510	< 50	72
12		H	OH		33	478	< 50	43
13		OC_2H_5			78	502	< 50	59
14					116	5641	> 50	> 50
15	C	OH			36	959	32	> 50
16	N				26	1157	> 50	> 50
17	C	H			20	540	52	> 50
18	C	NH_2			53	1757	n.i.	> 50
19	C	$NHSO_2CH_3$			15	403	> 50	> 50
20	C	$NHCOCH_3$			83	1239	> 50	n.i.

[a]Human placental, cytosolic fraction, substrate E1, 500 nM, cofactor NADH, 500µM; [b]Human placental, microsomal fraction, substrate E2, 500 nM, cofactor NAD^+, 1500µM; [c]Logit transformed values calculated from % inhibition at 50 nM inhibitor concentration, for inhibition values < 30% or > 70%, a trend is given; [d]Marmoset monkey placental, cytosolic fraction, substrate E1, 500 nM, cofactor NADH, 500µM; [e]Marmoset monkey placental, microsomal fraction, substrate E2, 500 nM, cofactor NAD^+, 1500µM; [f]Inhibitor concentration: 5nM; n.i.: no inhibition; Human IC_{50} values were retrieved from literature (corresponding references are indicated with the structural formulas in Fig. 3).

Homology modelling and MD simulations of marmoset 17β-HSD1

In order to obtain a more precise picture of the three-dimensional structure of the marmoset 17β-HSD1, a homology model was generated. A set of 100 models was built with MODELLER 9v7 [42] using the ternary complex E1-NADPH-human 17β-HSD1 as template. This complex was obtained by docking E1 into human 17β-HSD1 employing the Protein Data Bank (PDB) entry 1fdt with conformation B for residues 187-200 (in the following determined as 1fdtB). This 3D structure was chosen as it represents a ternary complex with $NADP^+$ and E2 in the closed enzyme conformation, as the βFαG'-loop is resolved, and as this protein structure was already successfully used in previous docking studies with the investigated compound classes [30,36]. The best model was chosen according to internal DOPE-score [43] and PROCHECK [44] tests. Notably, it presents a short α-helix (residues 190-196) in the region between the βF-sheet (residues 178-186) and the αG'-helix (residues 209-227), with Pro191 in the first turn of the helix (N1 position; Fig. 4), thus differing from the secondary structure of the template.

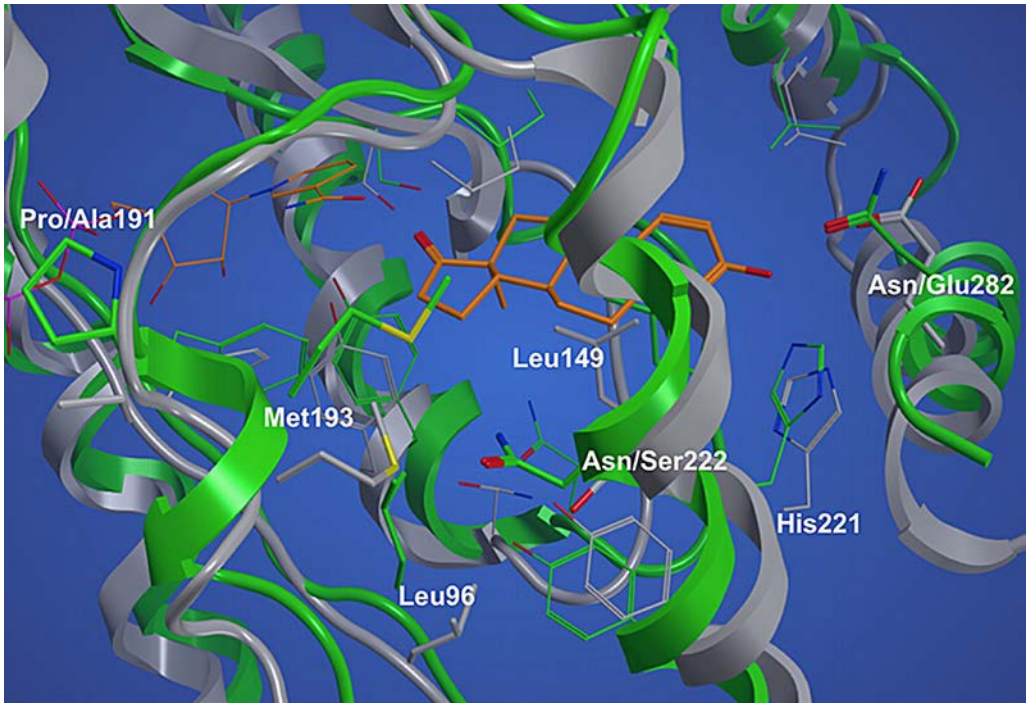

Figure 4. *Three-dimensional structure superimposition of marmoset and human 17β-HSD1. Low energy structure of marmoset 17β-HSD1 (green) in complex with E1 and NADPH (orange) from MD simulation superimposed onto the x-ray structure of human 17β-HSD1 (grey, PDB code: 1fdtB). When two residues are indicated, the first corresponds to marmoset 17β-HSD1 and the second to human 17β-HSD1*

The selected model was further refined both as holoenzyme with NADPH and as ternary complex with NADPH and E1 by MD simulations. The trajectories of the two MD simulations were stable with a α-carbon root-mean-square deviation (RMSD) to the starting structure below 3.0 Å (Fig. 5). No major structural differences were observed when comparing the simulated holoenzyme and the ternary complex. Therefore, the following results, based on analysis of the ternary complex, also apply to the holoform.

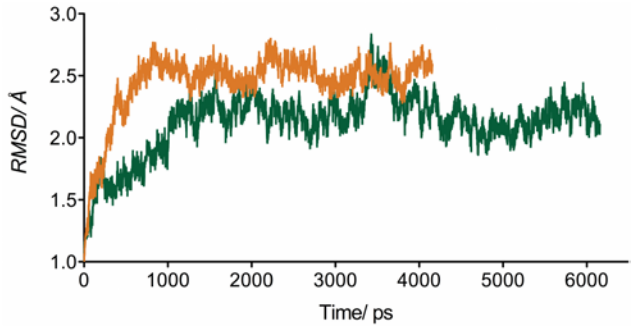

Figure 5. *RMSD analysis of the MD simulations of the marmoset 17β-HSD1 model. Time-dependent C_α-RMSD for all residues of the secondary (orange) and ternary (green) complex.*

After an initial inward rotation in the MD simulation, the short α-helix (residues 190-196) remained stable for the last 5 ns of the MD simulation, with an average backbone RMSD to the final conformation of 1.03 Å. Remarkably, a similar behaviour cannot be expected for the region between the βF-sheet and the αG'-helix in the human enzyme. The differences in the crystal structures suggest a high flexibility for the βFαG'-loop: it is not resolved in ten crystal structures and the remaining twelve show high b-factor values for this area. Some crystal structures present a short α-helix in the loop region whose position and length varies dependent on the presence of steroidal ligands, cofactor or inhibitor. In the apoform (PDB entry 1bhs) the helix is limited to the beginning of the loop, whereas in presence of steroidal ligands and/or cofactor it is shifted to the end (PDB entries 1dht, 1equ, and 1iol). Further, in the human enzyme, the βFαG'-loop axis occupies different orientations dependent on the presence of cofactor and ligands. In the marmoset however, both the holoform and the ternary complex show a helix starting already at the beginning of the βFαG'-loop with its axis in only one conformation.

The presence of the newly formed α-helix (residues 190-196) induced a different orientation of the side chain of Met193. Compared to the template structure, Met193 protrudes deeper into the substrate-binding site and stabilizes E1 by hydrophobic interactions (Fig. 4). Furthermore, during MD simulation a kink in the loop between the βD-sheet and the αE-helix was observed. Thereby the side chain of Leu96 was brought closer to E1 allowing Van der Waals contacts (Fig. 4). Summarizing, in the final part of the MD simulation E1 was stabilized by both lipophilic interactions and hydrogen bonds: Leu96, Leu149, Met193, and Phe259 constrained the steroidal scaffold while Ser142/Tyr155 and His221/Asn282 interacted with the carbonyl oxygen in 17-position and the 3 OH-group, respectively. The latter residue took over the H-bond acceptor abilities of Glu282, which is involved in forming an H-bond with the 3 OH-group of E1 in the human enzyme.

Employing CASTp [45], the active site volumes of human and marmoset 17β-HSD1 were calculated. The above-described conformational changes of Leu96 and Met193 as well as the S222N and V225I mutations resulted in a reduced volume of the marmoset 17β-HSD1 active site (478 $Å^3$) compared to that of the human ortholog (627 $Å^3$).

The stereochemical quality of the holoenzyme and the ternary complex models obtained from MD simulations was checked with PROCHECK [44]. The majority of the residues of the investigated structures were found to occupy the most favoured regions of the Ramachandran plots, while the other residues occupied the additional allowed regions. In detail, in the ternary complex 78.1 % of the residues were placed in the most favoured region, 20.2 % in the additional allowed region, 1.2 % in the generously allowed region, and only 0.4 % in the disallowed region (for the holoform: 81.8 %, 17.4 %, 0.8 % and 0 %).

Molecular docking

As the potent inhibitors of human 17β-HSD1 **12** and **19** are structurally diverse and exhibit different potencies toward marmoset 17β-HSD1 they were chosen as representatives to rationalize the observed species-specific inhibition profiles. Employing AutoDock 4 [46], both compounds were docked into the active sites of marmoset and human 17β-HSD1 using the equilibrated, ternary complex after 5537 ps and the x-ray structure 1fdtB (see experimental part), respectively. The inhibitor poses used for further investigation were selected considering binding energy and statistical representativity (cluster population; Table S1) and are shown in Figure 6.

In the human enzyme both inhibitors are placed in the substrate-binding site and they occupy an apolar subpocket consisting of the following amino acids: Gly94, Leu95, Leu96, Asn152, Tyr155, and Phe192 (Fig. 6A). While the carbonyl group of compound 12 mimics the D-ring keto function of E1, forming H-bonds with Ser142 and Tyr155, its para-OH group resembles the 3-OH of E1, which interacts with His221 via an H-bond. The meta-hydroxyphenyl moiety is projecting into the subpocket, where it forms an additional H-bond with Asn152 and is stabilized by π-π-interactions with Tyr155 and Phe192.

The (hydroxyphenyl)naphthol-core of compound 19 occupies the substrate-binding site and is stabilized by three H-bonds: the 2-OH group interacts with Ser142 as well as with Tyr155 and the OH group in meta position of the phenyl ring in 6-position interacts with His221. In this case, the sulfonamide substituted phenyl ring in 1-position of the naphthol core protrudes into the subpocket, where it is stabilized by H-bonds with Asn152 and with the -NH- of the backbone of Leu95 (Fig. 6A).

Table S1. Cluster analysis of molecular docking results.

Comp	No of clusters	Cluster	No of conformations	Best binding energy (ΔG_{bind})
Human x-ray structure (1fdtB)				
12	3	1	2	-4.77
		2	45	-4.65
		3	3	-4.58
19	5	**1**	24	-5.94
		2	1	-5.44
		3	19	-4.98
		4	1	-4.92
		5	5	-4.87
Marmoset monkey homology model				
12	3	**1**	21	-5.60
		2	27	-5.41
		3	1	-5.0
		4	1	-4.59
19	5	1	7	-5.79
		2	33	-5.74
		3	3	-5.11
		4	5	-4.41
		5	2	-4.10

All energies are expressed in kcal mol^{-1}. The lowest energy conformation of each cluster, which is marked in bold was used for further investigation.

Also in the marmoset enzyme both compounds occupy the substrate-binding site, but only 12 protrudes into the apolar subpocket (Fig. 6B). Due to the altered side chain conformation of Leu96 in the marmoset enzyme, compound 12 is slightly displaced toward the C-terminus (Fig. 6C). Regarding the interaction pattern, only minor changes were observed: the carbonyl group forms only an H-bond with Ser142 but for the para-OH group a second H-bond with Asn282 was observed (Fig. 6C).

Interestingly, compound 19 resulted in a completely different binding mode when docked into the homology model of marmoset 17β-HSD1 with respect to its position in the human crystal structure 1fdtB (Fig. 6D). The OH-group in meta position of the phenyl ring makes an H-bond with the backbone carbonyl oxygen of Cys185 and the 2-OH function forms H-bonds with His221 and Asn282 in a bifurcated fashion. The sulfonamide substituted phenyl ring is located in the C-terminal gate and might be stabilized by π-π-interactions with Phe259 and an H-bond with the backbone -NH- of Leu262.

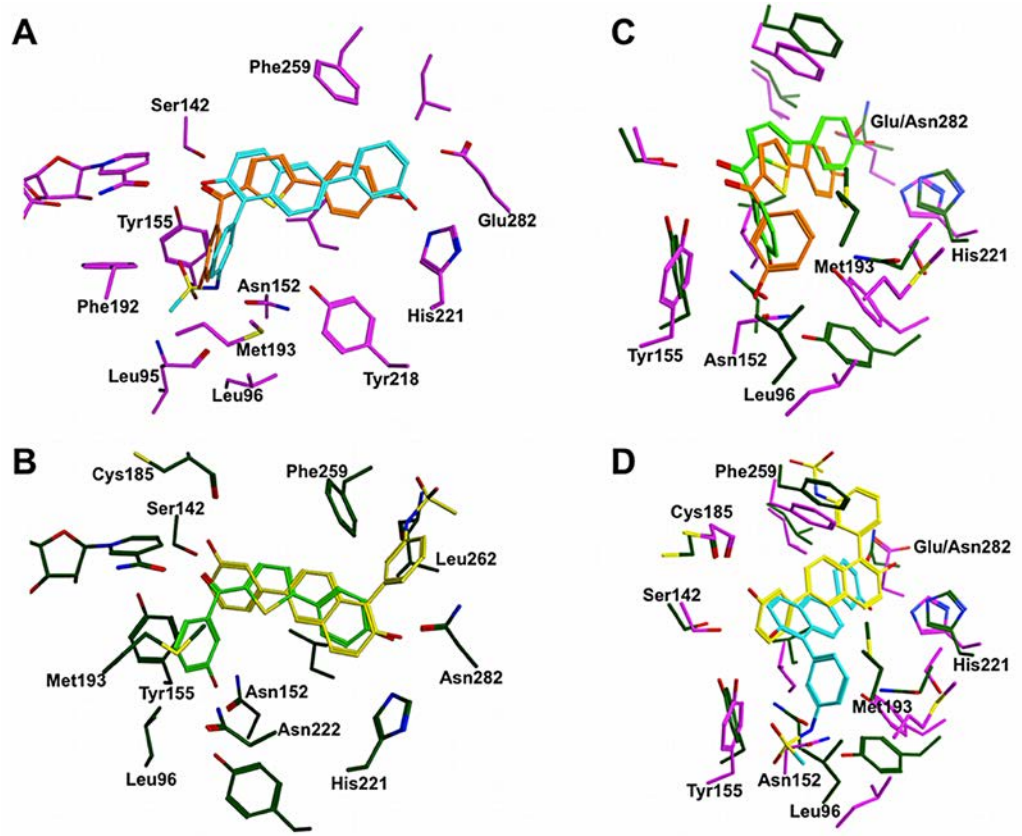

Figure 6. *Hypothetical binding modes of compounds* ***12*** *and* ***19.*** ***A)*** *Superimposition of lowest energy structures of* ***12*** *(orange) and* ***19*** *(cyan) obtained by docking into the x-ray structure of human 17β-HSD1 (magenta, PDB code: 1fdtB).* ***B)*** *Superimposition of lowest energy structures of* ***12*** *(light green) and* ***19*** *(yellow) obtained by docking into the marmoset 17β-HSD1 homology model (green).* ***C)*** *Superimposition of lowest energy structures of* ***12*** *(light green) docked into the marmoset 17β-HSD1 model (green) and of* ***12*** *(orange) docked into the x-ray structure of human 17β-HSD1 (magenta, PDB code: 1fdtB).* ***D)*** *Superimposition of lowest energy structures of* ***19*** *(yellow) docked into the marmoset 17β-HSD1 model (green) and of* ***19*** *(cyan) docked into the x-ray structure of human 17β-HSD1 (magenta, PDB code: 1fdtB).*

Validation of the docking complexes by means of MD simulations and free energy calculations (MM/PBSA)

With the aim to validate the docking results and to unravel possible induced-fit mechanisms, different MD simulations were run in explicit aqueous solution. Distance restraints were applied to inhibitors only in the first ns of the MD simulations with the aim of maintaining their proper orientation. For the rest of the MD simulation no restraints were used and the whole complexes were left free to move. This was done in order to avoid trapping the inhibitor in an unstable conformation, which could bias the results. The RMSD values of the heavy atoms of the inhibitors and of the Cα-atoms of the enzymes were analyzed as a function of time to assess the degree of conformational drift, as shown in Figure 7.

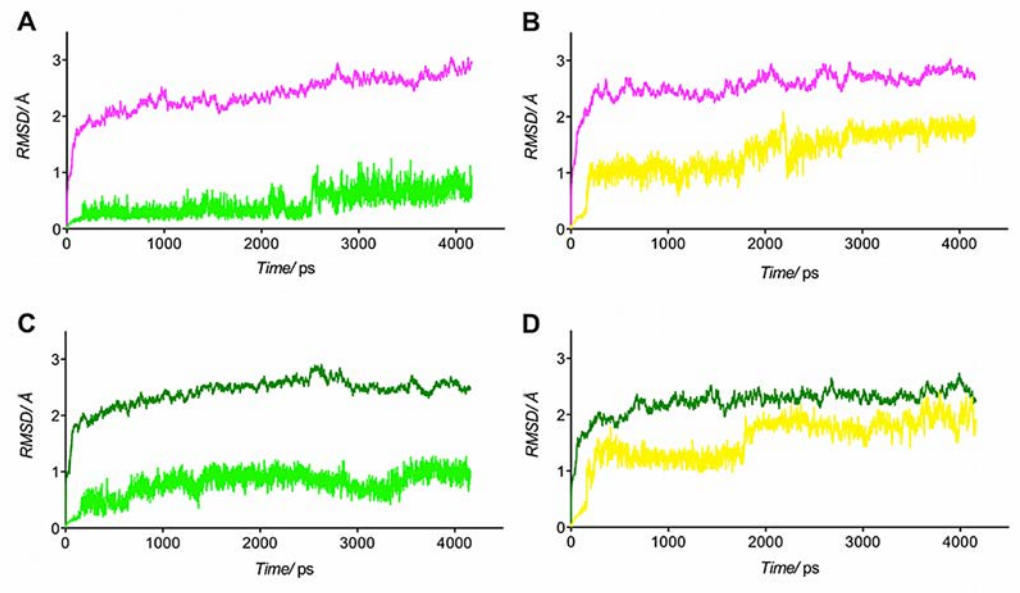

Figure 7. *Time dependent RMSD analysis of Cα of 17β-HSD1 and of the heavy atoms in the ligands.* ***A)*** *Cα-RMSD of human 17β-HSD1 is colored in magenta and the heavy atoms RMSD of compound* ***12*** *in light green.* ***B)*** *Cα-RMSD of human 17β-HSD1 is colored in magenta and the heavy atoms RMSD of compound* ***19*** *in yellow.* ***C)*** *Cα-RMSD of marmoset 17β-HSD1 is colored in green and the heavy atoms RMSD of compound* ***12*** *in light green.* ***D)*** *Cα-RMSD of marmoset 17β-HSD1 is colored green and the heavy atoms RMSD of compound* ***19*** *in yellow.*

In the simulation of **12** bound to human 17β-HSD1 the Cα-RMSD of the protein as well as the RMSD of the heavy atoms of **12** showed a stable plateau (~ 2.2 Å) from 1.0 to 2.5 ns (Fig. 7A). After 2.5 ns the Cα-RMSD of the protein increased and a minor fluctuation of the heavy atom RMSD of **12** was observed. The latter finding could be related to a slight shift of the inhibitor toward the C-terminal end of the enzyme. Notably, the hydrogen bonds between **12** and 17β-HSD1, which were observed in the initial structure, were conserved during the 4 ns simulation suggesting that both protein and **12** fluctuations do not impact the inhibitor binding.

Both human 17β-HSD1 and compound **19** were stable in the simulation of their complex (Fig 7B). During the simulation (after 1.5 ns) the hydrogen bond of the *meta*-OH group with His221 is replaced by an H-bond with Glu282. However, after 2.1 ns, this hydrogen bond is interrupted for 0.2 ns allowing the hydroxyphenyl ring to rotate freely around the axis of the bond to the naphthol core thereby inducing a minor fluctuation of the heavy atom RMSD of **19**. After this short interruption the H-bond interaction with Glu282 is re-established. On the other side, the hydrogen bonds between the 2-OH group and Ser142/Tyr155 as well as between the sulfonamide moiety and Asn152/Leu95 endured constant.

During the MD simulation of **12** in complex with marmoset 17β-HSD1, the *meta*-hydroxyphenyl moiety of **12** moved further out of the subpocket. This was reflected by the minor fluctuation of the RMSD of the heavy atoms of **12** after 1.4 ns (Fig. 7C). While this motion caused the break of the H-

bond with Asn152, it also placed the *meta*-OH group in an appropriate distance to Asn222, thus allowing a new H-bond formation.

The analysis of the MD simulation of the marmoset 17β-HSD1-**19** complex revealed an overall stable Cα-RMSD of the protein. However, after 1.8 ns, a ~ 0.5 Å fluctuation of the heavy atom RMSD of **19** was observed (Fig. 7D) corresponding to the rotation around the axis of the bond between the hydroxyphenyl ring and the naphthol core. Thereby the H-bond with the backbone amino group of Leu262 was lost.

Furthermore, for each of the four MD trajectories absolute free energy (ΔG) and relative binding affinity (ΔG_{bind}) were calculated applying MM/PBSA methods and NMODE analysis (Table 2).

Table 2. Free energy calculations for the MD simulations of the four docking complexes.

comp	ELEC	VDW mean	GAS mean	PBSOL mean	PBTOT (ΔG_{bind}) mean (±SE)	TSTOT mean (±SE)	ΔG mean (±SE)
Human x-ray structure (1fdtB)							
12	-15.4	-40.4	-55.7	35.1	-20.6±3.8	-15.9±6.6	-4.7±7.6
19	-36.7	-50.1	-86.8	64.2	-22.6±5.0	-15.3±6.8	-7.3±8.4
Marmoset monkey homology model							
12	-24.5	-38.1	-61.3	40.0	-21.3±4.9	-15.4±5.3	-5.8±7.2
19	-42.2	-34.4	-76.5	50.3	-26.3±4.4	-23.1±4.3	-3.2±6.1

ΔG and ΔGbind values correspond to the longest stable plateau for each MD. (ΔG) free binding energy; (PBTOT) (ΔGbind) relative binding energy; (ELEC) electrostatic contribution in gas phase; (VDW) Van der Waals contribution in gas phase; (GAS) free energy in vacuum; (PBSOL) solvation energy; (TSTOT) (TΔS) entropic contribution; (mean) mean value; (SE) standard error of the mean; all energies expressed in kcal mol^{-1}.

This was done for the following stable sectors: 1000 to 2500 ps for **12** in complex with human 17β-HSD1 (Fig. 7A), 2300 to 4160 ps for **19** in complex with human 17β-HSD1 (Fig. 7B), 1500 to 4160 ps for **12** in complex with marmoset 17β-HSD1 (Fig. 7C) and 1800 to 4160 ps for **19** in complex with marmoset 17β-HSD1 (Fig 7D). All four complexes showed favourable ΔG values, ranging from -7.3 kcal mol^{-1} to -3.2 kcal mol^{-1}. The free energies observed for compound **12** in complex with human (ΔG = -4.7 kcal mol^{-1}) and marmoset 17β-HSD1 (ΔG = -5.8 kcal mol^{-1}) are in the same range. This is in accordance with the inhibitory activities of **12**, which are comparable for both species (see Table 1). Regarding compound **19**, the complex with human 17β-HSD1 shows a more favourable free energy (ΔG = -7.3 kcal mol^{-1}) than the one with marmoset 17β-HSD1 (ΔG = -3.2 kcal mol^{-1}). This is mainly due to poor entropic contributions in the latter case. Remarkably, this finding is in concert with the experimentally determined inhibition data: compound **19** is a highly potent human 17β-HSD1 inhibitor (IC_{50} = 15nM) with reduced activity toward the marmoset enzyme (IC_{50} > 50 nM).

Analysis of the binding interactions using MM/GBSA methods

Focusing on the specific interactions, which mediate the binding of **12** and **19** to human and marmoset 17β-HSD1, we have analyzed the interaction energies of both inhibitors with the residues of the binding sites, employing a pairwise per-residue energy decomposition analysis.

Inspection of the interaction energies with human 17β-HSD1 (Table 3) showed that the hydrogen bonds of **12** (-4.1 kcal mol^{-1}) and **19** (-5.7 kcal mol^{-1}) with Asn152 contributed most to the interaction energies. Besides Asn152, further residues of the subpocket (Gly94, Leu95, Leu96) interact with both inhibitors revealing energies from -0.3 kcal mol^{-1} to -1.8 kcal mol^{-1}. The energies of the hydrogen bonds between **12** and the catalytic residues Ser142 as well as Tyr155 are -1.3 kcal mol^{-1} and -1.5 kcal mol^{-1}, respectively. In case of compound **19** the interaction energies are -1.3 kcal mol^{-1} for the H-bond with Ser142 and -1.3 kcal mol^{-1} for the H-bond with Tyr155. Further binding site residues, which significantly contribute to the binding of compounds **12** and **19** (Leu149, Pro187, Phe192, Met193, Val225, and Phe259) show interaction energies from -0.9 kcal mol^{-1} to -2.2 kcal mol^{-1}. Regarding the polar amino acids at the C-terminal end of the binding site, His221 takes primarily part in the binding of **12** (-1.8 kcal mol^{-1} for **12** vs. -0.2 kcal mol^{-1} for **19**) while Glu282 is mainly involved in binding compound **19** (-0.1 kcal mol^{-1} for **12** vs. -4.3 kcal mol^{-1} for **19**).

Table 3. Interaction energies between the inhibitors **12** and **19** and the proximal (4.0 Å) binding site residues of human 17β-HSD1.

comp	Gly94	Leu95	Leu96	Ser142	Leu149	Asn152	Tyr155	Cys185	Gly186	Pro187
12	-1.8	-0.3	-1.2	-1.3	-2.2	-4.1	-1.5	-0.2	-0.4	-1.3
19	-0.7	-0.7	-1.7	-1.3	-2.0	-5.7	-2.6	-0.3	-0.8	-2.0
comp	**Phe192**	**Met193**	**Tyr218**	**His221**	**Ser222**	**Val225**	**Arg258**	**Phe259**	**Leu262**	**Glu282**
12	-1.2	-1.0	-0.7	-1.8	-0.8	-1.7	-0.1	-1.2	-0.4	-0.1
19	-1.8	-1.9	-0.1	-0.2	-0.4	-1.9	-0.5	-0.9	-0.3	-4.3

All energies are expressed in kcal mol^{-1}.

The interaction energies of **12** and **19** with marmoset 17β-HSD1 are listed in Table 4. Remarkably, for inhibitor **12**, the energy contribution of the H-bond with the marmoset Asn152 (-1.6 kcal mol^{-1}) is 2.6 fold reduced compared to the human enzyme, while for compound **19** it is almost lost (-0.2 kcal mol^{-1}). Both for **12** and **19** reduced energies were also observed for interactions with Gly94, Leu95, and Leu96. Interestingly, inhibitor **12** showed an interaction with Asn222 in the marmoset enzyme (-3.3 kcal mol^{-1}), which was not observed for Ser222 in human 17β-HSD1 (-0.8 kcal mol^{-1}). This is not the case for **19**, as the interaction with Asn222 (-0.3 kcal mol^{-1}) does not contribute significantly to the interaction energy. In addition to Leu149, Pro187, Met193, Ile225, and Phe259, which interact with both compounds in the human enzyme, Gly186, His221, and Asn282 significantly contribute to the binding of **12** and **19** to marmoset 17β-HSD1 with interaction energies in the range from -0.4 kcal mol^{-1} to -3.6 kcal mol^{-1}. Interestingly, in marmoset 17β-HSD1 the interaction energy between **12** and Asn282 (-3.2 kcal mol^{-1}) is 32 fold increased compared to that with Glu282 in the human enzyme (-0.1

kcal mol^{-1}). In marmoset 17β-HSD1 an increased energy is also observed for the interaction of compound **19** with His221 (-2.6 kcal mol^{-1}) compared to the human enzyme (-0.2 kcal mol^{-1}).

Table 4. Interaction energies between the inhibitors **12** and **19** and the proximal (4.0 Å) binding site residues of marmoset monkey 17β-HSD1.

comp	Gly94	Leu95	Leu96	Ser142	Leu149	Asn152	Tyr155	Cys185	Gly186	Pro187
12	-0.0	-0.1	-0.8	-2.1	-2.0	-1.6	-0.8	-0.3	-0.7	-2.0
19	-0.0	-0.1	-0.2	-0.9	-1.1	-0.2	-0.3	-3.5	-2.0	-2.0
comp	**Phe192**	**Met193**	**Tyr218**	**His221**	**Asn222**	**Ile225**	**Arg258**	**Phe259**	**Leu262**	**Asn282**
12	-0.4	-1.3	-1.4	-0.8	-3.3	-1.9	-0.1	-1.3	-0.9	-3.2
19	-0.0	-0.4	-0.0	-2.6	-0.3	-2.6	-3.7	-1.9	-1.0	-3.6

All energies are expressed in kcal mol^{-1}.

Discussion

When the three-dimensional structures of marmoset and human 17β-HSD1 are compared, one of the most striking features is the small α-helix including the residues 190 to 196. It is formed in the segment between the βF-sheet and the αG'-helix starting from the interface residue Thr190, which is half in and half out of the helix (N-cap position). In contrast to the human enzyme, where this region is highly flexible, as suggested by the different crystal structures, the α-helix stayed stable during the MD simulation in both the holoform and the ternary complex. The observed conformational stability might be explained by the presence of a proline in position 191 instead of an alanine. Proline is a favourable candidate for N1 position because of its own conformational properties: with only one rotatable angle it loses less entropy than other amino acids in forming an α-helix and thereby it should have some stabilizing influence [47]. Furthermore, in an analysis of sequence-structural characteristics in protein crystal structures, proline was found to be a favoured residue at N1 position. Especially the residue pair involving threonine at N-cap and proline at N1 position, which is observed for marmoset 17β-HSD1, has a high prevalence [48].

In order to analyse the influence of the conformational changes in marmoset 17β-HSD1 on ligand binding, docking studies with subsequent MD simulations, free energy calculations, and energy decomposition analyses were carried out. While the conformational differences between the marmoset and the human enzyme did not affect the binding mode of **12** remarkably, the suggested binding mode of **19** differed strongly in 17β-HSD1 of both species. One possible explanation for that might be the lower sterical demand of **12** compared to **19**. However, the energy contribution of the interaction between **12** and the marmoset Asn152 is reduced, whereas it was outstanding in complex with the human enzyme. Due to the minimal shift of **12** in the marmoset binding pocket, the geometric parameters for the H-bond with Asn152 are no longer optimal. Interestingly, in the marmoset enzyme an additional interaction of **12** with Asn222 is observed, which seems to compensate the deficit in interaction energy due to the absent interaction with Asn152 resulting in comparable binding energies

for **12** in complex with human and marmoset 17β-HSD1. The latter finding is in accordance with the inhibition data observed for compound **12** and validates the marmoset 17β-HSD1 model.

Considering compound **19**, no particular interactions with the subpocket residues of the marmoset enzyme exist. Although weak interactions between **19** and the C-terminal region of marmoset 17β-HSD1 are observed, the binding free energy is less favourable compared to that calculated for the human 17β-HSD1-**19** complex. As the C-terminal part of the enzyme has already been discussed as a potential product exit gate of the enzyme [21], inhibitor **19** might be solvent exposed. This is consistent with the unfavourable entropy term of this complex resulting in the least favourable free energy.

Obviously, the presence of a proline in the flexible loop region and the thereby induced conformational changes in marmoset 17β-HSD1 are decisive for the species specific inhibition of **19**. On one hand interactions with subpocket residues like Asn152, recently discussed as relevant interaction partner [49], are prevented and on the other hand the inhibitor is forced in an unfavourable solvent exposed conformation.

The bis(hydroxyphenyl) substituted arenes (compounds **1**-**11**) show similar or increased inhibitory potencies toward marmoset 17β-HSD1 when comparing to human 17β-HSD1. Recently performed docking experiments proposed a steroidal binding mode when the human crystal structure 1fdtB was used [33]. The high inhibitory potencies toward marmoset 17β-HSD1 are in concert with the modelled structure of marmoset 17β-HSD1 as steroid-like binding is not affected by the proposed conformational changes. Obviously, they even stabilize the bis(hydroxyphenyl) substituted arenes in the marmoset 17β-HSD1 binding pocket as indicated by the observed inhibitory potencies.

Differing inhibitory potencies toward human 17β-HSD1 and 17β-HSD2 may arise from sequence variations in the regions 94-196 and 214-284 (numbering according to 17β-HSD1), which might lead to differences in the active sites of the two human subtypes. A lower selectivity of compounds toward non-target marmoset 17β-HSD2 was observed, when comparing to human 17β-HSD2. Obviously, the differences in the active sites of marmoset 17β-HSD1 and 17β-HSD2 are less pronounced compared to the human orthologs. However, as the available marmoset 17β-HSD2 sequence is missing the F/G segment and the C-terminal part this hypothesis cannot be proved.

The validity of the presented homology model is further substantiated by its ability to explain the reduced inhibitory potency of C-15 substituted estrone derivatives toward marmoset 17β-HSD1 [39]. The substituents in 15-position of the steroid were designed to occupy the hole between the flexible βFαG'-loop and the αG'-helix in the human enzyme [50]. Together with the helix formation and the conformational changes in the βD/αE-segment, the S222N mutation limits the size of the hole in marmoset 17β-HSD1 and thereby might reduce the inhibitory potency toward the marmoset enzyme.

Conclusion

An elegant strategy to gain more knowledge of active site topologies and, in particular, of protein-ligand interactions is to compare inhibition values obtained for one compound toward ortholog proteins from various species, which are highly conserved in sequence and differ only in few residues. Thereby, such an approach can be a valid alternative to site-directed mutagenesis. As human and marmoset 17β-HSD1 enzymes meet these criteria, selected human 17β-HSD1 inhibitors were assessed for their inhibitory potencies toward marmoset 17β-HSD1. While a species specific inhibition profile was observed in the class of the (hydroxyphenyl)naphthols, representatives of the other evaluated compound classes showed similar or even higher inhibition compared to those observed for the human enzyme. Using a combination of computational methods, including homology modeling, molecular docking, MD simulation, and binding energy calculation, a reasonable model of the three-dimensional structure of marmoset 17β-HSD1 was developed and inhibition data were rationalized on the structural basis. In the marmoset 17β-HSD1, residues 190 to 196 form a small α-helix, which is obviously stabilized by the presence of a proline in N-cap position (residue 191) and induces conformational changes that affect ligand binding. Furthermore energy decomposition analysis highlighted the important role of Asn152 as interaction partner for inhibitor binding.

This work could not only offer a better understanding of the active site topologies and of the protein-ligand interactions, but also provides novel structural clues that will help to design and optimize potent human 17β-HSD1 inhibitors with improved inhibitory potency toward marmoset 17β-HSD1. This is an important step to turn compounds, which show a promising pharmaceutical profile, into candidates for *in vivo* evaluation. Thus, our combined computational approach could also be considered as a valuable tool to achieve this goal.

Methods

Sequence Alignment and Model Building

The amino acid sequences of rat (accession number P51657), mouse (P51656) cynomolgus (Q4JK77) and marmoset 17β-HSD1 (Q9GME2) as well as human (P37059), cynomolgus (Q4JK76), marmoset (Q9GME5), mouse (P51658) and rat (Q62730) 17β-HSD2 were obtained from the uniprot webpage. These sequences were pairwise aligned with human 17β-HSD1 (PDB code: 1fdt) using MAFFT version 5 [51]. Using this alignment, a set of 100 comparative models of marmoset 17β-HSD1 was built employing Modeller9v7 [42], with the ternary complex E1-NADPH-human 17β-HSD1 as template. This complex resulted from docking of E1 to human 17β-HSD1 (PDB code: 1fdtB) (see below). The best homology model was then selected according to the Modeller energy score, DOPE score [43] and PROCHECK [44] tests. The reliability of the built homology models was checked by Prosa2003 [52] (Fig. S1), ERRAT [53], and Verify3D [54] (Fig. S2).

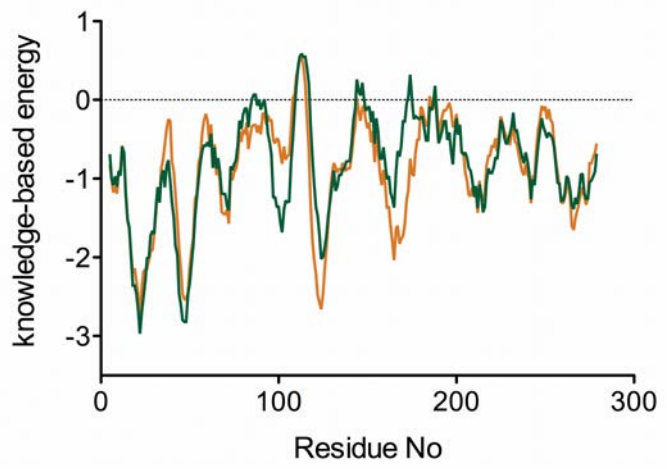

Figure S1. *Energy profile drawn for the marmoset 17β-HSD1 model using PROSA. Energy profiles of marmoset 17β-HSD1 in complex with NADPH (orange) and of marmoset 17β-HSD1 in complex with NADPH and E1 (green).*

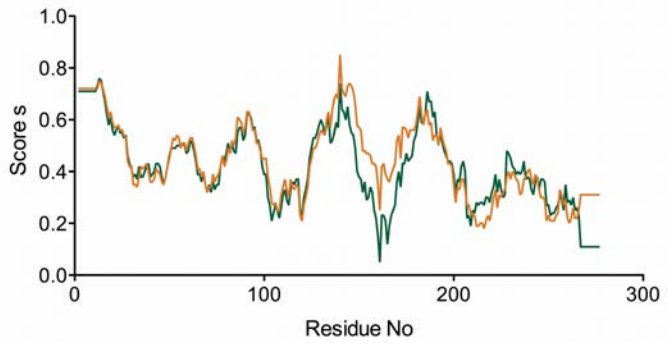

Figure S2 *Verify3D results for the marmoset 17β-HSD1 model.. Verify-3D results are shown for the secondary complex of marmoset 17β-HSD1 (orange) with NADPH and for ternary complex (green) with NADPH and E1; residues with positive score are reasonably folded.*

MD Simulations

MD simulations were performed using the AMBER 9.0 suite program [55]. The partial atomic charges for E1 and the inhibitors were derived from the molecular electrostatic potential (MEP) previously calculated using GAMESS [56], according to the RESP methodology [57]. For the protein, partial atomic charges were read from the AMBER 9.0 libraries. The AMBER99SB force field [58] was employed to define atom types and potentials for the protein, while the general AMBER force field (gaff) [59] was used to define all needed atom types and parameters for E1 and the inhibitors. For NADPH (charge -4), the parameters previously reported by Ulf Ryde were applied (http://www.teokem.lu.se/~ulf/).

The input files for the MD simulation were prepared with the xLEaP module of AMBER. Each system was solvated with an octahedral box of TIP3P water molecules of 10Å radius and neutralized by the addition of Na^+ ions. Finally, for each complex the topology and the coordinate files were written and used in the MD simulations.

Before starting the production-run phase, the following equilibration protocol was applied to all systems. At the beginning the system was energy-minimized in two stages: firstly, the solvent was relaxed while all the solute atoms were harmonically restrained to their original positions with a force constant of 100 kcal mol^{-1} $Å^{-2}$ for 1000 steps; and secondly, the whole molecular system was minimized for 2500 steps by conjugate gradient. Subsequently, the system was heated during 60 ps from 0 to 300 K at constant volume conditions (NTV, PBC conditions), and then equilibrated keeping both temperature and pressure constant (NTP, PBC conditions, 300 K, 1 atm) during 100 ps. Electrostatic interactions were computed using the Particle Mesh Ewald method [60], and the SHAKE [61] algorithm was employed to keep all bonds involving hydrogen atoms rigid. NADPH, E1 and the inhibitors were constrained during the equilibration with a force constant of 20 kcal mol^{-1} $Å^{-2}$. After equilibration, a MD production stage (NTP, PBC conditions, 300 K, 1 atm) was performed. The total simulation length differed for the various complexes ranging from 4 to 6 ns. Distance restraints were applied to substrate/inhibitor with the aim of maintaining their proper orientation at the beginning (first ns) of production stage.

For the ternary complex of marmoset 17β-HSD1 with E1 and NADPH, two additional distance restraints were used: between the keto-oxygen of E1 and the side chain oxygen of Ser142 (d=2.40-3.00 Å; force constant: 10 kcal mol^{-1} $Å^{-2}$) and between the oxygen of the OH-group in 17-position of E1 and the NE2 nitrogen of the His221 side chain (d=2.70-3.40 Å; force constant: 10 kcal mol^{-1} $Å^{-2}$).

For the ternary complex of human 17β-HSD1 with 12 and NADPH, three additional distance restraints were used: between the keto-oxygen of 12 and the side chain oxygen of Tyr155 (d=2.80-3.40 Å; force constant: 10 kcal mol^{-1} $Å^{-2}$), between the oxygen of the OH-group in *meta*-position of 12 and the OD1 oxygen of the Asn152 side chain (d=2.70-3.30 Å; force constant: 10 kcal mol^{-1} $Å^{-2}$), and between the oxygen of the *para* OH-group of 12 and the NE2 nitrogen of the His221 side chain (d=2.70-3.30 Å; force constant: 10 kcal mol^{-1} $Å^{-2}$).

For the ternary complex of marmoset 17β-HSD1 with 12 and NADPH three additional distance restraints were used: between the keto-oxygen of 12 and the side chain oxygen of Ser142 (d=2.50-3.10 Å; force constant: 10 kcal mol^{-1} $Å^{-2}$), between the oxygen of the OH-group in *meta*-position of 1 and the OD1 oxygen of the Asn152 side chain (d=2.40-3.00 Å; force constant: 10 kcal mol^{-1} $Å^{-2}$), and between the oxygen of the *para* OH-group of 12 and the OD1 oxygen of the Asn282 side chain (d=2.50-3.10 Å; force constant: 10 kcal mol^{-1} $Å^{-2}$).

For the ternary complex of human 17β-HSD1 with 19 and NADPH three additional distance restraints were used: between the oxygen of the OH-group in 2-position of the naphthol core and the side chain oxygen of Tyr155 (d=2.80-3.40 Å; force constant: 10 kcal mol^{-1} $Å^{-2}$), between the oxygen of the OH-group in *meta*-position of the phenyl ring and the NE2 nitrogen of the His221 side chain (d=3.00-4.20 Å; force constant: 10 kcal mol^{-1} $Å^{-2}$), and between the nitrogen of the sulfonamide moiety of 19 and the OD1 oxygen of the Asn152 side chain (d=2.70-3.40 Å; force constant: 10 kcal mol^{-1} $Å^{-2}$).

For the ternary complex of marmoset 17β-HSD1 with 19 and NADPH two additional distance restraints were used: between the oxygen of the OH-group in 2-position of the naphthol core and the NE2 nitrogen of the His221 side chain (d=2.70-3.40 Å; force constant: 10 kcal mol^{-1} $Å^{-2}$) and between the oxygen of the OH-group in *meta*-position of the phenyl ring of 19 and the backbone carbonyl oxygen of Cys185 (d=2.40-3.00 Å; force constant: 10 kcal mol^{-1} $Å^{-2}$).

Trajectories were analyzed using the AMBER ptraj module, the MMTSB toolset [62] and the molecular visualization program VMD (Visual Molecular Dynamics) [63]. The resulting low energy structures were extracted for the homology model (apoform and ternary complex) and subjected to a subsequent minimization of 1000 steps (500 steps of steepest descent followed by 500 steps of conjugate gradient), using the sander module of AMBER. The modified generalized Born solvation model (IGB=2) [64] was used. Active site volumes of low energy structures were calculated using the CASTp [45].

Molecular docking

The three-dimensional structures used for docking studies were either retrieved from the PDB (1fdt, conformation B for residues 187-200) or from the homology modelling with subsequent MD simulation (equilibrated ternary complex after 5537 ps). The cocrystallized E2 and water molecules were removed from the PDB file. Hydrogen atoms and neutral end groups were added, $NADP^+$ was turned into NADPH and correct atom types were set. Ionization states and hydrogen positions were assigned using the Protonate 3D utility of MOE2009.10 (Chemical Computing Group Inc., Montreal, Canada). Ligand structures were built in MOE and RESP charges were assigned as described above. The 17β-HSD1 three-dimensional structures and ligand structures were prepared for docking studies through the graphical user interface AutoDockTools4 [46]. For the ligands, non-polar hydrogen atoms were deleted, rotatable bonds were defined and RESP charges were kept. For the protein, non-polar hydrogen atoms were deleted and charges were added to the structure. Autodock4.2 [46] was used to dock the ligands in the steroidal binding site of the processed protein structures. A box, centered on

the steroid-binding site, was set to define the docking area. Grid points of 90 x 90 x 90 with 0.250 Å spacing were calculated around the docking area for all the ligand atom types using AutoGrid4.2. For each inhibitor, 50 separate docking calculations were performed. Each docking calculation consisted of $25x10^5$ energy evaluations using the Lamarckian genetic algorithm local search (GALS) method. Each docking run was performed with a population size of 250. A mutation rate of 0.02 and a crossover rate of 0.8 were used to generate new docking trials for subsequent generations. The docking results from each of the 50 calculations were clustered on the basis of root-mean-square deviation (RMSD = 2.0 Å) between the Cartesian coordinates of the ligand atoms and were ranked on the basis of the free binding energy.

Free energy calculations using the MM/PBSA method

The calculation of binding free energy was evaluated using the MM/PBSA (Molecular Mechanics/ Poisson Boltzmann Surface Area) method as implemented in AMBER11 [65]. The electronic and Van der Waals energies were calculated using the sander module in AMBER11. The solvation free energy contributions may be further decomposed into an electrostatic and hydrophobic contribution. The electrostatic portion is calculated using the linearized PB equation. The hydrophobic contribution is approximated by the LCPO method [66] implemented within sander. The changes in entropy upon ligand association ΔS are estimated by normal mode analysis. For stable plateaus of the MD trajectories, snapshots were collected every 20^{th} frame (every 20 ps) and used to calculate relative binding affinity (ΔG_{bind}) and absolute free energy (ΔG).

Energy decomposition using the MM/GBSA method

A free energy decomposition of the protein ligand complexes was performed on a pairwise per-residue basis using the MM/GBSA (Molecular Mechanics/ Generalized Born Surface Area) method as implemented in AMBER11. The GBSA implicit-solvent solvation model was used in order to avoid the retarding effect of the PBSA method.

Inhibition assay

[2, 4, 6, 7-^{3}H]-E1 and [2, 4, 6, 7-^{3}H]-E2 were bought from Perkin Elmer, Boston. Quickszint Flow 302 scintillator fluid was bought from Zinsser Analytic, Frankfurt. Marmoset 17β-HSD1 and 17β-HSD2 were obtained from marmoset placenta according to previously described procedures [41]. Fresh marmoset placenta was homogenized and cytosolic and microsomal fractions were separated by centrifugation. For the partial purification of 17β-HSD1, the cytosolic fraction was precipitated with ammonium sulfate. 17β-HSD2 was obtained from the microsomal fraction.

Inhibition of 17β-HSD1: Inhibitory activities were evaluated by an established method with minor modifications [41]. Briefly, the enzyme preparation was incubated with NADH [500 µM] in the presence of potential inhibitors at 37 °C in a phosphate buffer (50 mM) supplemented with 20 % of glycerol and EDTA (1 mM). Inhibitor stock solutions were prepared in DMSO. The final concentration of DMSO was adjusted to 1 % in all samples. The enzymatic reaction was started by addition of a mixture of unlabelled- and [2, 4, 6, 7-^{3}H]-E1 (final concentration: 500 nM, 0.15 µCi).

After 10 min, the reaction was stopped by the addition of $HgCl_2$ (10 mM) and the mixture was extracted with diethylether. After evaporation, the steroids were dissolved in acetonitrile. E1 and E2 were separated using acetonitrile/water (45:55) as mobile phase in a C18 reverse phase chromatography column (Nucleodur C18 Gravity, 3 µm, Macherey-Nagel, Düren) connected to an HPLC-system (Agilent 1200 Series, Agilent Technologies, Waldbronn). Detection and quantification of the steroids were performed using a radioflow detector (Agilent 1200 Series, Agilent Technologies, Waldbronn). The conversion rate was calculated after analysis of the resulting chromatograms according to the following equation: $\%conversion = \frac{\%E2}{\%E2 + \%E1} \times 100$. Each value was calculated from at least three independent experiments.

Inhibition of 17β-HSD2: The 17β-HSD2 inhibition assay was performed similarly to the 17β-HSD1 procedure. The microsomal fraction was incubated with NAD^+ [1500 µM], test compound and a mixture of unlabelled- and [2, 4, 6, 7-^{3}H]-E2 (final concentration: 500 nM, 0.11 µCi) for 20 min at 37 °C. Further treatment of the samples and HPLC separation was carried out as mentioned above. The conversion rate was calculated after analysis of the resulting chromatograms according to the following equation: $\%conversion = \frac{\%E1}{\%E1 + \%E2} \times 100$.

Acknowledgements

We thank Prof. Dr. Rolf W. Hartmann for helpful discussion and Prof. Dr. Almuth Einspanier for providing marmoset placenta

References

1. Poutanen M, Isomaa V, Peltoketo H, Vihko R (1995) Role of 17 beta-hydroxysteroid dehydrogenase type 1 in endocrine and intracrine estradiol biosynthesis. J Steroid Biochem Mol Biol 55: 525-532.
2. Travis RC, Key TJ (2003) Oestrogen exposure and breast cancer risk. Breast Cancer Res 5: 239-247.
3. Dizerega GS, Barber DL, Hodgen GD (1980) Endometriosis: role of ovarian steroids in initiation, maintenance and suppression. Fertil Steril 33: 649-653.
4. Saloniemi T, Jarvensivu P, Koskimies P, Jokela H, Lamminen T, et al. (2010) Novel Hydroxysteroid (17β) Dehydrogenase 1 Inhibitors Reverse Estrogen-Induced Endometrial Hyperplasia in Transgenic Mice. Am J Pathol 176: 1443-1451.
5. Gobbi S, Cavalli A, Rampa A, Belluti F, Piazzi L, et al. (2006) Lead optimization providing a series of flavone derivatives as potent nonsteroidal inhibitors of the cytochrome P450 aromatase enzyme. J Med Chem 49: 4777-4780.
6. Cavalli A, Bisi A, Bertucci C, Rosini C, Paluszcak A, et al. (2005) Enantioselective nonsteroidal aromatase inhibitors identified through a multidisciplinary medicinal chemistry approach. J Med Chem 48: 7282-7289.
7. Leonetti F, Favia A, Rao A, Aliano R, Paluszcak A, et al. (2004) Design, synthesis, and 3D QSAR of novel potent and selective aromatase inhibitors. J Med Chem 47: 6792-6803.
8. Aggarwal S, Thareja S, Verma A, Bhardwaj T, Kumar M (2010) An overview on 5alpha-reductase inhibitors. Steroids 75: 109-153.
9. Picard F, Schulz T, Hartmann RW (2002) 5-Phenyl substituted 1-methyl-2-pyridones and 4'-substituted biphenyl-4-carboxylic acids. synthesis and evaluation as inhibitors of steroid-5alpha-reductase type 1 and 2. Bioorg Med Chem 10: 437-448.
10. Baston E, Hartmann RW (1999) N-substituted 4-(5-indolyl)benzoic acids. Synthesis and evaluation of steroid 5alpha-reductase type I and II inhibitory activity. Bioorg Med Chem Lett 9: 1601-1606.
11. Baston E, Palusczak A, Hartmann RW (2000) 6-Substituted 1H-quinolin-2-ones and 2-methoxy-quinolines: synthesis and evaluation as inhibitors of steroid 5alpha reductases types 1 and 2. Eur J Med Chem 35: 931-940.
12. Wetzel M, Marchais-Oberwinkler S, Hartmann RW (2011) 17β-HSD2 inhibitors for the treatment of osteoporosis: Identification of a promising scaffold. Bioorg Med Chem 19: 807-815.
13. Jörnvall H, Persson B, Krook M, Atrian S, Gonzalez-Duarte R, et al. (1995) Short-chain dehydrogenases/reductases (SDR). Biochemistry 34: 6003-6013.
14. Peltoketo H, Isomaa V, Mäentausta O, Vihko R (1988) Complete amino acid sequence of human placental 17 beta-hydroxysteroid dehydrogenase deduced from cDNA. FEBS Lett 239: 73-77.
15. Ghosh D, Pletnev VZ, Zhu DW, Wawrzak Z, Duax WL, et al. (1995) Structure of human estrogenic 17beta- hydroxysteroid dehydrogenase at 2.20 Å resolution. Structure 3: 503-513.
16. Filling C, Berndt KD, Benach J, Knapp S, Prozorovski T, et al. (2002) Critical residues for structure and catalysis in short-chain dehydrogenase/reductase. J Biol Chem 277: 25677-25684.
17. Azzi A, Rehse PH, Zhu DW, Campbell RL, Labrie F, et al. (1996) Crystal structure of human estrogenic 17beta-hydroxysteroid dehydrogenase complexed with 17 beta-estradiol. Nat Struct Biol 3: 665-668.
18. Marchais-Oberwinkler S, Henn C, Möller G, Klein T, Negri M, et al. (2010) 17β-Hydroxysteroid dehydrogenases (17β-HSDs) as therapeutic targets: Protein structures, functions and recent progress in inhibitor development. J Steroid Biochem Mol Biol 125: 66-82 and references therein cited.
19. Mazumdar M, Chen J, Lin SX Molecular basis of sex-steroid translation. PDB ID: 3km0.
20. Mazumdar M, Chen J, Lin SX Molecular basis of sex-steroids: thier translational activity. PDB ID: 3klp.
21. Negri M, Recanatini M, Hartmann RW (2010) Insights in 17β-HSD1 Enzyme Kinetics and Ligand Binding by Dynamic Motion Investigation. PLoS ONE 5: e12026.
22. Brožic P, Lanišnik Rižner T, Gobec S (2008) Inhibitors of 17beta-hydroxysteroid dehydrogenase type 1. Curr Med Chem 15: 137-150 and references therein cited.
23. Poirier D (2009) Advances in development of inhibitors of 17beta hydroxysteroid dehydrogenases. Anticancer Agents Med Chem 9: 642-660.
24. Day JM, Tutill HJ, Purohit A (2010) 17β-Hydroxysteroid dehydrogenase inhibitors. Minerva Endocrinol 35: 87-108.

25. Day JM, Tutill HJ, Purohit A, Reed MJ (2008) Design and validation of specific inhibitors of 17beta-hydroxysteroid dehydrogenases for therapeutic application in breast and prostate cancer, and in endometriosis. Endocr Relat Cancer 15: 665-692.
26. Messinger J, Hirvelä L, Husen B, Kangas L, Koskimies P, et al. (2006) New inhibitors of 17beta-hydroxysteroid dehydrogenase type 1. Mol Cell Endocrinol 248: 192-198.
27. Karkola S, Lilienkampf A, Wähälä K (2008) A 3D QSAR model of 17beta-HSD1 inhibitors based on a thieno[2,3-d]pyrimidin-4(3H)-one core applying molecular dynamics simulations and ligand-protein docking. ChemMedChem 3: 461-472.
28. Frotscher M, Ziegler E, Marchais-Oberwinkler S, Kruchten P, Neugebauer A, et al. (2008) Design, synthesis, and biological evaluation of (hydroxyphenyl)naphthalene and -quinoline derivatives: potent and selective nonsteroidal inhibitors of 17β-hydroxysteroid dehydrogenase type 1 (17β-HSD1) for the treatment of estrogen-dependent diseases. J Med Chem 51: 2158-2169.
29. Marchais-Oberwinkler S, Frotscher M, Ziegler E, Werth R, Kruchten P, et al. (2009) Structure-activity study in the class of 6-(3'-hydroxyphenyl)naphthalenes leading to an optimization of a pharmacophore model for 17β-hydroxysteroid dehydrogenase type 1 (17β-HSD1) inhibitors. Mol Cell Endocrinol 301: 205-211.
30. Marchais-Oberwinkler S, Kruchten P, Frotscher M, Ziegler E, Neugebauer A, et al. (2008) Substituted 6-phenyl-2-naphthols. Potent and selective nonsteroidal inhibitors of 17β-hydroxysteroid dehydrogenase type 1 (17β-HSD1): design, synthesis, biological evaluation, and pharmacokinetics. J Med Chem 51: 4685-4698.
31. Marchais-Oberwinkler S, Wetzel M, Ziegler E, Kruchten P, Werth R, et al. (2011) New Drug-Like Hydroxyphenylnaphthol Steroidomimetics As Potent and Selective 17β-Hydroxysteroid Dehydrogenase Type 1 Inhibitors for the Treatment of Estrogen-Dependent Diseases. J Med Chem 54: 534-547.
32. Bey E, Marchais-Oberwinkler S, Kruchten P, Frotscher M, Werth R, et al. (2008) Design, synthesis and biological evaluation of bis (hydroxyphenyl) azoles as potent and selective non-steroidal inhibitors of 17β-hydroxysteroid dehydrogenase type 1 (17β-HSD1) for the treatment of estrogen-dependent diseases. Bioorg Med Chem 16: 6423-6435.
33. Bey E, Marchais-Oberwinkler S, Negri M, Kruchten P, Oster A, et al. (2009) New Insights into the SAR and Binding Modes of Bis(hydroxyphenyl)thiophenes and -benzenes: Influence of Additional Substituents on 17β-Hydroxysteroid Dehydrogenase Type 1 (17β-HSD1) Inhibitory Activity and Selectivity. J Med Chem 52: 6724-6743.
34. Bey E, Marchais-Oberwinkler S, Werth R, Negri M, Al-Soud YA, et al. (2008) Design, synthesis, biological evaluation and pharmacokinetics of bis(hydroxyphenyl) substituted azoles, thiophenes, benzenes, and aza-benzenes as potent and selective nonsteroidal inhibitors of 17β-hydroxysteroid dehydrogenase type 1 (17β-HSD1). J Med Chem 51: 6725-6739.
35. Oster A, Hinsberger S, Werth R, Marchais-Oberwinkler S, Frotscher M, et al. (2010) Bicyclic Substituted Hydroxyphenylmethanones as Novel Inhibitors of 17β-Hydroxysteroid Dehydrogenase Type 1 (17β-HSD1) for the Treatment of Estrogen-Dependent Diseases. J Med Chem 53: 8176-8186.
36. Oster A, Klein T, Henn C, Werth R, Marchais-Oberwinkler S, et al. (2011) Bicyclic Substituted Hydroxyphenylmethanone Type Inhibitors of 17β-Hydroxysteroid Dehydrogenase Type 1 (17β-HSD1): The Role of the Bicyclic Moiety. ChemMedChem 6: 476-487.
37. Oster A, Klein T, Werth R, Kruchten P, Bey E, et al. (2010) Novel estrone mimetics with high 17β-HSD1 inhibitory activity. Bioorg Med Chem 18: 3494-3505.
38. Negri M, Recanatini M, Hartmann RW (2011) Computational investigation of the binding mode of bis(hydroxylphenyl)arenes in 17β-HSD1: molecular dynamics simulations, free energy calculations, and molecular electrostatic potential maps. J Comput Aided Mol Des: submitted.
39. Möller G, Husen B, Kowalik D, Hirvelä L, Plewczynski D, et al. (2010) Species Used for Drug Testing Reveal Different Inhibition Susceptibility for 17beta-Hydroxysteroid Dehydrogenase Type 1. PLoS ONE 5: e10969.
40. Kruchten P, Werth R, Marchais-Oberwinkler S, Bey E, Ziegler E, et al. (2009) Development of biological assays for the identification of selective inhibitors of estradiol formation from estrone in rat liver preparations. C R Chim 12: 1110-1116.
41. Kruchten P, Werth R, Marchais-Oberwinkler S, Frotscher M, Hartmann RW (2009) Development of a biological screening system for the evaluation of highly active and selective 17β-HSD1-inhibitors as potential therapeutic agents. Mol Cell Endocrinol 301: 154-157.
42. Sali A, Blundell TL (1993) Comparative protein modelling by satisfaction of spatial restraints. J Mol Biol 234: 779-815.

43. Shen M-Y, Sali A (2006) Statistical potential for assessment and prediction of protein structures. Protein Sci 15: 2507-2524.
44. Laskowski RA, MacArthur MW, Moss DS, Thornton JM (1993) PROCHECK: a program to check the stereochemical quality of protein structures. J App Cryst 26: 283-291.
45. Dundas J, Ouyang Z, Tseng J, Binkowski A, Turpaz Y, et al. (2006) CASTp: computed atlas of surface topography of proteins with structural and topographical mapping of functionally annotated residues. Nucleic Acids Res 34: W116-118.
46. Morris GM, Huey R, Lindstrom W, Sanner MF, Belew RK, et al. (2009) AutoDock4 and AutoDockTools4: Automated Docking with Selective Receptor Flexibility. J Comput Chem 30: 2785-2791.
47. Richardson JS, Richardson DC (1988) Amino acid preferences for specific locations at the ends of alpha helices. Science 240: 1648-1652.
48. Kumar S, Bansal M (1998) Dissecting alpha-helices: position-specific analysis of alpha-helices in globular proteins. Proteins 31: 460-476.
49. Lilienkampf A, Karkola S, Alho-Richmond S, Koskimies P, Johansson N, et al. (2009) Synthesis and biological evaluation of 17β-hydroxysteroid dehydrogenase type 1 (17β-HSD1) inhibitors based on a thieno[2,3-d]pyrimidin-4(3H)-one core. J Med Chem 52: 6660-6671.
50. Messinger J, Husen B, Koskimies P, Hirvelä L, Kallio L, et al. (2009) Estrone C15 derivatives--a new class of 17β-hydroxysteroid dehydrogenase type 1 inhibitors. Mol Cell Endocrinol 301: 216-224.
51. Katoh K, Kuma K, Toh H, Miyata T (2005) MAFFT version 5: improvement in accuracy of multiple sequence alignment. Nucleic Acids Res 33: 511-518.
52. Sippl MJ (1993) Recognition of errors in three-dimensional structures of proteins. Proteins 17: 355-362.
53. Colovos C, Yeates TO (1993) Verification of protein structures: patterns of nonbonded atomic interactions. Protein Sci 2: 1511-1519.
54. Lüthy R, Bowie JU, Eisenberg D (1992) Assessment of protein models with three-dimensional profiles. Nature 356: 83-85.
55. Case D, Darden T, Cheatham T, III, Simmerling C, et al. (2006) AMBER 9. University of California, San Francisco.
56. Schmidt M, Baldridge K, Boatz J, Elbert S, Gordon M, et al. (1993) General atomic and molecular electronic structure system. J Comput Chem 14: 1347-1363.
57. Bayly CI, Cieplak P, Cornell WD, Kollman PA (1993) A well behaved electrostatic potential based method using charge restraints for determining atom-centered charges: the RESP model. J Phys Chem 97: 10269-10280.
58. Hornak V, Abel R, Okur A, Strockbine B, Roitberg A, et al. (2006) Comparison of multiple Amber force fields and development of improved protein backbone parameters. Proteins 65: 712-725.
59. Wang J, Wolf RM, Caldwell JW, Kollman PA, Case DA (2004) Development and testing of a general amber force field. J Comput Chem 25: 1157-1174.
60. Darden T, Perera L, Li L, Pedersen L (1999) New tricks for modelers from the crystallography toolkit: the particle mesh Ewald algorithm and its use in nucleic acid simulations. Structure 7: R55-60.
61. Ryckaert J-P, Ciccotti G, Berendsen HJC (1977) Numerical integration of the cartesian equations of motion of a system with constraints: molecular dynamics of n-alkanes. J Comput Phys 23: 327-341.
62. Feig M, Karanicolas J, Brooks CL (2004) MMTSB Tool Set: enhanced sampling and multiscale modeling methods for applications in structural biology. J Mol Graph Model 22: 377-395.
63. Humphrey W, Dalke A, Schulten K (1996) VMD: visual molecular dynamics. J Mol Graph 14: 33-38.
64. Onufriev A, Bashford D, Case DA (2004) Exploring protein native states and large-scale conformational changes with a modified generalized born model. Proteins 55: 383-394.
65. Kollman PA, Massova I, Reyes C, Kuhn B, Huo S, et al. (2000) Calculating structures and free energies of complex molecules: combining molecular mechanics and continuum models. Acc Chem Res 33: 889-897.
66. Weiser J, Shenkin PS, Still WC (1999) Approximate solvent-accessible surface areas from tetrahedrally directed neighbor densities. Biopolymers 50: 373-380.

3.2 New drug-like hydroxyphenylnaphthol steroidomimetics successfully developed as potent and selective 17β-HSD1 inhibitors for the treatment of estrogen-dependent diseases

Sandrine Marchais-Oberwinkler, Marie Wetzel, Erika Ziegler, Patrizia Kruchten, Ruth Werth, **Claudia Henn**, Rolf W. Hartmann, Martin Frotscher

Journal of Medicinal Chemistry **2011**, 54, (2), 534-547

Publication II

Abstract

Inhibition of 17β-hydroxysteroid dehydrogenase type 1 (17β-HSD1) is a novel and attractive approach to reduce the local levels of the active estrogen 17β-estradiol in patients with estrogen-dependent diseases like breast cancer or endometriosis. With the aim of optimizing the biological profile of 17β-HSD1 inhibitors from the hydroxyphenylnaphthol class, structural optimizations were performed at 1-position of the naphthalene by introduction of different heteroaromatic rings as well as substituted phenyl groups. In the latter class of compounds, which were synthesized applying Suzuki-cross coupling, the 3-methanesulfonamide **15** turned out to be a highly potent 17β-HSD1 inhibitor (IC_{50} = 15 nM in a cell-free assay). It was also very active in the cellular assay (T47D cells, IC_{50} = 71 nM) and selective toward 17β-HSD2 and the estrogen receptors α and β. It showed a good membrane permeation and metabolic stability and was orally available in the rat.

Introduction

The great importance of 17β-estradiol (E2)[1], the most potent estrogen, in the development and progression of estrogen-dependent diseases (EDD), like breast cancer[2,3] and endometriosis[4,5] is now well established. In case of estrogen-dependent tumors, current hormonal therapies are aimed either at blocking the action of estrogens (with anti-estrogens or selective estrogen receptor modulators (SERMs)) or at lowering the levels of both circulating and tissue E2 by inhibiting estrogen synthesis (by use of aromatase inhibitors (AI)[6-8] or GnRH analogs). Although the emergence of these therapies has led to major advances in the treatment of breast cancer, the tumor often develops resistance mechanisms during the treatment, leading to failure of these medications. Search for alternative therapies is therefore necessary. Restricting the estrogen decrease to the target cells only is an attractive approach for the treatment of EDD which should be associated with fewer side-effects. Such a therapeutic strategy (intracrine concept) had been shown to be successful in androgen dependent diseases like benign prostate hyperplasia by using 5α-alpha reductase inhibitors[9-12]. Such an approach could be implemented for EDD applying inhibitors of 17β-hydroxysteroid dehydrogenase type 1 (17β-HSD1), the enzyme which catalyzes the last step of estrogens biosynthesis, transforming estrone (E1) to E2. These inhibitors, decreasing the E2 levels in the target tissues only, should thus be superior to AI which influence the systemic levels of E1 and E2, leading to severe side-effects like osteoporosis.

High expression of 17β-HSD1 mRNA has been found in breast cancer tissues[13,14] and in endometriosis[15]. In addition, 17β-HSD1 is highly expressed in breast cancer cells while 17β-HSD2, the enzyme catalyzing the reverse reaction (deactivating E2 into E1) is frequently down-regulated in malignant cells. This disrupted 17β-HSD1/17β-HSD2 ratio suggests the important role of 17β-HSD1 in the production of E2 in breast tumors compared to normal breast tissue (E2 concentration is up to 2.3 times higher in malignant tissues[16,17]). Blocking the last step of estrogen biosynthesis by inhibition of 17β-HSD1 is therefore an attractive approach for the treatment of these diseases.

Recently in vivo efficacy of 17β-HSD1 inhibitors has been reported in two animal models. Immunodeficient mice were inoculated either with MCF-7 cells over-expressing human recombinant 17β-HSD1 enzyme[18,19] or with T47D cells naturally expressing 17β-HSD1[20]. In both models, the E1 induced tumor growth was reduced by 17β-HSD1 inhibitors. This effect was also demonstrated by Kruchten et al.[21] using an in vitro proliferation assay: in a control experiment equivalent tumor growth stimulation could be reached at equal concentration of E1 and E2 because of the very fast reduction of the weakly active EDD stimulator E1 to the highly potent E2 catalyzed by 17β-HSD1. Application of a 17β-HSD1 inhibitor could reduce significantly the cell proliferation induced by E1 only. The combination of these in vitro and in vivo experiments validates 17β-HSD1 as a novel target for the treatment of EDD. Up to date however, no 17β-HSD1 inhibitor has entered clinical trials.

17β-HSD1 belongs to the 17β-hydroxysteroid dehydrogenase (HSD) family. Together with type 7 and 12, the subtype 1 is able to catalyze the NADPH dependent reduction of E1 into E2. However, only

type 1 is considered to be efficient in the transformation of the sex steroid, type 7 and 12 are involved in cholesterol synthesis[22] and in lipid biosynthesis[20], respectively.

17β-HSD1 is a soluble cytosolic enzyme; it has been crystallized with different steroidal ligands[23-31]. The X-ray structures provided useful information about the enzyme active site for the design of potent inhibitors.

Several classes of 17β-HSD1 inhibitors have been described in the last years[32-38], most of them having a steroidal core. Within the nonsteroidal inhibitors, only five different templates revealed interesting activities: flavones and isoflavones[39], thienopyrimidinones[40,41], bishydroxyphenyl arenes[42-45], heterocyclic substituted biphenylols[46] and hydroxyphenylnaphthols[47-49], the three latter classes were described by our group. In the series of hydroxyphenylnaphthols, the steroidomimetic **A**[47] (Chart 1) was previously identified as a new scaffold for 17β-HSD1 inhibitors. The biological profile of **A** was optimized and the hit compound B[48,49] (Chart 1), bearing a phenyl ring at the 1-position of the naphthalene ring, was discovered as the most promising in this series of inhibitors with a good inhibitory activity (IC_{50} = 20 nM), a good selectivity toward 17β-HSD2 (selectivity factor (SF): 27) and a weak affinity to the estrogen receptors (ER) α and β.

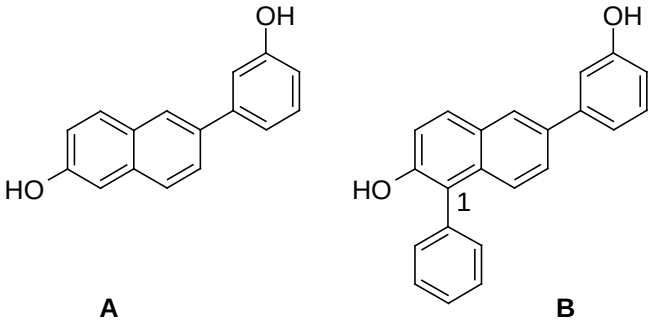

***Chart 1**: Previously identified hits as 17β-HSD1 inhibitors*

After introduction of various substituents at different positions on the hydroxyphenyl and/or naphthalene moiety, we identified a plausible binding mode for B in the active site: the hydroxyphenyl part mimics the A-ring of E2 and the naphthol-OH interacts with the catalytic tetrad. The 1-phenyl group is stabilized by π-π interactions with the amino acids Phe226 and Tyr155 and the nicotinamide ring of the cofactor[48].

As our goal is to develop new compounds demonstrating therapeutic efficacy, they should not only show good inhibitory activity but they should also have a good ADME/Tox profile and therefore should not be as lipophilic as compound **B** (logP 5.6). Considering the sharp structure-activity relationship (SAR) observed in this class of compounds[47] and in order to improve the in vivo activity of this compound class, we decided to perform structure modifications at the 1-position of the naphthalene.

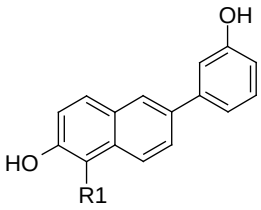

1-8

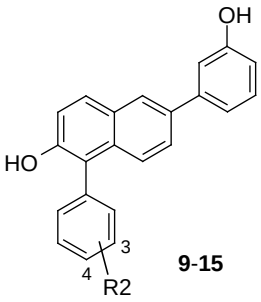

9-15

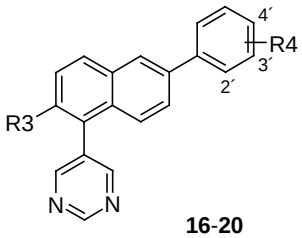

16-20

Cmpd	R1	Cmpd	R2	Cmpd	R3	R4
1		**9**	3-OH	**16**	H	2´-OH
2		**10**	3-COOH	**17**	H	3´-OH
3	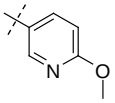	**11**	3-NH_2	**18**	OH	H
4		**12**	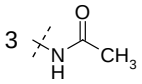	**19**	OH	2´-OH
5		**13**	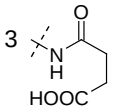	**20**	OH	4´-OH
6	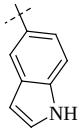	**14**	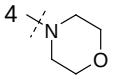			
7	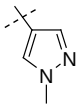	**15**	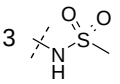			
8	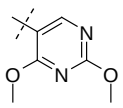					

***Chart 2**: Synthesized compounds.*

Two strategies were followed: a) exchange of the 1-phenyl moiety of B for different heterocycles (compounds **1-8**, Chart 2) and b) introduction of substituents on the 1-phenyl group (compounds **9-15**, Chart 2).

These substituents should on the one hand be able to establish H-bond interactions with amino acids from the active site located around the catalytic tetrad and on the other increase the hydrophilicity of the inhibitors.

Herein, we report about our efforts to improve the therapeutic properties of this class of compounds starting from B, developing new, potent and selective 17β-HSD1 inhibitors.

Chemistry

Introduction of aromatic heterocycles - compounds 1-8

Compounds **1-8** were prepared in two steps from 1-bromo-2-methoxy-6-(3-methoxyphenyl)naphthalene **1**b (Scheme 1). Demethylation using boron tribromide[50] (Method A) led to 1a, which was subsequently submitted to Suzuki coupling using the appropriate boronic acid[51] (Method B or C) to afford **1-5** and **8**. Compounds **6** and **7** were obtained from **1b** via a cross-coupling under microwave assisted conditions (Method C) and subsequent ether cleavage.

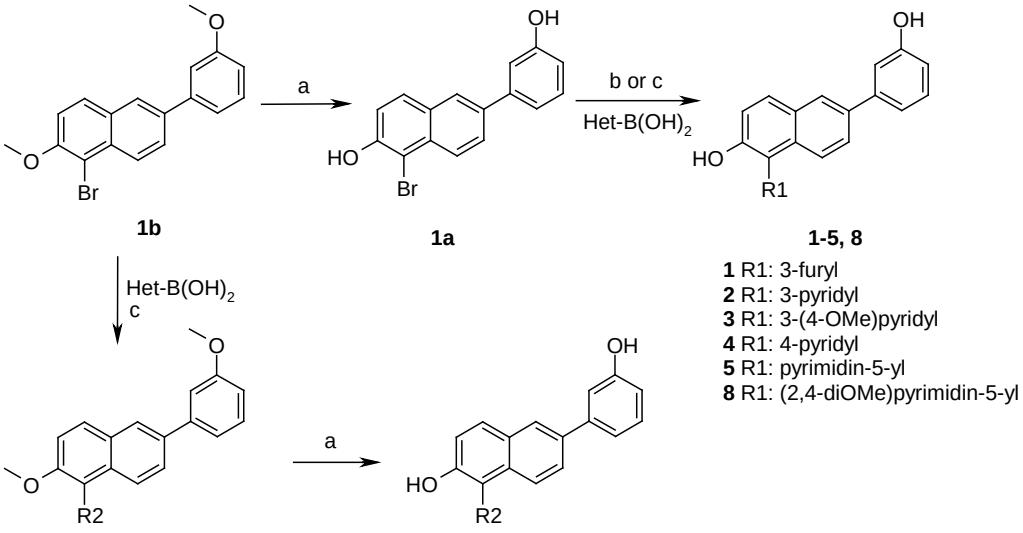

[a] Reagents and conditions: a. BBr_3, CH_2Cl_2, -78 °C to RT, overnight, Method A; b. $Pd(PPh_3)_4$, aq. Na_2CO_3, toluene/ethanol 5:1 for **1**, **3** and **4**, 2:1 for **2**, 5:3 for **5**, 80 °C for **1-3** and **5**, 100 °C for **4**, 1 h for **2** and **4**, 2 h for **1**, 3 h for **3**, 15 h for **5,** Method B; c. $Pd(PPh_3)_4$, aq. Cs_2CO_3, DME/EtOH/H_2O 1:1:1 microwave irradiation, 150 W, 150 °C, 15 bar, 25 min for **8**, **6a** and **7a,** Method C.

Scheme 1: *Synthesis of compounds **1-8**.*

Introduction of substituted aryls - compounds 9-15

Compound 9 was obtained by cross coupling reaction of 1,6-dibromo-2-naphthol **9**a with an excess of 3-hydroxybenzeneboronic acid following Method B (Scheme 2). Compounds **10** and **12-15** were prepared by coupling **1**a either to a boronic acid to give **10** and **14** or to a pinacolatoester in case of the amides **12**, **13** and the sulfonamide **15** (Method B, Scheme 2).

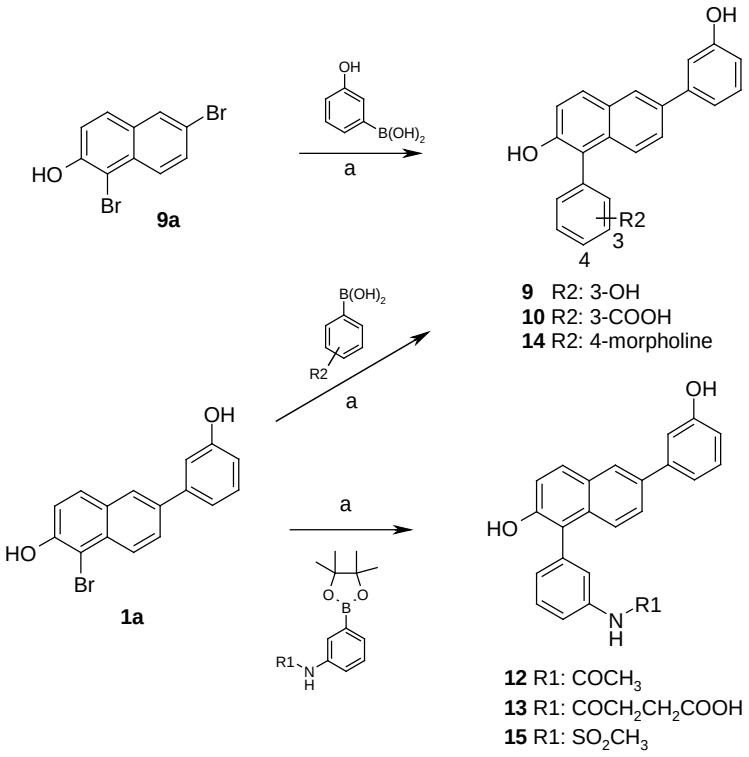

[a] Reagents and conditions: a. $Pd(PPh_3)_4$, aq. Na_2CO_3, toluene for **9**, toluene/ethanol 2:1 for **10** and **13**, 5:3 for **14** and 5:1 for **12** and **15** , 80 °C, 2 h for **10, 12** and **15**, 10 min for **13,** 1 h for **9** and 21 h for **14**, Method B.

Scheme 2: *Synthesis of compounds* ***9-10, 12-15****.*

The synthesis of compound **11** is depicted in Scheme 3. The dimethoxylated aniline derivative **11a** was prepared from **1b** by cross-coupling reaction following method B. Cleavage of the methoxy groups with boron tribromide (Method A) afforded **11** directly.

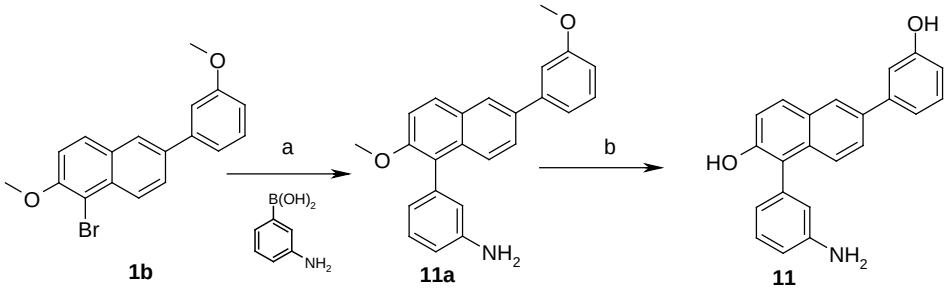

[a] Reagents and conditions: a. $Pd(OAc)_2$, Na_2CO_3, TBAB, water, 150 °C, 1 h, Method A; b. BBr_3, CH_2Cl_2, -78 °C to RT, overnight, Method A.

Scheme 3: *Synthesis of compound* ***11****.*

Investigation of the hydroxy group substitution pattern of the pyrimidine derivative - Compounds 16-20

Three monohydroxylated derivatives of the pyrimidine **5** (compounds **16-18**) were synthesized (Scheme 4 and 5).

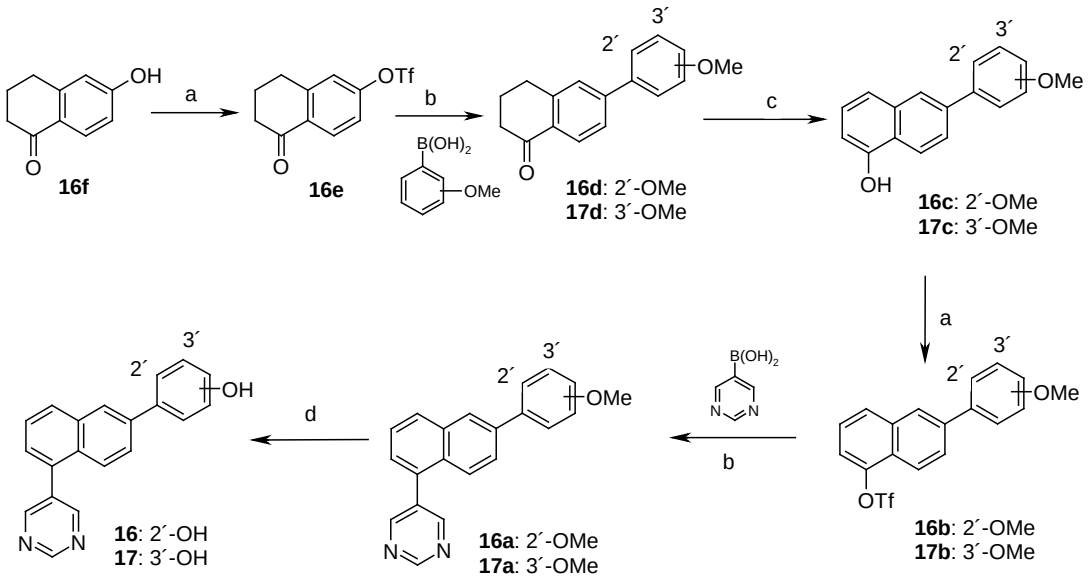

[a] Reagents and conditions: a. triflic anhydride, pyridine, CH_2Cl_2, 0 °C, 30 min; b. $Pd(PPh_3)_4$, aq. Na_2CO_3, toluene/ ethanol 5:1, 80 °C, 11 h for **16a** and 8 h for **17a**, Method B; c. 10% Pd/C, *p*-cymene, reflux, overnight; d. pyridinium hydrochloride, 220 °C, 3 h for **16**, BBr_3, CH_2Cl_2, -78 °C to RT, overnight for **17**, Method A.

Scheme 4: *Synthesis of compounds **16** and **17.***

Compounds **16** and **17** with the hydroxy group on the phenyl ring were prepared from the tetralone **16f**, which was converted to **16e**. A Suzuki reaction of the triflate **16e** and the corresponding methoxybenzeneboronic acid (Method B) led to the tetralones **16d** and **17d**[47,52], which were aromatized in presence of palladium on charcoal as catalyst. Subsequent triflation resulted in **16b** and **17b**[52]. Cross-coupling reaction with pyrimidine-5-boronic acid (Method B[52]) followed by ether cleavage with pyridinium hydrochloride or boron tribromide afforded compounds **16**[52] and **17**, respectively.

The synthesis of the monohydroxylated naphthalene **18** started from 6-bromo-2-methoxy-naphthalene **18c** (Scheme 5). Bromination with N-bromosuccinimide followed by regioselective Suzuki coupling with one equivalent of benzeneboronic acid (Method C) gave compound **18b**[53], which after coupling with pyrimidine-5-boronic acid (Method D) and subsequent ether cleavage with boron tribromide afforded **18**. For the synthesis of the dihydroxylated derivatives **19** and **20**, the hydroxylated phenyl group was introduced on 6-bromo-2-naphthol **19d** by Suzuki reaction (Method C). The resulting compounds **19c** and **20b**[52] were further brominated with N-bromosuccinimide to afford **19b** and **20a**[54] respectively. A second Suzuki coupling reaction with pyrimidine-5-boronic acid (Method D) gave compounds **19a** and **20**[53]. The ether group in **19a** was cleaved using boron tribromide to yield **19**[52].

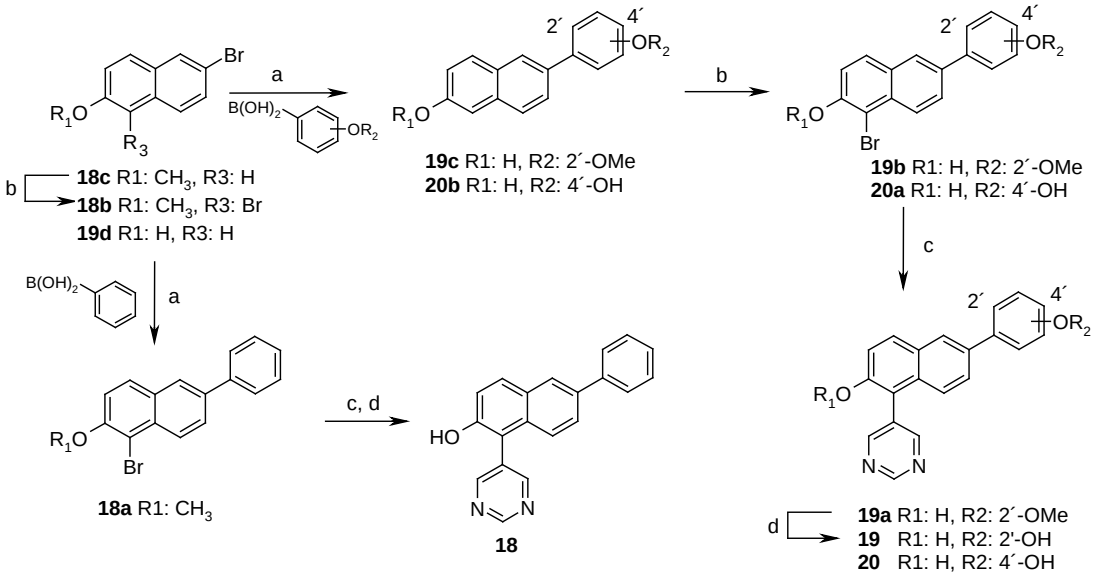

[a]Reagents and conditions: a. $Pd(PPh_3)_4$, aq. Cs_2CO_3, DME/EtOH/H_2O 1:1:1, microwave irradiation 150 W, 150 °C, 15 bar, 25 min, Method C; b. NBS, AcCN, RT, 5 min for **19b** and 1h for **18b and 20a**; c. pyrimidine-5-boronic acid, $Pd(OAc)_2$, PPh_3, 1,4-dioxane/EtOH 2:1, microwave irradiation 150 W, 150 °C, 15 bar, 15 min, Method D; d. BBr_3, CH_2Cl_2, -78 °C to RT, overnight, Method A.

Scheme 5: Synthesis of compounds **18-20.**

Results

Inhibition of human 17β-HSD1 and selectivity toward 17β-HSD2

17β-HSD1 and 17β-HSD2 inhibitory activities of the synthesized compounds were first evaluated in cell-free assays. 17β-HSD2 catalyzes the oxidation of E2 into E1, thus deactivates E2. It should not be affected by 17β-HSD1 inhibitors.

In the assays, both human recombinant and placental enzymes were used. In the 17β-HSD1 assay, incubations were run with tritiated E1, cofactor and inhibitor. The hybrid inhibitor (EM-1745) described by Poirier et al.[55] was used as reference compound and gave similar values as described (IC_{50} = 52 nM). The 17β-HSD2 assay was performed similarly using tritiated E2 as substrate. The percent inhibition values of all hydroxy compounds are shown in Tables 1-3. Compounds showing less than 10% inhibition at 1µM were considered to be inactive. IC_{50} values were determined for compounds showing more than 70% inhibition at 100 nM in the 17β-HSD1 assay and are shown in Table 4. All molecules with methoxy groups showed activity neither in the 17β-HSD1 nor in the 17β-HSD2 assays (data not shown). The 1-phenyl substituted naphthol **B** identified in a previous work[48] was used as internal reference. In an attempt to decrease the lipophilicity of **B** and to strengthen interactions with the enzyme, the 1-phenyl moiety was replaced by different 6- and 5-membered heteroaromatic cycles (**1**-**8**, Table 1).

Introduction of a nitrogen in the phenyl ring (3-pyridine **2** and 4-pyridine **4**) was well tolerated by the enzyme showing activity in the same range as the reference **B** (87%, 74% and 76% inhibition at 100 nM for **2**, **4** and **B** respectively) indicating that it is unlikely that supplementary interactions are achieved by the N. Addition of the electron donating methoxy group on the pyridine ring (**3**) is also

tolerated, it shows that there is some space around the heterocycle for introduction of a small substituent. Interestingly, introduction of a second nitrogen into the pyridine leading to the pyrimidine **5** led to an inactive compound (at 100 nM). The position of this N in the active site or the change of electronic distribution might be unfavorable, preventing **5** from integrating into the binding pocket. A moderate regain of activity (31% inhibition at 100 nM) was achieved by introduction of two methoxy groups into the pyrimidine core (**8**). The 2-OMe group of **8** certainly induces an *ortho* effect, constraining the pyrimidine to adopt a different geometry compared to **5** and restraining its free rotation. The *N*-methylpyrazole **7** also containing two nitrogens showed a weak inhibition (28% at 100 nM), indicating that only one nitrogen is tolerated in this area. Conversely, the furane **1** is a highly potent inhibitor (83% inhibition at 100 nM). The moderate activity of the indole **6** (50% inhibition at 100 nM) confirms that there is space available in this area for introduction of substituents on the phenyl ring as seen with **3**. A good (**3**, **4**, **6**, **7**, **8**) to moderate (**1**, **2**) selectivity toward 17β-HSD2 was observed for all compounds with the exception of **5** which was more potent for 17β-HSD2 (85% HSD2 inhibition *vs.* 41% HSD1 inhibition at 1 µM).
The logP values were calculated using the commercial ChemDrawPro 11.0 program and are indicated in Table 1 and 2. Compared to **B** the calculated logP suggested for all the compounds a better hydrophilicity, which should facilitate membrane permeation.

Various substituents were also introduced in the phenyl ring (Table 2). We focused on substituents which could establish interactions with the protein and which could increase the hydrophilicity of the lipophilic parent compound **B**. Introduction of a hydroxy (**9**) or an amino group (**11**) in position 3 did not dramatically change the inhibition compared to the naked **B** (83%, 74% and 76% inhibition at 100 nM for **9**, **11** and **B**, respectively). The unsubstituted carboxylic groups (compounds **10** and **13**) led to a decrease in activity (45% and no inhibition at 100 nM, respectively), which might be due to the absence of protonated amino acids in this area of the active site. The amides **12** and **13** bearing different substituents showed reasonable logP but only low or no activity. The most interesting compound in this series was the sulfonamide **15**, which exhibited the lowest logP (3.8) and a high potency. The most potent compounds **9**, **11** and **15** showed no to low inhibition of 17β-HSD2 (inhibition at 100 nM < 31% for **15**, Table 2) and therefore a good selectivity toward this enzyme.

Table 1: *Inhibition of human 17β-HSD1 and 17β-HSD2 by compounds* ***1-8.***

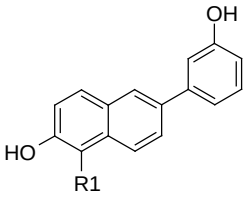

1-8

Cmpd	R1	Inhibition of 17β-HSD1 [%]		Inhibition of 17β-HSD2 [%]		LogP[e]
		100 nM	1 µM	100 nM	1 µM	
B		76[a]	89[a]	22[b]	77[b]	5.6
1		83[a]	89[a]	61[b]	92[b]	4.2
2		87[a]	92[a]	66[b]	90[b]	4.3
3	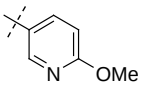	86[a]	89[a]	24[b]	67[b]	4.9
4		74[a]	86[a]	12[b]	49[b]	4.3
5		< 10[c]	41[c]	n.d.	85[d]	3.7
6		50[c]	87[c]	n.d.	19[d]	5.1
7		28[c]	71[c]	n.d.	24[d]	3.9
8	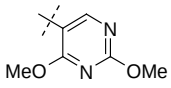	31[c]	79[c]	n.d.	9[d]	4.6

[a] Recombinant human 17β-HSD1, substrate [3H]-E1+ E1 [30 nM], cofactor NADPH [1 mM], Procedure A; mean value of two determinations, relative standard deviation < 20%, [b] Recombinant human 17β-HSD2, substrate [^{3}H]-E2 + E2 [30 nM], cofactor NAD^+ [1 mM], Procedure C, mean value of two determinations, relative standard deviation < 20%, [c] Human placenta, cytosolic fraction, substrate [^{3}H]-E1 + E1 [500 nM], cofactor NADH [0.5 mM], Procedure B, mean value of three determinations, relative standard deviation < 10% except for **7**: 20%, [d] Human placenta, microsomal fraction, substrate [^{3}H]-E2 + E2 [500 nM], cofactor NAD^+ [1.5 mM] Procedure D, mean value of three determinations, relative standard deviation < 10%, n.d.: not determined, [e] calculated logP data.

Table 2: *Inhibition of human 17β-HSD1 and 17β-HSD2 by compounds* ***9-15****.*

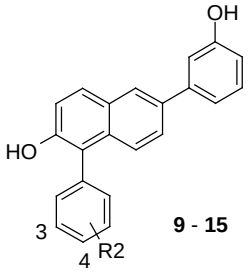

9 - 15

Cmpd	R2	Inhibition of 17β-HSD1 [%][a]		Inhibition of 17β-HSD2 [%][b]		LogP[c]
		100 nM	1 µM	100 nM	1 µM	
B	H	76	89	22	77	5.6
9	3-OH	83	93	< 10	40	5.2
10	3-COOH	45	80	< 10	34	5.2
11	3-NH_2	74	87	< 10	39	4.8
12	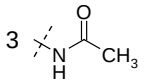	35	82	24	64	4.5
13	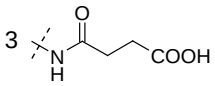	< 10	62	24	68	4.2
14	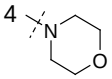	32	65	12	32	5.5
15	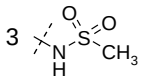	88	91	31	71	3.8

[a] Recombinant human 17β-HSD1, substrate [^{3}H]-E1+ E1 [30 nM], cofactor NADPH [1 mM], Procedure A; mean value of two determinations, relative standard deviation < 20%, [b] Recombinant human 17β-HSD2, substrate [^{3}H]-E2+ E2 [30 nM], cofactor NAD^+ [1 mM], Procedure C, mean value of two determinations, relative standard deviation < 20%, [c] calculated logP data.

Intrigued by the selectivity shown by pyrimidine **5** in favor of 17β-HSD2, a few pyrimidine derivatives (Table 3) lacking one OH group (**16-18**) or showing a changed hydroxysubstitution pattern (**19** and **20**) were examined with the goal to simplify and identify a new template for the further development of 17β-HSD2 inhibitors. Derivatives bearing one hydroxy group (**16-18**) turned out to be inactive on both 17β-HSD1 and 17β-HSD2. The potency could not be improved with derivatives bearing two hydroxy moieties (19-20). The distance between the two hydroxy groups might be either too long (20) or too short (19), to establish H-bond interactions.

***Table 3**: Inhibition of human 17β-HSD1 and 17β-HSD2 by compounds **16-20**.*

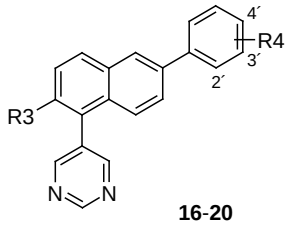

16-20

Cmpd	R3	R4	Inhibition of 17β-HSD1 [%][a,b] at 1 µM	Inhibition of 17β-HSD2 [%][b,c] at 1 µM
5	OH	3´-OH	41	85
16	H	2´-OH	< 10	< 10
17	H	3´-OH	< 10	< 10
18	OH	H	22	< 10
19	OH	2´-OH	< 10	< 10
20	OH	4´-OH	35	22

[a]Human placenta, cytosolic fraction, substrate [^{3}H]-E1 + E1 [500 nM], cofactor NADH [0.5 mM], Procedure B, [b] Mean value of three determinations, standard deviation < 10%, [c]Human placenta, microsomal fraction, substrate [^{3}H]-E2 + E2 [500 nM], cofactor NAD^+ [1.5 mM], Procedure D.

We focused therefore our efforts on the novel 17β-HSD1 inhibitors and measured IC_{50} values for the most potent ones (Table 4) and determined their SF. All tested compounds showed IC_{50} values in the low nanomolar range between 15 and 70 nM. The selectivity toward 17β-HSD2 could also be optimized with a SF up to 52.

As cell membrane permeation is an important criterion in the development of a drug, the potencies of the compounds were evaluated in a cellular assay using T47D cells (Table 4). All tested compounds, except the methoxy pyridine **3**, showed a better activity compared to the reference **B** (IC_{50} = 281 nM), the sulfonamide **15** being the best one with an IC_{50} of 71 nM. This finding also indicates, that **15** is metabolically stable in these cells.

Selectivity toward the ERα and ERβ

Designed as steroidomimetics the synthesized compounds might show some affinity to the ERα and ERβ. Agonistic properties would counteract the therapeutic concept of 17β-HSD1 inhibition and cannot be tolerated. This is also true for antagonistic effect which could lead to unwanted drug action similar to the ones observed for the anti-estrogens or SERMs. The most potent compounds were tested for their binding affinity to the ERs using the recombinant human proteins and applying a competition assay with [^{3}H]-E2. All tested compounds show a relative binding affinity of less than 0.1% to the estrogen receptors except for the reference compound **A**, which is included for comparison and is

considered as weak ligand of the ERs (Table 4). A RBA range between 0.01 and 0.1 means that the compound shows an affinity to the ERs between 0.01% and 0.1% compared to the affinity of E2 (RBA=100%). Due to these results the compounds are classified as low to very low affinity ligands of the ERs and are not expected to evoke ER-mediated effects under *in vivo* conditions.

Table 4: *IC_{50} values, selectivity factor and binding affinities for the ERα and ERβ for selected compounds.*

Cmpd	Cell free assay		SF[d]	Cell assay	ERα	ERβ
	17β-HSD1 IC_{50} [nM][a,b]	17β-HSD2 IC_{50} [nM][a,c]		17β-HSD1 IC_{50} [nM][a,e]	RBA (%)[a,f]	RBA (%)[a,f]
A	116	5641	49	229	0.1<RBA<1	0.1<RBA<1
B	20	540	27	281	0.01<RBA<0.1	0.01<RBA<0.1
1	70	527	7.5	n.d.	0.01<RBA<0.1	0.01<RBA<0.1
2	26	1157	45	165	0.01<RBA<0.1	0.01<RBA<0.1
3	33	530	16	670	<0.01	<0.01
4	64	3340	52	n.d.	<0.01	<0.01
9	36	959	27	115	<0.01	0.01<RBA<0.1
11	53	1757	33	n.d.	<0.01	<0.01
15	15	403	27	71	0.01<RBA<0.1	<0.01

[a] Mean value of three determinations except IC50 (17β-HSD2) for 4 two determinations, b Human placenta, cytosolic fraction, substrate [3H]-E1 +E1 [500 nM], cofactor NADH [0.5 mM], Procedure B, relative standard deviation < 10%, [c] Human placenta, microsomal fraction, substrate [3H]-E2+ E2 [500 nM], cofactor NAD+ [1.5 mM] Procedure D, relative standard deviation < 8%, [d] SF: selectivity factor = IC50 (17β-HSD2)/ IC_{50} (17β-HSD1), [e] T47D cells, substrate [3H]-E1 +E1 [50 nM], relative standard deviation < 13% f RBA: Relative Binding Affinity, E2 = 100%, n.d.: not determined.

Further in vitro assays

According to their potency (cell-free and cellular assays) and their selectivity toward 17β-HSD2 and ERs, compounds **2, 3, 9, 11** and **15** were the best compounds identified in this study. They were further evaluated in our screening system.[56] Metabolic stability of **2**, **3** and **11** was determined using rat liver microsomes and human liver microsomes for **15** (Table 5). For **2**, **3**, **11**
and **15** half-life and intrinsic body clearance were evaluated and compared to the references diazepam (high metabolic stability, $t_{1/2}$ = 41 min) and diphenhydramine (low metabolic stability, $t_{1/2}$ = 7 min). The short half-life of **2** ($t_{1/2}$ = 14 min) and the fast clearance of **11** (Cl_{int} = 93 µL/min/mg protein)

indicate a moderate metabolic stability. In the case of **15**, an exceptional metabolic stability was observed: 100% of the compound is still intact after 45 min incubation.

Subsequently the compounds were investigated for permeation of Caco-2 cells (Table 5), which are generally accepted to be an appropriate model for the prediction of peroral absorption[57]. All compounds showed medium to high cell permeation.

Table 5: *Metabolic stability using liver microsomes and Caco-2 cell permeation.*

Cmpd	$t_{1/2}$ [min][a, b]	Cl_{int}[a, c] [µL/min/mg protein]	P_{app}[a, d] [$\cdot 10^{-6}$ cm/sec]	Permeability[e]
B	n.d.	n.d.	9.3	medium
2	14[f]	340[f]	14	high
3	289[f]	n.d.[f]	8	medium
11	50[f]	93[f]	16	high
15	n.c.[g, h]	n.c.[g, h]	19	high
Diazepam	41[f]	113[f]	n.d.	n.d.
Diphenhydramine	7[f]	680[f]	n.d.	n.d.

[a] Mean value of three determinations; [b] $t_{1/2}$: half-life; [c] Cl_{int}: intrinsic body clearance; [d] P_{app}: apparent permeability, relative standard deviation < 9%, [e] Permeability of the investigated molecules was classified according to Yee[68], [f] Rat liver microsomes, [g] Human liver microsomes, [h] Not calculated as **15** was metabolically stable over 45 min, n.d.: not determined, n.c.: not calculated.

For the evaluation of potential drug-drug interactions, compounds **2**, **9** and **11** were tested for inhibition of the most important hepatic CYP enzymes (six human hepatic enzymes: CYP1A2, 2B6, 2C9, 2C19, 2D6, 3A4, Table 6). Compounds **2** and **9** show high inhibition of CYP3A4 (IC_{50} = 0.22 and 0.04 µM, respectively), which is responsible for 50% of drug metabolism. In the case of compound **11**, only CYP2C19 (IC_{50} = 0.68 µM), was slightly inhibited, indicating a rather low risk of drug-drug interactions

Table 6: *Inhibition of selected hepatic CYP enzymes by compounds **2**, **9** and **14** and control inhibitors*

	IC_{50} [µM][a]					
	CYP1A2	CYP2B6	CYP2C9	CYP2C19	CYP2D6	CYP3A4
B	7.16	7.96	1.64	1.41	15.49	2.77
2	0.014	5.34	0.15	0.88	22.90	0.221
9	19.04	11.84	0.27	6.03	24.8	0.04
14	10.45	10.4	1.25	0.680	40.00	1.07
Control inhibitor	Furafylline	Tranyl cypromine	Sulphenazole	Tranylcypromine	Quinidine	Ketoconazole
	3.04	6.96	0.250	3.04	0.011	0.054

[a] Mean value of three determinations, standard deviation < 10% except for **2**: 20%

In vivo pharmacokinetics in the rat

The pharmacokinetics of **2**, **9**, **11** and **15** were determined in Wistar male rats. Compounds **B**, **9**, **11** and **15** were administered (10 mg/kg, n = 4) in cassette dosing approach. Compound **11** as well as compound **2** were also administered in a single dose (50 mg/kg, n = 5). Plasma samples were collected over 24 h and concentrations of each compound were independently measured by LC-MS/MS quantification. The pharmacokinetic profiles are presented in Table 7.

Beside the advantage that data can be generated for more compounds and that fewer animals are used, cassette dosing is mainly used to rank compounds. The data shown in Table 7 indicates that compound B has the best area under the curve (AUC) and C_{max}, followed by **9**, **15** and **11**. In single dose application, compounds **2** and **11** (AUC = 203 and 337 ng·h/mL, respectively) showed insufficient pharmacokinetics. Accordingly **2** and **11** could not be considered as potential candidates for further development. Even tested at a 5 times higher dose, a poorer AUC value (337 *vs*. 539 ng·h/mL for single dose and cassette dosing, respectively) is observed for 11 in the single dose application compared to the one in the cassette dosing experiment. This might be explained by a high metabolism of 11 in case of the single dose application while in the cassette experiment metabolism might be lower because of the competition between the test compounds and the metabolizing enzymes.

Considering that the half-life of the compounds in plasma ($t_{1/2}$) and oral delivery (C_{max} and AUC) are the most important criteria, the hydroxyphenyl compound **9** presents the most favorable profile (AUC = 10681 ng·h/mL, C_{max} = 843 ng/mL, $t_{1/2}$ = 0.9 h). Compound **15** also showed acceptable pharmacokinetics (AUC = 1332 ng·h/mL, C_{max} = 110 ng/mL, $t_{1/2}$ = 1.1 h).

Regarding all biological data compound **15** can be considered as a good drug candidat while compound **9** inhibits hepatic CYP enzymes and shows faster metabolism.

Table 7: *Pharmacokinetic parameters of compounds **B**, **2**, **9**, **11** and **15** in rats after oral application in cassette dosing (10 mg/kg) and /or in single dose application (50 mg/kg).*

Compound	Parameters[a]						
	Dose	$C_{max\ obs}$	C_z	$t_{max\ obs}$	t_z	$t_{1/2z}$	$AUC_{0\text{-}tz}$
	[mg/kg]	[ng/mL]	[ng/mL]	[h]	[h]	[h]	[ng·h/mL]
Cassette dosing							
B	10	861	115	4	24	5.9	11702
9	10	844	557	6	10	0.9	10681
11	10	43	0.4	2	24	2.4	539
15	10	110	67	2	10	1.1	1332
Single dose							
2	50	16	18	2	8	1.5	203
11	50	44	14	2	8	1.6	337

[a] $C_{max\ obs}$: maximal measured concentration, C_z: last analytical quantifiable concentration, $t_{max\ obs}$: time to reach the maximum measured concentration, t_z: time of the last sample which has an analytically quantifiable concentration, $t_{1/2z}$: half-life of the terminal slope of a concentration – time curve, $AUC_{0\text{-}tz}$: area under the concentration-time curve up to the time t_z of the last sample, $AUC_{0\text{-}\infty}$: area under the concentration-time curve extrapolated to infinity.

Discussion and conclusion

In this study, starting from the hit candidate **B**, we have developed new highly active inhibitors of 17β-HSD1. Exchange of the phenyl moiety by different heteroaromatics is well tolerated but does not improve the activity. Introduction of substituents like carboxylic acid, amide or morpholine into the phenyl ring are detrimental for the activity. However in this study a very interesting steroidomimetic[47] was identified as an inhibitor of 17β-HSD1: the sulfonamide **15**. It is highly potent (cell-free assay IC_{50} = 15 nM), selective toward 17β-HSD2 and the ERs. In addition, its cellular activity (T47D cells, IC_{50} = 71 nM) was improved compared to **B** (T47D cells, IC_{50} = 281 nM). Such a good cellular activity, which is identified for the first time in this class of inhibitors, indicates that it can permeate membranes easily. This finding demonstrates that **15** is clearly superior to the hybrid inhibitor (EM-1745) and slightly better than **B**. Its favorable pharmacokinetic profile in the rat validates **15**, together with **B** as two promising drug candidates.

To be appropriate as a drug, a compound should have a favorable ADME/Tox profile as well as no or low toxicity. Hepatic CYP interactions and metabolic stability have been evaluated for the most interesting compounds. Compound **15** showed favorable properties. As toxicity remains a major cause of attrition during development, further toxicology studies should be undertaken for compound **15**.

Off-target effects should be investigated by performing metabolomic studies and reactive metabolites should be identified and tested as they often cause toxicity.

Sulfonamides are often considered as key polar replacement groups for amides. Interestingly, in this study the exchange amide (**12**) / sulfonamide (**15**) led to an important increase in activity. This might be explained by the different geometry of the two groups: the amide is planar while the sulfonamide exhibits a tetrahedral shape, allowing these functional groups to undergo H-bond interactions with partners located in different areas of the binding site. Additionally, the presence of the second oxygen in the sulfonamide group is responsible for an increased acidity.

The selectivity demonstrated by the compounds toward 17β-HSD2 and the ERs is an important aspect of this study. Selectivity toward 17β-HSD2 is important because this enzyme catalyzes the reverse reaction compared to 17β-HSD1. 17β-HSD2 inhibitory activity was measured for all compounds and for the most potent ones a SF was determined. Considering that the expression of 17β-HSD2 is down-regulated in EDD tissues, selectivity should be achieved to mainly avoid systemic effects. 17β-HSD2 is present in several organs (liver, small intestine, endometrium, adrenals, bones). It can be expected that inhibition of this enzyme would mainly lead to side-effects in estrogen sensitive tissues like endometrium. However it is difficult to estimate how high the SF should be to minimize potential side effects.

Selectivity toward the ERs is also an important issue. Neither agonistic nor antagonistic effects can be tolerated for ERs to avoid activation of the receptor or systemic effects as observed with the use of anti-estrogens. After analysis of the ERs X-ray structures, it became apparent that designing large compounds would be beneficial to achieve selectivity toward the ERs as the ER binding site is smaller than that of 17β-HSD1 (no cofactor binding pocket present). For the evaluation of the ER affinity, RBA values were determined for all compounds showing a SF (toward 17β-HSD2) higher than 10. All newly reported inhibitors exhibit less than 0.1% relative binding affinity and are therefore considered not to bind to the ERs under in vivo conditions (T47D cell line). This assumption is based on the comparison of the compound's binding affinity with the one of E1. Under 17β-HSD1 inhibitor treatment E2 levels are decreased and E1 levels are maintained or slightly increased. At an E1 concentration of 50 nM, 71 nM of **15** are needed to suppress E2 formation by 50% (Table 4). E1 itself is a ligand of the ERs with a relative binding affinity of about 10%[58,59]. Thus, the inhibitors compete with E1 for the ER binding. Due to their RBA values of less than 0.1%, they will be displaced by E1 from the ER binding site and are unlikely to exert an ER mediated effect in vivo.

In this study the pyrimidine **5** was identified as a 17β-HSD2 inhibitor (IC_{50} = 249 nM and 1387 nM for 17β-HSD2 and 17β-HSD1, respectively with a SF of 6 in favor of 17β-HSD2). Contrarily the pyridines **2** and **4** showed a high potency for 17β-HSD1 (IC_{50} = 26 and 64 nM, respectively), indicating that the position of the N is not critical for the inhibition. It is striking that introduction of one additional nitrogen in **2** induced a dramatic loss in 17β-HSD1 inhibitory activity. This might be due to a direct effect of the nitrogen, but also to an unfavorable electronic distribution increasing the

electron deficiency in the heterocycle. As a consequence the acidity of the naphthol-OH located in ortho position to the heteroring is increased and prevents tight interactions with amino acids in the binding pocket as observed for **2** or **B**. In case of the dimethoxypyrimidine **8**, a regain in activity was observed (79% inhibition at 1 µM for **8**). This might be due to the increase of electronic density caused by the dimethoxy substituents or to the ortho effect forcing the second nitrogen in a different area.

Attempts to identify a new template for 17β-HSD2 inhibitors with only one OH group failed. Change in the dihydroxysubstitution pattern led to a complete loss of activity. Obviously this protein is rather inflexible i.e. it cannot adopt a favorable conformation to bind the ligand. A similar phenomenon has been observed for 17β-HSD1[47], where sharp SARs were also proposed as a result of enzyme rigidity.

In this paper, we reported on the synthesis and biological evaluation of new 1-substituted hydroxyphenyl-2-naphthols as 17β-HSD1 inhibitors. The goal of the study was the identification of a drug-like steroidomimetic with a good in vivo profile and ADME/Tox properties. We discovered the highly potent methyl sulfonamide **15** (with a very good cellular activity), which proved to be selective toward 17b-HSD2 and ERs. It shows good membrane permeation, low metabolism and rather good pharmacokinetics after peroral application. The efficacy of this compound still needs to be demonstrated in an appropriate disease oriented animal model. The identification of the species, in which this compound will show the best 17β-HSD1 inhibitory activity, will be the goal of another study.

Acknowledgments

We thank Anja Palusczak, Martina Jankowski, Janine Ludwig and Beate Geiger for their help in performing the in vitro tests (17β-HSD1 procedure B, 17β-HSD2 procedure D, ERα and ERβ). We are grateful to Hormos Medical Corp. (Turku, Finland) for performing the inhibition test on 17β-HSD1 (procedure A), 17β-HSD2 (procedure C). We acknowledge Jorge Calleros, Dr. J. Messinger and Dr. H. Thole for fruitful discussion as well as Pharmacelsus GmbH for performing the metabolic stability experiments, CYP inhibition tests and in vivo pharmacokinetics. We express our gratitude to D. Poirier for the gift of EM-1745. We thank the Fonds der Chemischen Industrie and Abbott (former Solvay Pharmaceuticals) for financial support. Patricia Kruchten is grateful to the European Postgraduate School GRK532 (DFG) for a scholarship.

Experimental Section

Chemical Methods

IR spectra were measured neat on a Bruker Vector 33FT-infrared spectrometer.

1H-NMR spectra were recorded on a Bruker DRX-500 (500 MHz) instrument at 300 K in $CDCl_3$, CD_3OD, DMSO-d6 and acetone-d6. Chemical shifts are reported in δ values (ppm), the hydrogenated residues of deuteriated solvents were used as internal standard ($CDCl_3$: δ = 7.26 ppm in 1H-NMR and δ = 77 ppm in 13C-NMR, CD_3OD: δ = 3.35 ppm in 1H-NMR and δ = 49.3 ppm in 13C-NMR, DMSO-d6: δ = 2.50 ppm in 1H-NMR and δ = 39.5 ppm in 13C-NMR, acetone-d6: δ = 2.05 ppm in 1H-NMR and δ = 29.8 ppm and 206.3 ppm in 13C-NMR). Signals are described as s, d, t, dd, ddd, m, b for singlet, doublet, triplet, doublet of doublet, doublet of doublet of doublet, multiplet and broad, respectively. All coupling constants (J) are given in Hz.

Mass spectra (ESI) were measured on a TSQ Quantum instrument (ThermoFisher).

Chemical names follow IUPAC nomenclature.

All microwave irradiation experiments were carried out in a CEM-Discover microwave apparatus.

Column chromatography was performed using silica gel (70-200 μm) and the reaction progress was determined by TLC analyses on ALUGRAM SIL G/UV254 (Macherey-Nagel). Preparative chromatography was performed on glass plate SIL G-100/UV254 (TLC, silica, 1 mm thick) from Macherey-Nagel. Visualization was accomplished with UV light. Purifications with preparative HPLC were carried out on a Agilent 1200 series HPLC system from Agilent Technologies, using a RP C18 Nucleodur 100-5 column (30•100mm/50 μm – from Macherey-Nagel GmbH) as stationary phase with acetonitrile/water as solvent in a gradient from 20:80 to 100:0.

Tested compounds are ≥ 95% chemical purity as measured by HPLC. The methods for HPLC analysis and a table of purity for all tested compounds are provided in the supporting information.

Starting materials (different boronic acids and compounds 9a, 16f, 18c and 19d) were purchased from Aldrich, Acros, Lancaster or Fluka and were used without purification. No attempts were made to optimize yields.

The following compounds were prepared according to previously described procedures: 6-(3-hydroxyphenyl)-2-naphthol **A**[47]; 6-(3-hydroxyphenyl)-1-phenyl-2-naphthol **B**[48]; 1-bromo-6-(3-hydroxyphenyl)-2-naphthol **1a**[48]; 1-bromo-2-methoxy-6-(3-methoxyphenyl)naphthalene **1b**[48]; 5-oxo-5,6,7,8-tetrahydronaphthalen-2-yl trifluoromethanesulfonate **16e**[60]; 6-(3-methoxyphenyl)-3,4-dihydronaphthalen-1(2H)-one **17d**[61]; 6-(4-hydroxyphenyl)-2-naphthol **20b**[52].

General procedure for ether cleavage:

Method A: To a solution of methoxy derivative (1 equivalent (eq)) in dichloromethane cooled at -78 °C boron tribromide (1M solution in dichloromethane, 3 eq to 5 eq per methoxy function) was slowly added under N2. The reaction mixture was stirred at -78 oC for 1 h and at room temperature overnight. The reaction was quenched by the addition of 2% Na_2CO_3 and extracted with

dichloromethane. The combined organic layers were washed with brine and dried over magnesium sulfate and concentrated to dryness.

General procedures for Suzuki coupling:

Method B: A mixture of arylbromide (1 eq), boronic acid (1 eq), 10% aqueous solution of sodium carbonate (2 eq) and tetrakis(triphenylphosphine) palladium(0) (0.05 eq) in toluene/ethanol mixture (oxygen free) was stirred at 80 °C under nitrogen for several hours. The reaction mixture was cooled to room temperature, quenched by the addition of 2% HCl and extracted with ethyl acetate. The organic layer was washed with brine, dried over magnesium sulfate and concentrated to dryness.

Method C: A mixture of arylbromide (1 eq), boronic acid (1.3 eq), cesium carbonate (2 eq) and tetrakis(triphenylphosphine) palladium(0) (0.05 eq) was suspended in a DME/EtOH/water (1:1:1) solution. The reaction mixture was exposed to microwave irradiation (25 min, 150 W, 150 °C, 15 bar). After reaching room temperature, 1N NH_4Cl was added and the aqueous layer was extracted with ethyl acetate. The organic layer was washed with brine, dried over sodium sulfate, filtered and concentrated to dryness.

Method D: A mixture of arylbromide (1 eq), boronic acid (1.2 eq), potassium carbonate (2 eq), palladium acetate (0.1 eq) and triphenylphosphine (0.2 eq) was dissolved in a 1,4-dioxane/EtOH (2:1) solution. The reaction mixture was exposed to microwave irradiation (15 min, 150 W, 150 °C, 15 bar). After reaching room temperature, the solution was filtered off, water and dichloromethane were added to the filtrate. The aqueous layer was extracted with dichloromethane and the combined organic layers were washed with brine, dried over sodium sulfate, filtered and concentrated to dryness.

1-(3-Furyl)-6-(3-hydroxyphenyl)-2-naphthol (1). The title compound was prepared by reaction of 1-bromo-6-(3-hydroxyphenyl)-2-naphthol **1a** (80 mg, 0.25 mmol, 1 eq) with furan-3-boronic acid (28 mg, 0.25 mmol, 1 eq) in toluene/ethanol 5:1 at 80 °C for 2 h according to Method B. The analytically pure compound was obtained after purification by column chromatography under pressure (dichloromethane/methanol 98:2) in 46% yield (35 mg). $C_{20}H_{14}O_3$; MW 302; 1H-NMR (CD_3OD + 3 drops $CDCl_3$): δ 7.98 (d, J = 1.9 Hz, 1H), 7.86 (d, J = 8.8 Hz, 1H), 7.79 (d, J = 8.8 Hz, 1H), 7.71-7.70 (m, 1H), 7.68-7.67 (m, 1H), 7.64 (dd, J = 2.2 Hz, J = 8.8 Hz, 1H), 7.31-7.28 (m, 1H), 7.23 (d, J = 8.8 Hz, 1H), 7.20-7.19 (m, 1H), 7.18-7.17 (m, 1H), 6.81 (ddd, J = 0.9 Hz, J = 2.5 Hz, J = 7.9 Hz, 1H), 6.65 (dd, J = 0.9 Hz, J = 1.9 Hz, 1H); 13C-NMR (CD_3OD + 3 drops $CDCl_3$): δ 161.3, 156.1, 146.6, 146.3, 145.8, 139.4, 137.2, 133.5, 133.0, 132.8, 129.4, 128.7, 122.5, 122.1, 121.9, 117.7, 117.5, 116.9, 116.1; IR: 3340, 1601, 1493 cm^{-1}; MS (ESI): 301 $(M-H)^-$.

6-(3-Hydroxyphenyl)-1-(pyridin-3-yl)-2-naphthol (2). The title compound was prepared by reaction of 1-bromo-6-(3-hydroxyphenyl)-2-naphthol **1a** (100 mg, 0.32 mmol, 1 eq) with pyridine-3-boronic acid (39 mg, 0.32 mmol, 1 eq) in toluene/ethanol 2:1 at 80 °C for 1 h according to Method B. The analytically pure compound was obtained after purification by column chromatography under pressure (gradient hexane/ethyl acetate 3:2 to 0:1) in 59% yield (59 mg). $C_{21}H_{15}NO_2$; MW 313; 1H-NMR (CD_3OD): δ 9.03-9.02 (m, 1H), 8.95 (d, J = 5.7 Hz, 1H), 8.81-8.79 (m, 1H), 8.30 (dd, J = 5.7 Hz, J =

7.9 Hz, 1H), 8.12 (d, J = 1.9 Hz, 1H), 8.04 (d, J = 8.8 Hz, 1H), 7.75 (dd, J = 1.9 Hz, J = 8.8 Hz, 1H), 7.55 (d, J = 8.5 Hz, 1H), 7.35 (d, J = 9.1 Hz, 1H), 7.32 (t, J = 7.9 Hz, 1H), 7.23-7.21 (m, 1H), 7.18-7.17 (m, 1H), 6.83 (ddd, J = 0.9 Hz, J = 2.5 Hz, J = 7.9 Hz, 1H); 13C-NMR (CD_3OD): δ 159.1, 154.1, 151.0, 144.8, 143.2, 140.8, 133.3, 133.1, 131.0, 130.3, 128.4, 128.2, 127.2, 124.1, 119.3, 119.1, 115.4, 114.8; IR: 3091, 1581, 1493, 1276, 1209, 1180 cm^{-1}; MS (ESI): 314 $(M+H)^+$.

6-**(3-Hydroxyphenyl)-1-(4-methoxypyridin-3-yl)-2-naphthol (3).** The title compound was prepared by reaction of 1-bromo-6-(3-hydroxyphenyl)-2-naphthol **1a** (100 mg, 0.32 mmol, 1 eq) with 4-methoxypyridin-3-boronic acid (49 mg, 0.32 mmol, 1 eq) in toluene/ethanol 5:1 at 80 °C for 3 h according to Method B. The analytically pure compound was obtained after purification by column chromatography under pressure (hexane/ethyl acetate 8:2) in 84% yield (92 mg). $C_{22}H_{17}NO_3$; MW 343; 1H-NMR (CD_3OD): δ 8.15 (d, J = 2.5 Hz, 1H), 8.01 (d, J = 1.9 Hz, 1H), 7.84 (d, J = 8.8 Hz, 1H), 7.72 (dd, J = 2.5 Hz, J = 8.5 Hz, 1H), 7.61 (dd, J = 1.9 Hz, J = 8.8 Hz, 1H), 7.49 (d, J = 8.8 Hz, 1H), 7.29-7.26 (m, 1H), 7.26 (d, J = 8.8 Hz, 1H), 7.20-7.19 (m, 1H), 7.18-7.17 (m, 1H), 6.98 (dd, J = 0.6 Hz, J = 8.5 Hz, 1H), 6.81 (ddd, J = 0.9 Hz, J = 2.5 Hz, J = 8.2 Hz, 1H), 4.02 (s, 3H); 13C-NMR (CD_3OD): δ 164.8, 158.9, 153.6, 149.5, 143.7, 143.5, 136.8, 134.7, 130.9, 130.3, 126.9, 126.8, 125.5, 119.4, 118.9, 115.1, 114.8, 111.2, 54.2; IR: 3357, 2917, 2849, 1586, 1493 cm^{-1}; MS (ESI): 344 $(M+H)^+$.

6-**(3-Hydroxyphenyl)-1-(pyridin-4-yl)-2-naphthol (4).** The title compound was prepared by reaction of 1-bromo-6-(3-hydroxyphenyl)-2-naphthol **1a** (100 mg, 0.32 mmol, 1 eq) with pyridine-4-boronic acid (39 mg, 0.32 mmol, 1 eq) in toluene/ethanol 5:1 at 100 °C for 1 h according to Method B. The analytically pure compound was obtained after purification by column chromatography under pressure (hexane/ethyl acetate 8:2) in 44% yield (44 mg). $C_{21}H_{15}NO_2$; MW 313; 1H-NMR (CD_3OD): δ 8.95 (d, J = 6.9 Hz, 2H), 8.26 (d, J = 2.6 Hz, 2H), 8.13 (d, J = 1.9 Hz, 1H), 8.06 (d, J = 8.8 Hz, 1H), 7.77 (dd, J = 1.9 Hz, J = 8.8 Hz, 1H), 7.65 (d, J = 8.8 Hz, 1H), 7.34 (d, J = 8.8 Hz, 1H), 7.34-7.31 (m, 1H), 7.24-7.22 (m, 1H), 7.18-7.17 (m, 1H), 6.84 (ddd, J = 0.9 Hz, J = 2.2 Hz, J = 7.9 Hz, 1H); 13C-NMR (CD_3OD): δ 159.0, 153.0, 149.9, 148.1, 143.5, 137.1, 133.8, 133.1, 133.0, 131.6, 130.9, 130.0, 129.9, 128.4, 127.2, 126.8, 125.2, 119.4, 119.3, 115.2, 114.8; IR: 3080, 1631, 1596, 1580, 1359, 1276, 1201, 1179 cm^{-1}; MS (ESI): 314 $(M+H)^+$.

1,6-Bis(3-hydroxyphenyl)-2-naphthol (9). The title compound was prepared by reaction of 1,6-dibromo-2-naphthol **9a** (200 mg, 0.66 mmol, 1 eq) with 3-hydroxyphenylboronic acid (366 mg, 2.64 mmol, 4 eq) in toluene for 15 h according to Method B. The analytically pure compound was obtained after purification by column chromatography (gradient dichloromethane/methanol 99:1 to 90:10) in 20% yield (43 mg). $C_{22}H_{16}O_3$; MW 328; 1H-NMR ($CDCl_3$ + 3 drops CD_3OD): δ 7.92 (d, J = 1.6 Hz, 1H), 7.76 (d, J = 8.8 Hz, 1H), 7.53 (dd, J = 1.9 Hz, J = 8.8 Hz, 1H), 7.48 (d, J = 8.8 Hz, 1H), 7.39-7.36 (m, 1H), 7.26-7.23 (m, 1H), 7.20 (d, J = 8.8 Hz, 1H), 7.16-7.14 (m, 1H), 7.11-7.10 (m, 1H), 6.92 (ddd, J = 0.9 Hz, J = 2.5 Hz, J = 8.2 Hz, 1H), 6.89-6.87 (m, 1H), 6.85-6.84 (m, 1H), 6.78 (ddd, J = 0.9 Hz, J = 2.5 Hz, J = 7.9 Hz, 1H); 13C-NMR ($CDCl_3$ + 3 drops CD_3OD): 190.7, 157.5, 156.9, 150.3, 142.6,

135.9, 135.8, 132.5, 130.5, 129.8, 129.5, 125.7, 125.2, 122.4, 121.0, 118.9, 117.9, 117.8, 115.3, 114.0; IR: 3355, 1702, 1581, 1494, 1447, 1203, 1154 cm^{-1}; MS (ESI): 327 $(M-H)^{-}$

1-(3-Aminophenyl)-6-(3-hydroxyphenyl)-2-naphthol (11). The title compound was prepared by reaction of 3-[2-methoxy-6-(3-methoxyphenyl)-1-naphthyl]aniline **11a** (1.0 g, 2.82 mmol, 1 eq) with boron tribromide (14.1 mL, 14.1 mmol, 5 eq) according to Method A. The title compound was obtained pure in a quantitative yield (922 mg). $C_{22}H_{17}NO_2$; MW 327; 1H-NMR (CD_3OD): δ 8.00 (d, J = 1.6 Hz, 1H), 7.82 (d, J = 8.8 Hz, 1H), 7.58 (dd, J = 1.9 Hz, J = 8.8 Hz, 1H), 7.54 (d, J = 8.8 Hz, 1H), 7.32-7.29 (m, 1H), 7.29 (t, J = 7.9 Hz, 1H), 7.23 (d, J = 9.1 Hz, 1H), 7.22-7.20 (m, 1H), 7.17-7.16 (m, 1H), 6.87-6.85 (m, 1H), 6.81-6.79 (m, 2H), 6.75-6.73 (m, 1H); 13C-NMR (CD_3OD): δ 158.9, 152.4, 148.9, 143.9, 136.6, 134.6, 130.8, 130.2, 130.0, 126.5, 126.4, 126.3, 123.5, 122.1, 119.5, 119.4, 119.3, 115.7, 115.0, 114.8; IR: 3387, 3282 cm^{-1}; MS (ESI): 326 $(M-H)^{-}$.

N-(3-[2-Hydroxy-6-(3-hydroxyphenyl)-1-naphthyl]phenyl)methanesulfonamide (15). The title compound was prepared by reaction of 1-bromo-6-(3-hydroxyphenyl)-2-naphthol **1a** (100 mg, 0.32 mmol, 1 eq) with N-[3-(4,4,5,5-tetramethyl-1,3,2-dioxaborolan-2-yl)phenyl]methanesulfonamide (94 mg, 0.32 mmol, 1 eq) in toluene/ethanol 5:1 for 2 h according to Method B. The analytically pure compound was obtained after purification by column chromatography under pressure (hexane/ethyl acetate 3:2) in 64% yield (83 mg). $C_{23}H_{19}NO_4S$; MW 405; 1H-NMR (CD_3OD + 3 drops $CDCl_3$): δ 8.01 (d, J = 1.6 Hz, 1H), 7.85 (d, J = 9.1 Hz, 1H), 7.60 (dd, J = 1.9 Hz, J = 8.8 Hz, 1H), 7.53-7.50 (m, 2H), 7.39-7.37 (m, 1H), 7.32-7.31 (m, 1H), 7.29 (t, J = 7.9 Hz, 1H), 7.26 (d, J = 8.8 Hz, 1H), 7.23-7.20 (m, 2H), 7.17-7.16 (m, 1H), 6.82-6.80 (m, 1H), 3.07 (s, 3H); 13C-NMR (CD_3OD + 3 drops CDCl3): δ 161.4, 155.3, 146.3, 142.1, 141.7, 139.3, 136.8, 133.4, 133.1, 133.0, 132.8, 131.2, 129.3, 129.2, 128.6, 127.0, 124.9, 123.0, 122.0, 121.9, 117.6, 117.4, 64.1; IR: 3406, 1704, 1600, 1585, 1323, 1268 cm^{-1}; MS (ESI): 404 $(M-H)^{-}$

LogP determination

The LogP values of compounds B and **1-15** were calculated from CambridgeSoft Chem & Bio Draw 11.0 using the ChemDrawPro 11.0 program.

Biological Methods

[2,4,6,7-^{3}H]-E1 and [2,4,6,7-^{3}H]-E2 were purchased from Perkin Elmer, Boston. Quickszint Flow 302 scintillator fluid was bought from Zinsser Analytic, Frankfurt. T47D cells (passage 9) were obtained from ECACC, Salisbury. FCS was purchased from Pan Biotech GmbH. Cell culture media was bought from CCPRO, Oberdorla. Other chemicals were purchased from Sigma, Roth or Merck.

1. 17β-HSD1 and 17β-HSD2 Enzyme preparation

Recombinant human enzyme (17β-HSD1: Procedure A and 17β-HSD2: Procedure C):

Recombinant baculovirus was produced by the "Bac to Bac Expression System" (Invitrogen). Recombinant bacmid was transfected to Sf9 insect cells using "Cellfectin Reagent" (Invitrogen). Sixty hours later cells were harvested; the microsomal fraction was isolated as described by Puranen[62].

Aliquots containing 17β-HSD1 or 17β-HSD2 were stored frozen until determination of enzymatic activity.

Human placental enzyme (17β-HSD1: Procedure B and 17β-HSD2: Procedure D):

17β-HSD1 and 17β-HSD2 were obtained from human placenta according to previously described procedures[56,63]. Fresh human placenta was homogenized and the enzymes were separated by fractional centrifugation at 1000 g, 10000 g and 150000 g. For the purification of 17β-HSD1, the cytosolic fraction was precipitated with ammonium sulfate. 17β-HSD2 was obtained from the microsomal fraction. Aliquots containing 17β-HSD1 or 17β-HSD2 were stored frozen.

2. Inhibition of 17β-HSD1 in cell-free assay

The synthesized compounds were tested for their ability to inhibit 17β-HSD1 according to Procedure A (recombinant human enzyme, percentage of inhibition determination) or Procedure B (human placental enzyme). For selected compounds, IC_{50} values were determined according to Procedure B (human placental enzyme). Procedure A and B differ in enzyme source and substrate concentration. The two procedures have been compared and give similar results.

Procedure A using recombinant human enzyme

Assay: Recombinant human protein (0.1 µg/mL) was incubated in 20 mM KH_2PO_4 pH 7.4 with 30 nM [^{3}H]-estrone and 1mM NADPH for 30 min at room temperature, in the presence of potential inhibitors at concentrations of 1 µM or 100 nM. Inhibitor stock solutions were prepared in DMSO. Final concentration of DMSO was adjusted to 1% in all samples. The enzyme reaction was stopped by addition of 10% trichloroacetic acid (final concentration). Samples were centrifuged in a microtiter plate at 4000 rpm for 10 min. Supernatants were applied to reverse phase HPLC on a Waters Symmetry C18 column, equipped with a Waters Sentry Guard column. Isocratic HPLC runs were performed at room temperature at a flow rate of 1 mL/min of acetonitrile/water (48:52) as eluent. Radioactivity of the eluate was monitored by a Packard Flow Scintillation Analyzer. Total radioactivities for E1 and E2 were determined in each sample. The conversion rate was calculated according to the following formula: % conversion = 100 [(cpm E2 in sample with inhibitor)/(cpm E1 in sample with inhibitor + cpm E2 in sample with inhibitor)]/[(cpm E2 in sample without inhibitor)/(cpm E1 in sample without inhibitor + cpm E2 in sample without inhibitor)]. Percentage of inhibition was calculated according to the following equation: % inhibition = 100 - % conversion. Each value was calculated from two independent experiments.

Procedure B using human placental enzyme

Assay: Inhibitory activities were evaluated by an established method with minor modifications[56,63-65]. Briefly, the enzyme preparation was incubated with NADH [0.5 mM] in the presence of potential inhibitors at 37 °C in a phosphate buffer (50 mM) supplemented with 20% of glycerol and EDTA 1mM. Inhibitor stock solutions were prepared in DMSO. Final concentration of DMSO was adjusted to 1% in all samples. The enzymatic reaction was started by addition of a mixture of unlabelled- and [^{3}H]-E1 (final concentration: 500 nM, 0.15 µCi). After 10 min, the incubation was stopped with $HgCl_2$

and the mixture was extracted with ether. After evaporation, the steroids were dissolved in acetonitrile. E1 and E2 were separated using acetonitrile/water (45:55) as mobile phase in a C18 RP chromatography column (Nucleodur C18, 3µm, Macherey-Nagel, Düren) connected to a HPLC-system (Agilent 1100 Series, Agilent Technologies, Waldbronn). Detection and quantification of the steroids were performed using a radioflow detector (Berthold Technologies, Bad Wildbad). The conversion rate was calculated according to the following equation: $\%conversion = \frac{\%E2}{\%E2 + \%E1} \bullet 100$. Each value was calculated from at least three independent experiments. Compounds showing < 10% inhibition were considered to be inactive.

3. Inhibition of 17β-HSD2 in cell-free assay

The synthesized compounds were tested for their ability to inhibit 17β-HSD2 according to Procedure C (recombinant human enzyme) or D (human placental enzyme). For select compounds, IC_{50} values were determined according to Procedure D (human placental enzyme). Procedure C and D differ from enzyme source and substrate concentration. The two procedures have been compared and give similar results.

Procedure C using recombinant human enzyme

The 17β-HSD2 inhibition assay was performed as previously described for 17β-HSD1 according to procedure A from the recombinant human protein, using [^{3}H]-E2 as substrate [30 nM] and NAD^+ [1 mM] as cofactor.

Procedure D using human placental enzyme

The 17β-HSD2 inhibition assay was performed similarly to the 17β-HSD1 procedure B. The microsomal fraction was incubated with NAD^+ [1.5 mM], test compound and a mixture of unlabelled- and [^{3}H]-E2 (final concentration: 500 nM, 0.11 µCi) for 20 min at 37 °C. Further treatment of the samples and HPLC separation was carried out as mentioned above for 17β-HSD1. Compounds showing < 10% inhibition were considered to be inactive.

4. Inhibition of 17β-HSD1 in cellular assay

Cellular 17β-HSD1 activity was measured using the breast cancer cell line T47D. A stock culture of T47D cells was grown in RPMI 1640 medium supplemented with 10% FCS, L-glutamine (2 mM), penicillin (100 IU/mL), streptomycin (100 µg/mL), insulin-zinc-salt (10 µg/mL) and sodium pyruvate (1 mM) at 37 °C under 5% CO_2 humidified atmosphere.

The cells were seeded into a 24-well plate at $1 \bullet 10^6$ cells/well in DMEM medium with FCS, L-glutamine and the antibiotics added in the same concentrations as mentioned above. After 24 h the medium was changed for fresh serum free DMEM and a solution of test compound in DMSO was added. Final concentration of DMSO was adjusted to 1% in all samples. After a pre-incubation of 30 min at 37 °C with 5% CO_2, the incubation was started by addition of a mixture of unlabelled- and [2, 4, 6, 7-^{3}H]- E1 (final concentration: 50 nM, 0.15 µCi). After 30 min incubation, the enzymatic reaction

was stopped by removing of the supernatant medium. The steroids were extracted with ether. Further treatment of the samples was carried out as mentioned for the 17β-HSD1 assay (Procedure B).

5. ER affinity

The binding affinity of selected compounds to the ERα and ERβ was determined according to Zimmermann et al.[66] using recombinant human proteins. Briefly, 0.25 pM of ERα or ERβ, respectively, were incubated with [3H]-E2 (10 nM) and test compound for 1 h at room temperature. The potential inhibitors were dissolved in DMSO (5% final concentration). Evaluation of non-specific-binding was performed with diethylstilbestrol (10 µM). After incubation, ligand-receptor complexes were selectively bound to hydroxyapatite (5 g/ 60 ml TE-buffer). The formed complex was separated, washed and resuspended in ethanol. For radiodetection, scintillator cocktail (Quickszint 212, Zinsser Analytic, Frankfurt) was added and the samples were measured in a liquid scintillation counter (Rack Beta Primo 1209, Wallac, Turku). From these results the percentage of [3H]-E2 displacement by the compounds was calculated. The plot of % displacement versus compound concentration resulted in sigmoidal binding curves. The compound concentration to displace 50% of the receptor bound [3H]-E2 were determined. Unlabelled E2 was used as a reference. For determination of the relative binding affinity (RBA) the ratio was calculated according to the following equation: $RBA[\%] = \frac{IC_{50}(E2)}{IC_{50}(compound)} \bullet 100$.[67] This results in an RBA value of 100% for E2. After the assay was established and validated a modification was made to increase throughput. Compounds were tested at concentrations of $1000 \times IC_{50}$ (E2) and $10000 \times IC_{50}$ (E2). Results were reported as RBA ranges. Compounds with less than 50% displacement of [3H]-E2 at a concentration of $10000 \times IC_{50}$ (E2) were classified as RBA <0.01%, compounds that displace more than 50% at $10000 \times IC_{50}$ (E2) but less than 50% at $1000 \times IC_{50}$ (E2) were classified as 0.01%<RBA<0.1%.

6. Caco-2 Assay

Caco-2 cell culture and transport experiments were performed according to Yee[68] with small modifications. Cell culture time was reduced from 21 to 10 days by increasing seeding density from $6.3 \bullet 10^4$ to $1.65 \bullet 10^5$ cells per well. Four reference compounds (atenolol, testosterone, ketoprofene, erythromycin) were used in each assay for validation of the transport properties of the Caco-2 cells. The compounds were applied to the cells as a mixture (cassette dosing) to increase the throughput of the cell permeability tests. The initial concentration of the compounds in the donor compartment was 50 µM (for each compound, in buffer 0.2 M MES, pH: 6.5, containing either 1% ethanol or DMSO). Samples were taken from the acceptor side after 0 min, 60, 120 and 180 min and from the donor side after 0 and 180 min. Each experiment was run in triplicate. The integrity of the monolayers was checked by measuring the transepithelial electrical resistance (TEER) before the transport experiments and by measuring lucifer yellow permeability after each assay. All samples of the CaCo-2 transport experiments were analyzed by LC/MS/MS. The apparent permeability coefficients (P_{app}) were

calculated using equation $P_{app} = \frac{dQ}{dtAc_0}$, where $\frac{dQ}{dt}$ is the appearance rate of mass in the acceptor compartment, A the surface area of the transwell membrane, and c0 the initial concentration in the donor compartment.

7. Metabolic stability assay

The assay was performed with liver microsomes from male Sprague-Dawley rats (BD Gentest, Heidelberg, Germany). Stock solutions (10 mM in acetonitrile) were diluted to give working solutions in 20% acetonitrile. The incubation solutions consisted of a microsomal suspension of 0.33 mg/mL of protein in phosphate buffer 100 mM pH 7.4 and 90 µL NADP-regenerating system ($NADP^+$ 1 mM, glucose-6-phosphate 5 mM, glucose-6-phosphate dehydrogenase 5 U/mL, $MgCl_2$ 5 mM).

The reaction was initiated by the addition of test compound to the pre-incubated microsomes/buffer mix at 37 °C. The samples were removed from the incubations after 0, 15, 30 and 60 minutes and processed for acetonitrile precipitation. The samples were analyzed by LC-MS/MS. Two control groups were run in parallel: positive controls (PC; n= 1) using 7-ethoxycoumarin as reference compound to prove the quality of the microsomal enzymatic activity and negative controls (NC; n= 1), using boiled microsomes (boiling water bath, 25 minutes) without regenerating system to ensure that the potential apparent loss of parent compound in the assay incubation is due to metabolism. The amount of compound in the samples was expressed in percentage of remaining compound compared to time point zero (= 100%). These percentages were plotted against the corresponding time points and the half-life time was derived by a standard fit of the data.

Intrinsic clearance (Cl_{int}) estimates were determined using the rate of parent disappearance. The slope (-k) of the linear regression from log [test compound] versus time plot was determined as well as the elimination rate constant: k= ln2/t1/2. The equation expressing the microsomal Cl_{int} can be derived: $Cl_{int} = k \bullet V \bullet f_u$ [µL/min/mg protein], where fu is the unbound fraction. V gives a term for the volume of the incubation expressed in micro liters per mg protein. As fu is not known for the tested compound, the calculation was performed with $f_u = 1$ (V = incubation volume [µL]/microsomal protein [mg] = 6667).

8. Inhibition of human hepatic CYPs.

The commercially available P450 inhibition kits from BD Gentest (Heidelberg, Germany) were used according to the instructions of the manufacturer. Compounds were tested for inhibition of the following enzymes: CYP1A2, 2B6, 2C9, 2C19, 2D6 and 3A4. Inhibitory potencies were determined as IC_{50}-values.

9. Evaluation of plasma concentrations of compounds B, 9, 11 and 15 after peroral application to adult male rats in cassette dosing.

Four adult male Wistar rats (Janvier, France) were used. Animals were housed in a temperature-controlled room (20-22 °C) and maintained in a 12 h light/12 h dark cycle. Food and water were available ad libitum. Rats were anaesthetized with a ketamine (135 mg/kg) / xylazine (10 mg/kg) mixture and cannulated with silicone tubing via the right jugular vein. Prior to the first blood

sampling, animals were connected to a counterbalanced system and tubing, to perform blood sampling in the freely moving rat. The tested compounds, dissolved in labrasol/water (1:1) as vehicle, were administered in peroral doses of 10 mg/kg in a cassette dosing approach. At time 0, the tested compounds were applied and blood samples (200 µL) were taken at 1, 2, 3, 4, 6, 8, 10 and 24 h post-dose, collected in heparinized tubes and stored on ice. Plasma was harvested and kept at –20 °C until being assayed. HPLC-MS/MS analysis and quantification of the samples was carried out on a Surveyor-HPLC-system coupled with a TSQ Quantum (ThermoFisher) triple quadrupole mass spectrometer equipped with an electrospray ioninterface (ESI).

10. Evaluation of plasma concentrations of compounds 2 and 11 after peroral application to adult male rats in single dose application.

Five adult male Wistar rats (Janvier, France) were used in similar conditions as described in the cassette dosing experiment. The tested compounds, dissolved in labrasol/water (1:1) as vehicle, were administered in peroral doses of 50 mg/kg. At time 0, the tested compounds were applied and blood samples (200 µL) were taken at 1, 2, 3, 4, 6, 8, 10 and 24 h post-dose, and treated the same way as described in the cassette dosing experiment.

References

(1) Liehr, J. G. Is estradiol a genotoxic mutagenic carcinogen? Endocr. Rev. 2000, 21, 40-54.
(2) Thomas, D. B. Do hormones cause breast cancer? Cancer 1984, 53, 595-604.
(3) Russo, J.; Fernandez, S. V.; Russo, P. A.; Fernbaugh, R.; Sheriff, F. S.; Lareef, H. M.; Garber, J.; Russo, I. 11037587H. 17beta-estradiol induces transformation and tumorigenesis in human breast epithelial cells. FASEB J. 2006, 20, 1622-1634.
(4) Dizerega, G. S.; Barber, D. L.; Hodgen, G. D. Endometriosis: role of ovarian steroids in initiation, maintenance, and suppression. Fertil. Steril. 1980, 33, 649-653.
(5) Zeitoun, K.; Takayama, K.; Sasano, H.; Suzuki, T.; Moghrabi, N.; Andersson, S.; Johns, A.; Meng, L.; Putman, M.; Carr, B.; Bulun, S. E. Deficient 17beta-hydroxysteroid dehydrogenase type 2 expression in endometriosis: failure to metabolize 17beta-estradiol. J. Clin. Endocrinol. Metab. 1998, 83, 4474-4480.
(6) Gobbi, S.; Cavalli, A.; Rampa, A.; Belluti, F.; Piazzi, L.; Paluszcak, A.; Hartmann, R. W.; Recanatini, M.; Bisi, A. Lead optimization providing a series of flavone derivatives as potent nonsteroidal inhibitors of the cytochrome P450 aromatase enzyme. J. Med. Chem. 2006, 49, 4777-4780.
(7) Le Borgne, M.; Marchand, P.; Duflos, M.; Delevoye-Seiller, B.; Piessard-Robert, S.; Le Baut, G.; Hartmann, R. W.; Palzer, M. Synthesis and in vitro evaluation of 3-(1-azolylmethyl)-1H-indoles and 3-(1-azolyl-1-phenylmethyl)-1H-indoles as inhibitors of P450 arom. Arch. Pharm. (Weinheim) 1997, 330, 141-145.
(8) Jacobs, C.; Frotscher, M.; Dannhardt, G.; Hartmann, R. W. 1-imidazolyl(alkyl)-substituted di- and tetrahydroquinolines and analogues: syntheses and evaluation of dual inhibitors of thromboxane A(2) synthase and aromatase. J. Med. Chem 2000, 43, 1841-1851.
(9) Baston, E.; Hartmann, R. W. N-substituted 4-(5-indolyl)benzoic acids. Synthesis and evaluation of steroid 5alpha-reductase type I and II inhibitory activity. Bioorg. Med. Chem. Lett. 1999, 9, 1601-1606.
(10) Picard, F.; Baston, E.; Reichert, W.; Hartmann, R. W. Synthesis of N-substituted piperidine-4-(benzylidene-4-carboxylic acids) and evaluation as inhibitors of steroid-5alpha-reductase type 1 and 2. Bioorg. Med. Chem. 2000, 8, 1479-1487.
(11) Picard, F.; Schulz, T.; Hartmann, R. W. 5-Phenyl substituted 1-methyl-2-pyridones and 4'-substituted biphenyl-4-carboxylic acids. synthesis and evaluation as inhibitors of steroid-5alpha-reductase type 1 and 2. Bioorg. Med. Chem. 2002, 10, 437-448.
(12) Aggarwal, S.; Thareja, S.; Verma, A.; Bhardwaj, T. R.; Kumar, M. An overview on 5alpha-reductase inhibitors. Steroids 2010, 75, 109-153.
(13) Speirs, V.; Green, A. R.; Atkin, S. L. Activity and gene expression of 17beta-hydroxysteroid dehydrogenase type I in primary cultures of epithelial and stromal cells derived from normal and tumourous human breast tissue: the role of IL-8. J. Steroid Biochem. Mol. Biol. 1998, 67, 267-274.
(14) Gunnarsson, C.; Ahnström, M.; Kirschner, K.; Olsson, B.; Nordenskjöld, B.; Rutqvist, L. E.; Skoog, L.; Stål, O. Amplification of HSD17B1 and ERBB2 in primary breast cancer. Oncogene 2003, 22, 34-40.
(15) Šmuc, T.; Hevir, N.; Pucelj Ribič, M.; Husen, B.; Thole, H.; Lanišnik Rižner, T. Disturbed estrogen and progesterone action in ovarian endometriosis. Mol. Cell. Endocrinol. 2009, 301, 59-64.
(16) Suzuki, T.; Miki, Y.; Nakamura, Y.; Moriya, T.; Ito, K.; Ohuchi, N.; Sasano, H. Sex steroid-producing enzymes in human breast cancer. Endocr. Relat. Cancer 2005, 12, 701-720.
(17) Chetrite, G. S.; Cortes-Prieto, J.; Philippe, J. C.; Wright, F.; Pasqualini, J. R. Comparison of estrogen concentrations, estrone sulfatase and aromatase activities in normal, and in cancerous, human breast tissues. J. Steroid Biochem. Mol. Biol. 2000, 72, 23-27.
(18) Husen, B.; Huhtinen, K.; Poutanen, M.; Kangas, L.; Messinger, J.; Thole, H. Evaluation of inhibitors for 17beta-hydroxysteroid dehydrogenase type 1 in vivo in immunodeficient mice inoculated with MCF-7 cells stably expressing the recombinant human enzyme. Mol. Cell. Endocrinol. 2006, 248, 109-113.
(19) Husen, B.; Huhtinen, K.; Saloniemi, T.; Messinger, J.; Thole, H. H.; Poutanen, M. Human hydroxysteroid (17beta) dehydrogenase 1 expression enhances estrogen sensitivity of MCF-7 breast cancer cell xenografts. Endocrinology 2006, 147, 5333-5339.
(20) Day, J. M.; Foster, P. A.; Tutill, H. J.; Parsons, M. F. C.; Newman, S. P.; Chander, S. K.; Allan, G. M.; Lawrence, H. R.; Vicker, N.; Potter, B. V. L.; Reed, M. J.; Purohit, A. 17beta-hydroxysteroid dehydrogenase Type 1, and not Type 12, is a target for endocrine therapy of hormone-dependent breast cancer. Int. J. Cancer 2008, 122, 1931-1940.

(21) Kruchten, P.; Werth, R.; Bey, E.; Oster, A.; Marchais-Oberwinkler, S.; Frotscher, M.; Hartmann, R. W. Selective inhibition of 17beta-hydroxysteroid dehydrogenase type 1 (17betaHSD1) reduces estrogen responsive cell growth of T47-D breast cancer cells. J. Steroid Biochem. Mol. Biol. 2009, 114, 200-206.
(22) Moeller, G.; Adamski, J. Multifunctionality of human 17beta-hydroxysteroid dehydrogenases. Mol. Cell. Endocrinol. 2006, 248, 47-55.
(23) Azzi, A.; Rehse, P. H.; Zhu, D. W.; Campbell, R. L.; Labrie, F.; Lin, S. X. Crystal structure of human estrogenic 17 beta-hydroxysteroid dehydrogenase complexed with 17 beta-estradiol. Nat. Struct. Biol. 1996, 3, 665-668.
(24) Breton, R.; Housset, D.; Mazza, C.; Fontecilla-Camps, J. C. The structure of a complex of human 17beta-hydroxysteroid dehydrogenase with estradiol and NADP+ identifies two principal targets for the design of inhibitors. Structure 1996, 4, 905-915.
(25) Gangloff, A.; Shi, R.; Nahoum, V.; Lin, S. Pseudo-symmetry of C19 steroids, alternative binding orientations, and multispecificity in human estrogenic 17beta-hydroxysteroid dehydrogenase. FASEB J. 2003, 17, 274-276.
(26) Ghosh, D.; Pletnev, V. Z.; Zhu, D. W.; Wawrzak, Z.; Duax, W. L.; Pangborn, W.; Labrie, F.; Lin, S. X. Structure of human estrogenic 17 beta-hydroxysteroid dehydrogenase at 2.20 Å resolution. Structure 1995, 3, 503-513.
(27) Han, Q.; Campbell, R. L.; Gangloff, A.; Huang, Y. W.; Lin, S. X. Dehydroepiandrosterone and dihydrotestosterone recognition by human estrogenic 17beta-hydroxysteroid dehydrogenase. C-18/c-19 steroid discrimination and enzyme-induced strain. J. Biol. Chem. 2000, 275, 1105-1111.
(28) Mazza, C.; Breton, R.; Housset, D.; Fontecilla-Camps, J. C. Unusual charge stabilization of NADP+ in 17beta-hydroxysteroid dehydrogenase. J. Biol. Chem. 1998, 273, 8145-8152.
(29) Qiu, W.; Zhou, M.; Labrie, F.; Lin, S. Crystal structures of the multispecific 17beta-hydroxysteroid dehydrogenase type 5: critical androgen regulation in human peripheral tissues. Mol. Endocrinol. 2004, 18, 1798-1807.
(30) Sawicki, M. W.; Erman, M.; Puranen, T.; Vihko, P.; Ghosh, D. Structure of the ternary complex of human 17beta-hydroxysteroid dehydrogenase type 1 with 3-hydroxyestra-1,3,5,7-tetraen-17-one (equilin) and NADP+. Proc. Natl. Acad. Sci. U.S.A 1999, 96, 840-845.
(31) Mazumdar, M.; Fournier, D.; Zhu, D.; Cadot, C.; Poirier, D.; Lin, S. Binary and ternary crystal structure analyses of a novel inhibitor with 17beta-HSD type 1: a lead compound for breast cancer therapy. Biochem. J. 2009, 424, 357-366.
(32) Poirier, D. Inhibitors of 17 beta-hydroxysteroid dehydrogenases. Curr. Med. Chem. 2003, 10, 453-477.
(33) Day, J. M.; Tutill, H. J.; Purohit, A.; Reed, M. J. Design and validation of specific inhibitors of 17beta-hydroxysteroid dehydrogenases for therapeutic application in breast and prostate cancer, and in endometriosis. Endocr. Relat. Cancer 2008, 15, 665-692.
(34) Brožic, P.; Lanišnik Rižner, T.; Gobec, S. Inhibitors of 17beta-hydroxysteroid dehydrogenase type 1. Curr. Med. Chem. 2008, 15, 137-150.
(35) Poirier, D. Advances in development of inhibitors of 17beta hydroxysteroid dehydrogenases. Anticancer Agents Med. Chem. 2009, 9, 642-660.
(36) Poirier, D. 17beta-Hydroxysteroid dehydrogenase inhibitors: a patent review. Expert Opin Ther Pat 2010, 20, 1123-1145.
(37) Day, J. M.; Tutill, H. J.; Purohit, A. 17b-Hydroxysteroid dehydrogenase inhibitors. Minerva Endocrinol 2010, 35, 87-108.
(38) Marchais-Oberwinkler, S.; Henn, C.; Möller, G.; Klein, T.; Lordon, M.; Negri, M.; Oster, A.; Spadaro, A.; Werth, R.; Xu, K.; Frotscher, M.; Hartmann, R. W.; Adamski, J. 17β-Hydroxysteroid dehydrogenases (17β-HSD): novel therapeutic targets, protein structures and recent progress in inhibitor development. J. Steroid Biochem. Mol. Biol. in preparation.
(39) Deluca, D.; Krazeisen, A.; Breitling, R.; Prehn, C.; Möller, G.; Adamski, J. Inhibition of 17beta-hydroxysteroid dehydrogenases by phytoestrogens: comparison with other steroid metabolizing enzymes. J. Steroid Biochem. Mol. Biol. 2005, 93, 285-292.
(40) Messinger, J.; Hirvelä, L.; Husen, B.; Kangas, L.; Koskimies, P.; Pentikäinen, O.; Saarenketo, P.; Thole, H. New inhibitors of 17beta-hydroxysteroid dehydrogenase type 1. Mol. Cell. Endocrinol. 2006, 248, 192-198.
(41) Lilienkampf, A.; Karkola, S.; Alho-Richmond, S.; Koskimies, P.; Johansson, N.; Huhtinen, K.; Vihko, K.; Wähälä, K. Synthesis and biological evaluation of 17beta-hydroxysteroid dehydrogenase type 1 (17beta-HSD1) inhibitors based on a thieno[2,3-d]pyrimidin-4(3H)-one core. J. Med. Chem. 2009, 52, 6660-6671.
(42) Bey, E.; Marchais-Oberwinkler, S.; Kruchten, P.; Frotscher, M.; Werth, R.; Oster, A.; Algül, O.; Neugebauer, A.; Hartmann, R. W. Design, synthesis and biological evaluation of

bis(hydroxyphenyl) azoles as potent and selective non-steroidal inhibitors of 17beta-hydroxysteroid dehydrogenase type 1 (17beta-HSD1) for the treatment of estrogen-dependent diseases. Bioorg. Med. Chem. 2008, 16, 6423-6435.

(43) Bey, E.; Marchais-Oberwinkler, S.; Werth, R.; Negri, M.; Al-Soud, Y. A.; Kruchten, P.; Oster, A.; Frotscher, M.; Birk, B.; Hartmann, R. W. Design, synthesis, biological evaluation and pharmacokinetics of bis(hydroxyphenyl) substituted azoles, thiophenes, benzenes, and aza-benzenes as potent and selective nonsteroidal inhibitors of 17beta-hydroxysteroid dehydrogenase type 1 (17beta-HSD1). J. Med. Chem. 2008, 51, 6725-6739.

(44) Al-Soud, Y. A.; Bey, E.; Oster, A.; Marchais-Oberwinkler, S.; Werth, R.; Kruchten, P.; Frotscher, M.; Hartmann, R. W. The role of the heterocycle in bis(hydroxyphenyl)triazoles for inhibition of 17beta-Hydroxysteroid Dehydrogenase (17beta-HSD) type 1 and type 2. Mol. Cell. Endocrinol. 2009, 301, 212-215.

(45) Bey, E.; Marchais-Oberwinkler, S.; Negri, M.; Kruchten, P.; Oster, A.; Klein, T.; Spadaro, A.; Werth, R.; Frotscher, M.; Birk, B.; Hartmann, R. W. New insights into the SAR and binding modes of bis(hydroxyphenyl)thiophenes and -benzenes: influence of additional substituents on 17beta-hydroxysteroid dehydrogenase type 1 (17beta-HSD1) inhibitory activity and selectivity. J. Med. Chem. 2009, 52, 6724-6743.

(46) Oster, A.; Klein, T.; Werth, R.; Kruchten, P.; Bey, E.; Negri, M.; Marchais-Oberwinkler, S.; Frotscher, M.; Hartmann, R. W. Novel estrone mimetics with high 17beta-HSD1 inhibitory activity. Bioorg. Med. Chem. 2010, 18, 3494-3505.

(47) Frotscher, M.; Ziegler, E.; Marchais-Oberwinkler, S.; Kruchten, P.; Neugebauer, A.; Fetzer, L.; Scherer, C.; Müller-Vieira, U.; Messinger, J.; Thole, H.; Hartmann, R. W. Design, synthesis, and biological evaluation of (hydroxyphenyl)naphthalene and -quinoline derivatives: potent and selective nonsteroidal inhibitors of 17beta-hydroxysteroid dehydrogenase type 1 (17beta-HSD1) for the treatment of estrogen-dependent diseases. J. Med. Chem. 2008, 51, 2158-2169.

(48) Marchais-Oberwinkler, S.; Kruchten, P.; Frotscher, M.; Ziegler, E.; Neugebauer, A.; Bhoga, U.; Bey, E.; Müller-Vieira, U.; Messinger, J.; Thole, H.; Hartmann, R. W. Substituted 6-phenyl-2-naphthols. Potent and selective nonsteroidal inhibitors of 17beta-hydroxysteroid dehydrogenase type 1 (17beta-HSD1): design, synthesis, biological evaluation, and pharmacokinetics. J. Med. Chem. 2008, 51, 4685-4698.

(49) Marchais-Oberwinkler, S.; Frotscher, M.; Ziegler, E.; Werth, R.; Kruchten, P.; Messinger, J.; Thole, H.; Hartmann, R. W. Structure-activity study in the class of 6-(3'-hydroxyphenyl)naphthalenes leading to an optimization of a pharmacophore model for 17beta-hydroxysteroid dehydrogenase type 1 (17beta-HSD1) inhibitors. Mol. Cell. Endocrinol. 2009, 301, 205-211.

(50) Bhatt, M. V.; Kulkarni, S. U. Cleavage of Ethers. Synthesis 1983, 1983, 249-282.

(51) Miyaura, N.; Suzuki, A. Palladium-Catalyzed Cross-Coupling Reactions of Organoboron Compounds. Chem. Rev. 1995, 95, 2457-2483.

(52) Mewshaw, R. E.; Edsall, R. J.; Yang, C.; Manas, E. S.; Xu, Z. B.; Henderson, R. A.; Keith, J. C.; Harris, H. A. ERbeta ligands. 3. Exploiting two binding orientations of the 2-phenylnaphthalene scaffold to achieve ERbeta selectivity. J. Med. Chem. 2005, 48, 3953-3979.

(53) Koubachi, J.; El Kazzouli, S.; Berteina-Raboin, S.; Mouaddib, A.; Guillaumet, G. Synthesis of Polysubstituted Imidazo[1,2-a]pyridines via Microwave-Assisted One-Pot Cyclization/Suzuki Coupling/Palladium-Catalyzed Heteroarylation. J. Org. Chem. 2007, 72, 7650-7655.

(54) Carreño, M.; García Ruano, J.; Sanz, G.; Toledo, M.; Urbano, A. Orthobromination of phenols predominates in CS2. Synlett 1997, 1997, 1241-1242.

(55) Qiu, W.; Campbell, R. L.; Gangloff, A.; Dupuis, P.; Boivin, R. P.; Tremblay, M. R.; Poirier, D.; Lin, S. A concerted, rational design of type 1 17beta-hydroxysteroid dehydrogenase inhibitors: estradiol-adenosine hybrids with high affinity. FASEB J. 2002, 16, 1829-1831.

(56) Kruchten, P.; Werth, R.; Marchais-Oberwinkler, S.; Frotscher, M.; Hartmann, R. W. Development of a biological screening system for the evaluation of highly active and selective 17beta-HSD1-inhibitors as potential therapeutic agents. Mol. Cell. Endocrinol. 2009, 301, 154-157.

(57) Hidalgo, I. J. Assessing the absorption of new pharmaceuticals. Curr. Top. Med. Chem. 2001, 1, 385-401.

(58) Pillon, A.; Boussioux, A.; Escande, A.; Aït-Aïssa, S.; Gomez, E.; Fenet, H.; Ruff, M.; Moras, D.; Vignon, F.; Duchesne, M.; Casellas, C.; Nicolas, J.; Balaguer, P. Binding of estrogenic compounds to recombinant estrogen receptor-alpha: application to environmental analysis. Environ. Health Perspect 2005, 113, 278-284.

(59) Zhu, B. T.; Han, G.; Shim, J.; Wen, Y.; Jiang, X. Quantitative structure-activity relationship of various endogenous estrogen metabolites for human estrogen receptor alpha and beta

subtypes: Insights into the structural determinants favoring a differential subtype binding. Endocrinology 2006, 147, 4132-4150.
(60) Ahmad, S.; Doweyko, L.; Ashfaq, A.; Ferrara, F. N.; Bisaha, S. N.; Schmidt, J. B.; DiMarco, J.; Conder, M. L.; Jenkins-West, T.; Normandin, D. E.; Russell, A. D.; Smith, M. A.; Levesque, P. C.; Lodge, N. J.; Lloyd, J.; Stein, P. D.; Atwal, K. S. Tetrahydronaphthalene-derived amino alcohols and amino ketones as potent and selective inhibitors of the delayed rectifier potassium current IKs. Bioorg. Med. Chem. Lett. 2004, 14, 99-102.
(61) Zhang, P.; Kern, J. C.; Terefenko, E. A.; Trybulski, E. J. 5-Aryl-indan-1-ol and analogs useful as progesterone receptor modulators. United states patent application publication US2009/0325916A1, Dec. 31, 2009.
(62) Puranen, T. J.; Poutanen, M. H.; Peltoketo, H. E.; Vihko, P. T.; Vihko, R. K. Site-directed mutagenesis of the putative active site of human 17 beta-hydroxysteroid dehydrogenase type 1. Biochem. J. 1994, 304 (Pt 1), 289-293.
(63) Lin, S. X.; Yang, F.; Jin, J. Z.; Breton, R.; Zhu, D. W.; Luu-The, V.; Labrie, F. Subunit identity of the dimeric 17 beta-hydroxysteroid dehydrogenase from human placenta. J. Biol. Chem. 1992, 267, 16182-16187.
(64) Sam, K. M.; Auger, S.; Luu-The, V.; Poirier, D. Steroidal spiro-gamma-lactones that inhibit 17 beta-hydroxysteroid dehydrogenase activity in human placental microsomes. J. Med. Chem. 1995, 38, 4518-4528.
(65) Sam, K. M.; Boivin, R. P.; Tremblay, M. R.; Auger, S.; Poirier, D. C16 and C17 derivatives of estradiol as inhibitors of 17 beta-hydroxysteroid dehydrogenase type 1: chemical synthesis and structure-activity relationships. Drug Des. Discov. 1998, 15, 157-180.
(66) Zimmermann, J.; Liebl, R.; von Angerer, E. 2,5-Diphenylfuran-based pure antiestrogens with selectivity for the estrogen receptor alpha. J. Steroid Biochem. Mol. Biol. 2005, 94, 57-66.
(67) Hartmann, R. W. Influence of alkyl chain ramification on estradiol receptor binding affinity and intrinsic activity of 1,2-dialkylated 1,2-bis(4- or 3-hydroxyphenyl)ethane estrogens and antiestrogens. J. Med. Chem. 1986, 29, 1668-1674.
(68) Yee, S. In vitro permeability across Caco-2 cells (colonic) can predict in vivo (small intestinal) absorption in man--fact or myth. Pharm. Res. 1997, 14, 763-766.

3.3 Lead optimization of 17β-HSD1 inhibitors of the (hydroxyphenyl)naphthol sulfonamide type for the treatment of endometriosis

Claudia Henn, Almuth Einspanier, Sandrine -Marchais-Oberwinkler, Martin Frotscher and Rolf W. Hartmann

Journal of Medicinal Chemistry **2012,** 55, (7), 3307-3318

Publication III

Abstract

The reduction of estrone to estradiol, the most potent estrogen in human, is catalyzed by 17β-hydroxysteroid dehydrogenase type 1 (17β-HSD1). A promising approach for the treatment of estrogen dependent diseases is the reduction of intracellular estradiol formation by inhibition of 17β-HSD1. For the species specific optimization of the (hydroxyphenyl)naphthols a combinatorial approach was applied and enhanced by a focused synthesis that resulted in the aromatic substituted (hydroxyphenyl)naphthol sulfonamides. Rigidification of **12** led to the 4-indolylsulfonamide **30** which is a highly active and selective human 17β-HSD1 inhibitor, as well as a highly potent and selective inhibitor of 17β-HSD1 from *Callithrix jacchus*. It shows no affinity to the estrogen receptors α and β and good intracellular activity (T-47D). Thus, compound **30** shows good properties for further ADMET studies and might be a candidate for the *in vivo* proof of concept in *Callithrix jacchus*.

Introduction

Estradiol (E2), the most important estrogen in females is responsible for the development and differentiation of estrogen-sensitive tissues, e.g. breast and endometrial tissue. It is mainly produced in the granulosa cells of the ovaries. In a first step estrone (E1) is formed by aromatization of androstenedione, followed by the local conversion of E1 to E2 by 17β-hydroxysteroid dehydrogenase type 1 (17β-HSD1, Figure 1). Beside its physiological effects E2 is involved in the development and progression of estrogen dependent diseases (EDD) like breast cancer,[1,2] ovarian tumor,[3] endometriosis,[4,5] endometrial hyperplasia,[6] and uterine leiomyoma.[7] The conventional treatment for these diseases is the therapy with antiestrogens,[8] selective estrogen receptor modulators (SERMs) or aromatase inhibitors[9,10] to block the synthesis of estrogens on the systemic level.

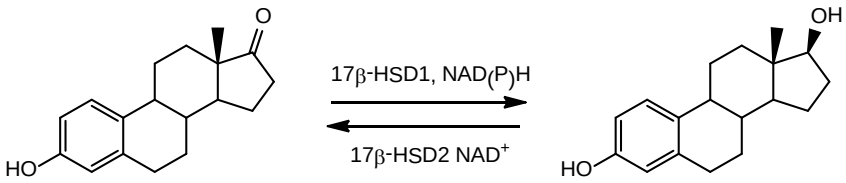

***Figure 1**: Interconversion of estrone (E1) to estradiol (E2)*

Notably, mRNA of 17β-HSD1, which is often used as prognostic marker, has been found highly expressed in breast cancer[11] and endometriotic tissue.[12] Therefore the development of 17β-HSD1 inhibitors is an attractive approach to reduce the intracellular E2 levels and to treat EDDs, particularly, since such an intracrine concept has already been proven to be successful for the treatment of the androgen dependent diseases BPH (benign prostatic hyperplasia) and alopecia by using 5α-reductase inhibitors.[13,14]

To decrease undesirable pharmacological effects, the 17β-HSD1 inhibitors should be selective toward 17β-hydroxysteroid dehydrogenase type 2 (17β-HSD2), which catalyzes the deactivation of E2 to E1 (Figure 1) and is downregulated in malignant breast cancer cells. Specific inhibition of 17β-HSD2 was recently published as a novel approach to prevent osteoporosis.[15-19] Further, potential inhibitors should not show any affinity to estrogen receptors α and β (ERα and β) in order to reduce the risk of estrogenic side effects.

Some 17β-HSD1 inhibitors are already described. Most of them are based on a steroidal skeleton.[20-22] In the last couple of years selective non-steroidal inhibitors were published by others[23-26] and our group. Our work is based on a long time experience in steroid mimetics which led to the development of selective inhibitors of CYP19,[27,28] CYP17,[29-31] CYP11B2[32-34] and CYP11B1[35,36] and resulted in three classes of non-steroidal 17β-HSD1 inhibitors: the bis(hydroxyphenyl)heterocycles,[37-42] hydroxyphenylmethanones[43-45] and the (hydroxyphenyl)naphthols.[46-48] Recently we reported on the optimization of the latter class that led to the identification of a highly active and selective sulfonamide substituted derivative **A** with no affinity to ERα and ERβ (Figure 2).[49]

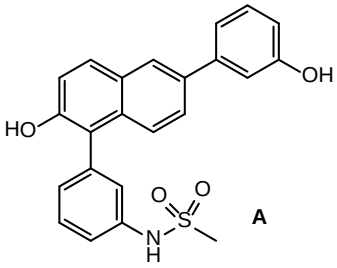

Figure 2: *Recently published inhibitor*

As this compound showed good intracellular activity and favourable pharmacokinetics it should be the starting point for the establishment of an *in vivo* proof of concept in a disease oriented animal model. Several animal models for breast cancer and endometriosis using different species are available.[50-54] For an *in vivo* experiment with rodents there are either rodent enzyme active inhibitors necessary or experiments with xenograft models or transgenic mice have to be performed. Previous studies had revealed that representative inhibitors of the aforementioned classes only show low inhibition of E2-formation in the rat and in the mouse.[42, 43, 45] Therefore we focus on a species, in which 17β-HSD1 shows high sequence identity to the human enzyme to increase the probability to find compounds for *in vivo* experiments. Due to the high phylogenetic similarity of monkeys and humans, models of the former species are preferable. An appropriate animal should be *Callithrix jacchus* (common marmoset), as there is an endometriosis model described.[54] The high overall sequence identity of 80% between human and *Callithrix jaccus* 17β-HSD1 (*cj*17β-HSD1) increases up to 87%, if only the steroidal binding site is considered, with five major amino acid variations observed in common marmoset: A191P, E194Q, S222N, V225I and E282N.[55] This high identity makes the animal model very appropriate for *in vivo* evaluation of designed inhibitors. Two different forms of endometriosis can be induced: developing and established endometriosis. Furthermore the pathogenesis of endometriosis and the relationship between local and central estrogen metabolism have been studied, which is important for validation of the intracrine concept of 17β-HSD1 inhibitors.

After having established an assay to screen our in house library for compounds showing good inhibition of *cj*17β-HSD1, the lead compound in the class of the sulfonamide substituted hydroxyphenylnaphthols (Figure 2), however, showed only very low inhibitory potency (16 % inhibition at 50 nM) and no selectivity toward *cj*17β-HSD2 (23 % inhibition at 50nM).[55] Therefore it is our aim to increase the potency toward *cj*17β-HSD1 without decreasing the activity toward *h*17β-HSD1 in this class of compounds to identify a potential candidate for the *in vivo* proof of concept in the common marmoset.

In this study we report on the optimization of the hydroxyphenylnaphthols at the sulfonamide core. In a previous study it was found that the exchange of aliphatic sulfonamides by aromatic sulfonamides led to an increase in activity toward *h*17β-HSD1.[45] Therefore we designed and synthesized a library (parallel synthesis) of aromatic substituted sulfonamides (Figure 3) and the compounds were evaluated

for inhibition of *h*17β-HSD1 in a cell-free assay. The most promising compounds were resynthesized in a larger amount, and were further evaluated biologically. To optimize and to derive a meaningful SAR, substituents in the phenyl moieties were varied regarding their electronic and lipophilic properties (Table 1).

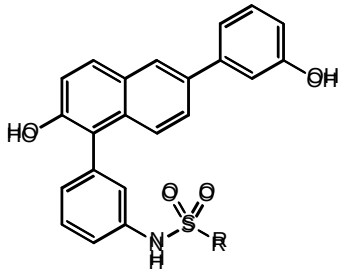

Cmpd	R	Cmpd	R	Cmpd	R	Cmpd	R
1	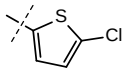	**2**	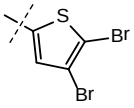	**3**	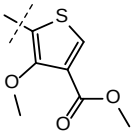	**4**	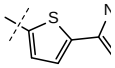
5	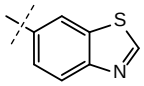	**6**	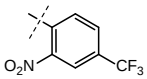	**7**	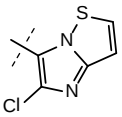	**8**	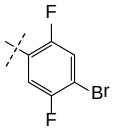
9	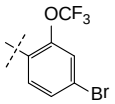	**10**	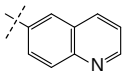	**11**		**14**	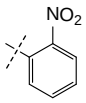
15	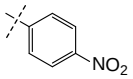	**17**	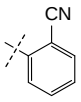				

Figure 3: Library compounds

Chemistry

The available 2-bromo-6-methoxynaphthalene was brominated with *N*-bromosuccinimide followed by Suzuki cross-coupling with 3-(methoxyphenyl) boronic acid, sodium carbonate and $Pd(PhP_3)_4$ in toluene/H_2O/MeOH (3:2:2) to obtain compound **1c.** In a second Suzuki cross-coupling with 3-(aminophenyl) boronic acid, caesium carbonate and $Pd(Ph_3P)_4$ in dimethoxyethane/EtOH/H_2O (1:1:1) compound **1b** was prepared (Scheme 1).

Scheme 1[a]: Synthesis of compound **1b**.

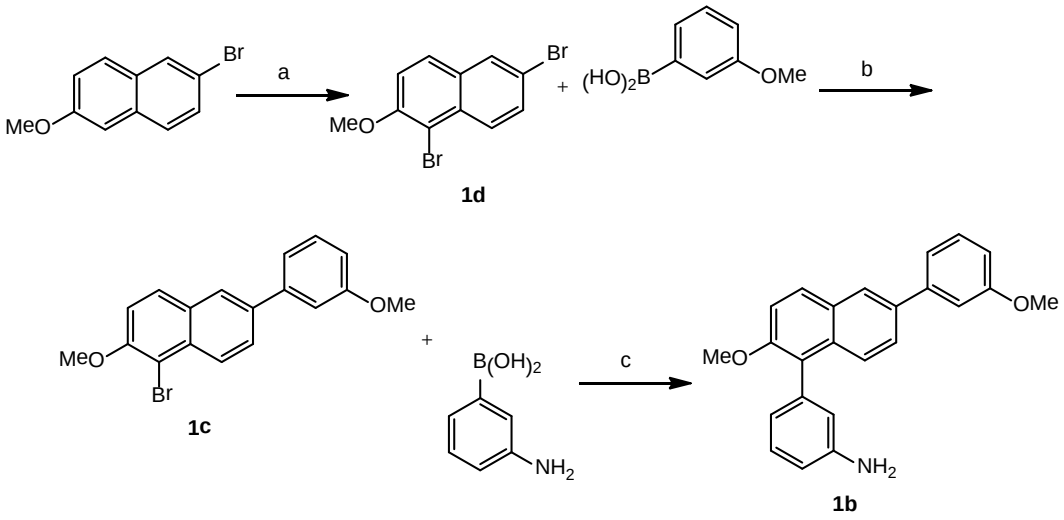

[a]**Reagents and conditions**: (a) NBS, reflux, 2 h; (b) Na_2CO_3, $Pd(PhP_3)_4$, toluene/H_2O/MeOH (3:2:2); (c) Cs_2CO_3, $Pd(PhP_3)_4$, dimethoxyethane/EtOH/H_2O (1:1:1), 15 min microwave irradiation (150 °C, 1.5 bar).

The library synthesis was started using 3-(2-methoxy-6-(3-methoxyphenyl)naphthalen-1-yl)aniline (**1b**) and an ether cleavage according to Method C was performed yielding the demethylated compound **1a**. The diversity was introduced with different commercially available sulfonyl chlorides (**1 – 11, 14, 15, 17,** Method A**,** Scheme 2).

Scheme 2[a]: Synthesis of library compounds **1-11, 14, 15** and **17.**

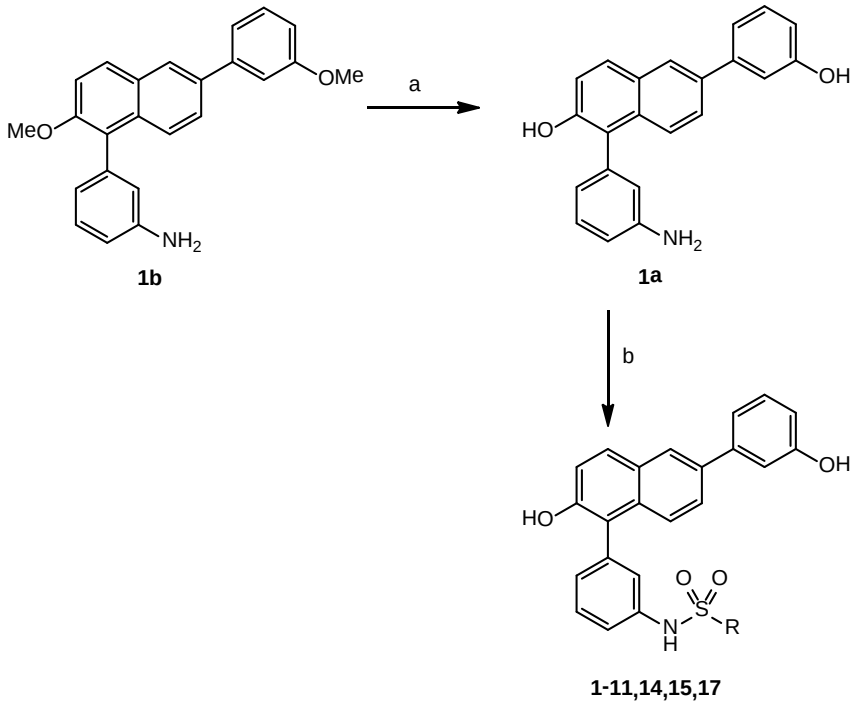

[a]**Reagents and conditions**: (a) BBr_3, CH_2Cl_2, -78 to RT, 18h, Method C; (b) PS-morpholine, PS-DMAP, THF, 48 h, RT, Method A.

The important intermediate **12b** was synthesized in four steps. After bromination of β-naphthol in glacial acetic acid the β-hydroxy function was protected with benzyl bromide **(12d**). Via two successive Suzuki cross-couplings with 3-(benzoxyphenyl) and 3-(aminophenyl) boronic acid **12b** was obtained (Scheme 3).

Scheme 3[a]: Synthesis of compound **12b**.

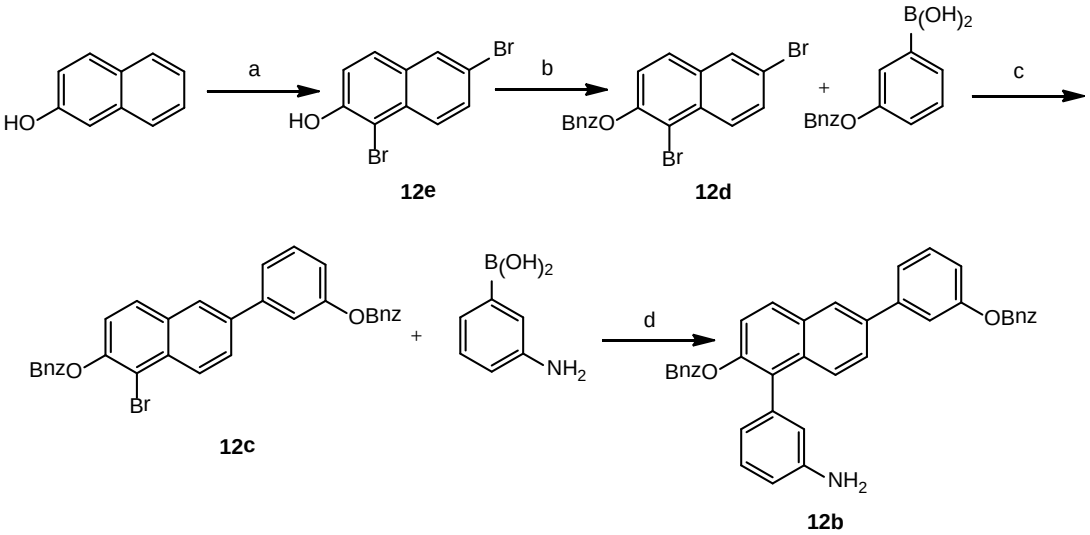

[a]**Reagents and conditions:** (a) Br_2, acetic acid, reflux, 3 h; (b) Benzyl bromide, K_2CO_3, EtOH, reflux, 15 h; (c) Cs_2CO_3, $Pd(Ph_3P)_4$, THF/H_2O (1:1), reflux, 4 h; (d) Cs_2CO_3, $Pd(Ph_3P)_4$, DME/EtOH/H_2O (1:1:1), 15 min microwave irradiation (150 °C, 1.5 bar).

The synthesis of the protected sulfonamides **8a–29a** and the deprotection yielding **8–29** is shown in scheme 4. The sulfonamide coupling with compound **1b** or compound **12b** and the commercially available sulfonyl chlorides was performed according to Method B (DMAP, pyridine, RT, 6 d). In a last step compounds **8a, 10a, 11a, 15a, 17a** and **18a** were demethylated with boron tribromide (Method C; BBr_3, CH_2Cl_2, -78°C to RT, 18h, Scheme 4). Compound **9a**, **12a**-**14a**, **16a** and **19a**–**29a** were debenzylated using the same reagent according to Method D (BBr_3, CH_2Cl_2, -25°C 1h, RT 2 h, Scheme 4).

For the synthesis of the rigidified sulfonamides **30** and **31,** the 4-indolylphenylsulfonamide and the 6-indolylphenylsulfonamide residues were introduced to compound **12c** by a Suzuki coupling with the corresponding indolyl boronic acids. A tetrabutyl ammonium chloride (TBAC) -catalyzed sulfonamide coupling resulted in compounds **30a** and **31a**. Cleavage of the benzyloxy moieties with boron tribromide (Method D) afforded **30** and **31** (Scheme 5).

Scheme 4[a]: Synthesis of compound **8 – 29.**

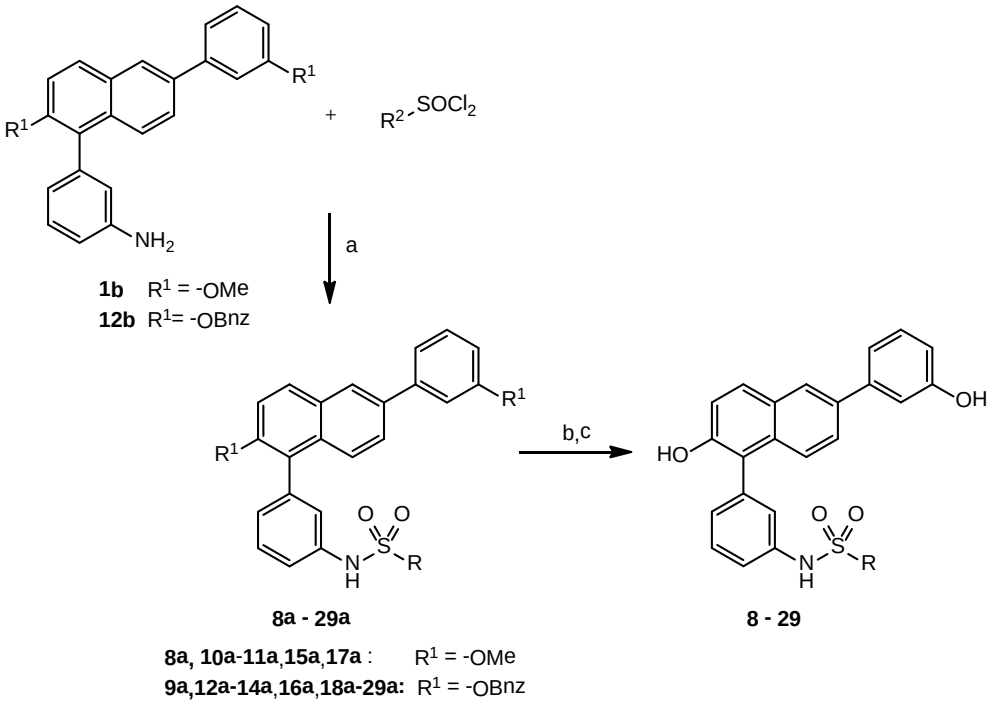

[a]**Reagents and conditions:** (a) DMAP, pyridine, rt, 6 d, Method B; (b) BBr_3, CH_2Cl_2, -78 °C to rt, 18 h, Method C; (c) BBr_3, CH_2Cl_2, -25 °C 1h, rt 2 h, Method D

Scheme 5[a]: Synthesis of compound **30 - 31.**

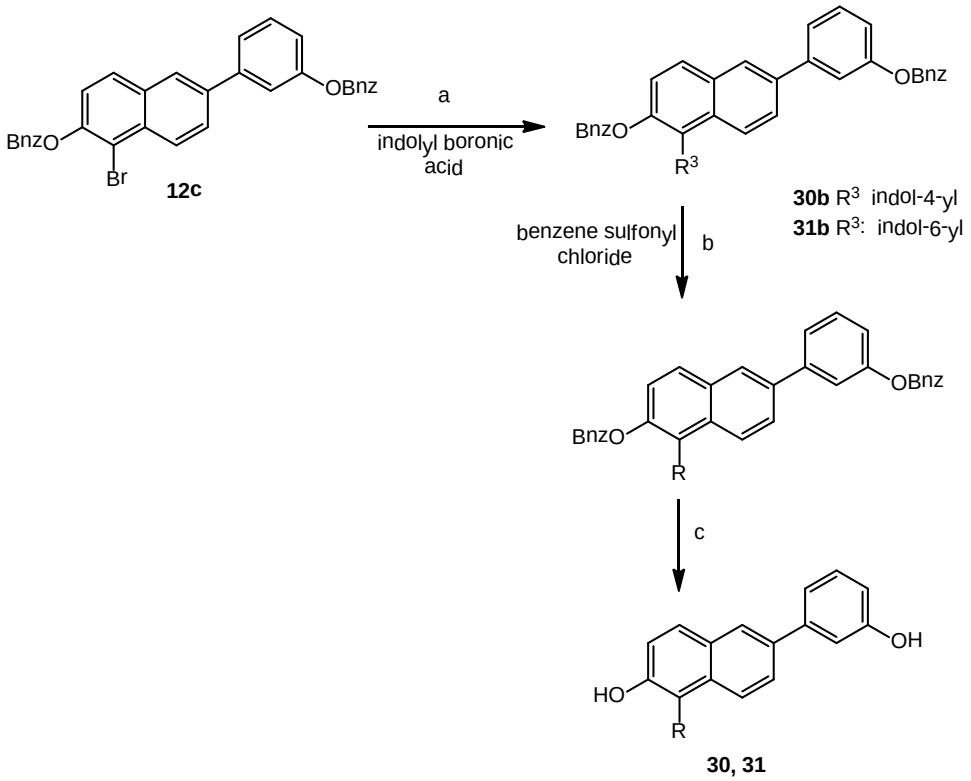

[a]**Reagents and conditions:** (a) Cs_2CO_3, $Pd(Ph_3P)_4$, DME/EtOH/H_2O (1:1:1), 15 Min microwave irradiation (150 °C, 1.5 bar); (b) DCM, TBAC, NaOH, 3h, 10°C; (c) BBr_3, CH_2Cl_2, -25 °C 1h, rt 2 h, Method D.

Biological results

Inhibition of 17β-HSD1, selectivity toward 17β-HSD2 in human and *Callithrix jacchus*

The assays were performed with placental enzymes from human and *Callithrix jacchus* (*cj*). For the 17β-HSD1 assay the cytosolic fraction, tritiated E1, cofactor and inhibitor were used. The 17β-HSD2 assay was performed similarly using the microsomal fraction and tritiated E2.

In a first step a synthetic library was designed to introduce aromaticity into the sulfonamide core (Figure 3). Biological evaluation of these compounds revealed that several are highly potent *h*17β-HSD1 inhibitors. Compounds which exhibited more than 30% inhibition of *h*17β-HSD1 at 10 nM were resynthesized, IC_{50} values and selectivity factors (SFs) toward *h*17β-HSD2 as well as percentage inhibition values against *cj*17β-HSD1 and 17β-HSD2 were determined (**8-11**, **14**, **15**, **17**). Further, in order to elaborate a meaningful SAR, substituents differing in their electronic and lipophilic properties were introduced in the aromatic moiety and the corresponding compounds were also tested against the human and *cj* enzymes (**12**, **13**, **16**, **18–31**, Table 1)

All compounds showed IC_{50} values toward *h*17β-HSD1 in the low nanomolar range (between 12 nM and 92 nM) as well as selectivity toward *h*17β-HSD2 (SF between 2 and 71).

The only exception is the di-nitro-substituted sulfonamide **16** with 30 fold reduced activity toward *h*17β-HSD1. Interestingly, **16** turned out to be a moderate *h*17β-HSD2 inhibitor. By introduction of *meta*- and *para*-substituents into the phenyl substituent of **12**, selectivity toward *h*17β-HSD2 could be further improved up to a SF of 71 for compound **23**.

To explore whether rigidification leads to an improvement of affinity toward the target, as it has been shown in previous studies[56] and to get more insights into the binding site two rigidified conformers were synthesized. The rigidification of **12** resulted in two compounds with different conformations in the sulfonamide moiety, the indoles **30** and **31**. Interestingly, one conformation remained highly active toward *h*17β-HSD1 (**30**) while the other conformer lost activity (**31**).

The activity toward *cj*17β-HSD1 and also the selectivity toward *cj*17β-HSD2 could be slightly optimized for all compounds. Remarkably, the rigidified **12 (**compound **30**) turned out to be a highly active and selective inhibitor of *cj*17β-HSD1 (79% inhibition of *cj*17β-HSD1 and 43% inhibition of *cj*17β-HSD2 at 50 nM).

A selection of the compounds (reference **A**, **12, 17, 23** and **29)** was also tested using the cytosolic and microsomal fraction of mouse liver homogenate, which are described to be responsible for the E1 and E2 conversion, respectively,[57] to examine whether the aromatic sulfonamides show activity in this species. In the cytosolic fraction E1 conversion was observed but the compounds did not show inhibitory activity. In the microsomal fraction E2 oxidation was monitored and the compounds exhibited moderate inhibition of estrone formation (Table 2).

Table 1[a]: IC_{50} values toward *h*17β-HSD1, selectivity factor toward *h*17β-HSD2 and inhibition of *cj*17β-HSD1 and *cj*17β-HSD2 for compounds **8-31**.

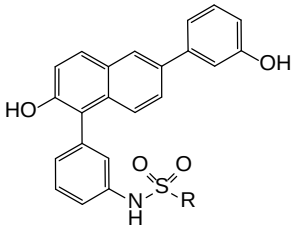

8 - 29

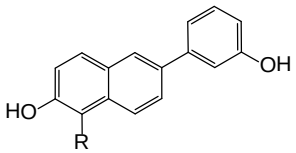

30-31

Cmpd	R	IC_{50} (nM)[a]		SF[d]	Inhibition at 50 nM (%)[a]	
		*h*17βHSD1[b]	*h*17βHSD2[c]		*cj*17β-HSD1[e]	*cj*17β-HSD2[f]
A[g]	-CH_3	15	403	27	16	23
8	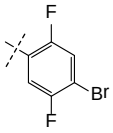	46	223	5	14	17
9	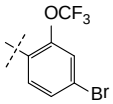	74	213	3	n.i.	n.i.
10	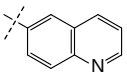	92	535	6	38	13
11		28	1104	39	25	18
12		15	403	27	19	n.i.
13	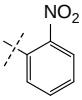	17	238	14	n.i.	21
14	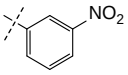	20	374	19	16	17
15	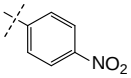	49	1058	22	28	13
16	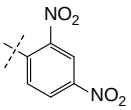	690	371	0.5	16	36
17	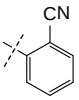	14	439	31	43	35
18	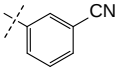	30	607	20	11	n.i.
19	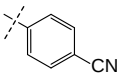	25	825	33	25	30

20	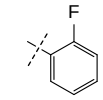	29	749	26	19	n.i.
21	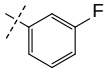	22	396	18	n.i.	33
22	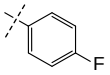	53	834	16	24	20
23	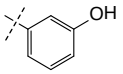	14	999	71	20	n.i.
24	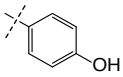	19	352	19	n.i.	30
25		31	188	6	20	n.i.
26	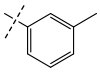	33	446	14	n.i.	11
27	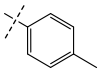	35	367	11	n.i.	11
28	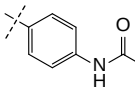	12	408	34	31	n.i.
29	$-CH_2CF_3$	32	1211	38	17	32
30	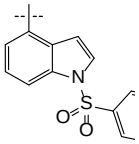	32	391	12	79	43
31	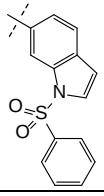	519	996	2	14	12

[a]mean values of three determinations, standard deviation less than 18 %,[b]human placenta, cytosolic fraction, substrate [^{3}H]-E1 + E1 [500 nM], cofactor NADH [500 µM]; [h]uman placenta, microsomal fraction, substrate [^{3}H]-E2 + E2 [500 nM], cofactor NAD^+ [1500 µM], [d]IC_{50} (17β-HSD2)/ IC_{50} (17β-HSD1), [e]Callithrix jacchus placenta, cytosolic fraction, substrate [^{3}H]-E1 + E1 [500 nM], cofactor NADH [500 µM]; [f]Callithrix jacchus placenta, microsomal fraction, substrate [^{3}H]-E2 + E2 [500 nM], cofactor NAD^+ [1500 µM],[h] n.i.: no inhibition, i.e. inhibition ≤ 10% , [g]aliphatic sulfonamide inhibitor **A**[49] is used as reference.

Selectivity toward estrogen receptors α and β (ERα & β)

Because of the similarity of the compounds to the estrogen scaffold it cannot be excluded that the phenyl naphthalene sulfonamides show affinity toward the estrogen receptors α and β. Agonistic as well as antagonistic effects are not compatible with the therapeutic concept for 17β-HSD1 inhibitors. Agonistic properties would stimulate cell proliferation and thus counteract the effect of these inhibitors. Antagonistic qualities are likely to lead to unwanted pharmacological effects and could reduce the advantages of the new therapeutic intracrine concept compared to antiestrogens or SERMs. The compounds were tested in an assay using the recombinant human ERs in competition with [^{3}H]-

E2. Affinity of E2 was set to 100%. A RBA of 0.1% means that the compound shows a 1000fold weaker affinity to the receptor than E2 and is considered as satisfactory.

All compounds, including reference A showed RBA values lower than 0.1 % toward ERα and ERβ and were classified as very low affinity ligands (Table 3).

Table 2 Percentage inhibition of estradiol and estrone formation in mice liver preparation

Compd	Inhibition at 1µM[a]	
	Estradiol formation (%)[b]	Estrone formation (%)[c]
A	n.i.	n.i.
14	n.i.	41
15	n.i.	28
23	n.i.	39
29	n.i.	29

[a]mean values of three determinations, standard deviation less than 18 %,[b]Mice liver, cytosolic fraction, substrate [^{3}H]-E1 + E1 [500 nM], cofactor NADH [500 µM]; [c]Mice liver, microsomal fraction, substrate [^{3}H]-E2+ E2 [500 nM], cofactor NAD^+ [1500 µM], n.i.: no inhibition, i.e. inhibition ≤ 10%.

Table 3: Estrogen Receptor α and β binding affinity

Cmpd	ERα RBA (%)[a,b]	ERβ RBA (%)[a,b]	Cmpd	ERα RBA (%)[a,b]	ERβ RBA (%)[a,b]
8	0.001<x<0.01	0.001<x<0.01	**20**	<0.1	<0.1
9	0.01<x<0,1	0.01<x<0.1	**21**	<0.1	<0.1
10	<0.001	<0.001	**22**	<0.1	<0.1
11	0.001<x<0.01	0.001<x<0.01	**23**	<0.1	<0.1
12	<0.1	<0.1	**24**	<0.1	<0.1
13	<0.1	<0.1	**25**	<0.1	<0.1
14	<0.001	0.001<x<0.01	**26**	<0.1	<0.1
15	<0.1	<0.1	**27**	<0.1	<0.1
16	<0.1	<0.1	**28**	<0.1	<0.1
18	<0.1	<0.1	**29**	<0.1	<0.1
19	<0.1	<0.1	**30**	<0.1	<0.1

[a]Mean value of three determinations, [b] RBA: Relative Binding Affinity, E2 = 100%;

Further biological evaluation

To get insights into cellular activity, the mammary tumor T-47D cell line, which expresses *h*17β-HSD1 and *h*17β-HSD2, was used to determine IC_{50} values for selected compounds (Table 2). All tested compounds showed IC_{50} values around or below 1000 nM. Compound **17** exhibiting an IC_{50} value of 157 nM turned out to be the most active one of this series.

Table 4[a]: IC_{50} values in the T-47D cell assay for selected compounds.

	Cell assay				
compd	IC_{50} (nM)[a] 17βHSD1	compd	IC_{50} (nM)[a] 17βHSD1	compd	IC_{50} (nM)[a] 17βHSD1
A	71	**17**	157	**25**	525
8	646	**18**	402	**26**	440
10	498	**19**	555	**27**	633
11	316	**20**	429	**28**	240
12	196	**21**	462	**29**	246
13	462	**22**	637	**30**	1100
14	396	**23**	701		
15	753	**24**	1009		

[a]Mean values of three determinations, standard deviation less than 25 %; [b]T47D cells, substrate [^{3}H]-E1 +E1 [50 nM].

To further characterise the inhibitors regarding their biophysical properties tPSA values were calculated using the commercial ChemDrawUltra 12.0 program and are shown in Table 5.

Except for **16,** (190.25 Å, Table 3) all compounds showed tPSA values which are in an adequate range for oral bioavailabity[58] (Table 5).

Discussion and Conclusion

The identification of a highly active *h*17β-HSD1 inhibitor (**A**) with properties suitable for further preclinical studies provided the starting point for the optimization concerning activity toward *cj*17β-HSD1. Starting with a parallel synthesis approach several highly potent *h*17β-HSD1 inhibitors were discovered. With the 4-indolyl substituted hydroxyphenyl naphthalene sulfonamide **30** a highly potent *h*- and *cj*17β-HSD1 inhibitor was identified, which might be an appropriate candidate for *in vivo* proof of concept.

The introduction of aromatic moieties differing in their electronic and lipophilic effects into the sulfonamide core is well tolerated by *h*17βHSD1, but did not resulted in higher activities. This finding cannot exclude additional beneficial interactions in the binding site initiated by the introduced substituents. However, they are obviously compensated by adverse effects, like losing a hydrogen bond from one of the two essential hydroxy groups[46] or by stripping the hydrate sheath for diffusion into the binding pocket

The strongly reduced activity of compound **16** could be explained by the high electron withdrawing effects of the two bulky nitro groups, disrupting potential π-π-interaction with the protein. A crystal structure will be necessary to shed light on the real binding mode of the synthesized compounds.

Rigidification is a common strategy in drug design to minimize entropic costs of binding and thus optimize the interaction. In this study, rigidification of the sulfonamide core led to the discovery of the highly active *human*- and *cj*17β-HSD1 inhibitor **30**. The structure of this compound obviously is very

close to the biologically active conformation of **12**. Contrarily, for the other conformation, rigidified in compound **31,** a significant reduced inhibition of *h*17β-HSD1 was found. This conformation is obviously not able to form sufficiently strong interactions in the active site of *h*17β-HSD1.

Table 5: Biophysical data of all compounds

Cmpd	tPSA (Å)[a]	MW (g/mol)	clogP [a]
A	86.63	403	3.82
8	86.63	581	7.15
9	95.86	630	8.37
10	98.99	518	6.09
11	86.63	455	6.01
12	86.63	467	6.12
13	138.44	512	6.14
14	138.44	512	6.14
15	138.44	512	6.14
16	190.25	557	6.10
17	140.43	492	6.04
18	140.43	492	6.04
19	140.43	492	6.04
20	86.63	485	6.17
21	86.63	485	6.17
22	86.63	485	6.17
23	106.83	483	5.62
24	106.83	483	5.62
25	86.63	481	6.50
26	86.63	481	6.50
27	86.63	481	6.50
28	115.73	524	4.92
29	86.63	473	4.98
30	86.63	492	6.59
31	86.63	492	6.59

[a]calculated values with ChemDrawUltra 12.0

Interestingly, the rigidification of **12** leading to **30** has a strong influence on inhibitory activity for the common marmoset enzyme compared to the human. The discovery of compound **30** as the

biologically active conformation of this class of inhibitors is of great importance and can be used for further structural optimization.

Through the introduction of aromatic substituents the activity toward *cj*17β-HSD1 could be increased significantly and also selectivity toward *cj*17β-HSD2 could be achieved for this class of compounds. H-bond-acceptors in *para*-position of the phenyl moiety seem to be beneficial for selectivity in *Callithrix jacchus*. Considering the fact, that the expression of 17β-HSD2 is downregulated in EDD tissues, it is nevertheless important to obtain selectivity toward this isozyme to avoid systemic enhancement of E2 levels and the side effects associated with it.

The differences in inhibitory activities between *h*- and *cj*17β-HSD1 in this compound class could be indications for different binding modes for the two species. However, an in depth investigation of the SAR for further elucidation is hampered by a somewhat blurred relationship.

All aromatic sulfonamides showed a decrease in cellular activity in T47-D cells, especially the indolyl-derivative **30** (IC_{50} = 1100 nM) which could be explained by the higher molecular weight and the increased clogP value compared to the reference **A** (491 g/mol vs. 405 g/mol and clogP 6.59 vs 3.91, respectively, supporting information Table 4). Intracellular metabolism might also play a role for the decreased cellular activity.

Another important issue in drug development is oral bioavailability. Molecular weight and lipophilicity are not sufficient for prediction of oral bioavailability. The polar surface area and the number of free rotatable bonds are more appropriate parameters[59] and should be considered for the development of potential drugs. The polar surface area of 77.84 $Å^2$ for compound **30** is in an excellent range (86.63 $Å^2$ for reference **A**) and also the more rigid structure is promising.

For mimetics of the steroidal scaffold, selectivity toward the estrogen receptors is very important. To avoid estrogenic side effects neither agonistic nor antagonistic activities can be tolerated. With RBA values below 0.1 % for ERα and β, all herein reported compounds are not expected to exert ER mediated effect.

In this paper we described a species specific optimization of hydroxyphenyl sulfonamide naphthols starting with a combinatorial library approach followed by optimization of discovered hits. The goal of the present study was the identification of *cj*17β-HSD1 inhibitors. Thus, it was successful, as we discovered the rigidified sulfonamide **30**, which is highly potent toward *h*17β-HSD1 as well as toward *cj*17β-HSD1 and shows selectivity toward 17β-HSD2 of both species and the ERs. This *h*- and *cj*17β-HSD1 inhibitor seems to be an appropriate candidate for the proof of concept in the endometriosis common marmoset model. Nevertheless, before performing an *in vivo* experiment further parameters like metabolic stability and pharmacokinetic properties will be investigated.

Acknowledgment

We thank Benjamin Kirsch for his help in performing the synthesis. We thank Jeannine Jung, Martina Jankowski and Janine Ludwig for their help in performing the *in vitro* tests.

Experimental Section

Chemistry

Chemical names follow IUPAC nomenclature. Starting materials were purchased from commercial suppliers and were used without further purification. Column flashchromatography was performed on silica gel (70 – 200 µm), preparative thin layer chromatography (PTLC) on 1mm SIL-G-100 UV_{254} glass plates (Macherey-Nagel) and reaction progress was monitored by TLC on TLC Silica Gel 60 F_{254} (Merck). NMR spectra were measured on a Bruker AM500 spectrometer (500MHz) at 300 K. Chemical shifts are reported in δ (parts per million: ppm), TMS was used as internal reference and hydrogenated residues of deuteriated solvent as internal standard ($CDCl_3$: δ = 7.24 ppm (^{1}H-NMR) and δ = 77 ppm (^{13}C-NMR); CD_3COCD_3: δ = 2.05 ppm (^{1}H-NMR) and δ = 29.8 ppm (^{13}C-NMR)). Signals are described as s, d, t, dd, m, dt, ddd for singlet, doublet, triplet, doublet of doublets, multiplet, doublet of triplets and doublet of doublet of doublets, respectively. All coupling constants (J) are given in Hertz (Hz). The purity of final products (≥95%) was confirmed by analytical HPLC. HPLC/MS was performed on a MSQ® electro spray mass spectrometer (Thermo Fisher). The system was operated by the standard software Xcalibur®. A RP C18 NUCLEODUR 100-5 (125 x 3 mm) column was used as stationary phase with water/acetonitrile mixtures as eluents. Mass spectra (ESI) were recorded on a TSQ Quantum (Thermofischer) instrument. Melting points were measured using melting point apparatus SMP3 (Stuart Scientific). The apparatus is uncorrected.

General procedure for sulfonamide library (1-11, 14, 15, 17). Method A. A solution of sulfonylchloride [1.2 eq] in 2 mL THF was added to a solution of 1-(3-aminophenyl)-6-(3-hydroxyphenyl)naphthalene-2-ol **1a** [1.0 eq] and PS-morpholine in 2 mL THF (55mg). After stirring for 15 h at rt a catalytic amount of PS-DMAP was added and the mixture was stirred another 15 h at rt. A catalytic amount PS-Tris(2-aminoethyl)-amine and PS-isocyanate were added to the mixture of compound **15** and **17**. After filtration and evaporation the compounds were purified by preparative HPLC (Varian Inertsil C18 50x21mm) (H_2O/CH_3CN + 0.1% TFA) (100:0) → (0:100). The remaining compounds were stirred for 15 h at 60°C and afterwards finished with the same procedure as **15** and **17**. After filtration and evaporation the compounds were purified by combi-flashchromatography (hexane/ethylacetate (2:1 → 1:1).

General procedure for the synthesis of the protected phenylnaphthalenesulfonamides. Method B.[60] 3-(2-methoxy-6-(3-methoxyphenyl)naphthalen-1-yl)aniline **(1b)** or 3-(2-benzyloxy)-6-(3-benzyloxy)phenyl)naphthalene-1-yl)aniline (**12b**) [1 eq.] was dissolved in pyridine abs. and was spiked with the accordant sulfonyl chloride [1.5 eq.] and DMAP as a catalyst. The reaction mixture was stirred 6 d by rt. The reaction was quenched by adding 10 mL of 2N HCl and extracted with ethyl acetate. The organic layers were washed with saturated $NaHCO_3$ and brine, dried over $MgSO_4$ and

were evaporated under vacuum. The product was purified by flashchromatography to give the title compounds.

General Procedure for Ether Cleavage. Method C.[61,62] A 3-(2-methoxy)-6-(3-methoxy)phenyl)naphthalene-1-yl)sulfonamide derivative [1 eq] was dissolved in dichloromethane abs. and was cooled to -78°C (acetone/dry ice). Boron tribromide (1M, 3.5 eq per methoxygroup) was added drop wise under stirring. The reaction mixture was stirred 18 h from -78 °C to rt. The reaction was quenched by adding 10 mL of water and extracted with ethyl acetate. The organic layers were washed with saturated $NaHCO_3$ and brine, dried over $MgSO_4$ and were evaporated under reduced pressure. The product was purified by flashchromatography to give the title compounds.

General Procedure for Ether Cleavage. Method D[61, 62]**.** A 3-(2-benzyloxy)-6-(3-benzyloxy)phenyl)naphthalene-1-yl)sulfonamide derivative [1 eq] was dissolved in dichloromethane abs. and was cooled to -25°C. Boron tribromide (1M, 10 eq per benzyloxygroup) was added drop wise under stirring. The reaction mixture was stirred 1h at -25°C and than 3h at rt. The reaction was quenched by adding 10 mL of water and extracted with ethyl acetate. The organic layers were washed with saturated $NaHCO_3$ and brine, dried over $MgSO_4$ and were evaporated under reduced pressure. The product was purified by flashchromatography to give the title compounds.

5-chloro-N-(3-(2-hydroxy-6-(3-hydroxyphenyl)naphthalen-1-yl)phenyl)thiophene-2-sulfonamide (1). The title compound was prepared by reaction of 1-(3-aminophenyl)-6-(3-hydroxyphenyl)naphthalen-2-ol **(1a)** and 5-chlorothiophene-2-sulfonyl chloride according to Method A, yield: 35 % (8.8 mg). MS (ESI): 508 $(M+H)^+$.

4,5-dibromo-N-(3-(2-hydroxy-6-(3-hydroxyphenyl)naphthalen-1-yl)phenyl)thiophene-2-sulfonamide (2): The title compound was prepared by reaction of 1-(3-aminophenyl)-6-(3-hydroxyphenyl)naphthalen-2-ol **(1a)** and 4,5-dibromothiophene-2-sulfonyl chloride according to Method A. yield: 21 % (6.6 mg). MS (ESI): 629 $(M+H)^+$.

Methyl 5-(*N*-(3-(2-hydroxy-6-(3-hydroxyphenyl)naphthalen-1-yl)phenyl)sulfamoyl)-4-methoxythiophene-3-carboxylate (3). The title compound was prepared by reaction of 1-(3-aminophenyl)-6-(3-hydroxyphenyl)naphthalen-2-ol **(1a)** and methyl 5-(chlorosulfonyl)-4-methoxythiophene-3-carboxylate according to Method A, yield: 19 % (5.4 mg). MS (ESI): 562 $(M+H)^+$.

***N*-(3-(2-hydroxy-6-(3-hydroxyphenyl)naphthalen-1-yl)phenyl)-5-(2-(methylthio)pyrimidin-4-yl)thiophene-2-sulfonamide (4).** The title compound was prepared by reaction of 1-(3-aminophenyl)-6-(3-hydroxyphenyl)naphthalen-2-ol **(1a)** and 5-(2-(methylthio)pyrimidin-4-yl)thiophene-2-sulfonyl chloride according to Method A, yield: 22 % (6.7 mg). MS (ESI): 598 $(M+H)^+$.

***N*-(3-(2-hydroxy-6-(3-hydroxyphenyl)naphthalen-1-yl)phenyl)benzo[d]thiazole-6-sulfonamide (5).** The title compound was prepared by reaction of 1-(3-aminophenyl)-6-(3-hydroxyphenyl)naphthalen-2-ol **(1a)** and benzo[d]thiazole-6-sulfonyl chloride according to Method A, yield: 42 % (11 mg). MS (ESI): 525 $(M+H)^+$.

***N*-(3-(2-hydroxy-6-(3-hydroxyphenyl)naphthalen-1-yl)phenyl)-2-nitro-4-(trifluoromethyl)benzenesulfonamide (6).** The title compound was prepared by reaction of 1-(3-aminophenyl)-6-(3-hydroxyphenyl)naphthalen-2-ol **(1a)** and 2-nitro-4-(trifluoromethyl)benzene-1-sulfonyl chloride according to Method A, yield: 18 % (5.1 mg).MS (ESI): 581 $(M+H)^+$.

5-chloro-N-(3-(2-hydroxy-6-(3-hydroxyphenyl)naphthalen-1-yl)phenyl)-6aH-pyrrolo[3,2-d]thiazole-6-sulfonamide (7). The title compound was prepared by reaction of 1-(3-aminophenyl)-6-(3-hydroxyphenyl)naphthalen-2-ol **(1a)** and 5-chloro-6aH-pyrrolo[3,2-d]thiazole-6-sulfonyl chloride according to Method A, yield: 24 % (6.6 mg). MS (ESI): 548 $(M+H)^+$.

Compounds **8–11, 14, 15 and 17** were synthesized in the parallel synthetic approach according to method A and afterwards resynthesized in a bigger scale according to descriptions below.

***N*-(3-(2-hydroxy-6-(3-hydroxyphenyl)naphthalen-1-yl)phenyl)-4-bromo-2,5-fluorobenzene-sulfonamide (8):** The title compound was synthesized by reaction of 4-bromo-2,5-difluoro-*N*-(3-(2-methoxy-6(3-methoxyphenyl)naphthalen-1-yl) phenyl) benzenesulfonamide **(8a)** (70 mg, 0.15 mmol) and boron tribromide (1.05 mmol) according to method C. The product was purified by preparative HPLC (Agilent PrepC18 (H_2O/CH_3CN + 0.1% TFA) (20:80) →(0:100) in 35 Min.; yield: 63 % (52 mg). MS (ESI): 583 $(M+H)^+$.

***N*-(3-(2-hydroxy-6-(3-hydroxyphenyl)naphthalen-1-yl)phenyl)-4-bromo-2-trifluoro-methoxybenzenesulfonamide (9)**: The title compound was synthesized by reaction of *N*-(3-(2-(benzyloxy)-6-(3-(benzyloxy)phenyl)naphthalen-1-yl)phenyl)-4-bromo-2-(trifluoro-methoxy)benzenesulfonamide **(9a)** (280 mg, 0.34 mmol) and boron tribromide (3.40 mmol) according to method D. The product was purified by flashchromatography hexane/ethylacetate (5:3); yield: 84 % (180mg). MS (ESI): 631 $(M+H)^+$.

***N*-(3-(2-hydroxy-6-(3-hydroxyphenyl)naphthalen-1-yl)phenyl)-quinolin-6-sulfonamide (10):** The title compound was synthesized by reaction *N*-(3-(2-methoxy-6(3-methoxyphenyl)naphthalen-1-yl) phenyl)quinoline-6-sulfonamide **(10a)** (61 mg, 0.12 mmol) and boron tribromide (0.9 mmol) according to method D. The product was purified by flashchromatography hexane/ethylacetate (1:1); yield: 63 % (30 mg). MS (ESI): 519 $(M+H)^+$.

***N*-(3-(2-hydroxy-6-(3-hydroxyphenyl)naphthalen-1-yl)phenyl)-thiophene-2-sulfonamide (11):** The title compound was synthesized by reaction *N*-(3-(2-methoxy-6(3-methoxyphenyl)naphthalen-1-yl) phenyl) thiophene-2-sulfonamide (**11a**) (50 mg, 0.1 mmol) and boron tribromide (0.75 mmol) according to method C. The product was purified by flashchromatography hexane/ethylacetate (1:1); yield: 34 % (16 mg). MS (ESI): 473 $(M+H)^+$.

***N*-(3-(2-hydroxy-6-(3-hydroxyphenyl)naphthalen-1-yl)phenyl)benzenesulfonamide (12)**: The title compound was synthesized by reaction of *N*-(3-(2-(benzyloxy)-6-(3-(benzyloxy)phenyl)naphthalen-1-yl)phenyl)-3-methylbenzene-sulfonamide **(12a)** (215 mg, 0.33 mmol) and boron tribromide (3.32 mmol) according to method D. The product was purified by preparative HPLC (Agilent PrepC18 (H_2O/CH_3CN + 0.1% TFA) (35:65) →(0:100) in 42 Min.; yield: 23 %. MS (ESI): 468 $(M+H)^+$.

***N*-(3-(2-hydroxy-6-(3-hydroxyphenyl)naphthalen-1-yl)phenyl)-2-nitrobenzene-sulfonamide (13):** The title compound was synthesized by reaction of *N*-(3-(2-(benzyloxy)-6-(3-(benzyloxy)phenyl)naphthalen-1-yl)phenyl)-2-nitrobenzenesulfonamide (**13a**) (190 mg, 0.27 mmol) and boron tribromide (2.70 mmol) according to method D. The product was purified by preparative HPLC (Agilent PrepC18 (H_2O/CH_3CN + 0.1% TFA) (35:65) →(0:100) in 42 Min.); yield: 9 % (12mg). MS (ESI): 530 $(M+H_2O)^+$. ***N*-(3-(2-hydroxy-6-(3-hydroxyphenyl)naphthalen-1-yl)phenyl)-3-nitrobenzene-sulfonamide (14):** The title compound was synthesized by reaction of *N*-(3-(2-(benzyloxy)-6-(3-(benzyloxy)phenyl)naphthalen-1-yl)phenyl)-3-nitrobenzene-sulfonamide (**14a**) (150 mg, 0.22 mmol) and boron tribromide (2.20 mmol) according to method D. The product was purified by preparative HPLC (Agilent PrepC18 (H_2O/CH_3CN + 0.1% TFA) (35:65) →(0:100) in 42 Min.); yield: 21 % (24 mg). MS (ESI): 513 $(M+H)^+$.

***N*-(3-(2-hydroxy-6-(3-hydroxyphenyl)naphthalen-1-yl)phenyl)-4-nitrobenzene-sulfonamide (15):** The title compound was synthesized by reaction *N*-(3-(2-methoxy-6(3-methoxyphenyl)naphthalen-1-yl) phenyl)4-nitrobenzene-sulfonamide (**15a**) (150 mg, 0.28 mmol) and boron tribromide (2.8 mmol) according to method C. The product was purified by flashchromatography hexane/ethylacetete (1:1); yield: 43 % (62 mg). MS (ESI): 512 $(M+H)^+$.

***N*-(3-(2-hydroxy-6-(3-hydroxyphenyl)naphthalen-1-yl)phenyl)-2,4-dinitrobenzene-sulfonamide (16):** The title compound was synthesized by reaction of *N*-(3-(2-(benzyloxy)-6-(3-(benzyloxy)phenyl)naphthalen-1-yl)phenyl)-2,4-dinitro-benzenesulfonamide (**16a**) (150 mg, 0.26 mmol) and boron tribromide (2.60 mmol) according to method D. The product was purified by flashchromatography hexane/ethyl acetate (5:1); yield: 21 % (24 mg). MS (ESI): 558 $(M+H)^+$.

2-Cyano-*N*-(3-(2-hydroxy-6-(3-hydroxyphenyl)naphthalen-1-yl)phenyl)benzene-sulfonamide (17): The title compound was synthesized by reaction of 2-Cyano-*N*-(3-(2-methoxy-6(3-methoxyphenyl)naphthalen-1-yl) phenyl)benzene sulfonamide (**17a**) (226 mg, 0.16 mmol) and boron tribromide (1.12 mmol) according to method C. The product was purified by flashchromatography hexane/ethyl acetate (15:1 → 5:1); yield: 23 % (38 mg). MS (ESI): 493 $(M+H)^+$.

***N*-(3-(2-hydroxy-6-(3-hydroxyphenyl)naphthalen-1-yl)phenyl)-3-cyanobenzene-sulfonamide (18):** The title compound was synthesized by reaction of *N*-(3-(2-(benzyloxy)-6-(3-(benzyloxy)phenyl)naphthalen-1-yl)phenyl)-3-cyanobenzene-sulfonamide (**18a**) (200 mg, 0.33 mmol) and boron tribromide (3.30 mmol) according to method D. The product was purified by flashchromatography hexane/ethyl acetate (10:1 → 6:1); yield: 49 % (72 mg). MS (ESI): 495 $(M+H)^+$.

***N*-(3-(2-hydroxy-6-(3-hydroxyphenyl)naphthalen-1-yl)phenyl)-4-cyanobenzene-sulfonamide (19)**: The title compound was synthesized by reaction of *N*-(3-(2-(benzyloxy)-6-(3-(benzyloxy)phenyl)naphthalen-1-yl)phenyl)-4-cyanobenzene-sulfonamide (**19a**) (170 mg, 0.25 mmol) and boron tribromide (2.50 mmol) according to method D. The product was purified by preparative TLC hexane/ethyl acetate (2:1); yield: 50 % (66 mg). MS (ESI): 493 $(M+H)^+$.

***N*-(3-(2-hydroxy-6-(3-hydroxyphenyl)naphthalen-1-yl)phenyl)-2-fluorobenzene-sulfonamide (20)**: The title compound was synthesized by reaction of *N*-(3-(2-(benzyloxy)-6-(3-(benzyloxy)phenyl)naphthalen-1-yl)phenyl)-2-fluorobenzene-sulfonamide (**20a**) (190 mg, 0.29 mmol) and boron tribromide (2.90 mmol) according to method D. The product was purified by preparative TLC hexane/ethyl acetate (3:2); yield: 71 % (100 mg). MS (ESI): 508 $(M+Na)^+$.

***N*-(3-(2-hydroxy-6-(3-hydroxyphenyl)naphthalen-1-yl)phenyl)-3-fluorobenzene-sulfonamide (21)**: The title compound was synthesized by reaction *N*-(3-(2-(benzyloxy)-6-(3-(benzyloxy)phenyl)naphthalen-1-yl)phenyl)-3-fluorobenzene-sulfonamide (**21a**) (150 mg, 0.23 mmol) and boron tribromide (2.30 mmol) according to method D. The product was purified by preparative TLC hexane/ethyl acetate (2:1); yield: 13 % (15 mg). MS (ESI): 508 $(M+Na)^+$.

***N*-(3-(2-hydroxy-6-(3-hydroxyphenyl)naphthalen-1-yl)phenyl)-4-fluorobenzene-sulfonamide (22):** The title compound was synthesized by reaction of *N*-(3-(2-(benzyloxy)-6-(3-(benzyloxy)phenyl)naphthalen-1-yl)phenyl)-4-fluorobenzene-sulfonamide (**22a**) (250 mg, 0.38 mmol) and boron tribromide (3.80 mmol) according to method D. The product was purified by flashchromatography hexane/ethyl acetate (5:3); yield: 44 % (80 mg). MS (ESI): 486 $(M+H)^+$.

***N*-(3-(2-hydroxy-6-(3-hydroxyphenyl)naphthalen-1-yl)phenyl)-3-hydroxybenzene-sulfonamide (23)**: The title compound was synthesized by reaction *N*-(3-(2-(benzyloxy)-6-(3-(benzyloxy)phenyl)naphthalen-1-yl)phenyl)-3-methoxybenzene-sulfonamide (**23a**) (100 mg, 0.15 mmol) and boron tribromide (2.10 mmol) according to method D. The product was purified by flash chromatography hexane/ethyl acetate (5:3); yield: 72 % (52 mg). MS (ESI): 484 $(M+H)^+$.

***N*-(3-(2-hydroxy-6-(3-hydroxyphenyl)naphthalen-1-yl)phenyl)-4-hydroxybenzene-sulfonamide (24):** The title compound was synthesized by reaction *N*-(3-(2-(benzyloxy)-6-(3-(benzyloxy)phenyl)naphthalen-1-yl)phenyl)-4-methoxybenzene-sulfonamide (**24a**) (150 mg, 0.22 mmol) and boron tribromide (2.20 mmol) according to method D. The product was purified by flash chromatography hexane/ethyl acetate (2:1→1:1); yield: 10 % (11 mg). MS (ESI): 484 $(M+H)^+$.

***N*-(3-(2-(hydroxy)-6-(3-(hydroxy)phenyl)naphthalen-1-yl)phenyl)-2-methylbenzene-sulfonamide (25).** The title compound was synthesized by reaction *N*-(3-(2-(benzyloxy)-6-(3-(benzyloxy)phenyl)naphthalen-1-yl)phenyl)-2-methylbenzene-sulfonamide (**25a**) (40 mg, 0.08 mmol) and boron tribromide (0.8 mmol) according to method D. The product was purified by HPLC (Agilent PrepC18 (H_2O/CH_3CN + 0.1% TFA) (60:40) →(0:100) in 42 Min.); yield: 10 % (11 mg). MS (ESI): 482 $(M+H)^+$. ***N*-(3-(2-hydroxy-6-(3-hydroxyphenyl)naphthalen-1-yl)phenyl)-3-methylbenzene-sulfonamide (26):** The title compound was synthesized by reaction *N*-(3-(2-(benzyloxy)-6-(3-(benzyloxy)phenyl)naphthalen-1-yl)phenyl)-3-methylbenzene-sulfonamide (**26a**) (150 mg, 0.23 mmol) and boron tribromide (2.30 mmol) according to method D. The product was purified by HPLC (Agilent PrepC18 (H_2O/CH_3CN + 0.1% TFA) (35:65) →(0:100) in 42 Min.); yield: 14 % (15 mg). MS (ESI): 499 $(M+H_2O)^+$.

N-(3-(2-hydroxy-6-(3-hydroxyphenyl)naphthalen-1-yl)phenyl)-4-methylbenzene- sulfonamide (27): The title compound was synthesized by reaction *N*-(3-(2-(benzyloxy)-6-(3-(benzyloxy)phenyl)naphthalen-1-yl)phenyl)-4-methylbenzene-sulfonamide (**27a**) (213 mg, 0.32 mmol) and boron tribromide (3.20 mmol) according to method D. The product was purified by HPLC (Agilent PrepC18 (H_2O/CH_3CN + 0.1% TFA) (35:65) →(0:100) in 35 Min.); yield: 45 % (70 mg). MS (ESI): 499 $(M+H_2O)^+$.

***N*-(4-(*N*-(3-(2-(hydroxy)-6-(3-(hydroxy)phenyl)naphthalen-1-yl)phenyl)sulfamoyl)-phenyl)-acetamide (28):** The title compound was synthesized by reaction *N*-(4-(*N*-(3-(2-(benzyloxy)-6-(3-(benzyloxy)phenyl)naphthalen-1-yl)phenyl)sulfamoyl)-phenyl)-acetamide (**28a**) (299 mg, 0.40 mmol) and boron tribromide (4.00 mmol) according to method C. The product was purified by HPLC (Agilent PrepC18 (H_2O/CH_3CN + 0.1% TFA) (55:45) →(0:100) in 42 Min.); yield: 37 % (70 mg). MS (ESI): 525 $(M+H)^+$.

***N*-(3-(2-hydroxy-6-(3-hydroxyphenyl)naphthalen-1-yl)phenyl)-2,2,2-trifluoro-ethanesulfonamide (29)**: The title compound was synthesized by reaction *N*-(3-(2-(benzyloxy)-6-(3-(benzyloxy)phenyl)naphthalen-1-yl)phenyl)-2,2,2-trifluoro-ethanesulfonamide **(29a)** (300 mg, 0.5 mmol) and boron tribromide (5.00 mmol) according to method D. The product was purified by HPLC (Agilent PrepC18 (H_2O/CH_3CN + 0.1% TFA) (35:65) →(0:100) in 38 Min.); yield: 25 % (60 mg). MS (ESI): 474 $(M+H)^+$.

6-(3-hydroxyphenyl)-1-(1-(phenylsulfonyl)-1H-indol-4-yl)naphthalen-2-ol (30):

The title compound was synthesized by reaction of 4-(2-(benzyloxy)-6-(3-(benzyloxy)phenyl)naphthalen-1-yl)-1-(phenylsulfonyl)-1*H*-indole **(30a)** (70 mg, 0.14 mmol) and boron tribromide (1.40 mmol)according to method D. The product was purified by HPLC (Agilent PrepC18 (H_2O/CH_3CN + 0.1% TFA) (75:25) →(0:100) in 55 Min.); yield: 10 % (5.00 mg). MS (ESI): 493 $(M+H)^+$.

5-(2-(benzyloxy)-6-(3-(benzyloxy)phenyl)naphthalen-1-yl)-1-(phenylsulfonyl)-1*H*-indole (31a) and **1-[1-(Benzensulfonyl)indol-6-yl]-6-(3-hydroxyphenyl)naphthalen-2-ol (31):**

Powdered sodium hydroxide (5 mg, 0.11 mmol) and a catalytic amount of tetra-butyl ammonium chloride were stirred for 10 Min in dichloromethane at 0 °C under nitrogen atmosphere. (6-(2-(benzyloxy)-6-(3-(benzyloxy)phenyl)naphthalen-1-yl)-1H-indole (**31b**) (20 mg, 0.038 mmol) was added without further purification and stirred for a while. A solution of benzenesulfonyl chloride (7 mg, 0.04 mmol) in dichloromethane was added drop wise during a period of 15 Min. The solution was stirred for 3 h under 10 °C. The product was extracted with ethyl acetate, the combined organic layers were dried over $MgSO_4$ and evaporated under vacuum. The product was used without further purification for the ether cleavage according to method D (3.60 mmol boron tribromide were used). The product was purified by HPLC (Agilent PrepC18 (H_2O/CH_3CN + 0.1% TFA) (75:25) →(0:100) in 40 Min.); yield: 11 % (2.3 mg). MS (ESI): 493 $([M+H])^+$.

Biophysical characterization

The molecular weight, clogP and tPSA values of all compounds were calculated from CambridgeSoft Chem & Bio Draw using the ChemDrawUltra 12.0 program.

Biological Methods

[2, 4, 6, 7-^{3}H]-E2 and [2, 4, 6, 7-^{3}H]-E1 were purchased from Perkin Elmer, Boston. Quickszint Flow 302 scintillator fluid was bought from Zinsser Analytic, Frankfurt. T-47D cells were obtained form ECACC, Salisbury. FCS war purchased from Sigma, Taufkirchen. Cell culture media and dextran coated charcoal stripped FCS (DCC-FCS) were ordered from CCPRO, Oberdorla. Other chemicals were purchased from Sigma, Roth or Merck

Enzyme preparation (17βHSD1 and 17βHSD2) of placenta from human and *Callithrix jacchus*

17β-HSD1 and 17β-HSD2 were obtained from human placenta and *Callithrix jacchus* placenta according to previously described procedures.[63, 64] Fresh human placenta and frozen *Callithrix jacchus* placenta was homogenized and separated by partial centrifugation. The pellet fraction contains the microsomal 17β-HSD2, while 17β-HSD1 was obtained after precipitation with ammonium sulfate from the cytosolic fraction. Aliquots of 17β-HSD1 and 17β-HSD2 were stored frozen at -80°C.

Inhibition of 17β-HSD1 in cell free assay

Inhibitory activities toward human and *Callithrix jacchus* enzymes were evaluated by a well-established method with minor modifications.[65-67] Briefly, the enzyme preparation was incubated with NADH [500 µM] in the presence of potential inhibitors at 37 °C in a phosphate buffer (50 mM) supplemented with 20 % of glycerol and EDTA. 10 mM inhibitor stock solutions were prepared in DMSO. Final concentration of DMSO was adjusted to 1 % in all samples. The enzymatic reaction was started by addition of a mixture of unlabelled- and [^{3}H]- E1 (final concentration: 500 nM, 0.15 µCi). After 10 min, the incubation was stopped with $HgCl_2$ (10 mM) and the mixture was extracted with diethylether. After evaporation, the steroids were dissolved in acetonitrile. E1 and E2 were separated using acetonitrile/water (45:55) as mobile phase in a C18 rp chromatography column (Nucleodur C18 Gravity, 3 µm, Macherey-Nagel, Düren) connected to a HPLC-system (Agilent 1200 Series, Agilent Technologies, Waldbronn). Detection and quantification of the steroids were performed using a radioflow detector (Ramona Star, Raytest, Straubenhardt). The conversion rate was calculated according to following equation:

$\%conversion = \frac{\%E2}{\%E2 + \%E1} \cdot 100$. Each value was calculated from at least three independent experiments.

Inhibition of 17β-HSD2

The 17β-HSD2 inhibition assays were performed similarly to the 17β-HSD1 procedure. The microsomal fraction was incubated with NAD^+ [1500 µM], test compound and a mixture of unlabelled- and [^{3}H]-E2 (final concentration: 500 nM, 0.14 µCi) for 20 min at 37 °C (the reaction was

stopped with 1mM $HgCl_2$). Further treatment of the samples and HPLC separation was carried out as mentioned above.

ER affinity

The binding affinity of selected compounds to the ERα and ERβ was determined according to Zimmermann et al.[68] Briefly, 0.25 pmol of ERα or ERβ, respectively, were incubated with [2, 4, 6, 7-^{3}H]-E2 (10 nM) and test compound for 1 h at rt. The potential inhibitors were dissolved in DMSO (5 % final concentration). Non-specific-binding was performed with diethylstilbestrol (10 µM). After incubation, ligand-receptor complexes were selectively bound to hydroxyapatite (5 g/ 60 mL TE-buffer). The formed complex was separated, washed and resuspended in ethanol. For radiodetection, scintillator cocktail (Quickszint 212, Zinsser Analytic, Frankfurt) was added and samples were measured in a liquid scintillation counter (Wallac Micro Beta TriLux, Perkin Elmer). For determination of the relative binding affinity (RBA), inhibitor and E2 concentrations required to displace 50 % of the receptor bound labelled E2 were determined. RBA values were calculated according to the following equation: $RBA[\%] = \frac{IC_{50}(E2)}{IC_{50}(compound)} \cdot 100$. The RBA value for E2 was arbitrarily set at 100 %.

Inhibition of 17β-HSD1 in cellular assay using T47-D

A stock culture of T-47D cells was grown in RPMI 1640 medium supplemented with 10 % FCS, L-glutamine (2 mM), penicillin (100 IU/mL), streptomycin (100 µg/mL), insulin-zinc-salt (10 µg/mL) and sodium pyruvate (1 mM) at 37 °C under 5 % CO_2 humidified atmosphere.

The cells were seeded into a 24-well plate at $5x10^5$ cells/well in DMEM medium with FCS, L-glutamine and the antibiotics added in the same concentrations as mentioned above. After 24 h the medium was changed for fresh serum free DMEM and a solution of test compound in DMSO was added. Final concentration of DMSO was adjusted to 1 % in all samples. After a pre-incubation of 30 min at 37°C with 5 % CO_2, the incubation was started by addition of a mixture of unlabelled- and [2, 4, 6, 7-^{3}H]- E1 (final concentration: 50 nM, 0.15 µCi). After 30 min incubation, the enzymatic reaction was stopped by removing of the supernatant medium. The steroids were extracted into diethylether. Further treatment of the samples was carried out as mentioned for the 17β-HSD1 assay.

References

[1] Miyoshi, Y.; Ando, A.; Shiba, E.; Taguchi, T.; Tamaki, Y.; Noguchi, S., Involvement of up-regulation of 17beta-hydroxysteroid dehydrogenase type 1 in maintenance of intratumoral high estradiol levels in postmenopausal breast cancers. *Int. J. Cancer* **2001,** 94, (5), 685-689.

[2] Jansson, A., 17beta-hydroxysteroid dehydrogenase enzymes and breast cancer. *J. Steroid Biochem. Mol. Biol.* **2009,** 144, (1-2), 64-67.

[3] Blomquist, C. H.; Bonenfant, M.; McGinley, D. M.; Posalaky, Z.; Lakatua, D. J.; Tuli-Puri, S.; Bealka, D. G.; Tremblay, Y., Androgenic and estrogenic 17beta-hydroxysteroid dehydrogenase/17-ketosteroid reductase in human ovarian epithelial tumors: evidence for the type 1, 2 and 5 isoforms. *J. Steroid Biochem. Mol. Biol.* **2002,** 81, (4-5), 343-351.

[4] Smuc, T.; Hevir, N.; Ribic□-Pucelj, M.; Husen, B.; Thole, H.; Rizner, T. L., Disturbed estrogen and progesterone action in ovarian endometriosis. *Mol. Cell. Endocrinol.* **2009,** 301, (1-2), 59-64.

[5] Dizerega, G. S.; Barber, D. L.; Hodgen, G. D., Endometriosis: role of ovarian steroids in initiation, maintenance and suppression. *Fertil. Steril.* **1980,** 33, (6), 649-653.

[6] Saloniemi, T.; Jarvensivu, P.; Koskimies, P.; Jokela, H.; Lamminen, T.; Ghaem-Maghami, S.; Dina, R.; Damdimopoulou, P.; Makela, S.; Perheentupa, A.; Kujari, H.; Brosens, J.; Poutanen, M., Novel Hydroxysteroid (17beta) Dehydrogenase 1 Inhibitors Reverse Estrogen-Induced Endometrial Hyperplasia in Transgenic Mice. *Am. J Pathol.* **2010,** 176, (3), 1443-1451.

[7] Kasai, T.; Shozu, M.; Murakami, K.; Segawa, T.; Shinohara, K.; Nomura, K.; Inoue, M., Increased Expression of Type I 17β-Hydroxysteroid Dehydrogenase Enhances in Situ Production of Estradiol in Uterine Leiomyoma. *J. Clin. Endocrinol. Metab.* **2004,** 89, (11), 5661-5668.

[8] Adamo, V.; Iorfida, M.; Montalto, E.; Festa, V.; Garipoli, C.; Scimone, A.; Zanghi, M.; Caristi, N., Overview and new strategies in metastatic breast cancer (MBC) for treatment of tamoxifen-resistant patients. *Ann. Oncol.* **2007,** 18, 53-57.

[9] Miller, W. R.; Bartlett, J. M.; Canney, P.; Verrill, M., Hormonal therapy for postmenopausal breast cancer: the science of sequencing. *Breast Cancer Res. Treat.* **2007,** 103, (2), 149-160.

[10] Bush, N. J., Advances in hormonal therapy for breast cancer. *Semin. Oncol. Nurs.* **2007,** 23, (1), 46-54.

[11] Gunnarsson, C.; Hellqvist, E.; Stål, O., 17beta-Hydroxysteroid dehydrogenases involved in local oestrogen synthesis have prognostic significance in breast cancer. *Br. J. Cancer* **2005,** 92, (3), 547-552.

[12] Šmuc, T.; Pucelj Ribič , M.; Šinkovec, J.; Husen, B.; Thole, H.; Lanišnik Rižner , T., Expression analysis of the genes involved in estradiol and progesterone action in human ovarian endometriosis. *Gynecol. Endocrinol.* **2007,** 23, (2), 105-111.

[13] Baston, E.; Palusczak, A.; Hartmann, R. W., 6-Substituted 1H-quinolin-2-ones and 2-methoxy-quinolines: synthesis and evaluation as inhibitors of steroid 5alpha reductases types 1 and 2. *Eur. J. Med. Chem.* **2000,** 35, (10), 931-940.

[14] Picard, F.; Baston, E.; Reichert, W.; Hartmann, R. W., Synthesis of N-substituted piperidine-4-(benzylidene-4-carboxylic acids) and evaluation as inhibitors of steroid-5alpha-reductase type 1 and 2. *Bioorg. Med. Chem.* **2000,** 8, (6), 1479-1487.

[15] Xu, K.; Al-Soud, Y. A.; Wetzel, M.; Hartmann, R. W.; Marchais-Oberwinkler, S., Triazole ring-opening leads to the discovery of potent nonsteroidal 17beta-hydroxysteroid dehydrogenase type 2 inhibitors. *Eur. J. Med.Chem.* **2011,** 46, (12), 5978-5990.

[16] Wetzel, M.; Marchais-Oberwinkler, S.; Perspicace, E.; Möller, G.; Adamski, J.; Hartmann, R. W., Introduction of an Electron Withdrawing Group on the Hydroxyphenylnaphthol Scaffold Improves the Potency of 17beta-Hydroxysteroid Dehydrogenase Type 2 (17beta-HSD2) Inhibitors. *J. Med. Chem.* **2011,** 54, (21), 7547-7557.

[17] Wetzel, M.; Marchais-Oberwinkler, S.; Hartmann, R. W., 17beta-HSD2 inhibitors for the treatment of osteoporosis: Identification of a promising scaffold. *Bioorg. Med. Chem.* **2011,** 19, (2), 807-815.

[18] Wetzel, M.; Gargano, E. M.; Hinsberger, S.; Marchais-Oberwinkler, S.; Hartmann, R. W., Discovery of a new class of bicyclic substituted hydroxyphenylmethanones as 17beta-hydroxysteroid dehydrogenase type 2 (17beta-HSD2) inhibitors for the treatment of osteoporosis. *Eur. J. Med. Chem.* **2012**, 47, 1-17..

[19] Xu, K.; Wetzel, M.; W. Hartmann, R.; Marchais-Oberwinkler, S., Synthesis and Biological Evaluation of Spiro--lactones as Inhibitors of 17-Hydroxysteroid Dehydrogenase Type 2 (17-HSD2). *Lett. Drug Des. Discovery* **2011,** 8, (5), 406-421.

[20] Brožic, P.; Lanišnik Rižner, T.; Gobec, S., Inhibitors of 17beta-hydroxysteroid dehydrogenase type 1. *Curr. Med. Chem.* **2008,** 15, 137-150 and references therein cited.

[21] Poirier, D., Advances in development of inhibitors of 17beta hydroxysteroid dehydrogenases. *Anticancer Agents Med. Chem.* **2009,** 9, 642-660 and references therein cited.
[22] Poirier, D., Inhibitors of 17 beta-hydroxysteroid dehydrogenases. *Curr. Med. Chem.* **2003,** 10, (6), 453-477 and references therein cited.
[23] Brozic, P.; Kocbek, P.; Sova, M.; Kristl, J.; Martens, S.; Adamski, J.; Gobec, S.; Lanisnik Rizner, T., Flavonoids and cinnamic acid derivatives as inhibitors of 17beta-hydroxysteroid dehydrogenase type 1. *Mol. Cell. Endocrinol.* **2009,** 301, 229-234.
[24] Karkola, S.; Lilienkampf, A.; Wähälä, K., A 3D QSAR model of 17beta-HSD1 inhibitors based on a thieno[2,3-d]pyrimidin-4(3H)-one core applying molecular dynamics simulations and ligand-protein docking. *ChemMedChem.* **2008,** 3, 461-472.
[25] Messinger, J.; Hirvelä, L.; Husen, B.; Kangas, L.; Koskimies, P.; Pentikäinen, O.; Saarenketo, P.; Thole, H., New inhibitors of 17beta-hydroxysteroid dehydrogenase type 1. *Mol. Cell. Endocrinol.* **2006,** 248, (1-2), 192-198.
[26] Lilienkampf, A.; Karkola, S.; Alho-Richmond, S.; Koskimies, P.; Johansson, N.; Huhtinen, K.; Vihko, K.; Wähälä, K., Synthesis and Biological Evaluation of 17beta-Hydroxysteroid Dehydrogenase Type 1 (17beta-HSD1) Inhibitors Based on a Thieno[2,3-d]pyrimidin-4(3H)-one Core. *J. Med. Chem.* **2009,** 52, (21), 6660-6671.
[27] Gobbi, S.; Cavalli, A.; Negri, M.; Schewe, K. E.; Belluti, F.; Piazzi, L.; Hartmann, R. W.; Recanatini, M.; Bisi, A., Imidazolylmethylbenzophenones as Highly Potent Aromatase Inhibitors. *J. Med. Chem.* **2007,** 50, (15), 3420-3422.
[28] Cavalli, A.; Bisi, A.; Bertucci, C.; Rosini, C.; Paluszcak, A.; Gobbi, S.; Giorgio, E.; Rampa, A.; Belluti, F.; Piazzi, L.; Valenti, P.; Hartmann, R. W.; Recanatini, M., Enantioselective Nonsteroidal Aromatase Inhibitors Identified through a Multidisciplinary Medicinal Chemistry Approach. *J. Med. Chem.* **2005,** 48, (23), 7282-7289.
[29] Leroux, F.; Hutschenreuter, T. U.; Charrière, C.; Scopelliti, R.; Hartmann, R. W., N-(4-Biphenylmethyl)imidazoles as Potential Therapeutics for the Treatment of Prostate Cancer: Metabolic Robustness Due to Fluorine Substitution? *Helv. Chim. Acta* **2003,** 86, (7), 2671-2686.
[30] Haidar, S.; Ehmer, P. B.; Barassin, S.; Batzl-Hartmann, C.; Hartmann, R. W., Effects of novel 17alpha±-hydroxylase/C17, 20-lyase (P450 17, CYP 17) inhibitors on androgen biosynthesis in vitro and in vivo. *J. Steroid Biochem. Mol. Biol.* **2003,** 84, (5), 555-562.
[31] Jagusch, C.; Negri, M.; Hille, U. E.; Hu, Q.; Bartels, M.; Jahn-Hoffmann, K.; Mendieta, M. A. E. P.-B.; Rodenwaldt, B.; Müller-Vieira, U.; Schmidt, D.; Lauterbach, T.; Recanatini, M.; Cavalli, A.; Hartmann, R. W., Synthesis, biological evaluation and molecular modelling studies of methyleneimidazole substituted biaryls as inhibitors of human 17alpha±-hydroxylase-17,20-lyase (CYP17). Part I: Heterocyclic modifications of the core structure. *Bioorg. Med. Chem.* **2008,** 16, (4), 1992-2010.
[32] Heim, R.; Lucas, S.; Grombein, C. M.; Ries, C.; Schewe, K. E.; Negri, M.; Müller-Vieira, U.; Birk, B.; Hartmann, R. W., Overcoming Undesirable CYP1A2 Inhibition of Pyridylnaphthalene-Type Aldosterone Synthase Inhibitors: Influence of Heteroaryl Derivatization on Potency and Selectivity. *J. Med. Chem.* **2008,** 51, (16), 5064-5074.
[33] Lucas, S.; Heim, R.; Negri, M.; Antes, I.; Ries, C.; Schewe, K. E.; Bisi, A.; Gobbi, S.; Hartmann, R. W., Novel Aldosterone Synthase Inhibitors with Extended Carbocyclic Skeleton by a Combined Ligand-Based and Structure-Based Drug Design Approach. *J. Med. Chem.* **2008,** 51, (19), 6138-6149.
[34] Lucas, S.; Heim, R.; Ries, C.; Schewe, K. E.; Birk, B.; Hartmann, R. W., In Vivo Active Aldosterone Synthase Inhibitors with Improved Selectivity: Lead Optimization Providing a Series of Pyridine Substituted 3,4-Dihydro-1H-quinolin-2-one Derivatives. *J. Med. Chem.* **2008,** 51, (24), 8077-8087.
[35] Hille, U. E.; Zimmer, C.; Haupenthal, J.; Hartmann, R. W., Optimization of the First Selective Steroid-11beta-hydroxylase (CYP11B1) Inhibitors for the Treatment of Cortisol Dependent Diseases. *Med. Chem. Lett.* **2011,** 2, (8), 559-564.
[36] Hille, U. E.; Zimmer, C.; Vock, C. A.; Hartmann, R. W., First Selective CYP11B1 Inhibitors for the Treatment of Cortisol-Dependent Diseases. *Med. Chem. Lett.* **2010,** 2, (1), 2-6.
[37] Bey, E.; Marchais-Oberwinkler, S.; Kruchten, P.; Frotscher, M.; Werth, R.; Oster, A.; Algul, O.; Neugebauer, A.; Hartmann, R. W., Design, synthesis and biological evaluation of bis(hydroxyphenyl) azoles as potent and selective non-steroidal inhibitors of 17beta-hydroxysteroid dehydrogenase type 1 (17beta-HSD1) for the treatment of estrogen-dependent diseases. *Bioorg. Med. Chem.* **2008,** 16, 6423-6435.
[38] Bey, E.; Marchais-Oberwinkler, S.; Werth, R.; Negri, M.; Al-Soud, Y. A.; Kruchten, P.; Oster, A.; Frotscher, M.; Birk, B.; Hartmann, R. W., Design, synthesis, biological evaluation and pharmacokinetics of bis(hydroxyphenyl) substituted azoles, thiophenes, benzenes and aza-

benzenes as potent and selective non-steroidal inhibitors of 17beta-hydroxysteroid dehydrogenase type 1 (17beta-HSD1). *J. Med. Chem.* **2008,** 51, 6725-6739.

[39] Al-Soud, Y. A.; Bey, E.; Oster, A.; Marchais-Oberwinkler, S.; Werth, R.; Kruchten, P.; Frotscher, M.; Hartmann, R. W., The role of the heterocycle in bis(hydroxyphenyl)triazoles for inhibition of 17beta-hydroxysteroid dehydrogenase (17beta-HSD) type 1 and type 2. *Mol. Cell. Endocrinol.* **2009,** 301, 212-215.

[40] Bey, E.; Marchais-Oberwinkler, S.; Negri, M.; Kruchten, P.; Oster, A.; Werth, R.; Frotscher, M.; Birk, B.; Hartmann, R. W., New insights into the SAR and binding modes of bis(hydroxyphenyl)thiophenes and benzenes: influence of additional substituents on 17β-hydroxysteroid dehydrogenase type 1 (17β-HSD1) inhibitory activity and selectivity. *J. Med. Chem.* **2009,** 52, 6724–6743.

[41] Kruchten, P.; Werth, R.; Bey, E.; Oster, A.; Marchais-Oberwinkler, S.; Frotscher, M.; Hartmann, R. W., Selective inhibition of 17beta-hydroxysteroid dehydrogenase type 1 (17betaHSD1) reduces estrogen responsive cell growth of T47-D breast cancer cells. *J. Steroid Biochem. Mol. Biol.* **2009,** 114, 200-206.

[42] Kruchten, P.; Werth, R.; Marchais-Oberwinkler, S.; Bey, E.; Ziegler, E.; Oster, A.; Frotscher, M.; Hartmann, R. W., Development of biological assays for the identification of selective inhibitors of estradiol formation from estrone in rat liver preparations. *C. R. Chim.* **2009,** 12, 1110-1116.

[43] Oster, A.; Klein, T.; Werth, R.; Kruchten, P.; Bey, E.; Negri, M.; Marchais-Oberwinkler, S.; Frotscher, M.; Hartmann, R. W., Novel estrone mimetics with high 17beta-HSD1 inhibitory activity. *Bioorg. Med. Chem.* **2010**.

[44] Oster, A.; Hinsberger, S.; Werth, R.; Marchais-Oberwinkler, S.; Frotscher, M.; Hartmann, R. W., Bicyclic Substituted Hydroxyphenylmethanones as Novel Inhibitors of 17β-Hydroxysteroid Dehydrogenase Type 1 (17β-HSD1) for the Treatment of Estrogen-Dependent Diseases. *J.Med.l Chem.* ***2010*** 53, (22), 8176-8186.

[45] Oster, A.; Klein, T.; Henn, C.; Werth, R.; Marchais-Oberwinkler, S.; Frotscher, M.; Hartmann, R. W., Bicyclic Substituted Hydroxyphenylmethanone Type Inhibitors of 17 β-Hydroxysteroid Dehydrogenase Type 1 (17 β-HSD1): The Role of the Bicyclic Moiety. *ChemMedChem* **2011,** 6, (3), 476-487.

[46] Frotscher, M.; Ziegler, E.; Marchais-Oberwinkler, S.; Kruchten, P.; Neugebauer, A.; Fetzer, L.; Scherer, C.; Müller-Vieira, U.; Messinger, J.; Thole, H.; Hartmann, R. W., Design, synthesis and biological evaluation of (hydroxyphenyl)-naphthalene and quinoline derivatives: potent and selective non steroidal inhibitors of 17beta-hydroxysteroid dehydrogenase type 1 (17beta-HSD1) for the treatment of estrogen-dependent diseases. *J. Med. Chem.* **2008,** 51, 2158-2169.

[47] Marchais-Oberwinkler, S.; Kruchten, P.; Frotscher, M.; Ziegler, E.; Neugebauer, A.; Bhoga, U. D.; Bey, E.; Müller-Vieira, U.; Messinger, J.; Thole, H.; Hartmann, R. W., Substituted 6-phenyl-2-naphthols. Potent and selective non-steroidal inhibitors of 17β-hydroxysteroid dehydrogenase type 1 (17beta-HSD1): design, synthesis, biological evaluation and pharmacokinetics. *J. Med. Chem.* **2008,** 51, 4685-4698.

[48] Marchais-Oberwinkler, S.; Frotscher, M.; Ziegler, E.; Werth, R.; Kruchten, P.; Messinger, J.; Thole, H.; Hartmann, R. W., Structure-activity study in the class of 6-(3'-hydroxyphenyl)naphthalenes leading to an optimization of a pharmacophore model for 17beta-hydroxysteroid dehydrogenase type 1 (17beta-HSD1) inhibitors. *Mol. Cell. Endocrinol.* **2009,** 301, 205-211.

[49] Marchais-Oberwinkler, S.; Wetzel, M.; Ziegler, E.; Kruchten, P.; Werth, R.; Henn, C.; Hartmann, R. W.; Frotscher, M., New Drug-Like Hydroxyphenylnaphthol Steroidomimetics As Potent and Selective 17beta-Hydroxysteroid Dehydrogenase Type 1 Inhibitors for the Treatment of Estrogen-Dependent Diseases. *J.Med. Chem.* **2011,** 54, (2), 534-547.

[50] Husen, B.; Huhtinen, K.; Poutanen, M.; Kangas, L.; Messinger, J.; Thole, H., Evaluation of inhibitors for 17beta-hydroxysteroid dehydrogenase type 1 in vivo in immunodeficient mice inoculated with MCF-7 cells stably expressing the recombinant human enzyme. *Mol. Cell. Endocrinol.* **2006,** 248, (1-2), 109-113.

[51] Husen, B.; Huhtinen, K.; Saloniemi, T.; Messinger, J.; Thole, H. H.; Poutanen, M., Human hydroxysteroid (17-beta) dehydrogenase 1 expression enhances estrogen sensitivity of MCF-7 breast cancer cell xenografts. *Endocrinology* **2006,** 147, (11), 5333-5339.

[52] Grummer, R.; Schwarzer, F.; Bainczyk, K.; Hess-Stumpp, H.; Regidor, P. A.; Schindler, A. E.; Winterhager, E., Peritoneal endometriosis: validation of an in-vivo model. *Hum Reprod* **2001,** 16, (8), 1736-1743.

[53] Lamminen, T.; Saloniemi, T.; Huhtinen, K.; Koskimies, P.; Messinger, J.; Husen, B.; Thole, H.; Poutanen, M., In vivo mouse model for analysis of hydroxysteroid (17beta) dehydrogenase 1 inhibitors. *Mol. Cell. Endocrinol.* **2009,** 301, (1-2), 158-162.

[54] Einspanier, A.; Lieder, K.; Bruns, A.; Husen, B.; Thole, H.; Simon, C., Induction of endometriosis in the common marmoset monkey (Callithrix jacchus). *Mol Hum Reprod* **2006,** 12, (5), 291-299.
[55] Klein, T.; Henn, C.; Negri, M.; Frotscher, M., Structural Basis for Species Specific Inhibition of 17beta-Hydroxysteroid Dehydrogenase Type 1 (17beta-HSD1): Computational Study and Biological Validation. *PLoS ONE* **2011,** 6, (8), e22990.
[56] Lucas, S.; Negri, M.; Heim, R.; Zimmer, C.; Hartmann, R. W., Fine-Tuning the Selectivity of Aldosterone Synthase Inhibitors: Structure Activity and Structure Selectivity Insights from Studies of Heteroaryl Substituted 1,2,5,6-Tetrahydropyrrolo[3,2,1-ij]quinolin-4-one Derivatives. *J.Med. Chem.* **2011,** 54, (7), 2307-2319.
[57] Milewich, L.; Garcia, R. L.; Gerrity, L. W., 17beta-Hydroxysteroid oxidoreductase: A ubiquitous enzyme. Interconversion of estrone and estradiol-17beta in BALBc mouse tissues. *Metabolism* **1985,** 34, (10), 938-944.
[58] Ertl, P.; Rohde, B.; Selzer, P., Fast Calculation of Molecular Polar Surface Area as a Sum of Fragment-Based Contributions and Its Application to the Prediction of Drug Transport Properties. *J. Med.Chem.* **2000,** 43, (20), 3714-3717.
[59] Veber, D. F.; Johnson, S. R.; Cheng, H.-Y.; Smith, B. R.; Ward, K. W.; Kopple, K. D., Molecular Properties That Influence the Oral Bioavailability of Drug Candidates. *J. Med. Chem.* **2002,** 45, (12), 2615-2623.
[60] Wilson, D. P.; Wan, Z.-K.; Xu, W.-X.; Kirincich, S. J.; Follows, B. C.; Joseph-McCarthy, D.; Foreman, K.; Moretto, A.; Wu, J.; Zhu, M.; Binnun, E.; Zhang, Y.-L.; Tam, M.; Erbe, D. V.; Tobin, J.; Xu, X.; Leung, L.; Shilling, A.; Tam, S. Y.; Mansour, T. S.; Lee, J., Structure-Based Optimization of Protein Tyrosine Phosphatase 1B Inhibitors: From the Active Site to the Second Phosphotyrosine Binding Site. *J. Med. Chem.* **2007,** 50, (19), 4681-4698.
[61] Bhatt, M. V.; Kulkarni, S. U., Cleavage of Ethers. *Synthesis* **1983**, 249-282.
[62] Felix, A. M., Cleavage of protecting groups with boron tribromide. *J. Org. Chem.* **1974,** 39, (10), 1427-1429.
[63] Qiu, W.; Campbell, R. L.; Gangloff, A.; Dupuis, P.; Boivin, R. P.; Tremblay, M. R.; Poirier, D.; Lin, S.-X., A concerted, rational design of type 1 17beta-hydroxysteroid dehydrogenase inhibitors: estradiol-adenosine hybrids with high affinity. *FASEB J.* **2002,** 16, (13), 1829-1831.
[64] Zhu, D. W.; Lee, X.; Breton, R.; Ghosh, D.; Pangborn, W.; Duax, W. L.; Lin, S.-X., Crystallization and preliminary X-ray diffraction analysis of the complex of human placental 17beta-hydroxysteroid dehydrogenase with $NADP^+$. *J. Mol. Biol.* **1993,** 234, (1), 242-244.
[65] Lin, S.-X.; Yang, F.; Jin, J. Z.; Breton, R.; Zhu, D. W.; Luu-The, V.; Labrie, F., Subunit identity of the dimeric 17beta-hydroxysteroid dehydrogenase from human placenta. *J. Biol. Chem.* **1992,** 267, (23), 16182-16187.
[66] Sam, K. M.; Auger, S.; Luu-The, V.; Poirier, D., Steroidal spiro-gamma-lactones that inhibit 17beta-hydroxysteroid dehydrogenase activity in human placental microsomes. *J. Med. Chem.* **1995,** 38, (22), 4518-4528.
[67] Sam, K. M.; Boivin, R. P.; Tremblay, M. R.; Auger, S.; Poirier, D., C16 and C17 derivatives of estradiol as inhibitors of 17beta-hydroxysteroid dehydrogenase type 1: chemical synthesis and structure-activity relationships. *Drug. Des. Discov.* **1998,** 15, (3), 157-180.
[68] Zimmermann, J.; Liebl, R.; von Angerer, E., 2,5-Diphenylfuran-based pure antiestrogens with selectivity for the estrogen receptor alpha. *J. Steroid Biochem. Mol. Biol.* **2005,** 94, (1-3), 57-66.

3.4 Catalytic Enzyme Activity on a Biosensor Chip: Combination of Surface Plasmon Resonance and Mass Spectrometry

Claudia Henn, Stefan Boettcher, Anke Steinbach and Rolf W. Hartmann

Analytical Biochemistry **2012**, 428, (1), 28-30

Publication IV

Abstract

Surface plasmon resonance as a label-free biosensor technique has become an important tool in drug discovery campaigns in the last couple of years. For good assay performance, it is of high interest to verify the functional activity upon the immobilization of the target protein on the chip. This study illustrates the verification of the catalytic activity of the drug target protein PqsD by monitoring substrate conversion as a decrease in SPR signal and product detection by UHPLC/MS2. This assay would be applicable to control surface activity of immobilized ligands.

Surface Plasmon Resonance (SPR)[1] spectroscopy is an outstanding method for the characterization of a variety of molecular interactions. The real-time measurement allows the determination of kinetic parameters, thermodynamics, concentrations and quantitative characterizations of ligand and analyte interactions [1]. The widespread application ranges, the low consumption of unlabelled protein and the monitoring of binding events and the high-throughput capability are striking advantages of the SPR technique [2]. Typically a ligand is permanently immobilized on a sensor surface and by the adsorption of an analyte a rise in signal can be detected [3]. It is known that the immobilization process affects the activity of a ligand [4], complicating data analysis [5]. Therefore it is of high interest to verify the ligand activity to obtain good quality data. However, this proof is normally performed using an antibody or a known binder [6] providing affinity data, but no activity data.

In this study, we describe a novel approach for the determination of ligand activity, the investigation of the "on-chip" enzymatic product formation using mass spectrometry. For the demonstration PqsD was used as an exemplary protein that is discussed as potential drug target for the development of antivirulence compounds. PqsD is involved in the PQS biosynthetic pathway, a signal molecule of the quorum sensing (*QS*) communication system in *Pseudomonas aeruginosa* [7-9]. It belongs to the bisubstrate enzymes and catalyzes the biosynthesis of HHQ [10] by the condensation of anthraniloyl-coenzyme A (ACoA) [11] and β-ketodecanoate (β-K) [12]. HHQ is a precursor of PQS and both interact with their receptor PqsR to control the transcription of PqsR-dependent target gene, e.g. virulence gene [13].

The principle of product formation measurement is described in Fig 1A. Immobilized PqsD is incubated successively with its two substrates. Firstly, PqsD is incubated with ACoA, whereof anthranilic acid binds covalently to Cys112 of the catalytic center in the active site of the protein [14] and the second, β-K, which is subsequently assembled in a condensation reaction with the covalently bound anthranilic acid to form HHQ. These steps are monitored by SPR and the formed product is determined by mass spectrometry.

After EDC/NHS surface activation, PqsD was covalently immobilized in a carboxymethyl dextran matrix under acidic conditions (10 mM NaAc, pH 4.5) to a high density surface. The PqsD loaded sensor was first treated with ACoA (K_D = 0.9 µM, Figure 1C) for 5 min at 37 °C to allow a covalent binding of anthranilic acid, excessive material was washed out by the buffer flow (5 min), until β-K was injected for additional 15 min. By the start of the second injection, the flow-through was collected for the mass spectrometric analysis. The SPR signal was monitored as shown in figure 1.

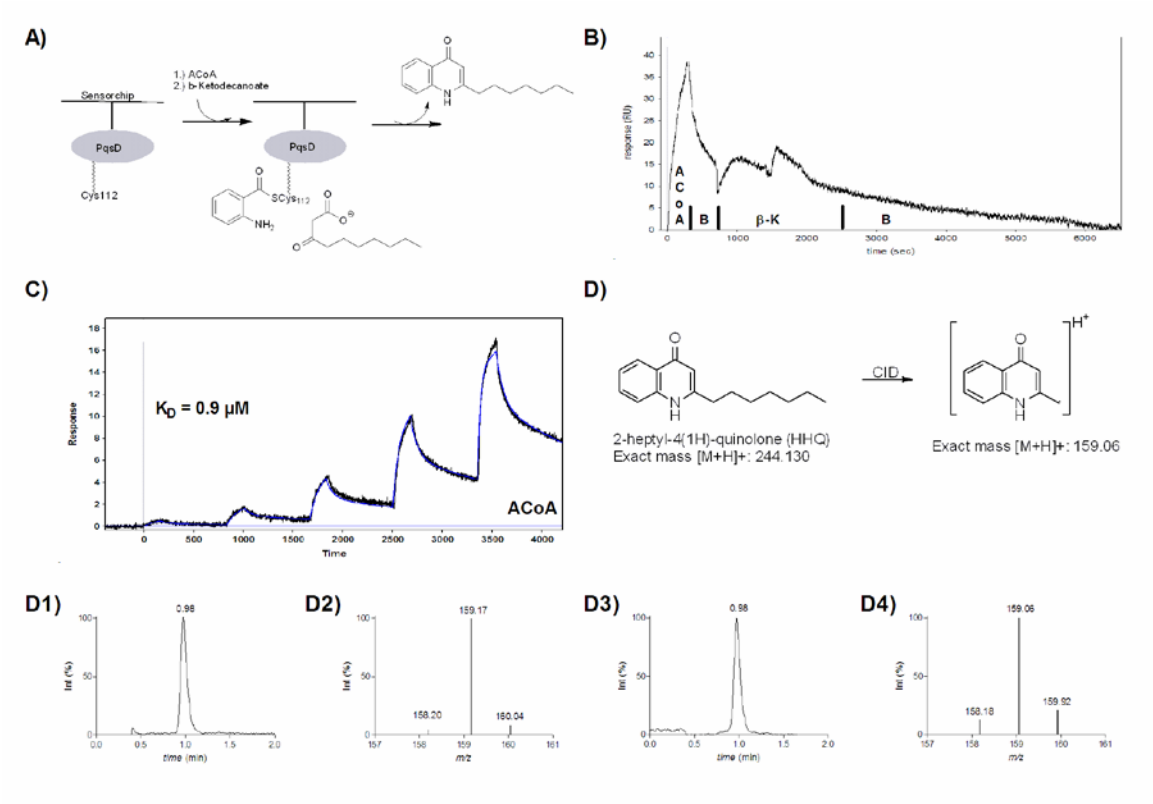

Figure 1. *(A) Schematic view to detect surface activity of an enzyme immobilized on biosensor chip. (B) Sensorgram of surface activity determination for PqsD immobilized on the surface. Injections are indicated in the figure: 5µM ACoA for 5 min and 10 µM β-K for 15 min, Sensorgram is blank surface referenced. (C) Binding affinity ACoA. Fit of the duplicate of the kinetic titration data from the H6-PqsD surface to a conformtional change model using Clamp (D) Fragmentation pattern of HHQ[15] (CID = collision induced decay) (D1) UHPLC-MS analysis of synthetic HHQ reference (D2) UHPLC-MS2 fragmentation pattern of synthetic HHQ reference at retention time 0.78 (D3) UHPLC-MS analysis of HHQ formed "on-chip" (D4) UHPLC-MS2 fragmentation pattern of HHQ formed "on-chip" at retention time 0.78 min. All data for the mass spectroscopy were obtained on a Thermo Fisher TSQ Access Max mass spectrometer.*

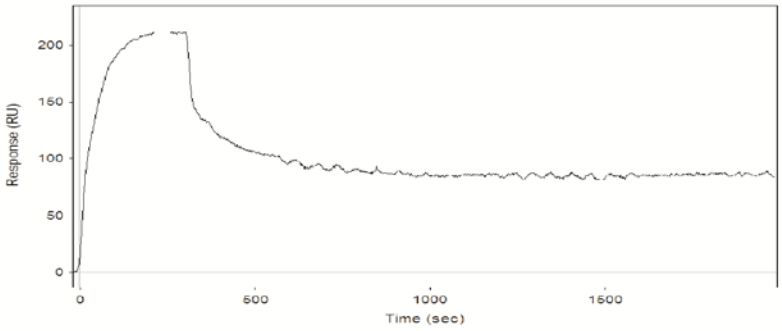

Figure 2*: Sensorgram for ACoA injection. The dissociation stopped at a defined level, indicating a covalent binding event.*

A clear signal increase was observed for ACoA, which did not decrease back to the baseline level during the dissociation phase (see also figure 2) demonstrating the covalent binding of anthranilic acid (ΔRU = 15). As a consequence of the β-K injection, the baseline decreased to the initial level (0 RU), indicating the elimination of HHQ from the active site by the condensation of the two substrates. The flow-through was analyzed to prove the product formation (HHQ) by ultra high performance liquid chromatography coupled to mass spectrometry (UHPLC-MS^2) which confirmed HHQ formation (137 pmol/pmol PqsD in 25 Min) on the PqsD-sensor by comparison of retention time and fragmentation pattern [15] to the synthetic reference [12]. (figure 1D, 1D1-D4, Supporting information). Thus, we provided successfully the direct experimental proof that PqsD, immobilized on a sensor surface, is catalytically active. For comparison of the activity of PqsD, experiments were performed with the enzyme in solution. PqsD is incubated in the same substrate order and the same time as in the biosensor-experiments and analyzed for HHQ-formation (336 pmol/pmol PqsD in 25 min). Ligand stability over time was demonstrated by measuring product-formation over a specified time period, resulting in quantifiable amounts until day 5. After 14 days HHQ-signals were still detectable. (Figure 3). This demonstrates that the ligand immobilization onto a surface does not interrupt the binding event and the functionality of the ligand confirming the use of SPR as a label-free technology. The proof of activity should be regarded as one of the initial, important steps in SPR assay development to enable efficient SPR studies. Evidencing the catalytic activity of an immobilized enzyme before starting intensive SPR-studies would be very helpful by interpreting the data. This finding gains the knowledge of the binding site´s accessibility of the immobilized ligand which wants to be targeted.

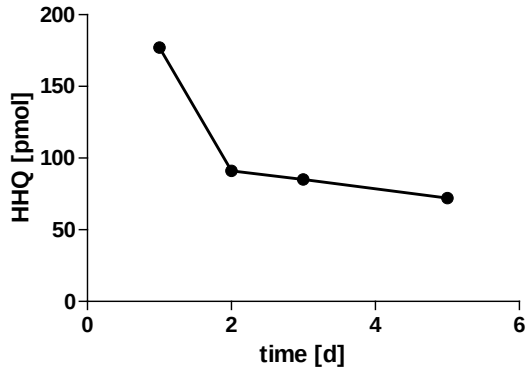

Figure 3: *Long term stability of H_6-PqsD-biosensor*

In conclusion, we succeeded to demonstrate real-time monitoring of an “on chip” enzymatic reaction by the combination of SPR and mass spectrometry. The current study provides useful information about functional activity and stability of the exemplary protein PqsD on the surface of a chip and illustrates an improved alternative for the biosensor surface evaluation. It can be used instead of an

antibody or known binder as positive control. Demonstrating product formation we have constrained that an immobilization process is not necessarily detrimental for activity of an immobilized ligand. Therefore the "on-chip" reaction is a method that can be applied to further activity monitoring of potential target proteins, which are to be examined by SPR.

Acknowledgement

We thank Simone Amman for the synthesis and purification of ACoA and Cenbin Lu for the synthesis of β-K and HHQ.

Experimental Section

Surface Plasmon Resonance

SPR binding studies were performed using Reichert SR7500DC instrument optical biosensor (Reichert Technologie, Depew, NY 14043 USA). CMD500 sensor chips were purchased from Xantec Analytics. (Düsseldorf, Germany).

Protein Expression and Purification

His-tagged-PqsD (H_6-PqsD) was expressed in *E. coli* and purified using a single affinity chromatography step. Briefly, *E. coli* BL21 (λDE3) cells containing the pET28a(+)/pqsD were grown in LB medium containing 50 µg ml-1 kanamycin at 37 °C to an OD600 of approximately 0.8 units and induced with 0.2 mM IPTG for 16 h at 16 °C. The cells were harvested by centrifugation (5000 rpm, 10 min, 4 °C) and the cell pellet was resuspended in 100 ml binding buffer (25 mM Tris-HCl pH 7.8, 500 mM NaCl, 20 mM imidazole, 5 mM β-mercaptoethanol) and lysed by sonication for a total process time of 2.5 min. Cell debris were removed by centrifugation (13000 rpm, 30 min) and the supernatant was filtered through a syringe filter (0.45 µm). The clarified lysate was immediately applied to a Ni-NTA column (GE Healthcare), washed with binding buffer and eluted with 500 mM imidazole. The protein containing fractions were buffer-exchanged into PBS pH 7.4, 10 % glycerol (*v/v*) for using a PD10 column (GE Healthcare) and judged pure by SDS-PAGE analysis. The H_6-PqsD was stored in aliquots at -80 °C.

Immobilization of H_6-PqsD

H_6-PqsD was immobilized on CMD500 sensor chips at 25 °C using standard amine coupling chemistry. H_2O was used as immobilization buffer. The carboxymethyl dextran surface was prepared with five sodium borate (1M pH 9.5) injections and was activated with a 7-min injection of a 1:1 ratio of 0.4 M 1-ethyl-3-(3-dimethylaminopropyl) carbodiimide hydrochloride (EDC)/0.1 M *N*-hydroxy succinimide (NHS). H_6-PqsD was diluted into sodium acetate (10 mM pH 4.5) to 100µg/mL and coupled to the surface with a 1.5 min injection. Remaining activated groups were blocked with a 7-min injection of 1 M ethanolamine (pH 8.5). H_6-PqsD (38400 Da) was immobilized at densities of 13,922 RU (Chip (I)), 13618 RU (Chip (II)) and 15628 RU (Chip III) for the experiments to determine

catalytic activity and at a density of 2922 RU (Chip IV) and 2322 RU (Chip V) for the kinetic titration experiments.

Amounts of protein were calculated belonging to the acquisition that 1RU is 1pg/mm^2. Flow cell size of the SPR instrument is 4.5 mm^2. A Anthranilsäurederivative [10] was used as initial positive control.

Binding affinity for ACoA

The binding experiments were performed with Chip IV and V at 12°C at a constant flow rate of 20 µl/min in instrument running buffer (50 mM TRIS-HCl pH = 8.0, 150 mM NaCl, 0.1% Triton-X-100 (*v/v*)). For the kinetic titration A 2.5 mM stock of *ACoA* in water was diluted to a concentration of 50 µM and then diluted in a 3-fold dilution series down to 617 nM. Before starting the experiments 12 warm-up blank injections were performed. Zero-buffer blank injections were included for double referencing. Within a single binding cycle, the ACoA samples were injected sequentially in order of increasing concentration over the ligand and the reference surfaces for 180 s association and 10 min dissociation time. Scrubber software was used for processing and Clamp software for analysing data. Kinetic Dissociation constant (K_D) was determined by simulation and fitting appropriate experimental data to a conformational change model using Clamp software [16].

Catalytic activity of H_6-PqsD-biosensor:

Tris (50 mM Tris-HCl pH 8.0, 150 mM NaCl, 0.1% Triton-X-100 (*v/v*)) was used as the running buffer. Anthraniloyl-CoA was provided as 5 mM stock solution in water and was diluted into running buffer to 10 µM. β-Ketodecanoate was dissolved in methanol to a 10 mM stock solution by mass and then diluted into running buffer to 20 µM. ACoA was injected for 5 min association and 5 min dissociation time, the injection was followed by the injection of β-ketodecanoate for 15 min association time and 10 min dissociation time. Experiments were performed at a flow rate of 25 µL and 37 °C. The flow-through was collected, evaporated and diluted in MeOH. HHQ-formation was detected using UHPLC-MS/MS.

Catalytic activity of H_6-PqsD:

Tris (50 mM Tris-HCl pH 8.0, 150 mM NaCl, 0.1% Triton-X-100) was used as the test buffer. Anthraniloyl-CoA was provided as 5 mM stock solution in water and was diluted into test buffer to 10 µM. β-Ketodecanoate was dissolved in methanol to a 10 mM stock solution by mass and then diluted into running buffer to 20 µM. 1 pmol PqsD was preincubated for 10 Min with ACoA followed by the addition of β-ketodecanoate for 25 min. Experiments were performed 37 °C. The reaction was stopped, HHQ was extracted, evaporated and diluted in MeOH. HHQ-formation was detected using UHPLC-MS/MS. 336 pmol HHQ were formed per pmol H_6PqsD in 25 min.

UHPLC-MS/MS analyses:

The analyses were performed using a TSQ Quantum Access Max mass spectrometer equipped with an ESI source and a triple quadrupole mass detector (Thermo Scientific Finnigan, San Jose, CA). The MS detection was carried out in heated ESI mode, at a spray voltage of 3.0 kV, a probe temperature of 500

°C, a nitrogen sheath gas pressure of 3.5×10^5 Pa, an auxiliary gas pressure of 1.75×10^5 Pa and a capillary temperature of 330 °C in positive ionization mode.

Xcalibur software was used for data acquisition and for the quantitative evaluation of the MS data and GraphPad Prism software (version 5.0) was used for plotting.

The chromatographic separation was carried out on an Accela UHPLC consisting of a quaternary pump, degasser and autosampler (Thermo Finnigan, San Jose, CA) using a Accucore RP-MS column (150 x 2.6µm) with an injection volume of 25 µL.

The solvent system consisted of water, containing 10 mM ammonium acetate and 0.1% TFA (A) and acetonitril containing 0.1% TFA (B). In a gradient run the percentage B was increased from an initial concentration of 45 % to 96 % in 1.50 min, kept for 0.1 min. The injection volume was 25 µL and the flow rate was set to 880 µL/min. The amount of HHQ was determined observing the precursor ion 244.191 m/z and the product ion 159.134 m/z, with a scan time of 0.1 sec and a collision voltage of 31V.

For HHQ a calibration of 39, 78, 156, 312, 1250, 2500, 5000 pM was used.

References

[1] I. Navratilova, and Myszka, D. G., Investigating Biomolecular Interactions and Binding Properties Using SPR Biosensors, Surface Plasmon Resonance Based Sensors, Springer Ser. Chem. Sens. Biosens. 4 (2006) 155-176.
[2] P. Pattnaik, Surface plasmon resonance, Appl. Biochem. Biotech. 126 (2005) 79-92.
[3] R. B. M. Schasfoort, and Tudos, A. Handbook of Surface Plasmon Resonance 2008, pp. 1-14.
[4] D. G. Myszka, Rich, R. L., and Matthew, A. C. Extracting affinity constants from biosensor binding responses. Label-Free Biosensors, Cambridge University Press 2009, pp. 48-84.
[5] D. G. Myszka, Improving biosensor analysis, J. Mol. Recognit. 12 (1999) 279-284.
[6] A. P. van der Merwe, Surface Plasmon Resonance
[7] E. C. Pesci, Milbank, J. B. J., Pearson, J. P., McKnight, S., Kende, A. S., Greenberg, E. P., and Iglewski, B. H., Quinolone signaling in the cell-to-cell communication system of Pseudomonas aeruginosa, Proc. Natl. Acad. Sci. 96 (1999) 11229-11234.
[8] L. A. Gallagher, McKnight, S. L., Kuznetsova, M. S., Pesci, E. C., and Manoil, C., Functions Required for Extracellular Quinolone Signaling by Pseudomonas aeruginosa, J. Bacteriol. 184 (2002) 6472-6480.
[9] Y.-M. Zhang, Frank, M. W., Zhu, K., Mayasundari, A., and Rock, C. O., PqsD Is Responsible for the Synthesis of 2,4-Dihydroxyquinoline, an Extracellular Metabolite Produced by Pseudomonas aeruginosa, J. Biol. Chem. 283 (2008) 28788-28794.
[10] D. Pistorius, Ullrich, A., Lucas, S., Hartmann, R. W., Kazmaier, U., and Müller, R., Biosynthesis of 2-Alkyl-4(1H)-Quinolones in Pseudomonas aeruginosa: Potential for Therapeutic Interference with Pathogenicity, ChemBioChem 12 (2011) 850-853.
[11] E. J. Simon, and Shemin, D., The Preparation of S-Succinyl Coenzyme A, J. Am. Chem. Soc. 75 (1953) 2520-2520.
[12] C. Lu, Kirsch, B., Zimmer, C., de Jong, J., Henn, C., Maurer, C., Müsken, M., Häussler, S., Steinbach, A., and Hartmann, R. W., Discovery of Antagonists of PqsR, a Key Player in 2-Alkyl-4-quinolone-dependent Quorum Sensing in Pseudomonas aeruginosa, Chem. Biol. (2012) doi:10.1016/j.chembiol.2012.01.015.
[13] J.-F. Dubern, Diggle, S. P., Quorum sensing by 2-alkyl-4-quinolones in Pseudomonas aeruginosa and other bacterial species, Mol. BioSystems 4 (2008) 882-888.
[14] A. K. Bera, Atanasova, V., Robinson, H., Eisenstein, E., Coleman, J. P., Pesci, E. C., and Parsons, J. F., Structure of PqsD, a Pseudomonas Quinolone Signal Biosynthetic Enzyme, in Complex with Anthranilate, Biochem. 48 (2009) 8644-8655.
[15] F. Lépine, Milot, S., Déziel, E., He, J., and Rahme, L., Electrospray/mass spectrometric identification and analysis of 4-hydroxy-2-alkylquinolines (HAQs) produced by *Pseudomonas aeruginosa*, J. Am. Soc. Mass Spectrom. 15 (2004) 862-869.
[16] D. G. Myszka and T. Morton, CLAMP©: a biosensor kinetic data analysis program, Trends Biochem. Sci. 23 (1998) 149-150.

3.5 Disclosure of the kinetic cycle of PqsD by enzyme kinetics and SPR and MD simulations

Matthias Negri, Christine Maurer, **Claudia Henn,** Anke Steinbach, Rolf W. Hartmann

Introduction

Quorum sensing (QS) is a chemical cell-to-cell communication system in bacteria ruled by small extracellular signal molecules. It coordinates the social life of bacteria by regulating many intraspecies and interkingdom group-related behaviors, such as biofilm formation and virulence factor production[1-3]. Anti-QS has been recognized as an attractive strategy in the fight against bacteria, which is based on an anti-virulence and anti-biofilm action and not on bacterial killing. The advantage of this approach relies in the expectation of a reduced selective pressure and, hence, minor resistance development.

The opportunistic Gram-negative pathogen *P. aeruginosa* has been shown to be a good model to study QS and QS-related pathogenicity [3]. Three distinct QS pathways are known, each with its own individual signal molecule as “autoinducer”. They regulate in a hierarchical manner the QS-dependent target gene expression and the biosynthesis of their “autoinducer”. The first two quorum sensing systems, las [4] and rhl [5, 6], utilize N-acyl homoserine lactones (AHL) (C4 and C12 AHL) and the receptors LasR and RhlR [7]. The third QS-system is 2-alkyl-4-hydroxyquinoline (HAQ) dependent and is specific for *P. aeruginosa* [8] and some *Burkholderia* strains [9] whereat only *P. aeruginosa* produces PQS (Pseudomonas Quinolone Signal). PQS and to a lesser extent its precursor HHQ (2-heptyl-4-hydroxyquinoline) activate PqsR (MvfR: Multiple virulence factor Regulator 10]). Besides many other genes, PqsR also controls the PQS signaling by positively regulating (McGrath et al, 2004) the expression of genes of its own biosynthesis operons (pqsABCD(E)[11] (HAQ biosynthesis) phnAB5[10] operons (anthranilic acid biosynthesis). A key enzyme of PQS biosynthesis pathway is PqsD (PQB biosynthetic 3-oxoacyl-[acyl-carrier-protein] synthase III; EC 2.3.1.180), which catalyzes the formation of HHQ by “head-to-head” decarboxylative condensation of anthranilic acid and 3-oxo-fatty acid moieties, i.e. anthraniloyl-CoA (ACoA) and β-ketodecanoate (βK)-ACP [12].

Target validation of PQS system: Several groups proved that *P. aeruginosa* pqsD-knockout-mutant as well as PQS-deficient *P. aeruginosa* strains have an attenuated virulence in nematode and mouse models, evidencing the significance of PQS signaling also in mammalian pathogenesis[10, 13-15]. The commitment to the PQS cell-to-cell communication system makes PqsD to a promising target, as inhibition of the biosynthesis of HHQ will also interrupt PQS formation. Consequently, inhibition of HHQ biosynthesis should reduce biofilm formation making the bacteria more susceptible to classic antibiotics.

PqsD is a homodimeric bi-substrate enzyme with high structural similarity to FabH and other KAS III (β-ketoacyl-acyl-carrier-protein [ACP] synthases III) enzymes sharing a virtually identical active site architecture with a long access channel and catalytic triad and common thiolase fold (αβαβα) [16].
Three crystal structures of PqsD exist [17] either as unligated apoform (E; PDB-ID 3H76), as Cys112-ligated anthranilate complex and additional ACoA molecules in the primary funnel (E*; PDB-ID 3H77) and as inactive Cys112Ala mutant with anthranilic acid (PDB-ID 3H78)[17]. Cys112, His257, and Asn287 form the FabH-like catalytic triad of PqsD, which can be accessed by two channels perpendicular (L-shaped) to each other: a primary, well exploited CoA/ACP-funnel, and a shorter, hydrophobic secondary channel. The three crystal structures contribute to elucidate entrance and active site binding of ACoA as well as the active site conformation after covalent bondage of anthranilate to Cys112, the molecular details as well as the dynamic motions governing the kinetic cycle of the HHQ-biosynthesis remain still unknown.

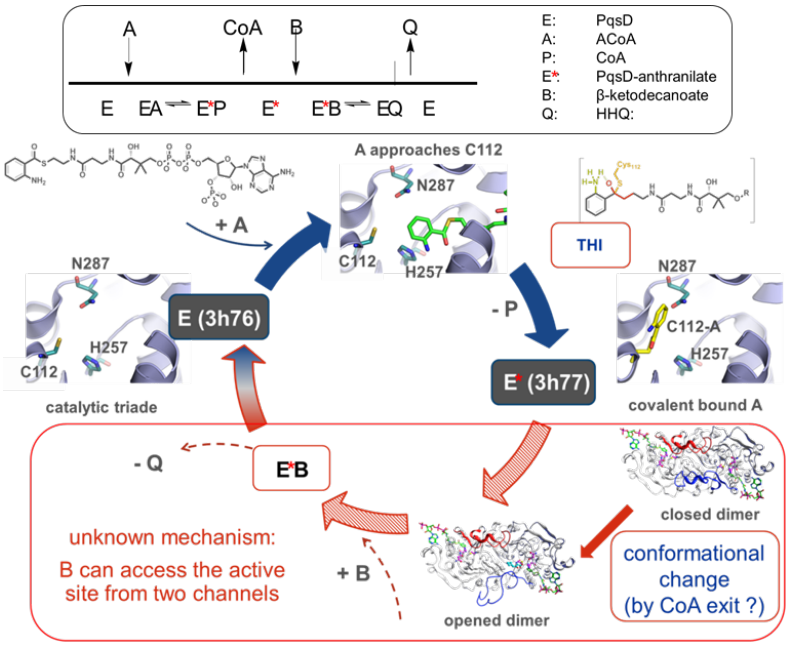

Figure 1. *Bi-bi ping-pong kinetic cycle of PqsD. Steps linked by blue arrows are supported by existing crystallographic data and the starting conformation of protein and ligands were derived from them. On contrary, no 3D-information was available for the steps linked by red arrows, thus the position of βK and HHQ, as well as the conformational changes within the hairpin-loop were derived from comparative studies with MtFabH (βK), docking studies (HHQ) and hinge-analysis/-prediction tools*

In this study we chose a multi-disciplinary approach to disclose the dynamic motions that guide the kinetics of PqsD in HHQ biosynthesis. We postulated a kinetic cycle model for the presumed ping-pong mechanism Thereby, we determined the kinetics of the HHQ-biosynthesis by surface plasmon resonance (SPR) biosensor experiments and classic enzyme kinetic analysis.

Results

The main steps of the kinetic cycle of PqsD were postulated from mechanistic insights of the kinetic cycle based on the crystal structures of PqsD [17] and molecular dynamic simulations (Figure1).

Surface Plasmon Resonance

Our first aim was to prove that PqsD follows a ping-pong mechanism in the HHQ-biosynthesis. PqsD was immobilized as a dimer with a His-tag to the chip. After the first substrate ACoA was added, an increase in response (Figure 2) was measured corresponding to the covalent linkage of anthranilate (A) to Cys112, confirmed also after washing processes. The CoA release was detected using mass spectrometry.

As expected, addition of the second substrate β-ketodecanoic acid (βK) could displace the anthranilate from its covalent binder Cys112 (Figure 2A) with consequent HHQ formation, as proven by determining HHQ via mass spectrometry (Figure 2B).

To further investigate the single steps of the bi-bi ping-pong kinetics the experiment was repeated but inverting the substrate order. Thereby, only a very small amount of HHQ could be determined indicating that a precise substrate addition order is necessary for catalytic activity, suggesting that the presence of βK in the enzyme could eventually block the access to the catalytic triad, drastically reducing the affinity of ACoA towards H_6PqsD (Figure 2B)

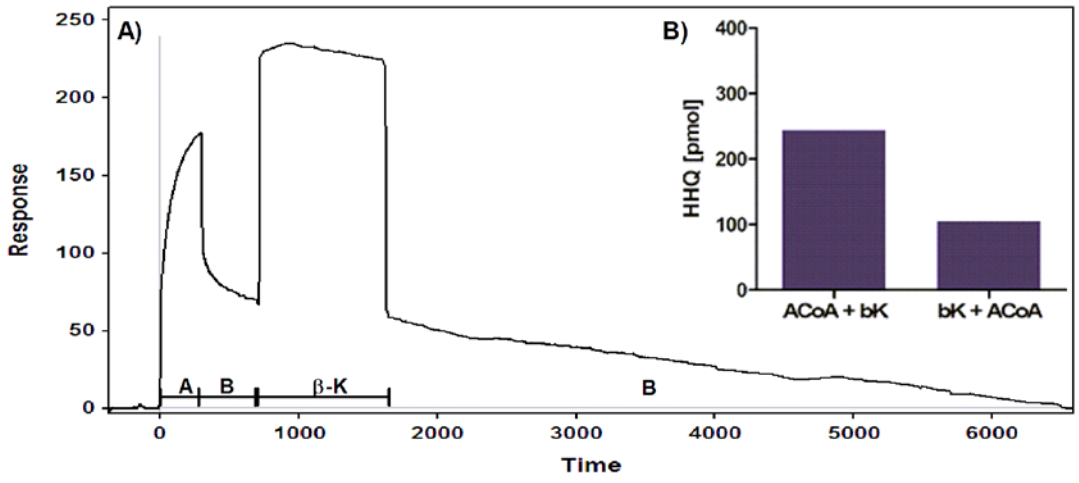

Figure 2. *A.) SPR experiments were performed at 37° C with Tris-buffer (50 mM Tris-HCl pH 8.0, 0.1% Triton-X-100) as running buffer, 1.6 pmol protein concentration and 10 µM ACoA and 20 µM βK. B) (Time-dependent) HHQ-formation as function of the substrate addition order determined by SPR experiments.*

Enzyme kinetic analysis

As resulted from the SPR experiments HHQ production is strongly influenced by the substrate addition order (Figure 2B). Thus, enzyme kinetic studies were performed to elucidate the kinetic parameters for each substrate.

Kinetic experiments were performed using a 96-well format based in vitro assay with the purified enzyme PqsD. Optimum enzymatic reaction conditions were determined in advance. Plotting product formation versus time at different constant PqsD concentrations we found that a reaction time of 4 min in combination with an enzyme concentration of 0.25 µM was suitable and that values in linear range within the progress curve could be obtained (data not shown). The initial velocity (v) was calculated by dividing the product concentration by the reaction time.

Plotting the data with the enzyme kinetics module of GraphPad Prism 5 software resulted in an array of parallel lines in the Lineweaver-Burk-Plot and a common Y-axis-intercept in the Hanes-Woolf-Plot (Figure 3). These results clearly demonstrate that PqsD follows a ping-pong kinetic mechanism and that ACoA is the substrate binding first.

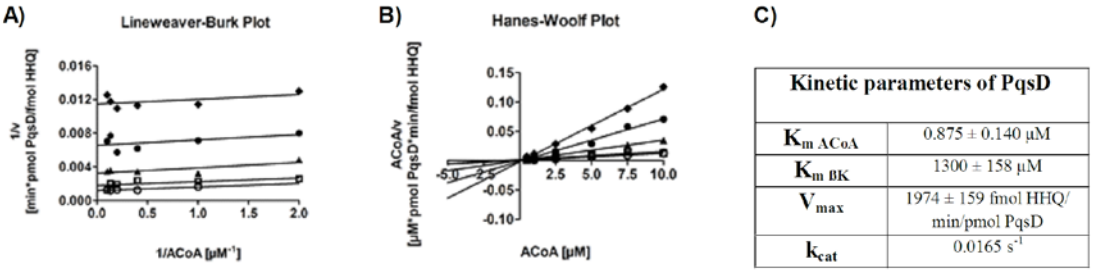

Figure 3. *Analysis of the PqsD kinetic mechanism. Lineweaver-Burk Plot (A) and Hanes-Woolf Plot (B) representing the activity of PqsD as a function of ACoA concentration in the presence of 60 (diamonds), 120 (black circles), 240 (triangles), 480 (open squares) and 1000 µM (open circles) ß-ketodecanoic acid. All data are mean values of four replicates. (C) Kinetic parameters of PqsD. All data were fitted using GraphPad Prism 5 software.*

kinetic parameters (s. Figure 3(C)) were determined by fitting the data with the ping-pong equation (1) [Segel, Enzyme kinetics, p. 609, equation IX-143]:

$$v = Vmax * [ACoA] / (Km\ ACoA + [ACoA] (1 + (Km\ ßkt / [ßkt]))) \quad (1)$$

Discussion

In this study we could clearly prove the results from molecular dynamic simulation (Figure 1). We could show via classic enzymology and, in particular, by SPR experiments, that PqsD is biosynthesizing HHQ following the ping-pong catalytic mechanism with a precise substrate addition order (Figure 3).

SPR biosensor experiments allowed real time measurements of the HHQ biosynthesis, starting from the covalent anthranilate loading on PqsD to the final βK-dependent HHQ-production we were able to trace the formation of the covalent linkage of anthranilate (A) to Cys112, but also of the displacement of anthranilate from its covalent binder Cys112 by addition of the second substrate βK. The CoA release as well as the HHQ production was confirmed by mass spectrometry as additional validation of the HHQ biosynthesis. Reversing the substrate addition order we could show that a clear substrate

order dependency exists for HHQ biosynthesis with PqsD. The mass spectrometry determination of the first step product CoA before addition of the second substrate was an important contribution supportive that PqsD follows a bi-bi kinetic mechanism. The obtained kinetic parameters were in accordance with previous findings by Pistorius *et al.* ($K_{mßK}$ = 598.5 ± 106 µM; V_{max} = 495.8 ± 37.5 fmol HHQ/min/pmol PqsD; k_{cat} (PqsD as monomer) = 0.01 s^{-1}). We explain the slightly increased catalytic activity of PqsD with more stable assay conditions and with optimized pH range (50 mM MOPS buffer at pH 7 versus 50 mM Tris-HCl) (data not shown). Taken the high K_m for ß-ketodecanoic acid and the very low kcat of the PqsD catalyzed formation of HHQ from anthraniloyl CoA and ß-ketodecanoic acid account for the presumption, that ßK might not be the natural substrate of PqsD in *P. aeruginosa* and that it might occur in vivo in its activated form bound to CoA or ACP.

In order to disclose the kinetic mechanism of PqsD kinetic analyses were performed using an in vitro assay with the purified enzyme. Different plots of the kinetic data reveal that PqsD follows a ping-pong kinetic mechanism (s. Figure 3A and B).

The kinetic parameters were derived from the variation of both substrates (s. Figure 3C) and are within the range of the apparent values previously determined by Pistorius et al. 2011 (app. $K_{mßK}$ = 598.5 ± 106 µM; V_{max} = 495.8 ± 37.5 fmol HHQ/min/pmol PqsD; k_{cat} (PqsD as monomer) = 0.01 s^{-1}). We believe that the higher catalytic activity in our assay system is due to an improvement of assay conditions, as the reactions were performed in 50 mM MOPS buffer at pH 7.0, which was found to be the pH optimum of the enzymatic reaction (data not shown; versus 50 mM Tris-HCl, pH 8.0) and as Triton X-100 was used in sub-CMC concentrations (0.005% versus 0.1%).

Nevertheless, taken together both results, the high K_m for ß-ketodecanoic acid and the very low k_{cat} of the PqsD catalyzed formation of HHQ from anthraniloyl CoA and ß-ketodecanoic acid account for the presumption, that ß-ketodecanoic acid is not the natural substrate of PqsD in *P. aeruginosa*. This hypothesis is supported by the fact that very high amounts of HHQ and PQS are found in *P. aeruginosa* cultures [18]. Thus, we think that in vivo ß-ketodecanoic acid occurs in an activated form, possibly as an ACP-bound thioester.

Conclusion

Herein we chose a multi-disciplinary approach to disclose the dynamic motions that guide the ping-pong kinetic mechanism, of PqsD in HHQ biosynthesis. We showed by surface plasmon resonance (SPR) biosensor experiments and classic enzyme analysis that PqsD synthesizes HHQ biosynthesis following a ping-pong kinetic mechanism with a preferential substrate order, Notably, PqsD is still catalytically active when attached to the chip and real time measurements by SPR could be performed with Cys112-liganded anthranilate being displaced by βK and HHQ formed.

Based on structural, biochemical and biophysical data we postulated the kinetic cycle of PqsD.

Our work described herein lays the basis for a better understanding of the kinetic mechanism of PqsD and of the dynamic motions therein. Moreover, as recently shown by Perez-Castillo [19] with *E. coli*

FabH exploration of a conformational ensemble generated via MD simulations led to enviable results in terms of molecular docking and binding free energy prediction. According to the structural similarity we conclude that analogous results are to be expected also for PqsD and that the conformer ensemble generated in this study will be a useful tool in virtual screening and ensemble docking to identify first PqsD inhibitors as potential drugs to treat *P. aeruginosa* infections and related biofilm formation. Concluding, given the high similarity to Burkholderia FabH2 all information derived in this study might also be applied to this enzyme and bacterial strains, representative for a more general character and importance of the investigations presented herein.

Acknowledgement

We thank Cenbin Lu for the synthesis of HHQ and ß-ketodecanoic acid and Prof. Müller for the kind provision of the plasmid pET28b(+)-pqsD.

Material and Methods

Experimental procedures

Coenzyme A trilithium salt dihydrate was purchased from Applichem and isatoic acid from Acros Organics.

Chemical and analytical methods

^{1}H and ^{13}C NMR spectra were recorded on a Bruker DRX-500 instrument. Chemical shifts are given in parts per million (ppm), and tetramethylsilane (TMS) was used as internal standard for spectra obtained in $CDCl_3$ and MeOH-d_4. All coupling constants (J) are given in hertz. Mass spectrometry (LC/MS) was performed on a MSQ® electro spray mass spectrometer (Thermo Fisher). The system was operated by the standard software Xcalibur®. A RP C18 NUCLEODUR® 100-5 (125 x 3 mm) column (Macherey-Nagel GmbH) was used as stationary phase with water/acetonitrile mixtures as eluents. All solvents were HPLC grade. Reagents were used as obtained from commercial suppliers without further purification. Flash chromatography was performed on silica gel 60, 70-230 mesh (Fluka) and the reaction progress was determined by thin-layer chromatography (TLC) analyses on silica gel 60, F254 (Merck). Visualization was accomplished with UV light. The melting points were measured using melting point apparatus SMP3 (Stuart Scientific). The apparatus is uncorrected.

Synthesis of Anthraniloyl-S-Coenzym A thioester (ACoA): ACoA was synthesized from isatoic anhydride and coenzyme A (CoA) using a previously described method (Simon EJ, Shemin D. The Preparation of S-Succinyl Coenzyme A. J. Am. Chem. Soc 1953;75:2520). ACoA was purified by HPLC (Agilent 1200 series consisting of a quaternary pump, a fraction collector and an MWD; Agilent Technologies, USA) after freeze drying of the aqueous reaction mixture (25 mL) and resuspending of the dried residue in 3 mL of a mixture of 50% methanol and water. A 10 µm RP C18 150-30 column (30 x 100 mm, Agilent) was used along with a mobile phase consisting of water

containing 1‰ TFA (A) and acetonitrile containing 1‰ TFA (B) with a flow rate of 5 mL/min. The following gradient was used: 0-35 min, linear gradient 10 % - 100 % B; 35-42 min, 100 % B; 42-43 min, 10 % B (initial conditions). ACoA containing fractions were pooled and freeze dried.

Synthesis of ethyl 3-oxodecanoate: To a THF solution of 2M LDA (20 ml, 40 mmol 2.4 equiv) was added ethyl acetoacetate (2.16 g, 16.6 mmol, 1.0 equiv) at 0 °C. The deep yellow clear solution was stirred at 0 °C for 1 h. To this solution the 1-iodohexane was added (4.20 g, 19.81 mmol, 1.2 equiv) at -78 °C. The temperature was allowed to reach an ambient temperature over 14 h and the solution was stirred at r.t. for 2 h. To the solution was added 10% HCl (200 ml) and the mixture was extracted with Et_2O (4 × 250 ml). The combined organic layers were dried over Na_2SO_4, filtered, and the filtrate was concentrated in vacuo. The residue was purified by column chromatography (n-hexane/ethyl acetate, 30/1) to give ethyl 3-oxodecanoate as a yellow oil (1.98 g, 9.24 mmol, 55%). 1H-NMR (500 MHz, $CDCl_3$): δ = 0.84 (t, J = 7.0 Hz, 3H), 1.23-1.28 (m, 11H), 1.54 (quint, J = 7.0 Hz, 2H), 2.49 (t, J = 7.0 Hz, 2H), 3.39 (s, 2H), 4.16 (m, 2H). LC/MS: m/z 457.98, 87.1% (Nguyen et al., 2006).

Synthesis of 3-oxodecanoic acid. Ethyl 3-oxodecanoate (300 mg, 1.4 mmol, 1 equiv) was stirred with NaOH (56 mg, 1.4 mmol, 1 equiv) in water (2 ml) overnight. Any remaining ester was removed by washing with Et_2O (10 ml). The aqueous layer was cooled and acidified with 32% HC1 to pH = 6. After filtration the 3-oxodecanoic acid was dried in vacuo and obtained as white solid (100 mg, 0.54 mmol, 38%). ^{1}H-NMR (500 MHz, $CDCl_3$): δ = 0.86 (t, J = 7.0 Hz, 3H), 1.25-1.29 (m, 8H), 1.58 (quint, J = 7.0 Hz, 2H), 2.54 (t, J = 7.5 Hz, 2H), 3.49 (s, 2H). LC/MS: m/z 242.04, 99.0% (Cook et al., 1987).

Synthesis of 2-heptylquinolin-4(1H)-one. 2-heptylquinolin-4(1H)-one was synthesized as described by Lu et al. 2012 [20].

Production and purification of recombinant PqsD in *E. coli.* The overexpression and purification of PqsD as an N-terminal His_6-tagged fusion protein in *E.coli* BL 21 (lambdaDE3) using the vector pET28b(+) -pqsD was performed using a previously described method (Pistorius et al. 2011) with the following modifications: bacterial cells were lysed by ultrasonic treatment (Bandelin Sonopuls HD60) in binding buffer consisting of 25 mM Tris-HCl, pH 7.9, 150 mM NaCl, 20 mM imidazole, 1 mM 2-mercaptoethanol (2-ME) and 10 % (v/v) glycerol. For purification, a 5 ml His Trap HP 5 column was used. The elution buffer consisted of binding buffer with 500 mM imidazole. The protein containing fractions were buffer exchanged to 50 mM Tris-HCl, pH 8.0, 50 mM NaCl, 1 mM 2-ME using PD10 columns (Amersham Biosciences).

To remove the His_6-tag, the obtained protein was subjected to a thrombin cleavage performed at 16°C for 16 h in a 50 mM Tris-HCl buffer, pH 8.0, containing 150 mM NaCl, 1 mM 2-ME, 2.5 mM CaCl2 and 1 unit thrombin per mg protein followed by a second passage through the His Trap HP 5 column. After addition of 10 % (v/v) glycerol, the final protein concentration was determined spectrophotometrically (A280 nm) and the protein was frozen in liquid nitrogen.

Computational Methods

Simulation protocol. System setup was performed as follows for all simulated systems. Atomic coordinates were taken from 3h76 for MD simulations A, B, C1, C2 and F, from 3h77 for D, E1, E2a and E2b. Protonation states for histidines and other titratable groups were determined at pH 7 and 8 by the PDB2PQR13 web server using PROPKA14 and manually verified. Water moleules as well as ions present in the crystals were removed. The enzyme complexes were minimized with MOE (ref) using the modules ligX and Protonate3D. All final systems were then setup using the AMBER11 [21] program xLeap with the AMBER99SB force field. A 9 Å pad of TIP3P waters was added to solvate to each system. Neutralizing counter ions were added to each system.

All MD simulations were performed with the parallelized PMEMD module from AMBER 11 [21]. The initial PqsD complexes were minimized and equilibrated, with the backbone atoms restricted by harmonic restraints of initially 10 kcal mol $^{-1}$ Å $^{-2}$.on the backbone atoms were progressively reduced to 5, 2, 1 and 0 kcal/mol. After minimization, the system was heated to 310 K in the canonical NVT ensemble (constant number of particles, N; constant volume, V; constant temperature, T) using a Langevin thermostat, with a collision frequency of 3.0 ps $^{-1}$ Å $^{-2}$ on the backbone atoms. Production runs were then made for 30-37 ns duration in the NPT ensemble at 300 K. As with the heating, the temperature was controlled with a Langevin thermostat (but with a 1.0 ps $^{-1}$ collision frequency). The time step used for all stages was 2 fs and all hydrogen atoms were constrained using the SHAKE algorithm. Long-range electrostatics were included on every step using the Particle Mesh Ewald algorithm [22] with a 4th order B-spline interpolation, a grid spacing of < 1.0 Å, and a direct space cutoff of 9 Å. For all trajectories, the random number stream was seeded using the wall clock time in microseconds.

RMSD, interatomic distances and B-factor calculations. B-factor, distances and RMSD time series were calculated using the cpptraj analysis tool of the AmberTool 1.5 package [21]. Structures were sampled at 20 ps intervals. Before performing each calculation, external translational and rotational motions were removed by minimizing the RMSD distance of the alpha-carbon atoms to the equivalent atoms of the first frame of the trajectory. RMSD and B-factor values were calculated for all heavy-atoms and in particular for each of the following regions: sL, h8-9, hL, h12.

Volume changes with FPOCKET. The volume changes for the five internal cavities in PqsD were tracked using the fpocket software package [23]. Default parameters for the identification of small cavities and channels were used.

Docking of βK and HHQ. βK and HHQ were docked with GOLDv5.0 using the GOLDSCORE function. The docking site was defined including all residues within 9 Å of the ACoA found in PDB 3H77 and both the apoform and the covalent ligated PqsD structure were used in the docking processes. βK and HHQ were docked each 50 times. The default gold parameters were used.

Figures and plots. Excel was used to generate all plots and molecular images were created using Pymol or MOE2010.

MM-PBSA Calculations. MM-GB/PBSA was used to calculate the relative binding free energies of ACoA, βK and HHQ to PqsD. The details of this method have been presented elsewhere. Briefly, the binding affinity for a protein/ligand complex corresponds to the free energy of association in solution as shown in

$$\Delta G_{bind} = G_{complex} - (_{Gunbound\ protein} + G_{free\ ligand}) \quad (1)$$

while the relative affinities for two ligands can be calculated using

$$\Delta\Delta G_{bind(1\rightarrow 2)} = \Delta G_{bind(2)} - \Delta G_{bind(1)} \quad (2)$$

In MM-PBSA, the binding affinity in eq 1 is typically calculated using

$$\Delta G_{bind} = \Delta E_{MM} + \Delta G_{solv} - T\Delta S_{solute} \quad (3)$$

where ΔE_{MM} represents the change in molecular mechanics potential energy upon formation of the complex, calculated using all bonded and nonbonded interactions. Solvation free energy, G_{solv}, is composed of the electrostatic component (G_{PB}) and a nonpolar component (G_{np}):

$$\Delta G_{solv} = \Delta G_{PB} + \Delta G_{np} \quad (4)$$

G_{PB} was calculated using the PBSA solver of AMBER11.

Surface Plasmon Resonance

SPR binding studies were performed using a Reichert SR7000DC optical biosensors instrument (Reichert Technologie, Depew, NY 14043 USA). HC1000m sensor chips were purchased from Xantec Analytics. (Düsseldorf, Germany).

Immobilisation of H_6PqsD. The overexpression and purification of PqsD as an N-terminal His_6-tagged fusion protein in *E.coli* BL 21 (λDE3) using the vector pET28b(+) -pqsD was performed as previously described (Henn *et al*. 2012). H_6PqsD was immobilized on HC1000m sensor chip using standard amine coupling chemistry at 25 °C. Water was used as the running buffer. The carboxymethyl dextran surface was activated with a 7-min injection of a 1:1 ratio of 0.4 M 1-ethyl-3-(3-dimethylaminopropyl) carbodiimide hydrochloride (EDC)/0.1 M N-hydroxy succinimide (NHS). H_6PqsD was diluted into 10 mM sodium acetate (pH 4.5) to a concentration of 100 µg/mL and coupled to the surfaces with a 18 min injection. Remaining activated groups were blocked with a 7-min injection of 1 M ethanolamine (pH 8.5). PqsD was immobilized at densities between 15000 and 20000 RU.

Catalytic activity of PqsD. Anthranoyl-CoA was provided as stock solution in water and was diluted into running buffer to 10 µM. β-ketodecanoate was dissolved in methanol to a 10 mM stock solution and then diluted into running buffer to 20 µM. In the first experiment ACoA was injected for 5 Min association and 10 Min dissociation time the injection was followed by the injection of β-Ketodecanoate for 20 Min association time. In the second experiment β-ketodecanoate was added to the running buffer (100 µM in 50mM TRIS pH 8.0, 150 mM NaCl, 0.1% Triton-X-100). The ACoA-injection (10 µM for 5 Min) followed when the binding site was saturated, indicated by a stable baseline.

In all experiments the flow through was collected. After ACoA addition CoA emission was detected using LC-MS/MS (method missing). After addition of the second substrate (experiment dependent) the flow through was extracted with 1 mL $CHCl_3$, evaporated and diluted in 50µL MeOH. HHQ-formation was detected using LC-MS/MS according the method described below.

LC-MS/MS analysis of CoA The analyses were performed using a TSQ Quantum Access Max mass spectrometer equipped with an ESI source and a triple quadrupole mass detector (Thermo Scientific Finnigan, San Jose, CA). The MS detection was carried out in heated ESI mode, at a spray voltage of 3.0 kV, a probe temperature of 500 °C, a nitrogen sheath gas pressure of 3.5 x 10^5 Pa, an auxiliary gas pressure of 1.75 x 10^5 Pa, a capillary temperature of 330 °C positive ionization mode.

Xcalibur software was used for data acquisition and GraphPad Prism software (version 5.0) was used for plotting.

The chromatographic separation was carried out on an Accela UHPLC consisting of a quaternary pump, degasser and autosampler (Thermo Finnigan, San Jose, CA) using a Accucore RP-MS column (150 x 2.6µm) with an injection volume of 25 µL.

The solvent system consisted of water, containing 10 mM ammonium acetate and 0.1% TFA (A) and acetonitril containing 0.1% TFA (B). In a gradient run the percentage B was increased from an initial concentration of 5 % to 96 % in 1.50 min, kept for 0.1 min. The injection volume was 25 µL and the flow rate was set to 1000 µL/min. CoA was determined observing the precursor ion 768.0 m/z and the product ion 260.977 m/z, with a scan time of 0.5 sec and a collision voltage of 27V.

LC-MS/MS analysis of HHQ.The analyses were performed using a TSQ Quantum Access Max mass spectrometer equipped with an ESI source and a triple quadrupole mass detector (Thermo Scientific Finnigan, San Jose, CA). The MS detection was carried out in heated ESI mode, at a spray voltage of 3.0 kV, a probe temperature of 500 °C, a nitrogen sheath gas pressure of 3.5 x 10^5 Pa, an auxiliary gas pressure of 1.75 x 10^5 Pa and a capillary temperature of 330 °C in positive ionization mode.

Xcalibur software was used for data acquisition and for the quantitative evaluation of the MS data and GraphPad Prism software (version 5.0) was used for plotting.

The chromatographic separation was carried out on an Accela UHPLC consisting of a quaternary pump, degasser and autosampler (Thermo Finnigan, San Jose, CA) using a Accucore RP-MS column (150 x 2.6µm) with an injection volume of 25 µL.

The solvent system consisted of water, containing 10 mM ammonium acetate and 0.1% TFA (A) and acetonitril containing 0.1% TFA (B). In a gradient run the percentage B was increased from an initial concentration of 45 % to 98 % in 1.50 min, kept for 0.1 min. The injection volume was 25 µL and the flow rate was set to 880 µL/min. The amount of HHQ was determined observing the precursor ion 244.191 m/z and the product ion 159.134 m/z, with a scan time of 0.1 sec and a collision voltage of 31V.

For HHQ a calibration of 39, 78, 156, 312, 1250, 2500, 5000 pM was used.

Enzyme kinetic analysis. The PqsD catalyzed formation of HHQ was analyzed using an LC-MS/MS based in vitro assay performed in 96 -well microtiter plates (Greiner) using the method of Pistorius et al. [12] with some modifications. First, the purified enzyme PqsD (0.8 µM; in 50 mM MOPS, pH 7.0, 0.016% (v/v) Triton X-100) was preincubated without substrates for 5 min at 37 °C. Then, the reaction buffer (15 µL; 50 mM MOPS, pH 7.0) and the substrates anthraniloyl CoA (20 µL; concentrations: 2, 4, 10, 20, 30, 40 µM; in 50 mM MOPS, pH 7.0) and ß-ketodecanoic acid (20 µL; concentrations: 240, 480, 960, 1440, 4000 µM; in 50 mM MOPS, pH 7.0, 8% (v/v) methanol) were distributed to the wells of the microtiter plate. The reaction was started by the addition of preincubated enzyme (25 µL; 0.8 µM; in 50 mM MOPS, pH 7.0, 0.016% (v/v) Triton X-100) resulting in a total reaction volume of 80 µL with the following final concentrations: PqsD 0.25 µM, anthraniloyl CoA 0.5, 1.0, 2.5, 5.0, 7.5, 10.0 µM and ß-ketodecanoic acid 60, 120, 240, 480, 1000 µM, Triton X-100 0.005%, methanol 2%. The reaction was stopped after 4 min at 37°C by adding 80 µL of methanol containing 1 µM of the internal standard amitriptyline to give a final concentration of 500 nM. Reagents and buffers were prepared in deionized MilliQ-filtered water. For each sample, the reactions were performed in quadruplicate. GraphPad Prism 5 software was used to plot the kinetic data.

LC-MS/MS analysis of HHQ for enzyme kinetics: The analyses were performed using a TSQ Quantum mass spectrometer equipped with an ESI source and a triple quadrupole mass detector (Thermo Finnigan, San Jose, CA). The MS detection was carried out at a spray voltage of 3.0 kV, a nitrogen sheath gas pressure of 4.0 x 10^5 Pa, an auxiliary gas pressure of 1.0 x 10^5 Pa, a capillary temperature of 270 °C, a tube lens offset of 155 V and source CID of 10 V.

Observed ions were (mother ion [m/z]; collision energy [V]; product ion [m/z]; scan time [s]; scan width [m/z]): HHQ: 243.988; 30; 159.181; 0.3; 3.000, internal standard (Amitriptyline): 278.000; 22; 233.000; 0.1; 3.000. Xcalibur software was used for data acquisition and quantification with the use of a calibration curve relative to the area of the internal standard. All samples were injected by autosampler (Surveyor®, Thermo Finnigan) with a volume of 15 µL. A Nucleodur C18® 3 µm (125 x 3.0 mm) column (Machery-Nagel, Düren, Germany) was used as stationary phase along with a mobile phase consisting of water containing 1‰ TFA (v/v; A) and acetonitril containing 1‰ TFA (v/v; B) and a flow rate of 0.5 mL/min. The following gradient was used: 0-2.8 min, linear gradient 45-100 % B; 2.8-4.5 min 100% B; 4.5-5.5 min initial conditions (45 % B).

References

[1] B. Lesic, Lépine, F., Déziel, E., Zhang, J., Zhang, Q., Padfield, K., Castonguay, M.-H., Milot, S., Stachel, S., Tzika, A. A., Tompkins, R. G., and Rahme, L. G., Inhibitors of pathogen intercellular signals as selective anti-infective compounds, PLoS Pathogens 3, (2007) 1229-1239.

[2] P. Williams, Quorum sensing, communication and cross-kingdom signalling in the bacterial world, Microbiology 153, (2007) 3923-3938.

[3] P. Williams, and Camara, M., Quorum sensing and environmental adaptation in Pseudomonas aeruginosa: a tale of regulatory networks and multifunctional signal molecules, Current Opinion in Microbiology 12, (2009) 182-191.

[4] L. Passador, Cook, J. M., Gambello, M. J., Rust, L., and Iglewski, B. H., Expression of Pseudomonas aeruginosa virulence genes requires cell-to-cell communication, Science 260, (1993) 1127.

[5] U. A. Ochsner, Koch, A. K., Fiechter, A., and Reiser, J., Isolation and characterization of a regulatory gene affecting rhamnolipid biosurfactant synthesis in Pseudomonas aeruginosa, Journal of Bacteriology 176, (1994) 2044-2054.

[6] U. A. Ochsner, and Reiser, J., Autoinducer-mediated regulation of rhamnolipid biosurfactant synthesis in Pseudomonas aeruginosa, Proceedings of the National Academy of Sciences of the United States of America 92, (1995) 6424-6428.

[7] E. K. Shiner, Rumbaugh, K. P., and Williams, S. C., Interkingdom signaling: Deciphering the language of acyl homoserine lactones, FEMS Microbiology Reviews 29, (2005) 935-947.

[8] E. C. Pesci, Milbank, J. B., Pearson, J. P., McKnight, S., Kende, A. S., Greenberg, E. P., and Iglewski, B. H., Quinolone signaling in the cell-to-cell communication system of Pseudomonas aeruginosa, Proceedings of the National Academy of Sciences of the United States of America 96, (1999) 11229-11234.

[9] S. P. Diggle, Lumjiaktase, P., Dipilato, F., Winzer, K., Kunakorn, M., Barrett, D. A., Chhabra, S. R., Cámara, M., and Williams, P., Functional genetic analysis reveals a 2-Alkyl-4-quinolone signaling system in the human pathogen Burkholderia pseudomallei and related bacteria., Chemistry & Biology 13, (2006) 701-710.

[10] H. Cao, Krishnan, G., Goumnerov, B., Tsongalis, J., Tompkins, R., and Rahme, L. G., A quorum sensing-associated virulence gene of Pseudomonas aeruginosa encodes a LysR-like transcription regulator with a unique self-regulatory mechanism, Proceedings of the National Academy of Sciences of the United States of America 98, (2001) 14613-14618.

[11] G. Xiao, Déziel, E., He, J., Lépine, F., Lesic, B., Castonguay, M.-H., Milot, S., Tampakaki, A. P., Stachel, S. E., and Rahme, L. G., MvfR, a key Pseudomonas aeruginosa pathogenicity LTTR-class regulatory protein, has dual ligands, Molecular microbiology 62, (2006) 1689-1699.

[12] D. Pistorius, Ullrich, A., Lucas, S., Hartmann, R. W., Kazmaier, U., and Müller, R., Biosynthesis of 2-Alkyl-4(1H)-Quinolones in Pseudomonas aeruginosa: Potential for Therapeutic Interference with Pathogenicity, Chembiochem : a European journal of chemical biology 12, (2011) 850-853.

[13] D. A. D´Argenio, Wu, M., Hoffman, L. R., Kulasekara, H. D., Déziel, E., Smith, E. E., Nguyen, H., Ernst, R. K., Larson Freeman, T. J., Spencer, D. H., Brittnacher, M., Hayden, H. S., Selgrade, S., Klausen, M., Goodlett, D. R., Burns, J. L., Ramsey, B. W., and Miller, S. I., Growth phenotypes of Pseudomonas aeruginosa lasR mutants adapted to the airways of cystic fibrosis patients., Molecular microbiology 64, (2007) 512-533.

[14] L. A. Gallagher, McKnight, S. L., Kuznetsova, M. S., Pesci, E. C., and Manoil, C., Functions required for extracellular quinolone signaling by Pseudomonas aeruginosa, Journal of Bacteriology 184, (2002) 6472-6480.

[15] E. Déziel, Gopalan, S., Tampakaki, A. P., Lépine, F., Padfield, K. E., Saucier, M., Xiao, G., and Rahme, L. G., The contribution of MvfR to Pseudomonas aeruginosa pathogenesis and quorum sensing circuitry regulation: multiple quorum sensing-regulated genes are modulated without affecting lasRI, rhlRI or the production of N-acyl-L-homoserine lactones, Molecular microbiology 55, (2005) 998-1014.

[16] J.-L. Ferrer, Jez, J. M., Bowman, M. E., Dixon, R. A., and Noel, J. P., Structure of chalcone synthase and the molecular basis of plant polyketide biosynthesis, Nat Struct Mol Biol 6, (1999) 775-784.

[17] A. K. Bera, Atanasova, V., Robinson, H., Eisenstein, E., Coleman, J. P., Pesci, E. C., and Parsons, J. F., Structure of PqsD, a Pseudomonas Quinolone Signal Biosynthetic Enzyme, in Complex with Anthranilate, Biochemistry 48, (2009) 8644-8655.

[18] E. Deziel, Lapine, F. o., Milot, S., He, J., Mindrinos, M. N., Tompkins, R. G., and Rahme, L. G., Analysis of Pseudomonas aeruginosa 4-hydroxy-2-alkylquinolines (HAQs) reveals a role for 4-hydroxy-2-heptylquinoline in cell-to-cell communication, Proceedings of the National Academy of Sciences of the United States of America 101, (2004) 1339-1344.

[19] Y. Pérez-Castillo, Froeyen, M., Cabrera-Pérez, M., and Nowé, A., Molecular dynamics and docking simulations as a proof of high flexibility in <i>E. coli</i> FabH and its relevance for accurate inhibitor modeling, Journal of Computer-Aided Molecular Design 25, 371-393.
[20] C. Lu, Kirsch, B., Zimmer, C., de Jong, Johannes C., Henn, C., Maurer, Christine K., Müsken, M., Häussler, S., Steinbach, A., and Hartmann, RolfÂ W., Discovery of Antagonists of PqsR, a Key Player in 2-Alkyl-4-quinolone-Dependent Quorum Sensing in Pseudomonas aeruginosa, Chemistry and Biology 19, (2012) 381-390.
[21] D. Case, Darden, T., Cheatham, T. I., and Simmerling, C., Amber 11, University of California, San Francisco. (2011)
[22] T. Darden, Perera, L., Li, L., and Pedersen, L., New tricks for modelers from the crystallography toolkit: the particle mesh Ewald algorithm and its use in nucleic acid simulations, Structure 7, (1999) R55-R60.
[23] V. Le Guilloux, Schmidtke, P., and Tuffery, P., Fpocket: An open source platform for ligand pocket detection, BMC Bioinformatics 10, (2009) 168.

3.6 Identification of Small-Molecule Antagonists of the *Pseudomonas aeruginosa* Transcriptional Regulator PqsR: Biophysically Guided Hit Discovery and Optimization

Tobias Klein[#], **Claudia Henn[#]**, Johannes C. de Jong, Christina Zimmer, Benjamin Kirsch, Christine K. Maurer, Dominik Pistorius, Rolf Müller, Anke Steinbach and Rolf W. Hartmann

[#] These authors contributed equalliy to this work

ACS Chemical Biology **2012**

Publication V

ABSTRACT: The Gram-negative opportunistic pathogen *Pseudomonas aeruginosa* produces an intercellular alkyl quinolone signaling molecule, the *Pseudomonas* quinolone signal. The *pqs quorum sensing* communication system that is characteristic for *P. aeruginosa* regulates the production of virulence factors. Therefore, we consider the *pqs* system as a novel target to limit *P. aeruginosa* pathogenicity. Here, we present small molecules targeting a key player of the *pqs* system, PqsR. A rational design strategy in combination with surface plasmon resonance biosensor analysis led to the identification of PqsR binders including four top candidates with good ligand efficiencies. Determination of thermodynamic binding signatures using isothemal titration calorimetry and functional characterization in a heterologous reporter gene assay in *E. coli* guided the optimization of the best hit that resulted in the potent hydroxamic acid-derived PqsR antagonist **11** (IC_{50} = 12.5 μM). This compound showed a K_D value of 4.1 μM and remarkably it displayed comparable potency in *P. aeruginosa* (IC_{50} = 23.6 μM) and is able to reduce the production of the virulence factor pyocyanin. Beyond this, site-directed mutagenesis together with thermodynamic analysis provided insights into the energetic characteristics of protein-ligand interactions suggesting the presence of hydrogen bonds and CH/π interactions. Thus the identified PqsR antagonists are promising scaffolds for further drug design efforts against this important pathogen.

Pseudomonas aeruginosa is an environmental highly adaptable opportunistic pathogen that is one of the leading causes for nosocomial infections[1] and is responsible for chronic lung infections in the majority of cystic fibrosis patients.[2] It coordinates group behaviours via a cell density dependent cell-to-cell communication system known as *quorum sensing* (QS).[3] Besides the *las*[4, 5] and the *rhl*[6, 7] communication systems, which use *N*-acyl homoserine lactones as autoinducers, *P. aeruginosa* employs a characteristic *pqs* QS system.[8] It functions via the signal molecules PQS (2-heptyl-3-hydroxy-4-quinolone) and its precursor HHQ (2-heptyl-4-quinolone) that interact with their receptor PqsR to control production of a number of virulence factors such as pyocyanin and biofilm formation.[9-11] Due to growing antibiotic resistance there is an urgent need for therapeutics with novel modes of action. Targeting bacterial virulence or disrupting the interaction between the host and the pathogen are attractive options that are increasingly being explored.[12] Therefore we consider PqsR as a novel, promising target to disrupt PqsR-dependent gene expression thereby limiting *P. aeruginosa* pathogenicity without affecting bacterial viability.[13] Recently, we reported on the discovery of the first PqsR antagonists.[14] However, as their structures are derived from the natural effector HHQ they have insufficient physicochemical properties to be used as a drug. Herein, we describe the discovery and optimization of small molecules targeting the transcriptional regulator PqsR using a rational design strategy guided by biophysical methods. Combination of site-directed mutagenesis and thermodynamic analysis enabled us to study protein-ligand interactions into details.

The κ-opioid receptor agonist (±)-*trans*-U50488 (**1**) was recently found to stimulate the transcription of *pqsABCDE* in *P. aeruginosa* PAO1 indicating that it could act via PqsR.[15] Employing surface plasmon resonance (SPR) biosensor analysis and isothermal titration calorimetry (ITC) we confirmed that **1** binds to PqsR (Figure 1) thereby providing a promising starting point for the identification of small-molecule PqsR ligands.

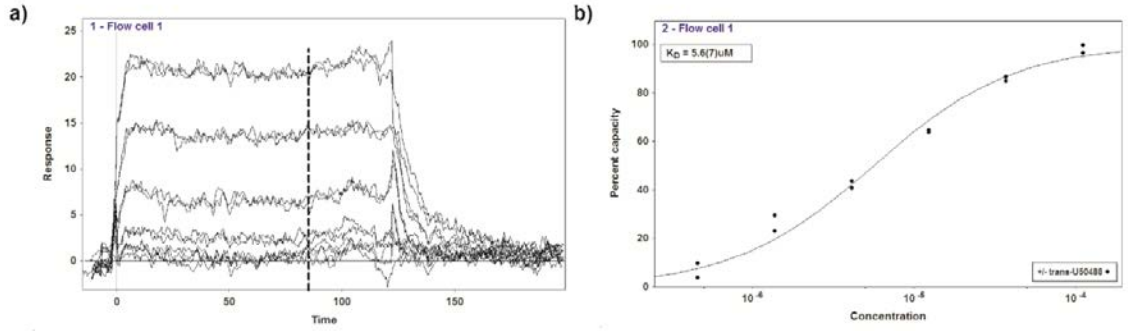

Figure 1. *Binding affinity for (±)-trans-U50488* ***a)*** *Overlay of sensorgrams for confirmed hit binding to H_6SUMO-PqsR^{C87} measured in duplicates at 12°C; double referenced.* ***b)*** *Fit of the duplicate (±)-trans-U50488 equilibrium response data from the H_6SUMO-PqsR^{C87} surface to a 1:1 interaction.*

We applied a rational design strategy that involves the simplification of **1** into smaller fragments and analogues. In the context of antibacterial discovery, fragment-based design is a promising strategy since it allows to address the key issues namely insufficient physicochemical properties and the lack of

chemical diversity.[16, 17] The derived in house library included (i) *N*-heteroaromatic substituted benzamides, (ii) substituted benzyl- and benzamides, and (iii) *N*-phenyl substituted isonicotin- and nicotinamides (Figure 2). Screening of the focussed library (106 compounds) in a SPR biosensor assay monitoring the affinity toward PqsR (biotinylated PqsR was immobilized on a streptavidin coated sensorchip) revealed binders including four top candidates with outstanding ligand efficiencies (LE, Figure 2).

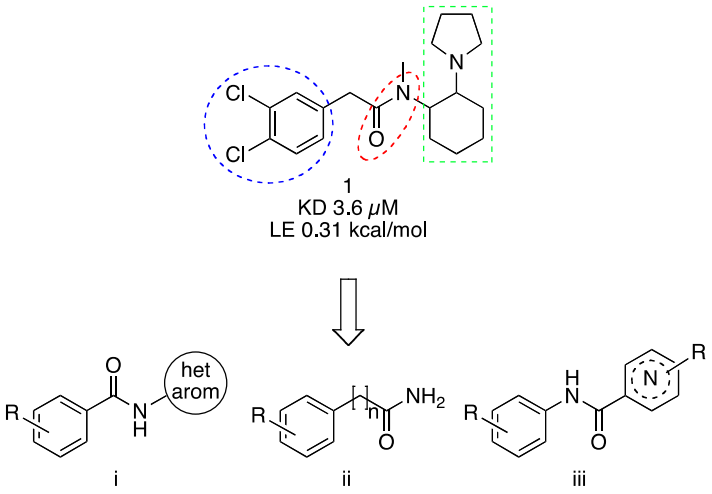

Figure 2. *Ligand-based design strategy. Structure of the PqsR ligand (±)-trans-U50488 1 (top) and general structures i-iii of the derived focused library (below).* K_D *value and ligand efficiency (LE) were determined using ITC.*

The major drawback of screening small simple molecules is that the binding affinity is usually low.[17] Therefore, LE, which is calculated as the binding energy of the ligand per heavy atom thereby normalizing the affinity and molecular size of a compound, was used for effective hit selection.[18] To account for heteroatoms the binding efficiency index (BEI), that engages the total molecular weight instead of the number of non-hydrogen atoms[19] is superior but here the ranking did not change. To verify and further characterize the best hit **4**, we carried out a thermodynamic analysis and evaluated its agonistic and antagonistic activity (Table 1). Using ITC a dissociation constant (K_D) of 25.5 µM was determined for **4** binding to PqsR and the LE of 0.63 kcal/mol confirmed the high potential of **4** as starting point for optimization. Further, we examined the PqsR-mediated transcriptional effect in a reporter gene assay by measuring the β-galactosidase activity in *E. coli* harbouring the pEAL08-2 plasmid containing the tacP-pqsR and pqsAP-lacZ fusion genes.[20] *E.coli* was used as it provides a system to characterize the functionality of PqsR ligands independent of the entire pqs system present in *P. aeruginosa*.[21] Remarkably, in the *E. coli* reporter gene assay 1 did not stimulate the transcription of pqsABCDE as described,[15] rather it acts as a weak PqsR antagonist. More important, for ligand **4** a significant reduction of the PqsR stimulation was observed. Considering the promising LE and the antagonistic activity compound **4** was chosen as starting point for structural modifications.

Table 1. Thermodynamic parameters of ligands 1, 4, and 6-12 binding to PqsR and their agonistic and antagonistic activities.

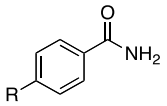

4, 6-10

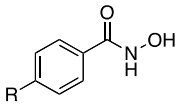

11, 12

Ligand	R	K_D [μM]	Δ*G* [kcal mol^{-1}]	Δ*H* [kcal mol^{-1}]	-*T*Δ*S* [kcal mol^{-1}]	LE [kcal mol^{-1}]	Agonistic activity [%]	Antagonistic activity [%]
1		3.6±0.4	-7.4±0.1	-4.7±0.1	-2.7±0.1	0.31	n.a.	18±3$^{\bigstar}$
4	Cl	25.5±2.5	-6.3±0.1	-4.1±0.2	-2.1±0.2	0.63	n.a.	53±7$^{\bigstar}$
6	Me	31.2±3.4	-6.1±0.1	-2.2±0.1	-3.9±0.1	0.62	33±2*	n.i.
7	Et	7.3±0.6	-7.0±0.1	-4.6±0.3	-2.4±0.3	0.64	122±13*	n.i.
8	*i*Pr	3.0±0.4	-7.5±0.1	-6.3±0.3	-1.3±0.4	0.63	111±10*	n.i.
9	*t*Bu	0.9±0	-8.3±0	-9.7±0.3	1.5±0.3	0.63	43±3*	48±1*
10	*i*Bu	5.7±0.9	-7.2±0.2	-7.9±0.4	0.7±0.1	0.55	32±3$^{\bigstar}$	45±8$^{\bigstar}$
11	*t*Bu	4.1±0.6	-7.4±0.1	-8.9±0.2	1.5±0.3	0.53	n.a.	78±12$^{\bigstar}$
12	Et	19.7±1.2	-6.4±0	-4.8±0.2	-1.6±0.2	0.64	n.a.	50±9*

ITC titrations were performed at 298 K. Data represent mean ± SD from at least three independent experiments. Agonistic activity was determined by measuring the PqsR stimulation induced by 100 μM of the test compound compared to 50 nM PQS (= 100%); n.a. = no agonism (agonistic activity ≤ 10%). Antagonistic activity was determined by measuring the inhibition of the PqsR stimulation induced by 50 nM PQS in the presence of 100 μM test compound (full inhibition = 100%); n.i. = no inhibition (antagonistic activity ≤ 10%). Mean value of at least two independent experiments with n = 4, standard deviation less than 25%. Significance: For the agonist test, induction compared to the basal value; for the antagonist test, decrease of the PQS-induced induction. * $p < 0.003$; $^{\bigstar}$ $p < 0.05$.

Variation of the length of the alkyl chain in PQS[21, 22] as well as in HHQ and its derivatives[14] had demonstrated a chain length dependency of agonistic and antagonistic activities revealing the alkyl chain as a key feature. Therefore, alkyl chains varying from C1 to C4 were introduced in the *para*-position of the benzamide core that led to compounds **6**-**10** (Table 1; Figure 3a). Compared to **4** (K_D = 25.5 μM) the *tert*-butyl substituted benzamide (**9**, K_D = 0.9 μM) showed a 29-fold increase in binding affinity and the LE remained constant at a value of 0.63 kcal/mol. However, changing the constitution from *tert*- to *iso*-butyl (compound **10**, K_D = 5.7 μM) reduced the affinity again. Analysis of the thermodynamic signatures revealed that ligands **7**-**10** are enthalpy driven binders indicating a good non-covalent bond complementary between the protein and the compounds.[23] Though, with increasing enthalpic contribution in this series the entropic terms became more unfavorable, thereby partially compensating the enthalpic gain (Figure 3b).

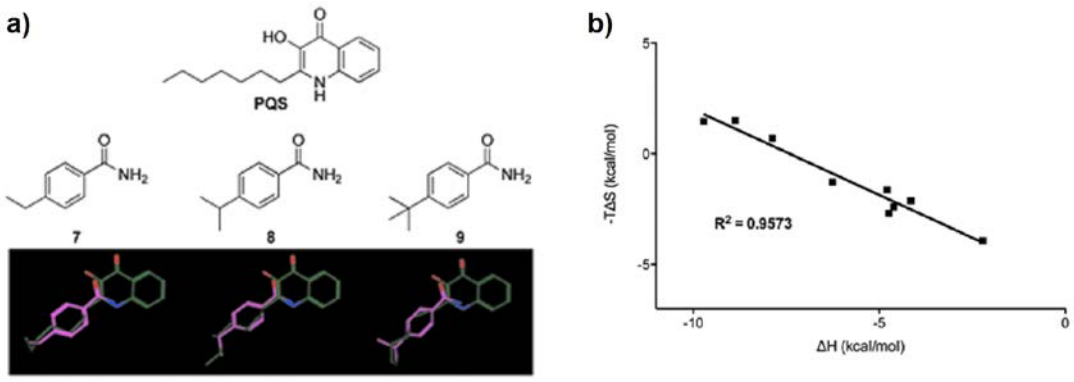

Figure 3. a) *Flexible alignment of **7**, **8**, and **9** (magenta) with the natural ligand PQS (green). Alignment was done using the flexible alignment utility of MOE2009.10 (Chemical Computing Group Inc., Montreal, Canada).* ***b)*** *Plot of enthalpy (ΔH) vs entropy (-TΔS). ΔH and –TΔS are highly correlated thereby clearly evidencing an enthalpy-entropy compensation effect in the protein-ligand complexes of the current study.*

The replacement of the Cl-substituent in *para*-position of **4** by alkyl-residues (compounds **6**-**10**) inverted the functional properties from antagonistic (**4**) to agonistic activity (**6**-**10**). Interestingly, the ligands with the bulkiest substituents **9** and **10** showed in addition to their moderate agonistic activity a significant reduction of the PqsR stimulation. These findings demonstrate the impact of the alkyl moiety on binding affinity as well as on functional properties.

Table 2. Effect of the Q194A mutation on the thermodynamic parameters of ligand binding.

Ligand	$\Delta\Delta G$ [kcal mol^{-1}]	$\Delta\Delta H$ [kcal mol^{-1}]	$-T\Delta\Delta S$ [kcal mol^{-1}]
1	0.0±0.1	0.1±0.1	-0.1±0.1
8	-1.3±0.3*	-4.0±0.3*	2.7±0.4*
9	-1.3±0*	-4.4±0.3*	3.1±0.3*
11	-0.5±0.1*	-4.1±0.4*	3.6±0.4*

$\Delta\Delta G$, $\Delta\Delta H$, and $-T\Delta\Delta S$ are $\Delta G_{WT} - \Delta G_{mutant}$, $\Delta H_{WT} - \Delta H_{mutant}$, and $-T(\Delta S_{WT} - \Delta S_{mutant})$, respectively. Negative values indicate a loss; positive values, a gain compared to wild-type. Errors indicate SD calculated via Gaussian error propagation. Significance: effect of the Q194A mutation on the thermodynamic parameters of ligand binding compared to the wild-type. * $p < 0.003$.

In order to elucidate the role of the amide function, we exchanged it by a hydroxamic acid in the ligand with the highest affinity and the most favorable enthalpic contribution (compound **9**). The resulting compound **11** (K_D = 4.1 µM) displayed a 4.6-fold reduced affinity compared to **9** that is due to a decrease in ΔH. Interestingly, the antagonistic potency was improved and the agonistic activity was completely lost. To investigate whether in the alkyl-substituted series the replacement of the amide by a hydroxamic acid in general can turn agonists into antagonists the corresponding derivative of **7** (compound **12**) was synthesized. Indeed, **12** (K_D = 19.7 µM) is also a pure PqsR antagonist.

Combining ITC with site-directed mutagenesis provides a valuable thermodynamic tool to identify the effects of specific residues in interaction with ligands.[24] Gln194, the only polar residue in the PQS-

binding pocket,[25, 26] was mutated and the binding of **1**, **8**, **9**, and **11** to the resulting PqsR Q194A mutant was analyzed by ITC (Table 2).

While the point mutation of Gln194 to Ala did not affect the binding of **1**, the affinity of **8**, **9**, and **11** was significantly decreased. The latter reveals that Gln194 is only involved in the binding of **8**, **9**, and **11**, but, competition experiments confirmed that **1** and **11** though bind to the same binding site (Figure 4).

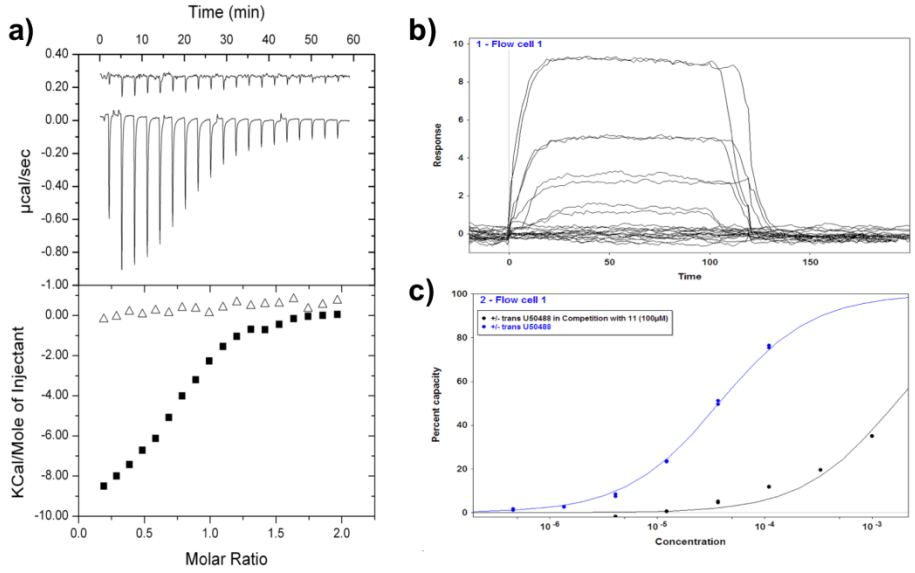

***Figure 4**. Competitive binding of ligands to PqsRC[87] as measured by ITC and SPR. a) Raw ITC data (top) and integrated normalized data (bottom) for titrations of 94 µM H_6SUMO-PqsR^{C87} with 900 µM **11** (■) in the absence of **1** and in the presence of 1 mM compound 1 (Δ). b) Overlay of sensorgrams for compound 1 in competition with **11** to H_6SUMO-PqsR^{C87} measured in duplicates at 12°C; double referenced and DMSO calibrated. c) Blue line: Fit of the duplicate (±)-trans-U50488 equilibrium response data from the H_6SUMO-PqsR^{C87} surface to a 1:1 interaction; black line: Fit of the duplicate (±)-trans-U50488 equilibrium response data from the H_6SUMO-PqsR^{C87} surface to a 1:1 interaction in the presence of 100µM of compound **11**.*

Interestingly, for the interaction of **8**, **9**, and **11** with the Q194A mutant a comparable loss in Δ*H* was observed with values ranging from 4.0 to 4.4 kcal/mol. Considering that a well-placed H-bond can make a favorable enthalpic contribution in the order of -4 to -5 kcal/mol,[27] the results suggest that Gln194 forms H-bonds with **8**, **9**, and **11**. Further, the binding of the latter ligands to the Q194A mutant showed positive -*T*Δ*S* values relative to those of the wild-type. This might be due to the increased conformational flexibility both of the ligand and the protein in the absence of the H-bond. As shown in Table 1, variation of the alkyl chain (compounds **6**-**10**) affects the enthalpy Δ*H* demonstrating that the alkyl chain is involved in the formation of non-covalent interactions like CH/π hydrogen bonds. The latter have their origin in dispersion forces, which have an impact on the enthalpic term of free energy.[28] To probe for CH/π interactions Phe221 that is lining the PQS-binding pocket[25, 26] was mutated to Ala. Ligand **9**, which showed the highest affinity toward PqsR (K_D = 0.9

µM) was selected for analysis and the thermodynamic signatures for the binding of **9** to wild-type and F221A mutant PqsR are shown in Figure 5.

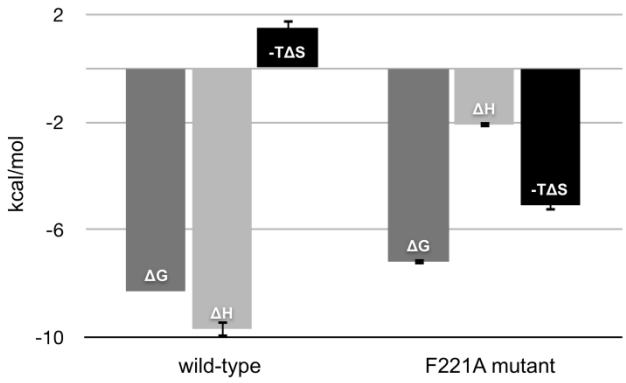

Figure 5. *Thermodynamic profiles determined by ITC for the binding of ligand* ***9*** *to wild-type and F221A mutant PqsR. Data shown are mean ± SD, n = 3.*

Indeed, the F221A point mutation affected the binding of **9** and with a deficit of 7.6 kcal/mol the enthalpic contribution was significantly reduced compared to the wild-type. A salient feature of the CH/π hydrogen bond is that it works cooperatively and for cases involving aliphatic CH groups as the hydrogen donor, the energy of a CH/π hydrogen bond is between -1.5 and -2.5 kcal/mol.[29] This indicates that Phe221 might form three CH/π bonds with the *t*Bu-moiety of **9** as described for the interaction of benzene with isobutane. [30]

Given that *P. aeruginosa* is characterized by an intrinsic resistance to a variety of antimicrobial agents, which is due to the synergy between drug efflux pumps with broad substrate specificity and low outer membrane permeability[31] we examined whether the most potent antagonist **11** also shows an effect when tested in a *P. aeruginosa* background. Remarkably, the antagonistic activity could be confirmed (IC_{50} in *E. coli* = 12.5 µM vs. IC_{50} in *P. aeruginosa* = 23.6 µM; Figure 6a). Two possible explanations for this finding might be that the penetration of the hydrophilic hydroxamic acid **11** (logP = 2.1) across the outer membrane overwhelms its efflux or that the antagonist **11** is no substrate of the efflux pumps. Additionally, **11** is able to reduce the production of the virulence factor pyocyanin in *P. aeruginosa* (IC_{50} = 87.2 µM; Figure 6b). In summary, through application of rational design and biophysical methods, we developed to the best of our knowledge the first small-molecule PqsR ligands. LEs and functional properties were used to guide the elaboration process that resulted in the potent hydroxamic acid-derived PqsR antagonist **11**. Compared to the recently described HHQ analogues[14] compound **11** is a less potent antagonist but, as a consequence of its low molecular weight and its activity in *P. aeruginosa*, it has a high potential for further optimization. Beyond this, site-directed mutagenesis together with thermodynamic analysis disclosed that Gln194 and Phe221 are involved in ligand binding, probably by making hydrogen bonds and CH/π interactions, respectively. The rational simplification strategy in combination with biophysical methods, using LE as a primary filter, revealed promising hits. Accordingly, this approach is a valuable tool in drug design. Future experiments will

address hit to lead optimization to open the door for antibiotics with novel modes of action for the treatment of *P. aeruginosa.*

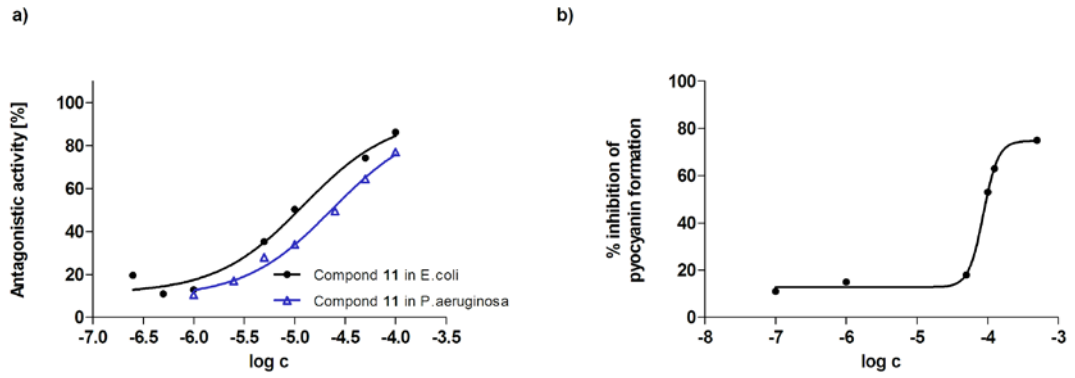

Figure 6. a) *Determination of IC_{50} values in E.coli and P. aeruginosa. IC_{50} values were determined in the reporter gene assays. Compound 11 was tested at seven concentrations in competition with 50 nM PQS. IC_{50} value in E.coli: 12.5 µM; mean value of three experiments. IC_{50} value in P. aeruginosa: 23.6 µM; mean value of two experiments with n = 4. The log (inhibitor) vs. response model (Prism 5.0) was applied for nonlinear regression and determination of IC_{50}-values; the Hill slope was constrained equal to 1.0.* ***b)*** *Effect of* ***11*** *on the pyocyanin production in P. aeruginosa PA14. For the determination of the IC_{50} value the pyocyanin levels in P. aeruginosa PA14 were spectrophotometrically determined at A_{520} nm in the presence of compound* ***11*** *at six concentrations. IC_{50} value in: 87.3 µM; mean value of two experiments. The log (inhibitor) vs. response-variable slope model (Prism 5.0) was applied for nonlinear regression and determination of the IC_{50}-value.*

Supporting Information

Synthetic and analytical methods for the compounds described herein. Detailed description of the reporter gene assays and pyocyanin assay. Supplementary Figures. This material is available free of charge via the Internet at http://pubs.acs.org.

ACKNOWLEDGMENT

The authors thank Simone Amann for her help in performing the reporter gene assay. We are very grateful to Dr. Cugini and Dr. Hogan (Dartmouth Medical School, Hanover, NH, USA) for kindly supplying the plasmid pEAL08-2. The *Pseudomonas aeruginosa* PA14 strain was kindly provided by Prof. Susanne Häussler (Helmholtz Centre for Infection Research, Braunschweig, Germany).

METHODS

Construction of pSUMO3_ck4_*pqsR*^{C87}. For generation of pSUMO3_ck4_*pqsR*^{C87} containing the truncated *pqsR*^{C87} gene of *P. aeruginosa* PA14, the *pqsR* gene from nucleotide 259 to the stop codon was PCR-amplified from genomic DNA using the forward primer 5'-TATGAGTACTAATCTCAACAAGGGTCCGCGC-3′ and reverse primer 5′-TGTACAATTGCTACTCTGGTGCGGCGCGCT-3′ (*Sca*I/*Mfe*I sites underlined) and subsequently cloned into the *Sca*I/*Mfe*I sites of the pSUMO3_ck4 vector in order to express it as a H_6SUMO-fusion

protein. The construct was confirmed by DNA sequencing. This plasmid adds 104 amino acids to the N-terminus of the PqsR sequence starting at N87 .

Preparation of pSUMO3_ck4_Q194A*pqsR*^{C87} and pSUMO3_ck4_F221A*pqsR*^{C87}. The Q194A and the F221A mutants was generated using the QuikChange Site-Directed Mutagenesis Kit (Stratagene, La Jolla, CA) according to the manufacturer's instructions using the pSUMO3-ck4-*pqsR*^{C87} plasmid as an template. Briefly, the forward primer 5'-CTGGCCAATTACCGGGCGATCAGCCTCGGCAGC-3' (A194 underlined) and the reverse primer 5'-GCTGCCGAGGCTGATCGCCCGGTAATTGGCCAG-3' (A194 underlined) were used to amplify the Q194A gene through 16 cycles of PCR (35 s denaturation at 95 °C, 60 s annealing at 55 °C, and 6.5 min extension at 68 °C). The forward primer 5' CTCTTCGTGGAAAACGCGGACGACATGCTGCGTCTG 3' (A221 underlined) and the reverse primer 5' CAGACGCAGCATGTCGTCCGCGTTTTCCACGAAGAG 3' (A221 underlined) were used to amplify the F221A gene through 16 cycles of PCR using the same conditions as described above. After treatment with *Dpn*I, the PCR product was transformed into *E. coli* strain XL1-Blue. Plasmid DNA was then purified from transformants using the GenElute^{TM} HP Plasmid Miniprep Kit (Sigma-Aldrich, St. Louis, MO) and sequenced to confirm the Q194A and the F221A mutations.

Protein Expression and Purification. Wild-type, Q194A mutant, and F221A mutant H_6SUMO-PqsR^{C87} were expressed in *E. coli* and purified using a single affinity chromatography step. Briefly, *E. coli* BL21 (DE3) cells containing the pSUMO3_ck4_*pqsR*^{C87}, the pSUMO3_ck4_Q194A*pqsR*^{C87} or the the pSUMO3_ck4_F221A*pqsR*^{C87} plasmid were grown in LB medium containing 50 µg ml^{-1} kanamycin at 37 °C to an OD_{600} of approximately 0.8 and induced with 0.2 mM IPTG for 16 h at 16 °C. The cells were harvested by centrifugation (5000 rpm, 10 min, 4 °C) and the cell pellet was resuspended in 100 ml binding buffer (50 mM Tris-HCl, pH 7.8, 150 mM NaCl, 20 mM imidazole, 10% glycerol (*v/v*)) and lysed by sonication for a total process time of 2.5 min. Cell debris were removed by centrifugation (13000 rpm, 30 min) and the supernatant was filtered through a syringe filter (0.2 µm). The clarified lysate was immediately applied to a Ni-NTA column (GE Healthcare), washed with 50 mM Tris-HCl, pH 7.8, 150 mM NaCl, 20 mM imidazole, 10% glycerol (*v/v*), and eluted with 500 mM imidazole. The protein containing fractions were buffer-exchanged into 20 mM Tris, pH 7.4, 150 mM NaCl, 10% glycerol (*v/v*) for the wild-type and into 20 mM Tris, pH 7.8, 300 mM NaCl, 10% glycerol (*v/v*) for the Q194A and the F221A mutants, using a PD10 column (GE Healthcare) and judged pure by SDS-PAGE analysis. The H_6SUMO-tagged proteins were stored at -80 °C and used for **biophysical studies.**

Minimal biotinylation of H_6SUMO-PqsR^{C87}. Minimal biotinylation of the H_6SUMO-PqsR^{C87} was achieved by mixing 56 nmol of H_6SUMO-PqsR^{C87} (1 eq.) with 28 nmol of EZ-link sulfoNHS LC-LC-biotin (0.5 eq.; Thermofisher Scientific) that was freshly dissolved in water. Biotinylation reaction mixture was incubated on ice for 2 hours. To remove unreacted biotin reagent, the entire biotinylation mixture was subjected to size exclusion chromatography on a Superdex200 HR (16/600) column equilibrated in storage buffer (1x PBS, pH 7.4, 10% glycerol (*v/v*)). A protein peak containing

biotinylated H_6SUMO-PqsR^{C87} protein was collected (0.3 mg/ml), stored at -80 °C and used for SPR studies.

Surface Plasmon Resonance. SPR binding studies were performed using a Reichert SR7500DC instrument optical biosensor (Reichert Technologie, Depew, NY 14043 USA). SAD500 sensor chips from Xantec (Xantec Analytics, Düsseldorf) were used. Dimethyl sulfoxide (DMSO), biotin and (±)-*trans*-U50488 methanesulfonate were purchased from Sigma. Library collection consisted of 106 compounds with molecular weight range of 100 to 350 Da.

Immobilization of biotinylated H_6Sumo-PqsR^{C87}. Biotinylated H_6SUMO-PqsR^{C87} was immobilized on a SAD500 (Streptavidin coated) sensor chip at 25 °C. HEPES (50 mM HEPES, pH 7.4, 150 mM NaCl) was used as the running buffer. The streptavidin carboxymethyl dextran surface was preconditioned 30 min with running buffer until the baseline was stable. Biotinylated H_6SUMO-PqsR^{C87}was diluted into running buffer to a concentration of 100 µg/mL and coupled to the surface with a 2-min injection. Remaining streptavidin and the reference cell were blocked with a 3-min injection of biotin (3µg/mL). Biotinylated H_6SUMO-PqsR^{C87} (39494 Da) was immobilized at density of 2200 RU for the binding affinity experiment of (±)-*trans*-U50488 methanesulfonate and at a density of 5506 RU for the library screen.

Binding affinity for (±)-trans-U50488 methanesulfonate. The binding experiment was performed at 12°C at a constant flow rate of 80 µl/min in instrument running buffer (50 mM HEPES, 150 mM NaCl, pH 7.4, 5% DMSO (*v/v*), 0.05% P20 (*v/v*). A 10 mM stock of *trans*-U50488 methanesulfonate in running buffer was directly diluted to a concentration of 1 mM and then diluted in a 3-fold dilution series from 111 µM down to 457 nM. Before starting the experiments 12 warm-up blank injections were performed. Zero-buffer blank injections and DMSO calibrations were included for double referencing. Individual concentrations were injected in duplicates from lowest to highest concentrations for 120 s association and 5 min dissociation time. Scrubber software was used for processing and analysing data. Equilibrium dissociation constant (K_D) was determined by locally fitting appropriate experimental data to a 1:1 model using fitting procedure available within Scrubber software. Overlay plot of sensorgrams and affinity plot in adequate logarithmic units for the concentrations[32] are shown in Supplementary Figure 1.

Library Screening. Concentrations of ligand stock solutions in DMSO were determined by the weight of the compound. Compounds as 10 mM DMSO stocks were diluted in DMSO to 2 mM. Final ligand concentrations (100 µM) were achieved by diluting 1:20 (*v/v*) in the experimental buffer (50 mM HEPES, pH 7.4, 150 mM NaCl, 0.05% P20 (*v/v*)) resulting in a final DMSO concentration of 5% (*v/v*). Binding experiments were performed at 12°C at a constant flow rate of 100 µl/min in instrument running buffer (50 mM HEPES, pH 7.4, 150 mM NaCl, 5% DMSO (*v/v*), 0.05% P20 (*v/v*). Each compound was injected for 26 s association - and 120 s dissociation time. Positive control ((±)-*trans*-U50488 methanesulfonate) was injected each 25th injection at 20 µM to assess stability and reproducibility of the assay. 110 compounds were screened within 6 hours in 96 well plates. Data

evaluation was performed using Scrubber (http://www.biologic.com.au) and Microsoft Excel software for data processing and analysis. Using Scrubber software, SPR signals in flow cell containing captured biotinylated protein were transformed, referenced against the blank surface (streptavidin) and further corrected for DMSO refractive index change (excluded volume effect). Compounds showing promiscuous binding response[33] were removed from the screening data. Report binding points, taken for each fragment injection after a contact interval of 19-s were analyzed. K_D values were estimated using Eq. (1) derived from the Langmuir adsorption isotherm.

$$K_D = (R_{max}*C/R)-C \quad (1)$$

R_{max}, R, and C correspond to the normalized saturation response of the compound, the normalized response of the test compound, and the concentration of the test solution, respectively. For the ranking of the best hits, the LE was calculated as previously described[18, 34] from Eq. (2),

$$LE = -RT\ln K_D/(\text{heavy atom count}) \quad (2)$$

T is the absolute temperature, and R = 1.98 cal/mol/K.

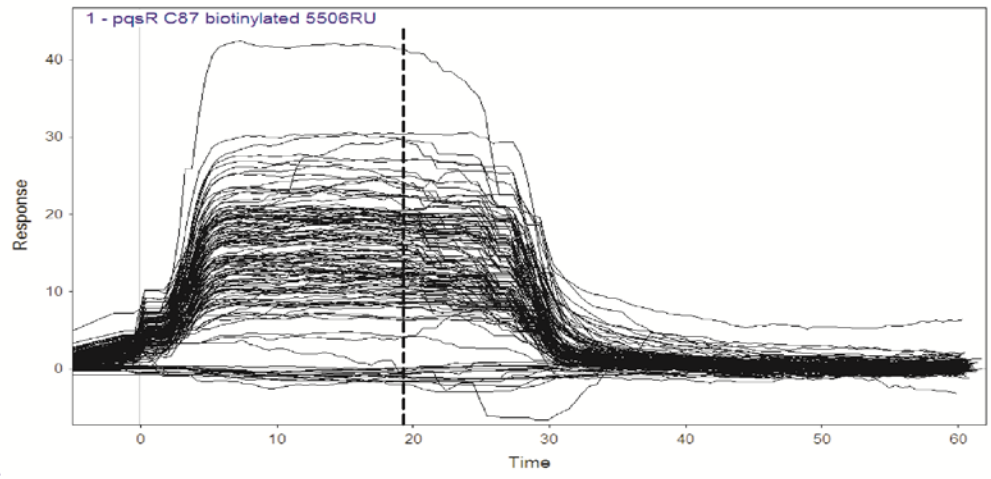

Figure 7. *Overlay of 110 sensorgrams for tested compounds against biotinylated H_6SUMO-PqsR$^{C87'}$. The data read-out line is indicated by the dashed line.*

Competition experiments for (±)-trans-U50488 methanesulfonate and compound 11. The competition experiment was performed at 12°C at a constant flow rate of 25 µl/min in instrument running buffer (50 mM HEPES, 150 mM NaCl, pH 7.4, 5% DMSO (*v/v*), 0.05% P20 (*v/v*), 100µM compound 11. A 10 mM stock of *trans*-U50488 methanesulfonate in running buffer was directly diluted to a concentration of 1 mM and then diluted in a 3-fold dilution series from 333 µM down to 4,57 µM. Before starting the experiments 12 warm-up blank injections were performed. Zero-buffer blank injections and DMSO calibrations were included for double referencing. Individual

concentrations were injected in duplicates from lowest to highest concentrations for 120 s association and 5 min dissociation time. Scrubber software was used for processing and analysing data. Equilibrium dissociation constant (K_D) was determined by locally fitting appropriate experimental data to a 1:1 model using fitting procedure available within Scrubber software. Overlay plot of sensorgrams and affinity plot in adequate logarithmic units for the concentrations[32] are shown in Figure 7.

Isothermal titration calorimetry. ITC experiments were carried out using an ITC_{200} instrument (Microcal Inc., GE Healthcare). Concentrations of ligand stock solutions in DMSO were determined by the weight of the compound. Final ligand concentrations were achieved by diluting 1:20 (*v/v*) in the experimental buffer resulting in a final DMSO concentration of 5% (*v/v*). Protein concentration was determined by measuring the absorbance at 280 nm using a theoretical molarity extinction coefficient of 22,900 $M^{-1}cm^{-1}$. DMSO concentration in the protein solution was adjusted to 5% (*v/v*). ITC measurements were routinely performed at 25 °C in 20 mM Tris, pH 7.4, 150 mM NaCl, 10% glycerol (*v/v*), 5% DMSO (*v/v*) for the wild-type $PqsR^{C87}$and in 20 mM Tris, pH 7.4, 300 mM NaCl, 10% glycerol (*v/v*), 5% DMSO (*v/v*) for the Q194A and the F221A mutants, respectively. The titrations were performed on 66-200 µM H_6SUMO-$PqsR^{C87}$, H_6SUMO-Q194A$PqsR^{C87}$ or H_6SUMO-F221A$PqsR^{C87}$ in the 200 µl sample cell using 2-2.7 µl injections of 0.7-2.5 mM ligand solution every 180 s. The competition experiment was performed on 94 µM H_6SUMO-$PqsR^{C87}$, which was incubated with 1mM compound **1** for 30 min at 25 °C. Raw data were collected and the area under each peak was integrated. To correct for heats of dilution and mixing the final base line consisting of small peaks of the same size at the end of the experiment was subtracted. The experimental data were fitted to a theoretical titration curve (one site binding model) using MicroCal Origin 7 software, with ΔH (enthalpy change in kcal/mol), K_A (association constant in M^{-1}), and N (number of binding sites) as adjustable parameters. Thermodynamic parameters were calculated from Eq. (3),

$$\Delta G = \Delta H - T\Delta S = RT\ln K_A = -RT\ln K_D \qquad (3)$$

where ΔG, ΔH, and ΔS are the changes in free energy, enthalpy, and entropy of binding, respectively, T is the absolute temperature, and R = 1.98 cal/mol/K. The LE for each compound was calculated from Eq. (4),

$$\text{LE} = -\Delta G/(\text{heavy atom count}) \qquad (4)$$

where ΔG is the change in free energy and heavy atom count is the number of non-hydrogen atoms of the compound. For each ligand at least three independent experiments were performed. Representative ITC titrations are shown in Supporting Information.

Synthesis. Complete chemical and analytical methods are descrided in the Supporting Information.

Reporter Gene assays. The β-galactosidase reporter gene assays in *E.coli* and *P. aeruginosa* PA14 were performed as previously described and are explained into details in the Supporting Information.

Pyocyanin assay. The pyocyanin assay in *P. aeruginosa* PA14 was performed as previously described and is explained into details in the Supporting Information.

References

(1) Blanc, D. S., Petignat, C., Janin, B., Bille, J., and Francioli, P. (1998) Frequency and molecular diversity of Pseudomonas aeruginosa upon admission and during hospitalization: a prospective epidemiologic study. *Clin. Microbiol. Infect. 4*, 242-247.

(2) Koch, C., and Høiby, N. (1993) Pathogenesis of cystic fibrosis. *Lancet 341*, 1065-1069.

(3) Swift, S., Downie, J. A., Whitehead, N. A., Barnard, A. M., Salmond, G. P., and Williams, P. (2001) Quorum sensing as a population-density-dependent determinant of bacterial physiology. *Adv. Microb. Physiol. 45*, 199-270.

(4) Gambello, M. J., and Iglewski, B. H. (1991) Cloning and characterization of the Pseudomonas aeruginosa lasR gene, a transcriptional activator of elastase expression. *J. Bacteriol. 173*, 3000-3009.

(5) Passador, L., Cook, J. M., Gambello, M. J., Rust, L., and Iglewski, B. H. (1993) Expression of Pseudomonas aeruginosa virulence genes requires cell-to-cell communication. *Science 260*, 1127-1130.

(6) Ochsner, U. A., Koch, A. K., Fiechter, A., and Reiser, J. (1994) Isolation and characterization of a regulatory gene affecting rhamnolipid biosurfactant synthesis in Pseudomonas aeruginosa. *J. Bacteriol. 176*, 2044-2054.

(7) Ochsner, U. A., and Reiser, J. (1995) Autoinducer-mediated regulation of rhamnolipid biosurfactant synthesis in Pseudomonas aeruginosa. *Proc. Natl. Acad. Sci. USA 92*, 6424-6428.

(8) Pesci, E. C., Milbank, J. B., Pearson, J. P., McKnight, S., Kende, A. S., Greenberg, E. P., and Iglewski, B. H. (1999) Quinolone signaling in the cell-to-cell communication system of Pseudomonas aeruginosa. *Proc. Natl. Acad. Sci. USA 96*, 11229-11234.

(9) Allesen-Holm, M., Barken, K. B., Yang, L., Klausen, M., Webb, J. S., Kjelleberg, S., Molin, S., Givskov, M., and Tolker-Nielsen, T. (2006) A characterization of DNA release in Pseudomonas aeruginosa cultures and biofilms. *Mol. Microbiol. 59*, 1114-1128.

(10) Dubern, J.-F., and Diggle, S. P. (2008) Quorum sensing by 2-alkyl-4-quinolones in Pseudomonas aeruginosa and other bacterial species. *Mol. Biosyst. 4*, 882-888.

(11) Déziel, E., Gopalan, S., Tampakaki, A. P., Lépine, F., Padfield, K. E., Saucier, M., Xiao, G., and Rahme, L. G. (2005) The contribution of MvfR to Pseudomonas aeruginosa pathogenesis and quorum sensing circuitry regulation: multiple quorum sensing-regulated genes are modulated without affecting lasRI, rhlRI or the production of N-acyl-L-homoserine lactones. *Mol. Microbiol. 55*, 998-1014.

(12) Clatworthy, A. E., Pierson, E., and Hung, D. T. (2007) Targeting virulence: a new paradigm for antimicrobial therapy. *Nat. Chem. Biol. 3*, 541-548.

(13) Xiao, G., Déziel, E., He, J., Lépine, F., Lesic, B., Castonguay, M.-H., Milot, S., Tampakaki, A. P., Stachel, S. E., and Rahme, L. G. (2006) MvfR, a key Pseudomonas aeruginosa pathogenicity LTTR-class regulatory protein, has dual ligands. *Mol. Microbiol. 62*, 1689-1699.

(14) Lu, C., Kirsch, B., Zimmer, C., de Jong, J. C., Henn, C., Maurer, C. K., Müsken, M., Häussler, S., Steinbach, A., and Hartmann, R. W. (2012) Discovery of Antagonists of PqsR, a Key Player in 2-Alkyl-4-quinolone-Dependent Quorum Sensing in Pseudomonas aeruginosa. *Chem. Biol. 19*, 381-390.

(15) Zaborina, O., Lepine, F., Xiao, G., Valuckaite, V., and Chen, Y. (2007) Dynorphin activates quorum sensing quinolone signaling in Pseudomonas aeruginosa. *PLoS Pathog.*

(16) Mochalkin, I., Miller, J. R., Narasimhan, L., Thanabal, V., Erdman, P., Cox, P. B., Prasad, J. V. N. V., Lightle, S., Huband, M. D., and Stover, C. K. (2009) Discovery of antibacterial biotin carboxylase inhibitors by virtual screening and fragment-based approaches. *ACS Chem. Biol. 4*, 473-483.

(17) Waldrop, G. L. (2009) Smaller is better for antibiotic discovery. *ACS Chem. Biol. 4*, 397-399.

(18) Hopkins, A. L., Groom, C. R., and Alex, A. (2004) Ligand efficiency: a useful metric for lead selection. *Drug Discov. Today 9*, 430-431.

(19) Abad-Zapatero, C., and Metz, J. T. (2005) Ligand efficiency indices as guideposts for drug discovery., In *Drug Discov. Today*, pp 464-469.

(20) Cugini, C., Calfee, M. W., Farrow, J. M., Morales, D. K., Pesci, E. C., and Hogan, D. A. (2007) Farnesol, a common sesquiterpene, inhibits PQS production in Pseudomonas aeruginosa. *Mol. Microbiol. 65*, 896-906.

(21) Fletcher, M. P., Diggle, S. P., Crusz, S. A., Chhabra, S. R., Cámara, M., and Williams, P. (2007) A dual biosensor for 2-alkyl-4-quinolone quorum-sensing signal molecules. *Environ. Microbiol. 9*, 2683-2693.

(22) Hodgkinson, J., Bowden, S. D., Galloway, W. R. J. D., Spring, D. R., and Welch, M. (2010) Structure-activity analysis of the Pseudomonas quinolone signal molecule. *J. Bacteriol. 192*, 3833-3837.

(23) Ladbury, J. E., Klebe, G., and Freire, E. (2010) Adding calorimetric data to decision making in lead discovery: a hot tip. *Nat. Rev. Drug Discov. 9*, 23-27.
(24) Ciulli, A., Williams, G., Smith, A. G., Blundell, T. L., and Abell, C. (2006) Probing Hot Spots at Protein−Ligand Binding Sites: A Fragment-Based Approach Using Biophysical Methods. *J. Med, Chem. 49*, 4992-5000.
(25) de Bentzmann, S., and Plésiat, P. (2011) The Pseudomonas aeruginosa opportunistic pathogen and human infections. *Environ. Microbiol. 13*, 1655-1665.
(26) Williams, P. (2011) Book of Abstracts. *1st International HIPS Symposium, Saarbrücken, Germany*, June 16.
(27) Freire, E. (2008) Do enthalpy and entropy distinguish first in class from best in class? *Drug Discov. Today 13*, 869-874.
(28) Ramírez-Gualito, K., Alonso-Ríos, R., Quiroz-García, B., Rojas-Aguilar, A., Díaz, D., Jiménez-Barbero, J., and Cuevas, G. (2009) Enthalpic nature of the CH/pi interaction involved in the recognition of carbohydrates by aromatic compounds, confirmed by a novel interplay of NMR, calorimetry, and theoretical calculations. *J. Am. Chem. Soc. 131*, 18129-18138.
(29) Nishio, M. (2011) The CH/π hydrogen bond in chemistry. Conformation, supramolecules, optical resolution and interactions involving carbohydrates. *Phys. Chem. Chem. Phys. 13*, 13873-13900.
(30) Ran, J., and Wong, M. W. (2006) Saturated hydrocarbon-benzene complexes: theoretical study of cooperative CH/pi interactions. *J. Phys. Chem. A 110*, 9702-9709.
(31) Ma, D., Cook, D. N., Hearst, J. E., and Nikaido, H. (1994) Efflux pumps and drug resistance in gram-negative bacteria. *Trends Microbiol. 2*, 489-493.
(32) Rich, R. L., and Myszka, D. G. (2010) Grading the commercial optical biosensor literature-Class of 2008: 'The Mighty Binders'. *J. Mol. Recognit. 23*, 1-64.
(33) Giannetti, A. M., Koch, B. D., and Browner, M. F. (2008) Surface plasmon resonance based assay for the detection and characterization of promiscuous inhibitors. *J. Med. Chem. 51*, 574-580.
(34) Navratilova, I., and Hopkins, A. L. (2010) Fragment screening by surface plasmon resonance. *ACS Med. Chem. Lett. 1*, 44-48.

4 Zusammenfassende Diskussion

4.1 Design, Synthese und Validierung von 17β-HSD1 Hemmstoffen zur Erbringung des *in vivo Proof of Concepts*

17β-HSD1 stellt als Schlüsselenzym der E2-Biosynthese ein neues, vielversprechendes Target für die Therapie von estrogen-abhängigen Erkrankungen dar. Durch die Hemmung dieses Enzyms verspricht man sich eine lokale Estradiolabsenkung im erkrankten Gewebe und dadurch die Reduzierung von unerwünschten Nebeneffekten, wie sie bei herkömmlichen Therapien vorkommen. Zur Validierung neuer Targets ist das Erbringen des *Proof of Principle* und des *Proof of Concepts* im geeigneten Tiermodell unerlässlich. Da die gefundenen Leitverbindungen an 17β-HSD1 von Rattenleberpreparationen keine ausreichende Aktivität gezeigt haben (Kruchten 2008), ist es notwendig eine alternative Spezies zu identifizieren.

In Kapitel 3.1 ist der Vergleich von 17β-HSD1 verschiedener Spezies beschrieben. Für die Spezies in denen Tiermodelle etabliert sind, wurde für den Vergleich von 17β-HSD1 von Maus, Ratte, Cynomolgus, *Callithrix jacchus* und Mensch ein Sequenzalignment durchgeführt. Vergleicht man für die ersten 287 Aminosäuren die Ähnlichkeit von Ratte/Maus und humaner 17β-HSD1 (*h*17β-HSD1), so kommt man lediglich auf 69 % Identität. Insbesondere der Austausch von H221 der humanen Sequenz in Glycin (H221G) ist in den murinen Sequenzen sehr weitreichend. Diese Aminosäure befindet sich in der Steroidbindetasche und ist maßgeblich an der Steroidbindung beteiligt (Azzi *et al*., 1996). Zusätzlich sind weitere Aminosäuren der murinen Substratbindetasche durch sperrige Reste ausgetauscht. Das Fehlen von H221 und das reduzierte Volumen der Substratbindetasche mag eine Erklärung für die Inaktivität der 17β-HSD1 Leitstrukturen darstellen. Vergleicht man dann die humane Sequenz mit der von *C. jacchus* erhält man eine Identität von 80%, die sich auf 87 % erhöht, wenn man nur die Steroidbindetasche berücksichtigt. Auch aufgrund der hohen phylogenetischen Ähnlichkeit von Affe und Mensch ist die Spezies *C. jacchus* für die Validierung von 17β-HSD1 Hemmstoffen der Nagerspezies vorzuziehen. Ein geeignetes Tiermodell in *C. jacchus* ist das Endometriosemodell, hier können zwei verschiedene Formen von Endometriose induziert werden (Einspanier *et al*., 2006). Das Endometriosegewebe hat seinen Ursprung also in *C. jacchus*. Deshalb ist es von großer Bedeutung, dass potentielle Kandidaten für das *in vivo Proof of Concept* Aktivität an 17β-HSD1 dieser Spezies zeigen. Ein weiterer Vorteil, den dieses Endometriosemodell bietet, ist zusätzlich zur intensiven Studie der Endometrioseläsionen die Untersuchung des lokalen und zentralen Estrogenmetabolismus. Durch diese Daten könnte man auch das intrakrine Konzept der 17β-HSD1 Hemmstoffen validieren. Durch die Überexpression von 17β-HSD1 im erkrankten Gewebe käme es also nur lokal zur Absenkung der E2-Spiegel und E2 könnte im Organismus weiterhin seine normale Funktion ausüben.

Zum Aufbau eines biochemischen Assays für die Evaluierung der vorhandenen Inhibitoren am isolierten Target ist es notwendig die 17β-HSD1 von *C. jacchus* (*cj*17β-HSD1) in ausreichender Menge zur Verfügung zu haben. Prinzipiell gibt es zwei Möglichkeiten an *cj*17β-HSD1 zu kommen; durch eine Transfektion in geeignete Zellen oder durch die Aufreinigung aus Gewebe, das das Protein in ausreichender Menge exprimiert. Bei letzterer Methode ist es jedoch wichtig sicherzustellen, wie sich das Expressionsmuster von weiteren Enzymen, die in der Lage sind dieselbe Reaktion zu katalysieren, verhält. Studien haben gezeigt, dass das Plazentagewebe von *C. jacchus* hauptsächlich 17β-HSD1 und in sehr geringen Mengen auch 17β-HSD7, die in der Lage ist E1 zu reduzieren, enthält (Schwabe *et al.*, 2001). Dieses Expressionsmuster ist in diesem Fall jedoch von geringer Bedeutung, da es sich bei 17β-HSD1 um ein cytosolisch gelöstes und bei 17β-HSD7 um ein zellmembranständiges Enzym handelt. Bei der Aufarbeitung werden durch fraktionierte Zentrifugation zuerst Zelldebris und die schweren Zellbestandteile abgetrennt, wodurch die 17β-HSD7 auch aus dem Gemisch entfernt wird. Anschließend werden cytosolische und mikrosomale Fraktion durch Ultrazentrifugation voneinander getrennt. Die cytosolische Fraktion wird für die Etablierung des Hemmstoffassays verwendet. Geht man davon aus, dass das Expressionsmuster der *C. jacchus*-Plazenta annähernd identisch mit dem der humanen Plazenta ist, dann enthält die mikrosomale Fraktion 17β-HSD2 und 17β-HSD4, die beide in der Lage sind die Oxidation von Estradiol zu katalysieren. Beide Enzyme kann man durch Zentrifugation nicht weiter voneinander trennen. 17β-HSD2 liegt jedoch in deutlich höheren Konzentrationen vor und zusammengenommen mit der Tatsache, dass 17β-HSD2 auch die deutlich höhere Affinität zu E2 hat (Wu *et al.*, 1993; Adamski *et al.*, 1995), kann die mikrosomale Fraktion für Evaluierung von Selektivitäten verwendet werden. Die Aktivitätsmessungen erfolgen über HPLC-Separation und anschließender Radiodetektion, es wird der Umsatz von E1 zu E2, bzw. von E2 zu E1 detektiert, so dass andere NADPH- und NAD^+- abhängige Reaktion keine Rolle spielen.
An diesem Testsystem wurden eine Reihe hochpotenter *h*17β-HSD1 Inhibitoren hinsichtlich ihrer Aktivität an *cj*17β-HSD1 und Selektivität gegenüber *cj*17β-HSD2 evaluiert. Es wurden Verbindungen drei verschiedener Substanzklassen getestet (Abbildung 22), die Bis(hydroxyphenyl)-substituierten Arene **I/1-I/11**[†], die bizyklisch substituierten Hydroxyphenylmethanone **I/12-I/13** und die (Hydroxyphenyl)naphthole **I/14-I/20**. Die Ergebnisse sind zweigeteilt. Für die ersten beiden Klassen hat man vergleichbare oder höhere Aktivitäten an *cj*17β-HSD1 wie für die *h*17β-HSD1 gefunden.
Für die Klasse der Hydroxyphenylnaphthole hat man für Verbindung **I/14** als einzige Substanz dieser Klasse vergleichbare Aktivitäten von *h*- und *cj*17β-HSD1 gefunden. Alle Vergrößerungen an der Corestruktur (**I/15 – I/20**), die zu verbesserten humanen Aktivitäten führten, waren nachteilig für die Potenz an *cj*17β-HSD1.

---

†Alle Verbindungen, auf die sich in Kapitel 3 bezogen wird, können durch Nennung der Römischen Ziffer der entsprechenden Publikation zugeordnet werden. Die Arabische Ziffer steht für die jeweilige Verbindung in der entsprechenden Publikation (z.B.**I/8** bezieht sich auf Verbindung Nr. **8** in Publikation Nr. **I**)

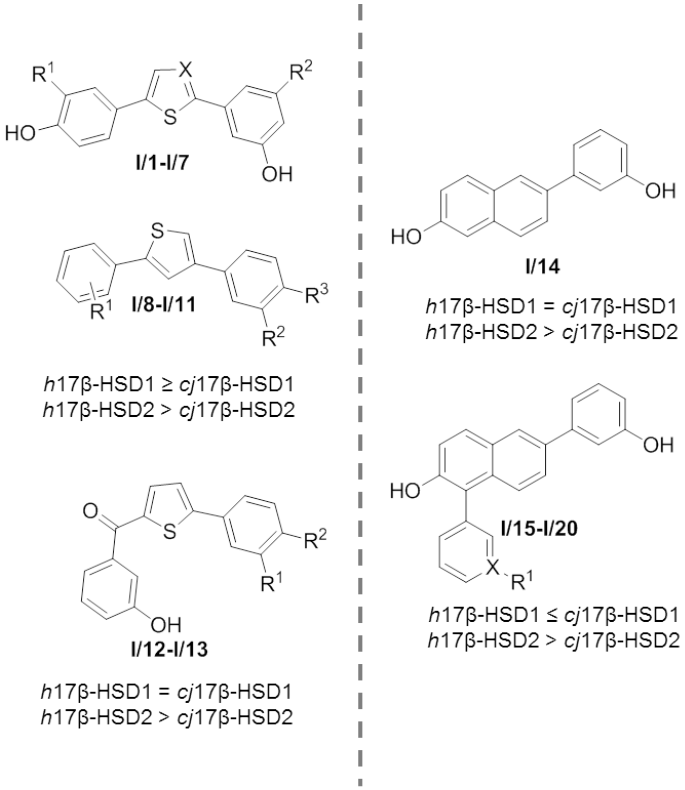

Abbildung 21: Getestete Verbindung verschiedener Substanzklassen und Inhibitionstrend von h17β-HSD Typ 1 & 2 und cj17β-HSD Typ 1 und Typ 2. Linke Seite: gleichbleibende Inhibitionstendenz, rechte Seite: verändertes Inhibitionsprofil

Eine mögliche Erklärung für das spezies-spezifische Inhibitionsprofil an 17β-HSD1 für die Klasse der (Hydroxyphenyl)naphthole kann der hohe sterische Anspruch dieser Klasse sein. Vergleicht man die Strukturen auf der linken und rechten Seite von Abbildung 21 so kann man erkennen, dass es sich bei der Klasse der (Hydroxyphenyl)naphthole um die sterisch weniger flexiblen Substanzen handelt. Zusätzlich ist in der Aminosäuresequenz der *cj*17β-HSD1 Ala191 gegen ein starres Prolin (A191P) ausgetauscht. Dies sitzt in der in α-Helix, die in den humanen Kristallstrukturen als hoch flexibel gefunden wurde (Negri *et al*., 2010). Durch die speziellen Konformationseigenschaften von Prolin, mit nur einer frei drehbaren Bindung, wird die Flexibilität dieser α-Helix (AS 190-196) stark eingeschränkt und stabilisiert. Durch die beiden Faktoren besteht die Möglichkeit, dass die (Hydroxyphenyl)naphthole einen anderen Bindungsmodus in *cj*17β-HSD1 einnehmen, als im humanen Enzym (Abbildung 22).

In beiden Modellen findet man beim Docking Verbindung **I/19** in der Substratbindetasche, jedoch sind die beiden Bindungsmodi um circa 180° verdreht (Abbildung 22B). So dass im humanen Modell die 2-Hydroxygruppe mit Ser142 und Tyr155, sowie die meta-Hydroxygruppe des Phenylrings mit H221 Wasserstoffbrückenbindungen bilden. Der in 1-Position substituierte Phenylring ragt in die Subtasche und wird durch Wasserstoffbrücken mit Asn 152 und dem NH aus dem Rückgrat von Leu95 stabilisiert. Im *cj*-Modell bildet die Hydroxyfunktion des Phenylrings eine Wasserstoffbrücke mit dem Carbonylsauerstoff des Rückgrats von Cys185 und die 2-Hydroxygruppe wird durch

Wasserstoffbrücken mit H221 und Asn282 in ihrer Postition stabilisiert. Der Sulfonamidring ist am C-terminalen Ausgang der Bindetasche wahrscheinlich durch π-π-Wechselwirkungen mit Phe259 stabilisiert. Durch die räumliche Nähe zum Produktausgang des Enzyms könnte Verbindung **I/19** schon Wechselwirkungen mit Wasser ausgesetzt sein, wodurch ungünstige Entropieterme entstehen, die zu weniger günstigen freien Energien führten und dadurch die verringerte Hemmpotenz zustande kommen könnte.

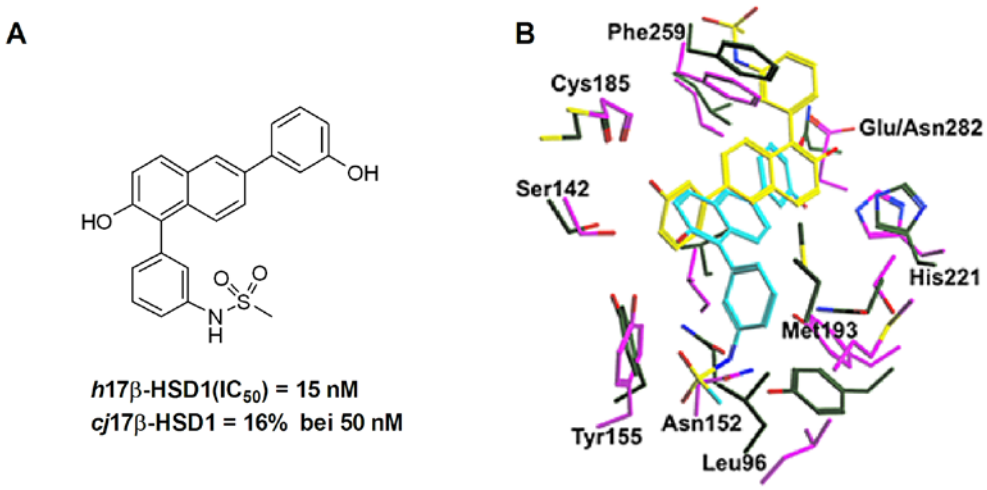

*Abbildung 22: A) Verbindung **I/19** mit Hemmdaten gegenüber h- und cj17β-HSD1 (cj = prozentuale Hemmung bei 50 nM Inhibitorkonzentration). B) Überlagerung von Verbindung **I/19** (cyan) in die Kristallstruktur 1fdt der h17βHSD1 (magenta) gedockt und Verbindung **I/19** (gelb) in das cj17β-HSD1 Modell (grün) gedockt*

Um Aussagen über ihre Selektivität treffen zu können, wurden die Verbindungen auch auf Potenz gegenüber *cj*17β-HSD2 (katalysiert die Oxidation von E2 zu E1) getestet (Abbildung 21). Hier verhalten sich die drei Verbindungsklassen gleich, die Selektivitäten gegenüber *cj*17β-HSD2 sind durchgängig geringer als die gegenüber der *h*17β-HSD2. Dies könnte ein Hinweis darauf sein, dass sich die beiden *cj*-Enzyme strukturell ähnlicher sind, als es *h*17β-HSD Typ 1 und 2 sind. Da in der *cj*17β-HSD2 Sequenz jedoch wichtige Teile, wie das F/G-Segment und das C-terminale Ende fehlen, kann diese Hypothese nicht klar belegt werden. Es können anhand dieser Daten keine Studien durchgeführt werden, die genaue Aussagen über Homologien und Similaritäten von 17β-HSD2 der beiden Spezies geben. Berücksichtigen muss man aber auch, dass es zum Expressionsmuster von 17β-HSD Typ 2 und 4 in *C. jacchus* Plazenta keine Studien gibt. Die geringeren Selektivitäten könnten auch durch eine 17β-HSD4-Inhibition zustande kommen, da die Möglichkeit besteht, dass dieses Enzym in höherem Maße im Plazentagewebe von *C. jacchus* exprimiert wird, als *cj*17β-HSD2. Man könnte hier also auch von einer Hemmung der E1-synthetisierenden Enzymen ausgehen. Um dies jedoch genau zu belegen, müssten Studien an den isolierten Enzymen separat für jeden Subtyp durchgeführt werden.

Vielmehr stellen jedoch die Aktivitäten der (Hydroxyphenyl)naphthole gegenüber der *cj*17β-HSD1 ein Ausschlusskriterium für das *in vivo Proof of Concept* in *C. jacchus* dieser Verbindungsklasse dar. Insbesondere das Sulfonamid **I/19** (auch als **II/15** und **III/A** in dieser Arbeit zu finden, im Folgenden der Einfachheit halber immer als **I/19** benannt.) stellt in dieser Verbindungsklasse eine sehr interessante, hoch potente Verbindung mit sehr guten pharmakokinetischen Parametern dar (Abbildung 23) und erfüllt die Kriterien, die man sich für einen Kandidaten zur Erbringung des *in vivo Proof of Concepts* vorstellt (Abbildung 23).

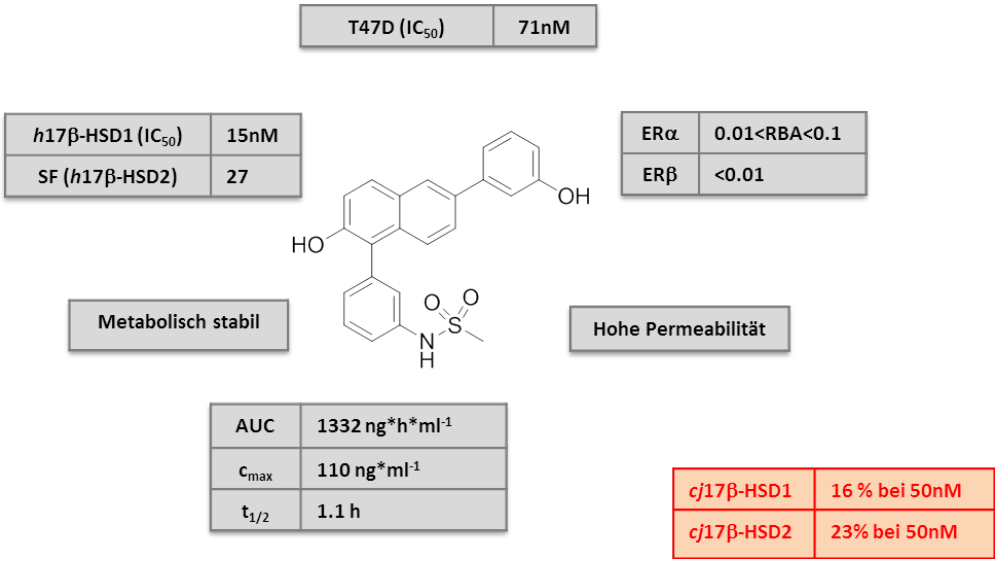

*Abbildung 23: Biologisches Profil des Methylsulfonamids **I/19** der (Hydroxyphenyl)Naphtholklasse*

Das Ziel der Studie **III** in Kapitel 3.1.3 dieser Arbeit war es nun die ungenügende Aktivität an *cj*17β-HSD1 und die Selektivität gegenüber *cj*17β-HSD2 dieser Verbindung zu optimieren und zwar ohne dabei die humane Aktivität zu beeinflussen. Startpunkt war ein parallelsynthetischer Ansatz zur Synthese von aromatischen Sulfonamiden, die auf ihre Aktivität an *h*17β-HSD1 getestet wurden. Die vielversprechendsten Verbindungen wurden dann im größeren Maßstab synthetisiert und weiter charakterisiert. Da die aromatischen Sulfonamide sich als sehr potent am humanen Enzym erwiesen, wurde eine Bibliothek synthetisiert, in der die Substituenten hinsichtlich ihrer lipophilen und elektronischen Effekte variieren (Abbildung 24). Alle Verbindungen wurden hinsichtlich ihrer Aktivität an *h*- und *cj*17β-HSD1 und ihrer Selektivität gegenüber *h*- und *cj*17β-HSD2 evaluiert. Die Aktivitäten an *h*17β-HSD1 liegen für alle Substanzen im niedrigen nanomolaren Bereich (12 – 92 nM), die Selektivitäten gegenüber *h*17β-HSD2 reichen von Faktor 6 – 36. Einzige Ausnahme bildet die 2,4-di-Nitro substituierte Verbindung **III/16**, die an *h*17β-HSD2 bessere Aktivität zeigt als an *h*17β-HSD1. Das könnte am hohen sterischen Anspruch dieser Substituenten liegen und deutet darauf hin, dass *h*17β-HSD2 größere Substituenten besser toleriert.

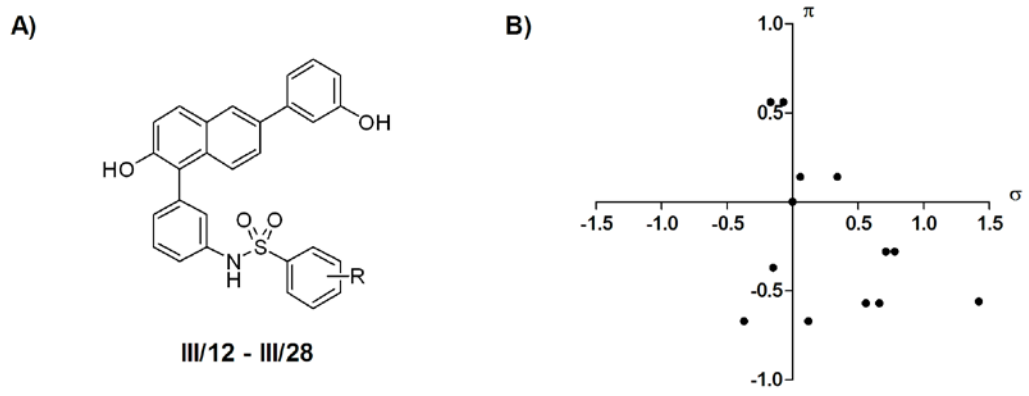

Abbildung 24: A) Übersichtsstruktur der synthetisierten Bibliotheksubstanzen B) Übersicht über die in der Bibliothek eingeführten Substituenten hinsichtlich Sigma-Hammet-Faktoren und lipophilen Eigenschaften.

Dass man keine signifikanten Steigerungen der Aktivität beobachten kann, ist aufgrund der verschiedenen Substituenten (Abbildung 24) und deren Einfluss auf die Elektronendichte im Phenylring und die Lipophilie verwunderlich. Geht man davon aus, dass die phenylsubstituierten Sulfonamide (Abbildung 24 A) den gleichen Bindungsmodus in der *h*17β-HSD1 einnehmen, wie das methylsubstituierte Sulfonamid **I/19**, wären zusätzliche π-π-Wechselwirkungen des Phenylrings am Sulfonamid mit Phe192 denkbar (Abbildung 25 A). Nicht zu begründen sind dadurch die fehlenden Einflüsse der Substituenten. Eine mögliche Erklärung hierfür wäre die Kompensation durch den Verlust einer der oben beschriebenen H-Brücken mit dem Protein. Denkbar für die phenylsubstituierten Verbindungen wäre aber auch ein Bindungsmodus der dem von Verbindung **I/19** in *cj*17β-HSD1 ähnelt (Abbildung 25B). Hier wären stabilisierende π-π-Wechselwirkungen des Phenylrings am Naphthalenkern mit Phe259 möglich. Die weiteren eingeführten Substituenten würden so aus der Bindetasche rausragen, könnten dadurch auch keine Effekte erzielen und wären zusätzlich noch Solvenzeffekten an der Proteinoberfläche ausgesetzt. Diese hier diskutierten verschiedenen Möglichkeiten der Bindungsmodi können nur durch ein Co-Kristallisat belegt werden. Auf der einen Seite sind die gleichbleibenden Aktivitäten dieser Verbindungsklasse durch die dadurch fehlenden SAR-Studien von Nachteil, andererseits könnten sie auch von Vorteil sein. Man hat so die Möglichkeit, die Verbindungen hinsichtlich ihrer physikochemischen und biochemischen Eigenschaften zu optimieren ohne dabei eventuell ihre Wirksamkeit abzuschwächen. Dies würde einen großen Vorteil in der nachfolgenden ADMET-Optimierung bieten.

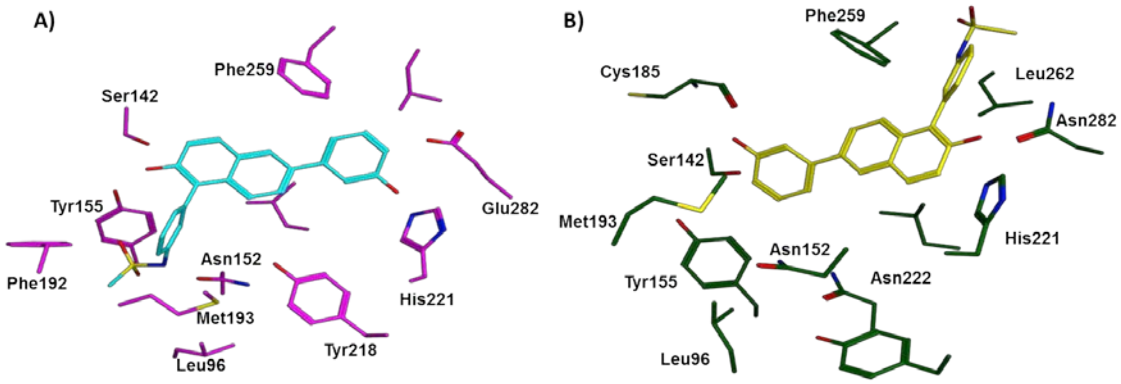

*Abbildung 25: A) Bindungsmodus von **I/19** gedockt in 1fdt (www.uniprot.org) B) Bindungsmodus von **I/19** gedockt in das Homologiemodell von cj17β-HSD1.*

Die Aktivitäten an *cj*17β-HSD1 und auch die Selektivitäten konnten durch das Einfügen der Aromatizität am Sulfonamid von **I/19** geringfügig verbessert werden. Auch hier konnten keine klaren Strukturwirkungsbeziehungen ausgemacht werden. Durchgängig zeigen die Verbindungen (**III/8** – **III/29**) schlechtere Hemmdaten an *cj*17β-HSD1.

Eine allgemeine Strategie in der medizinischen Chemie zur Steigerung der Aktivität ist die Rigidisierung einer Verbindung. Durch das Einfrieren einer Konformation verringert man den entropischen Anteil einer Bindung und kann so möglicherweise seine Affinität steigern. Um diesen Ansatz zu verfolgen wurde Verbindung **III/12** am Sulfonamid rigidisiert und dabei zwei Konformere erhalten (**III/30** und **III/31**). Konformer **III/30** behält seine Aktivität gegenüber *h*17β-HSD1 bei und Konformer **III/31** büßt sehr stark an Aktivität ein. Man hat mit

Verbindung **III/30** die biologisch aktive Konformation gefunden, während Verbindung **III/31** offensichtlich nicht in der Lage ist die nötigen Interaktionen mit der Bindungstasche einzugehen. Bemerkenswert ist jedoch die Aktivität an *cj*17β-HSD1 und auch die Selektivität gegenüber *cj*17β-HSD2. Konformer **III/30** (Abbildung 26) zeigt als einzige der synthetisierten Verbindungen eine sehr hohe Aktivität an *cj*17β-HSD1 und auch eine deutliche Selektivität, während das andere Konformer **III/31** genauso wenig aktiv ist wie die Ausgangsverbindung **I/19**.

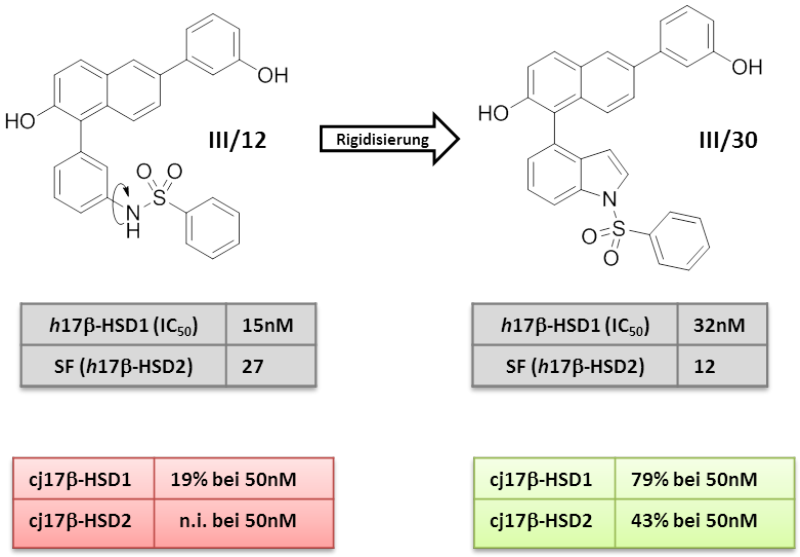

*h*17β-HSD1 (IC_{50})	15nM
SF (*h*17β-HSD2)	27

cj17β-HSD1	19% bei 50nM
cj17β-HSD2	n.i. bei 50nM

*h*17β-HSD1 (IC_{50})	32nM
SF (*h*17β-HSD2)	12

cj17β-HSD1	79% bei 50nM
cj17β-HSD2	43% bei 50nM

*Abbildung 26: **III/12**, aktives Konformer **III/30** und deren Inhibitionsprofile*

Das Einfrieren der Verbindung **III/12** in einer Konformation nahe der biologisch aktiven Konformation beeinflusst die Aktivität an *cj*17β-HSD1 deutlich mehr am humanen Pendant. Eine Erklärung hierfür mag in der durch Pro191 eingeschränkten Flexibilität der Bindetasche von *cj*17β-HSD1 liegen, die womöglich nur die Bindung der biologisch aktiven Konformation zulässt. Durch die größere Bindetasche der *h*17β-HSD1 stellt Verbindung **III/30** wohl nur eine der möglichen Konformationen nahe der biologisch aktiven Konformation, die vom Enzym toleriert werden, dar. Handelt es sich tatsächlich um die biologisch aktive Konformation würde man einen deutlichen Aktivitätszuwachs an *h*17β-HSD1 erwarten. Für die Verbindungen mit freier Drehbarkeit am Sulfonamid bedeuten diese Ergebnisse, dass der Energieaufwand von energetisch günstiger Konformation in Lösung zu biologisch aktiver Konformation in der Bindetasche größer ist, als der Energiegewinn durch die Bindung im aktiven Zentrum. Für die rigidisierte Verbindung **III/30** ist dieser Energieverlust nicht gegeben und man erhält daher die gesteigerte Potenz der Verbindung an *cj*17β-HSD1.

Die weiteren biologischen Daten, die für diese Verbindung evaluiert wurden, deuten auf einen vielversprechenden Kandidaten für das *in vivo Proof of Concept* im beschriebenen Tiermodell hin. Sie ist selektiv gegenüber ER α und β und zeigt Aktivität im zellulären System T47D. Der nächste Schritt in Richtung *Proof of Concept* wäre die Evaluierung der metabolischen Stabilität und auch die Bestimmung der Pharmakokinetik des Kandidaten.

Das Hauptziel des ersten Teils dieser Arbeit war die Identifizierung einer geeigneten Spezies und die Auswahl einer geeigneten Verbindung für das *in vivo Proof of Concept* für 17βHSD1 Inhibitoren in einem Tiermodell. Die Auswahl der geeigneten Spezies wurde durch computer-gestützte Methoden erzielt. Hier stellt *C. jacchus* und das darin etablierte Endometriosemodell eine gute Möglichkeit für die Validierung der entwickelten Hemmstoffe dar. Im anschließend entwickelten biochemischen Assay stellte sich heraus, dass die Verbindungsklasse mit dem vielversprechendsten biologischen

Profil an dieser Spezies nur geringe Aktivität zeigt. Deswegen wurde in einem rationalen Optimierungsprozess die Verbindungsklasse hinsichtlich ihrer Aktivität an *cj*17β-HSD1 verbessert. Hierbei wurde die hochaktive Verbindung **III/30** als potentieller Kandidat für das *in vivo Proof of Concept* in *C. jacchus* entwickelt.

4.2 SPR-Spektroskopie zum Einsatz im Drug Discovery Prozess

Um weiteren Antibiotikaresistenzen entgegenzuwirken, müssen neue Ansätze gefunden werden diese Mechanismen zu umgehen. Das für *P. aeruginosa* charakteristische *pqs-QS* System stellt einen vielversprechenden Ansatzpunkt dar. Der Eingriff über das Kommunikationssystem bringt den Vorteil, dass die Pathogenität der Bakterien abgeschwächt wird, ohne dabei ihre Viabilität zu beeinflussen. Der natürliche Selektionsdruck und somit auch die Resistenzentwicklung würde dadurch reduziert werden. Die Entwicklung von *QSIs*, die über PqsD und/oder PqsR ihre Wirkung ausüben, gehört zu einer vielversprechenden Alternative gegenüber der herkömmlichen Antibiotikatherapie (Kapitel 1.2). Ziel der Arbeit war die Entwicklung von validen SPR-Biosensor-Assays für beide Targets, die es erlauben die SPR-spektroskopische Methode in der Entwicklung von *QSIs* effizient einzusetzen.

Ein SPR-Biosensor-Assay lässt sich in drei Teile gliedern; Immobilisierung, Bindungsstudien und Interpretation der Daten. Zur Vorbereitung des Target-Proteins spielt die Auswahl der Immobilisierungsmethode eine wichtige Rolle. Die am häufigsten verwendete Immobilisierungsart ist die Aminkupplung (siehe Kapitel 1.3.2.1), welche auch für die Immobilisierung von PqsD an der Sensoroberfläche ausgewählt wurde. Hierbei spielt nicht nur der pH-Wert des Immobilisierungspuffers, sondern auch dessen Ionenstärke und Zusammensetzung eine große Rolle. Da der Zusatz von Nucleophilen, wie TRIS oder Detergenzien wie DTT oder β-Mercaptoethanol die Immobilisierungsreaktion stören, wurde PqsD nach der Expression und Aufreinigung in PBS-Puffer gelagert. Um den optimalen Immobilisierungspuffer zu identifizieren, wurden zur Präkonzentrierung (Kapitel 1.3.2.1) vier verschiedene Puffer verwendet (Abbildung 27A). 10 mM Natriumacetat bei pH 4.5 eignet sich am besten zur Präkonzentrierung, was an der Intensität des Signals deutlich wird (Abbildung 27A) und wurde deshalb als Puffer für die Aminkupplung verwendet (Abbildung 27B). Dieses Puffersystem erweist sich als sehr effizient. Man erreicht schnell eine hohe Beladungsdichte (Abbildung 27B).

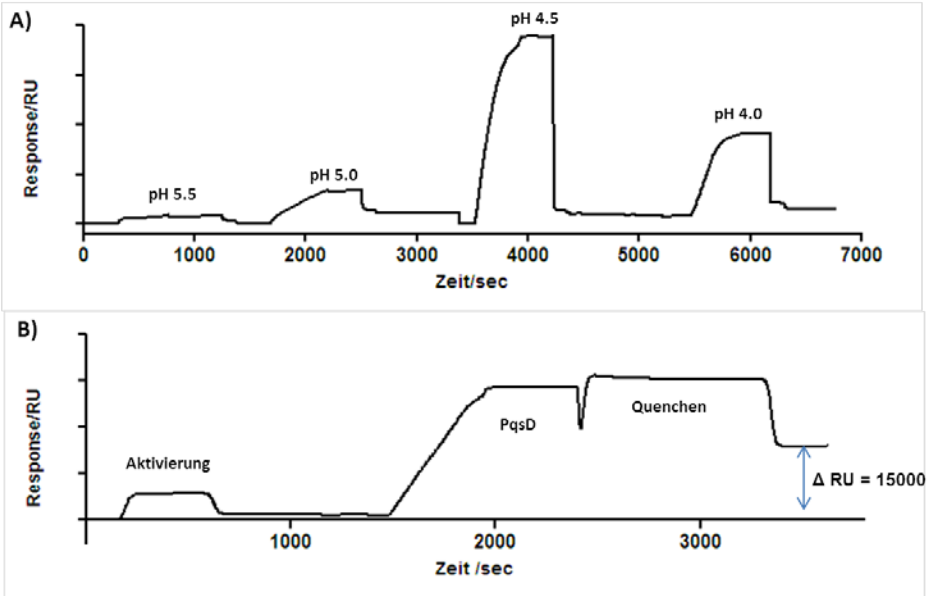

Abbildung 27: A) pH-Scouting mit 10 mM NaAc für H_6-PqsD. B) Immobilisierung von H_6-PqsD.

Um nach der Immobilisierung die Aktivität des Liganden zu überprüfen, ist es unbedingt notwendig einen Referenzbinder für das Protein als Positivkontrolle zu haben. Bei der für PqsD verwendeten Referenzsubstanz handelt es sich um ein Anthranilsäurederivat **IV/1** (Abbildung 28 B), für das im funktionalen Kompetitionsassay (Pistorius *et al.*, 2011) eine Hemmung von 65 µM (IC_{50}) bestimmt wurde. Die Verbindung zeigt am immobilisierten Target eine Equilibriumbindungskonstante K_{Deq} von 435 µM (Abbildung 28). Wie man jedoch am Fit der Equilibrium Response sehen kann, ist die Proteinoberfläche nur zu ca. 60 % gesättigt. Um den Sättigungszustand zu erreichen, müssten deutlich höhere Konzentrationen des Hemmstoffes eingesetzt werden, für die man hier an die Löslichkeitsgrenze der Verbindung im Puffersystem stoßen würde. In Studien wurde gezeigt, dass es nicht zwingend notwendig ist die Sättigung zu erreichen um einen verlässlichen Fit zu erhalten (Myszka and Rich, 2011). Solche Ergebnisse sollten jedoch immer kritisch hinterfragt und analysiert werden. Eine Alternative zum K_{Deq} ist die Bestimmung des K_D-Wertes über die Assoziations- und Dissoziationsgeschwindigkeiten (k_{on} und k_{off}). Da das Anthranilsäurederivat **IV/1** aber die typischen SPR-Signale für einen schwach affinen Binder zeigt, also schnelle Assoziation und auch schnelle Dissoziation, ist diese Methode in diesem Fall weniger gut geeignet. Durch die Bindung von **IV/1** an PqsD wurde klar gezeigt, dass nach der Immobilisierung Affinitätsstudien mit dem Protein problemlos möglich sind. Die Aminkupplung bei pH 4.5 ist für die PqsD-Immobilisierung also eine geeignete Methode. Mit dem Beweis der Bindung von **IV/1** können jedoch keine Aussagen über den Einfluss der Immobilisierung auf die katalytische Aktivität des Proteins getroffen werden. PqsD katalysiert die Biosynthese von HHQ aus Anthraniloyl-CoA (ACoA) und β-Ketodecanoat (Pistorius *et al.*, 2011). Deshalb wurde ein Assay entwickelt (Kapitel 3.4), mit dem es möglich ist, die Produktformation am Chip zu untersuchen, indem die SPR-Spektroskopie mit der massenspektrometrischen Analyse gekoppelt wurde.

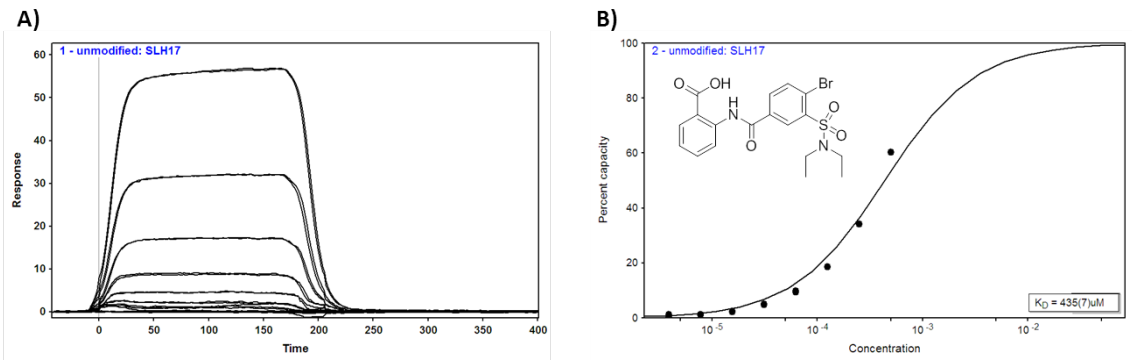

*Abbildung 28: Bindungsaffinität für **IV/1** **A)** Overlay der Sensorgramme für die Bindung von **IV/1** an H_6-PqsD gemessen als Duplikate bei 25°C; DMSO kalibriert und doppelt referenziert. **B)** Fit der Duplikate der Equilibrium Response für die Bindung von **IV/1** an H6-PqsD nach einer 1:1 Interaktion.*

Der PqsD-Biosensor wurde mit ACoA inkubiert und der Durchfluss auf HHQ-Formation untersucht. Als Kontrolle wurde synthetisches HHQ eingesetzt (Abbildung 29). Die Ergebnisse zeigen, dass die katalytische Aktivität des Proteins durch die Immobilisierung nicht verloren geht. Im Vergleich zum nativen Protein in Lösung ist sie zwar geringer, was aber auf die relativ hohe Proteindichte am Chip und die damit verbundene eingeschränkte Flexibilität zurückzuführen sein mag.

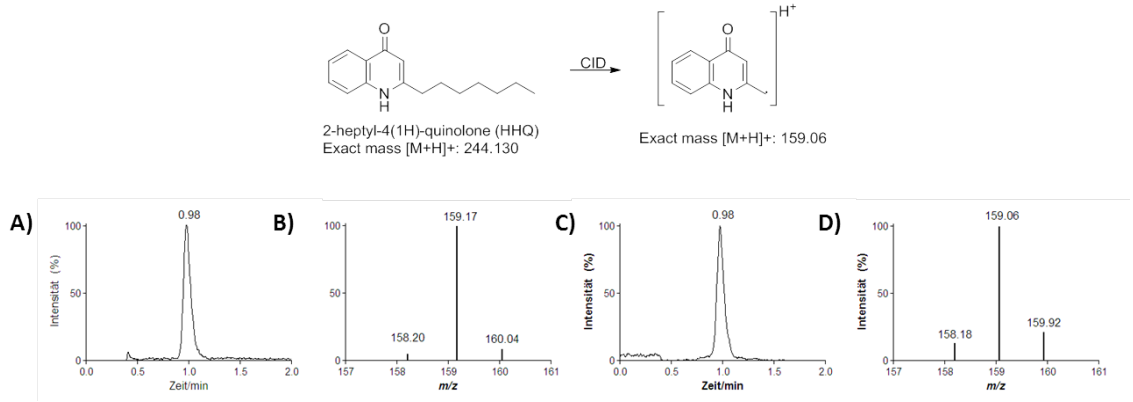

Abbildung 29: Fragmentationsmuster von HHQ (CID = collision induced decay) A) UHPLC-MS Analyse der synthetischen HHQ Referenz B) UHPLC-MS^2 Fragmentierungsmuster der synthetischen HHQ Referenz bei einer Retentionszeit von 0.98 C) UHPLC-MS Analysis des "on-chip" gebildete HHQ D) UHPLC-MS^2 Fragmetierungsmuster des „on-chip" gebildeten HHQ.

Überaus bemerkenswert ist aber die Stabilität des Proteins am Chip. Selbst nach zwei Wochen kann noch katalytische Aktivität nachgewiesen werden. Diese Ergebnisse demonstrieren deutlich, dass eine kovalente Immobilisierung die katalytische Aktivität des Proteins nur geringfügig beeinflusst und man die SPR-Spektroskopie durchaus als Label-freies System bezeichnen kann. Weiterhin ist die Überprüfung der katalytischen Aktivität als Alternative oder zusätzlich zur Positivkontrolle für immobilisierte Enzyme zu sehen. Oftmals gibt es neue Targets für die es noch keine bekannten Analyten gibt, hier wäre die Messung des Substratumsatzes zur Überprüfung der Aktivität nach der Immobilisierung von deutlichem Vorteil.

Da der katalytische Mechanismus von PqsD bisher noch ungeklärt ist, wurde eine Kombination aus Molekularem Modelling, konventioneller Enzymkinetik und SPR-Spektroskopie verfolgt, um den Mechanismus genauer zu untersuchen (Kapitel 3.5). In silico wurde ein Ping-Pong-Bi-Bi-Mechanismus für das Bi-Substratenzym postuliert, welcher dann durch experimentelle Nachweise validiert wurde. Der beschriebene SPR-Assay zur Bestimmung der katalytischen Aktivität wurde dazu verwendet verschiedene Parameter, die für einen Ping-Pong-Bi-Bi-Mechanismus charakteristisch sind, zu belegen und damit die konventionellen enzymkinetischen Methoden zu unterstützen (Abbildung 30).

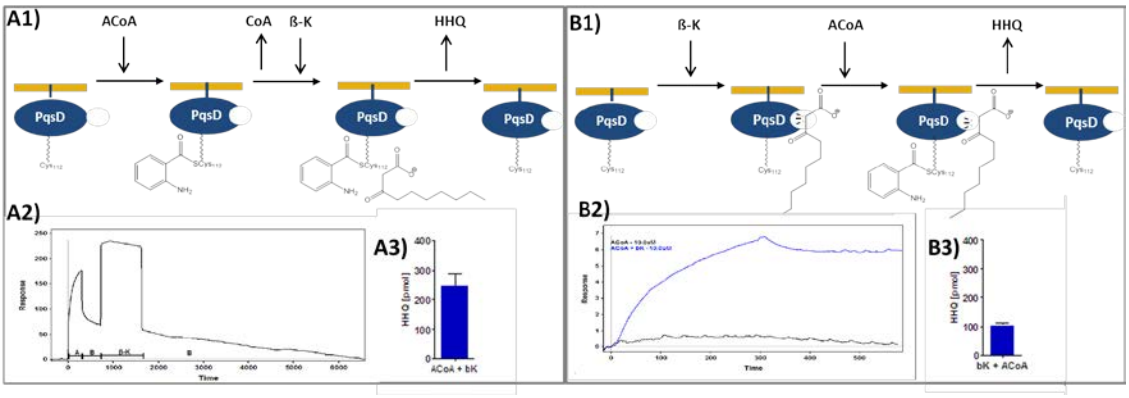

Abbildung 30: Validierung des Ping-Pong-Mechanismus (β-K = β-Ketodecanoat, B = Puffer) A) Bevorzugte Reihenfolge der Substratzugabe. A1) Übersichtsschema, A2) Sensorgramm: PqsD wird mit ACoA inkubiert, Anthranilat bleibt kovalent gebunden, durch Zugabe von β-K entsteht HHQ und die Basislinie erreicht ihr Ausgangslevel, A3) HHQ-Bestimmung mittels HPLC-MS^2 B) Nachteilige Substratzugabe: B1)Übersichtsschema, B2) Sensorgramm: Blaue Kurve: Affinität von ACoA zu PqsD. Schwarze Kurve: PqsD vorbehandelt mit β-K, keine Bindung von ACoA möglich, B3) HHQ-Bestimmung mittels HPLC-MS^2.

Um einen Ping-Pong-Bi-Bi-Mechanismus nachzuweisen, muss man zwingend zwischen zwei Bi-Bi-Mechanismen unterscheiden. Beim sequenziellen Bi-Bi-Mechanismus müssen zuerst alle Substrate an das Enzym binden, bevor die Reaktion ablaufen kann und die Produkte freigesetzt werden (Voet and Voet, 1992). Der Unterschied zum Ping-Pong-Bi-Bi-Mechanismus besteht darin, dass bei diesem Mechanismus ein oder mehrere Produkte freigesetzt werden bevor alle Substrate gebunden haben (Voet and Voet, 1992).

Wichtig für den Nachweis des Ping-Pong-Bi-Bi-Mechanismus ist, dass die Produktformation des ersten Produktes nachgewiesen werden kann, für PqsD also das Coenzym A. Häufig ist es für einen Ping-Pong-Bi-Bi-Mechanismus auch der Fall, dass ein Substrat zuerst kovalent bindet (Voet and Voet, 1992). Dieser Faktor stützt zusätzlich die These des Ping-Pong-Bi-Bi-Mechanismus für PqsD. Die SPR-Experimente (Abbildung 30A, Kapitel 3.4) haben gezeigt, dass Anthranilat kovalent am Enzyme gebunden bleibt und Coenzym A frei wird. Dann erst kann β-Ketodecanoat als weiteres Substrat binden und die zweite Produktbildung (HHQ) erfolgt. In Abbildung 30B ist die Negativkontrolle für

diesen Mechanismus dargestellt. Nach Inkubation mit β-Ketodecanoat, kann ACoA als zweites Substrat nicht mehr an PqsD binden, was sich auch an der HHQ-Formation bemerkbar macht.
Durch den entwickelten SPR-Assay konnte die katalytische Aktivität von PqsD als weiterführende Kontrolle zur Oberflächenstabilität etabliert und in einem multi-disziplinären Ansatz zur Validierung des kinetischen Mechanismus von PqsD eingesetzt werden. Die hohe Stabilität des Enzyms, wenn es am Sensorchip gebunden vorliegt, ermöglicht die Anwendung des Assays auch für das Screening von großen Substanzbibliotheken, was zur Identifizierung neuer Strukturklassen für die Inhibitorentwicklung von wichtiger Bedeutung ist.

PqsR ist der Rezeptor, über den PQS und auch in geringem Maße HHQ ihre Funktionen im *pqs*-System ausüben. Das Konzept mit dem Rezeptor zu interagieren, sieht die Entwicklung von Rezeptorantagonisten vor, die mit dem natürlichen Substrat um die PQS-Bindestelle konkurrieren. Da es sich beim kompletten Rezeptor um ein unlösliches Protein handelt, wurde dieser in einer verkürzten Version (C^{87}) mit einem SUMO-Tag zur Erhöhung der Löslichkeit kloniert, exprimiert und aufgereinigt. Um das empfindliche Protein nicht der niedrigen Salzkonzentration und dem niedrigen pH-Wert der Aminkupplung auszusetzen, wurde der Rezeptor nach der Expression biotinyliert um ihn anschließend über Streptavidin-Biotin-Interaktionen auf dem Sensorchip zu immobilisieren (Kapitel 1.3.2.2 und Kapitel 3.6). Die Biotinylierung kann in jedem für das Protein geeigneten Puffersystem durchgeführt werden. Studien haben gezeigt, dass hier auch TRIS-Puffer keine negative Auswirkung auf den Biotinylierungsgrad hat (Papalia and Myszka, 2010), obwohl die Biotinylierung auch über freie NH_2-Gruppen abläuft. Wichtig vor der Immobilisierung ist nur die vollständige Entfernung von nichtreagiertem Biotin. Als Positivkontrolle zur Assayvalidierung diente ein κ-Opiod **VI/1**, das in der Literatur als Stimulator der Transkription des *pqsABCDE Operons* beschrieben ist und für das eine Bindung an PqsR im ITC-Experiment nachgewiesen wurde. SPR-Experimente bestätigten die hohe Affinität von **VI/1** an $PqsRC^{87}$ (Abbildung 31).
Im Unterschied zur **IV/1** erreicht man mit dieser Verbindung den Sättigungszustand, man erhält einen verlässlichen Fit und einen K_{Deq} von 5.6 µM. Dieser Wert stimmt mit der über ITC bestimmen Bindungskonstante (K_D = 3.6 µM) sehr gut überein, so dass man die Immobilisierungsmethode und auch den entwickelten Assay als valide betrachten kann.

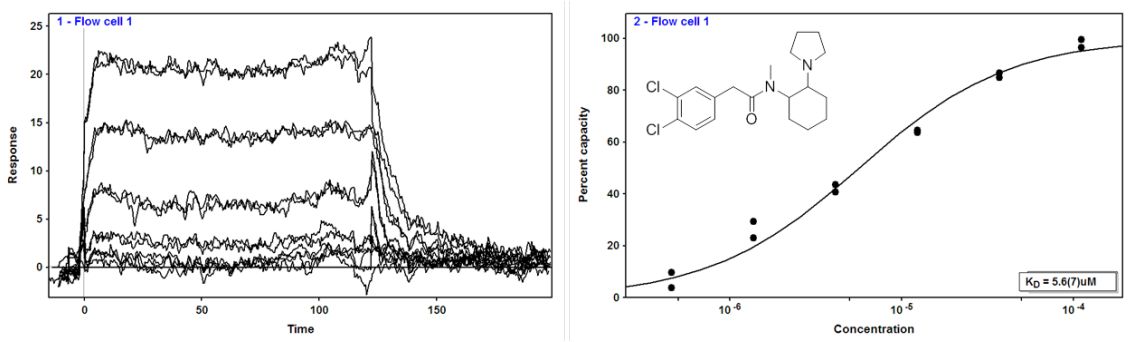

*Abbildung 31: Bindungsaffinität für κ-Opiod **VI/1 A)** Overlay der Sensorgramme für die Bindung von **VI/1** an H_6-PqsRC[87] gemessen als Duplikate bei 12°C; DMSO kalibriert und doppelt referenziert. **B)** Fit der Duplikate der Equilibrium Response für die Bindung von **VI/1** an H_6-PqsRC[87] nach einer 1:1 Interaktion.*

Ausgehend von dieser Verbindung wurde eine Fragmentbibliothek zusammengestellt um neue Leitstrukturen mit verbesserten physikochemischen Eigenschaften gegenüber den Substratanaloga (Kapitel 1.2 und (Lu *et al.*, 2012) zu identifizieren. Insbesondere im Kontext des antibakteriellen Drug Discovery stellt die Strategie der fragmentbasierten Wirkstofffindung ein vielversprechender Ansatz zur Überwindung der Antibiotikaresistenzen dar (Mochalkin *et al.*, 2009; Waldrop, 2009). Nachteile beim Screening von kleinen Molekülen ergeben sich jedoch aus deren meist schwachen Bindungsaffinitäten und damit auch geringen Signalintensitäten. Eine Möglichkeit diese zu umgehen ist eine hohe Screeningkonzentration der Fragmente, was aber auch gleichzeitig unspezifische Bindung am Target fördern kann (Giannetti and Lawrence, 2011). Deshalb wurde das PqsR-Screening bei einer geringen Konzentration von 100 µM und bei erniedrigter Temperatur von 12°C durchgeführt. Die erniedrige Temperatur ist zum einen förderlich für die Proteinstabiliät, zum anderen ist die k_{off}-Geschwindigkeit herabgesetzt, so dass man die deutlicheren Bindungskurven erhält. Zur effizienten Klassifizierung der Fragmente bezüglich ihrer Affinität wurde die Ligandeneffizienz (LE) als Kriterium ausgewählt (Hopkins *et al.*, 2004). Diese berechnet sich aus der Bindungsenergie des Liganden pro schweres Atom und erlaubt die Normalisierung der Affinität gegenüber dem Molekulargewicht (je größer der Zahlenwert, desto besser die LE).

Durch die Kombination aus Simplifizierung eines bekannten Liganden, geringer Konzentration der Fragmente, niedriger Assay-Temperatur und der Einstufung nach LE ist es gelungen ein effektives Screening durchzuführen. Es wurde ein hochaktiver Hit identifiziert, der ohne weitere Optimierung zwar schwächere Affinität als die Ausgangverbindung zeigt, die sich jedoch unter Berücksichtigung des Molekulargewichts normalisieren lässt (LE **VI/1** = 0.31 versus LE **VI/4** = 0.63). Zusätzlich zeigt Verbindung **VI/4** eine höhere antagonistische Aktivität als **VI/1**. Ausgehend von dieser Verbindung wurden Optimierungen durchgeführt, was zu einem hochpotenten PqsR-Antagonisten (**VI/11)** führte, der um dieselbe Bindungsstelle konkurriert wie Ausgangsverbindung **VI/1**. Um eine Bindung an dieselbe Substratbindestelle nachzuweisen, wurden Kompetitionsexperimente durchgeführt, die diese

Annahme bestätigten (Abbildung 32). **VI/1** ist in der Lage, Verbindung **VI/11** konzentrationsabhängig aus der Bindetasche zu verdrängen. Sowohl am isolieren System in *E.coli* (IC_{50} = 12.5µM) als auch im komplexen *QS*-System in *P. aeruginosa* (IC_{50} = 23.6 µM) zeigt die Hitverbindung ein sehr gutes Hemmprofil. Hinsichtlich der beschriebenen Beobachtungen, dass *E.coli* die höheren Sensitivitäten gegenüber Substraten aufweist (Fletcher *et al.*, 2007; Hodgkinson *et al.*, 2010), ist der geringe Unterschied der Hemmpotenz zwischen *E.coli* und *P. aeruginosa* sehr bemerkenswert. Möglicherweise liegt diese hohe Potenz der Hydroxamsäure **VI/11** in ihrer Hydrophilie (logP = 2.1), die zur Penetration der *P. aeruginosa* Membran von Vorteil ist, oder aber die Verbindung stellt kein Substrat der für *P. aeruginosa* spezifischen Effluxpumpen dar, die mitunter für die hohe Resistenz gegenüber Antibiotika verantwortlich sind (Ma *et al.*, 1994).

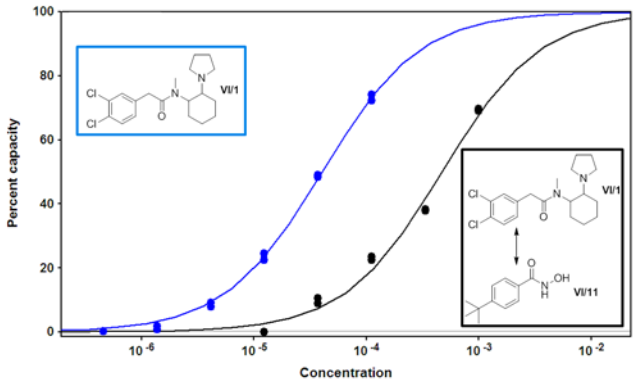

*Abbildung 32: Kompetitionsexperiment für die Bindung von **VI/1** und **VI/11**. **A)** Blaue Kurve: Fit der Duplikate der Equilibrium Response von **IV/1** an H_6SUMO-PqsR^{C87} nach einer 1:1 Interaktion; Schwarze Kurve: Fit der Duplikate der Equilibrium Response von **IV/1** an H_6SUMO-PqsR^{C87} nach einer 1:1 Interaktion in Anwesenheit von 100µM **VI/11**.*

Durch die Kombination aus rationalem Design und biophysikalischen Methoden ist es gelungen, die ersten antagonistischen kleinen Moleküle als PqsR-Liganden zu entwickeln. Sie sind zwar deutlich schwächer antagonistisch als die bereits beschriebenen Substratanaloga (Lu et al., 2012), aber hinsichtlich ihres geringen Molekulargewichtes und ihrer Aktivität in *P. aeruginosa* bieten sie hohes Potenzial zur weiteren Optimierung.

Diese Ergebnisse unterstreichen den Einsatz der SPR-Spektroskopie als ausgezeichnete Methode zur Hitstrukturfindung im fragmentbasierten Drug Discovery Prozess.

Der Fokus dieser Arbeit lag auf der Entwicklung von neuen Substanzen zur Behandlung von Infektions- und Krebserkrankungen, die die Problematik der Resistenzentwicklung umgehen und so vielversprechende Ansätze in der Therapie dieser Krankheiten bilden. Die im Rahmen dieser Arbeit entwickelten 17β-HSD1-Inhibitoren stellen eine vielversprechende Strukturklasse für das *in vivo Proof of Concept* am Endometriosemodell in *C. jacchus* dar. Der entwickelte spezies-spezifische Kompetitionsassay kann sowohl für die weitere Charakterisierung von selektiven 17β-HSD1-Hemmstoffen als auch für die Charakterisierung von 17β-HSD2-Hemmstoffen angewendet werden.
Die Etablierung der SPR-Biosensor-Assays ermöglicht weitere Untersuchung zur Target-Charakterisierung an PqsD und PqsR. Sie können sowohl für die Identifizierung neuer Strukturklassen als auch zur Optimierung des kinetischen Profils bereits bekannter Liganden eingesetzt werden. Das Hydroxamsäurederivat (**VI/11**) als PqsR-Antagonist bietet einen vielversprechenden Ausgangspunkt für medizinisch-chemische Modifikationen in der Entwicklung von hochpotenten PqsR-Antagonisten.

5 Referenzen

Abdiche, Y.N., and Myszka, D.G. Probing the mechanism of drug/lipid membrane interactions using Biacore. *Analytical Biochemistry* **2004** 328 233-243.

Abdulhaq, H., and Geyer, C. Safety of Adjuvant Endocrine Therapy in Postmenopausal Women With Breast Cancer. *American Journal of Clinical Oncology* **2008** 31 595-605 510.1097/COC.1090b1013e31816d39171.

Adamo, V., Iorfida, M., Montalto, E., Festa, V., Garipoli, C., Scimone, A. et al. Overview and new strategies in metastatic breast cancer (MBC) for treatment of tamoxifen-resistant patients. *Annals of Oncology* **2007** 18 vi53-vi57.

Adamski, J., Normand, T., Leenders, F., Monté, D., Begue, A., Stéhelin, D. et al. Molecular cloning of a novel widely expressed human 80 kDa 17 beta-hydroxysteroid dehydrogenase IV. *Biochemical Journal* **1995** 311
437-443.

Ahmad, A., Ramakrishnan, A., McLean, M.A., and Breau, A.P. Use of surface plasmon resonance biosensor technology as a possible alternative to detect differences in binding of enantiomeric drug compounds to immobilized albumins. *Biosensors and Bioelectronics* **2003** 18 399-404.

Akinola, L.A., Poutanen, M., and Vihko, R. Cloning of rat 17 beta-hydroxysteroid dehydrogenase type 2 and characterization of tissue distribution and catalytic activity of rat type 1 and type 2 enzymes. *Endocrinology* **1996** 137 1572-1579.

Al-Soud, Y.A., Bey, E., Oster, A., Marchais-Oberwinkler, S., Werth, R., Kruchten, P. et al. The role of the heterocycle in bis(hydroxyphenyl)triazoles for inhibition of 17β-Hydroxysteroid Dehydrogenase (17β-HSD) type 1 and type 2. *Molecular and Cellular Endocrinology* **2009** 301 212-215.

Allaire, C. Endometriosis and Infertility: A Review *The Journal of Reproductive Medicine* **2006** 51 164-168.

Allan, G.M., Bubert, C., Vicker, N., Smith, A., Tutill, H.J., Purohit, A. et al. Novel, potent inhibitors of 17β-hydroxysteroid dehydrogenase type 1. *Molecular and Cellular Endocrinology* **2006a** 248 204-207.

Allan, G.M., Vicker, N., Lawrence, H.R., Tutill, H.J., Day, J.M., Huchet, M. et al. Novel inhibitors of 17β-hydroxysteroid dehydrogenase type 1: Templates for design. *Bioorganic & Medicinal Chemistry* **2008** 16 4438-4456.

Allan, G.M., Lawrence, H.R., Cornet, J., Bubert, C., Fischer, D.S., Vicker, N. et al. Modification of Estrone at the 6, 16, and 17 Positions: Novel Potent Inhibitors of 17β-Hydroxysteroid Dehydrogenase Type 1. *Journal of Medicinal Chemistry* **2006b** 49 1325-1345.

Amara, N., Mashiach, R., Amar, D., Krief, P., Spieser, S.p.A.H., Bottomley, M.J. et al. Covalent Inhibition of Bacterial Quorum Sensing. *Journal of the American Chemical Society* **2009** 131 10610-10619.

Azzi, A., Rehse, P.H., Zhu, D.-W., Campbell, R.L., Labrie, F., and Lin, S.-X. Crystal structure of human estrogenic 17[beta]-hydroxysteroid dehydrogenase complexed with 17[beta]-estradiol. *Nature Structural & Molecular Biology* **1996** 3 665-668.

Baird, C.L., Courtenay, E.S., and Myszka, D.G. Surface plasmon resonance characterization of drug/liposome interactions. *Analytical Biochemistry* **2002** 310 93-99.

Beckett, D., Kovaleva, E., and Schatz, P.J. A minimal peptide substrate in biotin holoenzyme synthetase-catalyzed biotinylation. *Protein Science* **1999** 8 921-929.

Bey, E., Marchais-Oberwinkler, S., Kruchten, P., Frotscher, M., Werth, R., Oster, A. et al. Design, synthesis and biological evaluation of bis(hydroxyphenyl) azoles as potent and selective non-steroidal inhibitors of 17β-hydroxysteroid dehydrogenase type 1 (17β-HSD1) for the treatment of estrogen-dependent diseases. *Bioorganic & Medicinal Chemistry* **2008a** 16 6423-6435.

Bey, E., Marchais-Oberwinkler, S., Werth, R., Negri, M., Al-Soud, Y.A., Kruchten, P. et al. Design, Synthesis, Biological Evaluation and Pharmacokinetics of Bis(hydroxyphenyl) substituted Azoles, Thiophenes, Benzenes, and Aza-Benzenes as Potent and Selective Nonsteroidal Inhibitors of 17β-Hydroxysteroid Dehydrogenase Type 1 (17β-HSD1). *Journal of Medicinal Chemistry* **2008b** 51 6725-6739.

Bey, E., Marchais-Oberwinkler, S., Negri, M., Kruchten, P., Oster, A., Klein, T. et al. New Insights into the SAR and Binding Modes of Bis(hydroxyphenyl)thiophenes and -benzenes: Influence of Additional Substituents on 17β-Hydroxysteroid Dehydrogenase Type 1 (17β-HSD1) Inhibitory Activity and Selectivity. *Journal of Medicinal Chemistry* **2009** 52 6724-6743.

Biacore Biacore Sensor Surface Handbook. **2005**

Bjarnsholt, T., and Givskov, M. Quorum-sensing blockade as a strategy for enhancing host defences against bacterial pathogens. *Philosophical transactions of the Royal Society of London. Series B, Biological sciences* **2007** 362 1213-1222.

Bjarnsholt, T., Jensen, P.O., Rasmussen, T.B., Christophersen, L., Calum, H., Hentzer, M. et al. Garlic blocks quorum sensing and promotes rapid clearing of pulmonary Pseudomonas aeruginosa infections. *Microbiology* **2005** 151 3873-3880.

Brown, W.M., Metzger Iv, L.E., Barlow, J.P., Hunsaker, L.A., Deck, L.M., Royer, R.E., and Vander Jagt, D.L. 17-β-Hydroxysteroid dehydrogenase type 1: computational design of active site inhibitors targeted to the Rossmann fold. *Chemico-Biological Interactions* **2003** 143-144 481-491.

Brozic, P., Lanisik Rizner, T., and Gobec, R. Inhibitors of 17β-Hydroxysteroid dehydrogenase type 1 *Current Medicinal Chemistry* **2008** 15 137-150.

Bulun, S.E. Endometriosis. *New England Journal of Medicine* **2009** 360 268-279.

Bulun, S.E., Zeitoun, K.M., Takayama, K., and Sasano, H. Estrogen biosynthesis in endometriosis: molecular basis and clinical relevance. *Journal of Molecular Endocrinology* **2000** 25 35-42.

Bulun, S.E., Yang, S., Fang, Z., Gurates, B., Tamura, M., Zhou, J., and Sebastian, S. Role of aromatase in endometrial disease. *The Journal of Steroid Biochemistry and Molecular Biology* **2001** 79 19-25.

Cao, H., Krishnan, G., Goumnerov, B., Tsongalis, J., Tompkins, R., and Rahme, L.G. A quorum sensing-associated virulence gene of Pseudomonas aeruginosa encodes a LysR-like transcription regulator with a unique self-regulatory mechanism. *Proceedings of the National Academy of Sciences of the United States of America* **2001** 98 14613-14618.

Cimitan, S., Lindgren, M.T., Bertucci, C., and Danielson, U.H. Early Absorption and Distribution Analysis of Antitumor and Anti-AIDS Drugs: Lipid Membrane and Plasma Protein Interactions. *Journal of Medicinal Chemistry* **2005** 48 3536-3546.

Collier, D.N., Anderson, L., McKnight, S.L., Noah, T.L., Knowles, M., Boucher, R. et al. A bacterial cell to cell signal in the lungs of cystic fibrosis patients. *FEMS Microbiology Letters* **2002** 215 41-46.

Cooper, M.A. Optical biosensors in drug discovery. *Nature Reviews Drug Discovery* **2002** 1 515-528.

Costerton, J.W., Stewart, P.S., and Greenberg, E.P. Bacterial Biofilms: A Common Cause of Persistent Infections. *Science* **1999** 284 1318-1322.

Costerton, J.W., Lewandowski, Z., Caldwell, D.E., Korber, D.R., and Lappin-Scott, H.M. Microbial Biofilms. *Annual Review of Microbiology* **1995** 49 711-745.

Cushman, M., He, H.-M., Katzenellenbogen, J.A., Lin, C.M., and Hamel, E. Synthesis, Antitubulin and Antimitotic Activity, and Cytotoxicity of Analogs of 2-Methoxyestradiol, an Endogenous Mammalian Metabolite of Estradiol That Inhibits Tubulin Polymerization by Binding to the Colchicine Binding Site. *Journal of Medicinal Chemistry* **1995** 38 2041-2049.

Danelian, E., Karlson, A., Karlsson, R., Winiwarter, S., Hansson, A., Löfas, S. et al. SPR Biosensor Studies of the Direct Interaction between 27 Drugs and a Liposome Surface: Correlation with Fraction Absorbed in Humans. *Journal of Medicinal Chemistry* **2000** 43 2083-2086.

Darby, C., Cosma, C.L., Thomas, J.H., and Manoil, C. Lethal paralysis of Caenorhabditis elegans by Pseudomonas aeruginosa. *Proceedings of the National Academy of Sciences* **1999** 96 15202-15207.

Day, J.M., Tutill, H.J., and Purohit, A. 17β-Hydroxysteroid dehydrogenase inhibitors. *Minvera Endocrinology* **2010** 35 87-108.

Day, J.M., Tutill, H.J., Purohit, A., and Reed, M.J. Design and validation of specific inhibitors of 17β-hydroxysteroid dehydrogenases for therapeutic application in breast and prostate cancer, and in endometriosis. *Endocrine-Related Cancer* **2008a** 15 665-692.

Day, J.M., Tutill, H.J., Newman, S.P., Purohit, A., Lawrence, H.R., Vicker, N. et al. 17β-Hydroxysteroid dehydrogenase Type 1 and Type 2: Association between mRNA expression and activity in cell lines. *Molecular and Cellular Endocrinology* **2006** 248 246-249.

Day, J.M., Foster, P.A., Tutill, H.J., Parsons, M.F.C., Newman, S.P., Chander, S.K. et al. 17β-hydroxysteroid dehydrogenase Type 1, and not Type 12, is a target for endocrine therapy of hormone-dependent breast cancer. *International Journal of Cancer* **2008b** 122 1931-1940.

Day, Y.S.N., and Myszka, D.G. Characterizing a drug's primary binding site on albumin. *Journal of Pharmaceutical Sciences* **2003** 92 333-343.

Day, Y.S.N., Baird, C.L., Rich, R.L., and Myszka, D.G. Direct comparison of binding equilibrium, thermodynamic, and rate constants determined by surface- and solution-based biophysical methods. *Protein Science* **2002** 11 1017-1025.

de Bentzmann, S., and Plésiat, P. The Pseudomonas aeruginosa opportunistic pathogen and human infections. *Environmental Microbiology* **2011** 13 1655-1665.

Deluca, D., Möller, G., Rosinus, A., Elger, W., Hillisch, A., and Adamski, J. Inhibitory effects of fluorine-substituted estrogens on the activity of 17beta-hydroxysteroid dehydrogenases. *Molecular and Cellular Endocrinology* **2006** 248 218-224.

DeMichele, A., Troxel, A.B., Berlin, J.A., Weber, A.L., Bunin, G.R., Turzo, E. et al. Impact of Raloxifene or Tamoxifen Use on Endometrial Cancer Risk: A Population-Based Case-Control Study. *Journal of Clinical Oncology* **2008** 26 4151-4159.

Déziel, E., Gopalan, S., Tampakaki, A.P., Lépine, F., Padfield, K.E., Saucier, M. et al. The contribution of MvfR to Pseudomonas aeruginosa pathogenesis and quorum sensing circuitry regulation: multiple quorum sensing-regulated genes are modulated without affecting lasRI, rhlRI or the production of N-acyl-L-homoserine lactones. *Molecular microbiology* **2005** 55 998-1014.

Diggle, S.P., Winzer, K., Chhabra, S.R., Worrall, K.E., Cámara, M., and Williams, P. The Pseudomonas aeruginosa quinolone signal molecule overcomes the cell density-dependency of the quorum sensing hierarchy, regulates rhl-dependent genes at the onset of stationary phase and can be produced in the absence of LasR. *Molecular microbiology* **2003** 50 29-43.

Donaldson, S.H., and Boucher, R.C. Die Pathophysiologie der Mukoviszidose. *Annales Nestlé© (Deutsche Ausg.)* **2006** 64 103-111.

Dubern, J.-F., and Diggle, S.P. Quorum sensing by 2-alkyl-4-quinolones in Pseudomonas aeruginosa and other bacterial species. *Molecular bioSystems* **2008** 4 882-888.

Einspanier, A., Lieder, K., Brüns, A., Husen, B., Thole, H., and Simon, C. Induction of endometriosis in the marmoset monkey (Callithrix jacchus). *Molecular Human Reproduction* **2006** 12 291-299.

Emons, G., Gründker, C., Günthert, A.R., Westphalen, S., Kavanagh, J., and Verschraegen, C. GnRH antagonists in the treatment of gynecological and breast cancers. *Endocrine-Related Cancer* **2003** 10 291-299.

Filling, C., Berndt, K.D., Benach, J., Knapp, S., Prozorovski, T., Nordling, E. et al. Critical Residues for Structure and Catalysis in Short-chain Dehydrogenases/Reductases. *Journal of Biological Chemistry* **2002** 277 25677-25684.

Firnhaber, S. (2006) Expression und Regulationvon Enzymen des Östrogenmetabolismus in humanen Endometriumläsionen kultiviert in der Nacktmaus. In *Biologie und Geographie*. Essen: Duisburg-Essen.

Fletcher, M.P., Diggle, S.P., Camara, M., and Williams, P. Biosensor-based assays for PQS, HHQ and related 2-alkyl-4-quinolone quorum sensing signal molecules. *Nature Protocols* **2007** 2 1254-1262.

Frostell-Karlsson, A., Remaeus, A., Roos, H., Andersson, K., Borg, P., Hämäläinen, M., and Karlsson, R. Biosensor Analysis of the Interaction between Immobilized Human Serum Albumin and Drug Compounds for Prediction of Human Serum Albumin Binding Levels. *Journal of Medicinal Chemistry* **2000** 43 1986-1992.

Frotscher, M., Ziegler, E., Marchais-Oberwinkler, S., Kruchten, P., Neugebauer, A., Fetzer, L. et al. Design, Synthesis, and Biological Evaluation of (Hydroxyphenyl)naphthalene and -quinoline Derivatives: Potent and Selective Nonsteroidal Inhibitors of 17β-Hydroxysteroid Dehydrogenase Type 1 (17β-HSD1) for the Treatment of Estrogen-Dependent Diseases. *Journal of Medicinal Chemistry* **2008** 51 2158-2169.

Fuqua, C., Winans, S.C., and Greenberg, E.P. Census and consensus in bacterial ecosystems: the LuxR-LuxI family of quorum-sensing transcriptional regulators. *Annual review of microbiology* **1996** 50 727-751.

Fuqua, W.C., Winans, S.C., and Greenberg, E.P. Quorum sensing in bacteria: the LuxR-LuxI family of cell density-responsive transcriptional regulators. *Journal of Bacteriology* **1994** 176 269-275.

Gallagher, L.A., McKnight, S.L., Kuznetsova, M.S., Pesci, E.C., and Manoil, C. Functions required for extracellular quinolone signaling by Pseudomonas aeruginosa. *Journal of Bacteriology* **2002** 184 6472-6480.

Geske, G.D., Wezeman, R.J., Siegel, A.P., and Blackwell, H.E. Small Molecule Inhibitors of Bacterial Quorum Sensing and Biofilm Formation. *Journal of the American Chemical Society* **2005** 127 12762-12763.

Ghosh, D., and Vihko, P. Molecular mechanisms of estrogen recognition and 17-keto reduction by human 17Î²-hydroxysteroid dehydrogenase 1. *Chemico-Biological Interactions* **2001** 130-132 637-650.

Ghosh, D., Pletnev, V.Z., Zhu, D.-W., Wawrzak, Z., Duax, W.L., Pangborn, W. et al. Structure of human estrogenic 17β-hydroxysteroid dehydrogenase at 2.20 Ã resolution. *Structure* **1995** 3 503-513.

Giannetti, A.M., and Lawrence, C.K. (2011) Chapter Eight - From Experimental Design to Validated Hits: A Comprehensive Walk-Through of Fragment Lead Identification Using Surface Plasmon Resonance. In *Methods in Enzymology*: Academic Press, pp. 169-218.

Gradishar, W.J. Tamoxifen:What Next? *The Oncologist* **2004** 9 378-384.

Grümmer, R., Schwarzer, F., Bainczyk, K., Hess-Stumpp, H., Regidor, P.-A., Schindler, A.E., and Winterhager, E. Peritoneal endometriosis: validation of an in-vivo model. *Human Reproduction* **2001** 16 1736-1743.

Gunnarsson, C., Hellqvist, E., and Stal, O. 17[beta]-Hydroxysteroid dehydrogenases involved in local oestrogen synthesis have prognostic significance in breast cancer. *British Journal of Cancer* **2005** 92 547-552.

Gustafsson, S.S., Vrang, L., Terelius, Y., and Danielson, U.H. Quantification of interactions between drug leads and serum proteins by use of "binding efficiency" *Analytical Biochemistry* **2011** 409 163-175.

Hale, G., Rebello, P., Al Bakir, I., Bolam, E., Wiczling, P., Jusko, W.J. et al. Pharmacokinetics and Antibody Responses to the CD3 Antibody Otelixizumab Used in the Treatment of Type 1 Diabetes. *The Journal of Clinical Pharmacology* **2010** 50 1238-1248.

Haun, M., and Wasi, S. Biotinylated antibodies bound to streptavidin beads: A versatile solid matrix for immunoassays. *Analytical Biochemistry* **1990** 191 337-342.

Heinrich, L., Tissot, N., Hartmann, D.J., and Cohen, R. Comparison of the results obtained by ELISA and surface plasmon resonance for the determination of antibody affinity. *Journal of Immunological Methods* **2010** 352 13-22.

Hentzer, M., Wu, H., Andersen, J.B., Riedel, K., Rasmussen, T.B., Bagge, N. et al. Attenuation of Pseudomonas aeruginosa virulence by quorum sensing inhibitors. *The EMBO journal* **2003** 22 3803-3815.

Hodgkinson, J., Bowden, S.D., Galloway, W.R.J.D., Spring, D.R., and Welch, M. Structure-Activity Analysis of the Pseudomonas Quinolone Signal Molecule. *Journal of Bacteriology* **2010** 192 3833-3837.

Hoiby, N., Krogh Johansen, H., Moser, C., Song, Z., Ciofu, O., and Kharazmi, A. Pseudomonas aeruginosa and the in vitroand in vivo biofilm mode of growth. *Microbes and Infection* **2001** 3 23-35.

Hopkins, A.L., Groom, C.R., and Alex, A. Ligand efficiency: a useful metric for lead selection. *Drug Discovery Today* **2004** 9 430-431.

Hurvitz, S.A., and Pietras, R.J. Rational management of endocrine resistance in breast cancer. *Cancer* **2008** 113 2385-2397.

Husen, B., Huhtinen, K., Poutanen, M., Kangas, L., Messinger, J., and Thole, H. Evaluation of inhibitors for 17β-hydroxysteroid dehydrogenase type 1 in vivo in immunodeficient mice inoculated with MCF-7 cells stably expressing the recombinant human enzyme. *Molecular and Cellular Endocrinology* **2006a** 248 109-113.

Husen, B., Huhtinen, K., Saloniemi, T., Messinger, J., Thole, H.H., and Poutanen, M. Human Hydroxysteroid (17-β) Dehydrogenase 1 Expression Enhances Estrogen Sensitivity of MCF-7 Breast Cancer Cell Xenografts. *Endocrinology* **2006b** 147 5333-5339.

Jansson, A. 17Beta-hydroxysteroid dehydrogenase enzymes and breast cancer. *The Journal of Steroid Biochemistry and Molecular Biology* **2009** 114 64-67.

Joernvall, H., Persson, B., Krook, M., Atrian, S., Gonzalez-Duarte, R., Jeffery, J., and Ghosh, D. Short-chain dehydrogenases/reductases (SDR). *Biochemistry* **1995** 34 6003-6013.

Johnsson, B., Löfas, S., and Lindquist, G. Immobilization of proteins to a carboxymethyldextran-modified gold surface for biospecific interaction analysis in surface plasmon resonance sensors. *Analytical Biochemistry* **1991** 198 268-277.

Jordan, V.C., and O'Malley, B.W. Selective Estrogen-Receptor Modulators and Antihormonal Resistance in Breast Cancer. *Journal of Clinical Oncology* **2007** 25 5815-5824.

Karkola, S., Alho-Richmond, S., and Wahala, K. Pharmacophore modelling of 17β-HSD1 enzyme based on active inhibitors and enzyme structure. *Molecular and Cellular Endocrinology* **2009** 301 225-228.

Karlsson, R., Kullman-Magnusson, M., Hämäläinen, M.D., Remaeus, A., Andersson, K., Borg, P. et al. Biosensor Analysis of Drug Target Interactions: Direct and Competitive Binding Assays for Investigation of Interactions between Thrombin and Thrombin Inhibitors. *Analytical Biochemistry* **2000** 278 1-13.

Kerem, B., Rommens, J.M., Buchanan, J.A., Markiewicz, D., Cox, T.K., Chakravarti, A. et al. Identification of the cystic fibrosis gene: genetic analysis. *Science* **1989** 245 1073-1080.

Key, T.J., Allen, N.E., Spencer, E.A., and Travis, R.C. Nutrition and breast cancer. *The Breast* **2003** 12 412-416.

Kruchten, P., Werth, R., Marchais-Oberwinkler, S., Frotscher, M., and Hartmann, R.W. Development of a biological screening system for the evaluation of highly active and selective 17β-HSD1-inhibitors as potential therapeutic agents. *Molecular and Cellular Endocrinology* **2009a** 301 154-157.

Kruchten, P., Werth, R., Bey, E., Oster, A., Marchais-Oberwinkler, S., Frotscher, M., and Hartmann, R.W. Selective inhibition of 17β-hydroxysteroid dehydrogenase type 1 (17βHSD1) reduces estrogen responsive cell growth of T47-D breast cancer cells. *The Journal of Steroid Biochemistry and Molecular Biology* **2009b** 114 200-206.

Kruchten, P., Werth, R., Marchais-Oberwinkler, S., Bey, E., Ziegler, E., Oster, A. et al. Development of biological assays for the identification of selective inhibitors of estradiol formation from estrone in rat liver preparations. *Comptes Rendus Chimie* **2009c** 12 1110-1116.

Kulak, J., Fischer, C., Komm, B., and Taylor, H.S. Treatment with Bazedoxifene, a Selective Estrogen Receptor Modulator, Causes Regression of Endometriosis in a Mouse Model. *Endocrinology* **2011** 152 3226-3232.

Lamminen, T., Saloniemi, T., Huhtinen, K., Koskimies, P., Messinger, J., Husen, B. et al. In vivo mouse model for analysis of hydroxysteroid (17β) dehydrogenase 1 inhibitors. *Molecular and Cellular Endocrinology* **2009** 301 158-162.

Laschke, M.W., Elitzsch, A., Vollmar, B., and Menger, M.D. In vivo analysis of angiogenesis in endometriosis-like lesions by intravital fluorescence microscopy. *Fertility and Sterility* **2005** 84, Supplement 2 1199-1209.

Laschke, M.W., Elitzsch, A., Scheuer, C., Vollmar, B., and Menger, M.D. Selective cyclo-oxygenase-2 inhibition induces regression of autologous endometrial grafts by down-regulation of vascular endothelial growth factor-mediated angiogenesis and stimulation of caspase-3-dependent apoptosis. *Fertility and sterility* **2007** 87 163-171.

Latifi, A., Foglino, M., Tanaka, K., Williams, P., and Lazdunski, A. A hierarchical quorum-sensing cascade in Pseudomonas aeruginosa links the transcriptional activators LasR and RhlR (VsmR) to expression of the stationary-phase sigma factor RpoS. *Molecular microbiology* **1996** 21 1137.

Latifi, A., Winson, M.K., Foglino, M., Bycroft, B.W., Stewart, G.S.A.B., Lazdunski, A., and Williams, P. Multiple homologues of LuxR and LuxI control expression of virulence determinants and secondary metabolites through quorum sensing in Pseudomonas aeruginosa PAO1. *Molecular Microbiology* **1995** 17 333-343.

Lawrence, H.R., Vicker, N., Allan, G.M., Smith, A., Mahon, M.F., Tutill, H.J. et al. Novel and Potent 17β-Hydroxysteroid Dehydrogenase Type 1 Inhibitors. *Journal of Medicinal Chemistry* **2005** 48 2759-2762.

Leese, M.P., Leblond, B., Newman, S.P., Purohit, A., Reed, M.J., and Potter, B.V.L. Anti-cancer activities of novel D-ring modified 2-substituted estrogen-3-O-sulfamates. *The Journal of Steroid Biochemistry and Molecular Biology* **2005** 94 239-251.

Lépine, F., Milot, S., Déziel, E., He, J., and Rahme, L.G. Electrospray/mass spectrometric identification and analysis of 4-hydroxy-2-alkylquinolines (HAQs) produced by Pseudomonas aeruginosa. *Journal of the American Society for Mass Spectrometry* **2004** 15 862-869.

Lilienkampf, A., Karkola, S., Alho-Richmond, S., Koskimies, P., Johansson, N., Huhtinen, K. et al. Synthesis and Biological Evaluation of 17β-Hydroxysteroid Dehydrogenase Type 1 (17β-HSD1) Inhibitors Based on a Thieno[2,3-d]pyrimidin-4(3H)-one Core. *Journal of Medicinal Chemistry* **2009** 52 6660-9971.

Lower, E.E., Blau, R., Gazder, P., and Stahl, D.L. The effect of estrogen usage on the subsequent hormone receptor status of primary breast cancer. *Breast Cancer Research and Treatment* **1999** 58 205-210.

Lu, C., Kirsch, B., Zimmer, C., de Jong, Johannes C., Henn, C., Maurer, ChristineÂ K. et al. Discovery of Antagonists of PqsR, a Key Player in 2-Alkyl-4-quinolone-Dependent Quorum Sensing in Pseudomonas aeruginosa. *Chemistry and Biology* **2012** 19 381-390.

Ma, D., Cook, D.N., Hearst, J.E., and Nikaido, H. Efflux pumps and drug resistance in Gram-negative bacteria. *Trends in Microbiology* **1994** 2 489-493.

Mahajan-Miklos, S., Tan, M.-W., Rahme, L.G., and Ausubel, F.M. Molecular Mechanisms of Bacterial Virulence Elucidated Using a Pseudomonas aeruginosaâ€“ Caenorhabditis elegans Pathogenesis Model. *Cell* **1999** 96 47-56.

Mäkelä, S., Poutanen, M., Lehtimäki, J., Kostian, M.L., Santti, R., and Vihko, R. Estrogen-specific 17 beta-hydroxysteroid oxidoreductase type 1 (E.C. 1.1.1.62) as a possible target for the action of phytoestrogens. *Proceeding of the Society of Experimental Biology and Medicine* **1995** 208 51-59.

Manefield, M., and Turner, S.L. Quorum sensing in context: out of molecular biology and into microbial ecology. *Microbiology* **2002** 148 3762-3764.

Marchais-Oberwinkler, S., Frotscher, M., Ziegler, E., Werth, R., Kruchten, P., Messinger, J. et al. Structure activity study in the class of 6-(3´-hydroxyphenyl)naphthalenes leading to an optimization of a pharmacophore model for 17β-hydroxysteroid dehydrogenase type 1 (17β-HSD1) inhibitors. *Molecular and Cellular Endocrinology* **2009** 301 205-211.

Marchais-Oberwinkler, S., Kruchten, P., Frotscher, M., Ziegler, E., Neugebauer, A., Bhoga, U. et al. Substituted 6-Phenyl-2-naphthols. Potent and Selective Nonsteroidal Inhibitors of 17β-Hydroxysteroid Dehydrogenase Type 1 (17β-HSD1): Design, Synthesis, Biological Evaluation, and Pharmacokinetics. *Journal of Medicinal Chemistry* **2008** 51 4685-4698.

Marchais-Oberwinkler, S., Henn, C., Möller, G., Klein, T., Negri, M., Oster, A. et al. 17β-Hydroxysteroid dehydrogenases (17β-HSDs) as therapeutic targets: Protein structures, functions, and recent progress in inhibitor development. *The Journal of Steroid Biochemistry and Molecular Biology* **2011** 125 66-82.

Markgren, P.-O., Schaal, W., Hämäläinen, M., Karlén, A., Hallberg, A., Samuelsson, B., and Danielson, U.H. Relationships between Structure and Interaction Kinetics for HIV-1 Protease Inhibitors. *Journal of Medicinal Chemistry* **2002** 45 5430-5439.

Matsui, H., Verghese, M.W., Kesimer, M., Schwab, U.E., Randell, S.H., Sheehan, J.K. et al. Reduced Three-Dimensional Motility in Dehydrated Airway Mucus Prevents Neutrophil Capture and Killing Bacteria on Airway Epithelial Surfaces. *The Journal of Immunology* **2005** 175 1090-1099.

Mazumdar, M., Chen, J., and Lin, S.-X. Molecular Basis of sex-steroid translation PDB ID: 3klp. **2009a**

Mazumdar, M., Chen, J., and SX, L. Molecular Basis of sex-steroid translation. PDB ID:3km0. **2009b**

Mazumdar, M., Fournier, D., Zhu, D.-W., Cadot, W., Poirier, D., and Lin, C.M. Binary and ternary crystal structure analyses of a novel inhibitor with 17β-HSD type 1: a lead compound for breast cancer therapy. *Biochemical Journal* **2009c** 2009 357-366.

McKnight, S.L., Iglewski, B.H., and Pesci, E.C. The Pseudomonas quinolone signal regulates rhl quorum sensing in Pseudomonas aeruginosa. *Journal of Bacteriology* **2000** 182 2702-2708.

Menger, M.D., Laschke, M.W., and Vollmar, B. Viewing the Microcirculation through the Window: Some Twenty Years Experience with the Hamster Dorsal Skinfold Chamber. *European Surgical Research* **2002** 34 83-91.

Messinger, J., Schoen, U., Husen, B., Thole, H., Koskimies, P., and Kallio, L. (2008a) Therapeutically active triazoles and their use. In.

Messinger, J., Husen, B., Schoen, U., Thole, H., Koskimies, P., and Unkila, M. (2008b) Substituted estratrien derivatives as 17beta HSD inhibitors. In.

Messinger, J., Husen, B., Koskimies, P., HirvelÃ¤, L., Kallio, L., Saarenketo, P., and Thole, H. Estrone C15 derivative-A new class of 17β-hydroxysteroid dehydrogenase type 1 inhibitors. *Molecular and Cellular Endocrinology* **2009** 301 216-224.

Messinger, J., Hirvela¤, L., Husen, B., Kangas, L., Koskimies, P., PentikÃ¤inen, O. et al. New inhibitors of 17β-hydroxysteroid dehydrogenase type 1. *Molecular and Cellular Endocrinology* **2006** 248 192-198.

Michiels, P.J.A., Ludwig, C., Stephan, M., Fischer, C., Möller, G., Messinger, J. et al. Ligand-based NMR spectra demonstrate an additional phytoestrogen binding site for 17Î²-hydroxysteroid dehydrogenase type 1. *The Journal of Steroid Biochemistry and Molecular Biology* **2009** 117 93-98.

Miller, W., Bartlett, J., Canney, P., and Verrill, M. Hormonal therapy for postmenopausal breast cancer: the science of sequencing. *Breast Cancer Research and Treatment* **2007** 103 149-160.

Mindnich, R., Haller, F., Halbach, F., Moeller, G., de Angelis, M.H., and Adamski, J. Androgen metabolism via 17β-hydroxysteroid dehydrogenase type 3 in mammalian and non-mammalian vertebrates: comparison of the human and the zebrafish enzyme. *Journal of Molecular Endocrinology* **2005** 35 305-316.

Mochalkin, I., Miller, J.R., Narasimhan, L., Thanabal, V., Erdman, P., Cox, P.B. et al. Discovery of Antibacterial Biotin Carboxylase Inhibitors by Virtual Screening and Fragment-Based Approaches. *ACS Chemical Biology* **2009** 4 473-483.

Molin, S., and Tolker-Nielsen, T. Gene transfer occurs with enhanced efficiency in biofilms and induces enhanced stabilisation of the biofilm structure. *Current opinion in biotechnology* **2003** 14 255-261.

Möller, G., Husen, B., Kowalik, D., Hirvela, L., Plewczynski, D., Rychlewski, L. et al. Species Used for Drug Testing Reveal Different Inhibition Susceptibility for 17beta-Hydroxysteroid Dehydrogenase Type 1. *PLoS ONE* **2010** 5 e10969.

Müh, U., Schuster, M., Heim, R., Singh, A., Olson, E.R., and Greenberg, E.P. Novel Pseudomonas aeruginosa Quorum-Sensing Inhibitors Identified in an Ultra-High-Throughput Screen. *Antimicrobial Agents and Chemotherapy* **2006** 50 3674-3679.

Myszka D. G., Abdiche Y. N., F., A., O., B., Eisenstein, E., Hensley, P. et al. The ABRF-MIRG'02 Study: Assembly State, Thermodynamic, and Kinetic Analysis of an Enzyme/Inhibitor Interaction. *Journal of Biomolecular Technology* **2003** 14 247-269.

Myszka, D.G., and Rich, R.L. Implementing surface plasmon resonance biosensors in drug discovery. *Pharmaceutical Science & Technology Today* **2000** 3 310-317.

Myszka, D.G., and Rich, R.L. (2011) Biosensor Tools, Handbook of Advanced Biosensor Workshop. In.

Nadal Jimenez, P., Koch, G., Thompson, J.A., Xavier, K.B., Cool, R.H., and Quax, W.J. The Multiple Signaling Systems Regulating Virulence in Pseudomonas aeruginosa. *Microbiology and Molecular Biology Reviews* **2012** 76 46-65.

Navratilova, I., Papalia, G.A., Rich, R.L., Bedinger, D., Brophy, S., Condon, B. et al. Thermodynamic benchmark study using Biacore technology. *Analytical Biochemistry* **2007** 364 67-77.

Negri, M., Recanatini, M., and Hartmann, R.W. Insights in 17β-HSD1 Enzyme Kinetics and Ligand Binding by Dynamic Motion Investigation. *PLoS ONE* **2010** 5 e12026.

Nokelainen, P., Puranen, T., Peltoketo, H., Orava, M., Vihko, P., and Vihko, R. Molecular Cloning of Mouse 17β-Hydroxysteroid Dehydrogenase Type 1 and Characterization of Enzyme Activity. *European Journal of Biochemistry* **1996** 236 482-490.

Olusjano, M.S., Li, Y., Isomaa, V.V., Mantyniema, A., Pulkka, A.E., Soini, Y., and Vihko, P.T. Inhibition of 17β-hydroxysteroid dehydrogenase (17β-hsd) by imidazole-based compounds. *Letters in Drug Design and Discovery* **2004** 5 48-51.

Ortmann, O., Cufer, T., Dixon, J.M., Maass, N., Marchetti, P., Pagani, O. et al. Adjuvant endocrine therapy for perimenopausal women with early breast cancer. *The Breast* **2009** 18 2-7.

Oster, A., Hinsberger, S., Werth, R., Marchais-Oberwinkler, S., Frotscher, M., and Hartmann, R.W. Bicyclic Substituted Hydroxyphenylmethanones as Novel Inhibitors of 17β-Hydroxysteroid Dehydrogenase Type 1 (17β-HSD1) for the Treatment of Estrogen-Dependent Diseases. *Journal of Medicinal Chemistry* **2010a** 53 8176-8186.

Oster, A., Klein, T., Henn, C., Werth, R., Marchais-Oberwinkler, S., Frotscher, M., and Hartmann, R.W. Bicyclic Substituted Hydroxyphenylmethanone Type Inhibitors of 17 β-Hydroxysteroid Dehydrogenase Type 1 (17 β-HSD1): The Role of the Bicyclic Moiety. *ChemMedChem* **2010b** 6 476-487.

Oster, A., Klein, T., Werth, R., Kruchten, P., Bey, E., Negri, M. et al. Novel estrone mimetics with high 17β-HSD1 inhibitory activity. *Bioorganic & Medicinal Chemistry* **2010c** 18 3494-3505.

Papalia, G., and Myszka, D. Exploring minimal biotinylation conditions for biosensor analysis using capture chips. *Analytical Biochemistry* **2010** 403 30-35.

Pearson, J.P., Pesci, E.C., and Iglewski, B.H. Roles of Pseudomonas aeruginosa las and rhl quorum-sensing systems in control of elastase and rhamnolipid biosynthesis genes. *Journal of Bacteriology* **1997** 179 5756-5767.

Pedersen, S.S., Shand, G.H., Hansen, B.L., and Hansen, G.N. Induction of experimental chronic Pseudomonas aeruginosa lung infection with P. aeruginosa entrapped in alginate microspheres. *APMIS* **1990** 98 203-211.

Peltoketo, H., Isomaa, V., Maentausta, O., and Vihko, R. Complete amino acid sequence of human placental 17β-hydroxysteroid dehydrogenase deduced from cDNA. *FEBS Letters* **1988** 239 73-77.

Penning, T.M. Molecular Endocrinology of Hydroxysteroid Dehydrogenases. *Endocrine Reviews* **1997** 18 281-305.

Perez, E.A. Safety profiles of tamoxifen and the aromatase inhibitors in adjuvant therapy of hormone-responsive early breast cancer. *Annals of Oncology* **2007** 18 viii26-viii35.

Pesci, E.C., Milbank, J.B., Pearson, J.P., McKnight, S., Kende, A.S., Greenberg, E.P., and Iglewski, B.H. Quinolone signaling in the cell-to-cell communication system of Pseudomonas aeruginosa. *Proceedings of the National Academy of Sciences of the United States of America* **1999** 96 11229-11234.

Pistorius, D., Ullrich, A., Lucas, S., Hartmann, R.W., Kazmaier, U., and Müller, R. Biosynthesis of 2-Alkyl-4(1H)-Quinolones in Pseudomonas aeruginosa: Potential for Therapeutic Interference with Pathogenicity. *Chembiochem : a European journal of chemical biology* **2011** 12 850-853.

Poirier, D. Inhibitors of 17β–Hydroxysteroid dehydrogenases. *Current Medicinal Chemistry* **2003** 10 642-660.

Poirier, D. Advances in Development of Inhibitors of 17β-Hydroxysteroid Dehydrogenases *Anticancer Agents in Medicinal Chemistry* **2009** 9 642-660.

Qiu, W., Campbell, R.L., Gangloff, A., Dupuis, P., Boivin, R.P., Tremblay, M.R. et al. A concerted, rational design of type 1 17b-hydroxysteroid dehydrogenase inhibitors: estradiol-adenosine hybrids with high affinity. *The FASEB Journal* **2002**

Racine, A.C., Legrand, E., Lefebvre-Lacoeuille, C., Hoppe, E., Catala, L., Sentilhes, L., and Descamps, P. Treatment of endometriosis by aromatase inhibitors: Efficacy and side effects. *Gynécologie Obstétrique & Fertilité* **2012** 38 318-323.

Rahme, L.G., Stevens, E.J., Wolfort, S.F., Shao, J., Tompkins, R.G., and Ausubel, F.M. Common virulence factors for bacterial pathogenicity in plants and animals. *Science (New York, NY)* **1995** 268 1899-1902.

Rasmussen, T.B., and Givskov, M. Quorum-sensing inhibitors as anti-pathogenic drugs. *International journal of medical microbiology : IJMM* **2006** 296 149-161.

Rasmussen, T.B., Bjarnsholt, T., Skindersoe, M.E., Hentzer, M., Kristoffersen, P., KÃ¶te, M. et al. Screening for Quorum-Sensing Inhibitors (QSI) by Use of a Novel Genetic System, the QSI Selector. *Journal of Bacteriology* **2005** 187 1799-1814.

Reisner, A., Hoiby, N., Tolker-Nielsen, T., and Molin, S. Microbal Pathogenesis and Biofilm Development. *Contribribution to Microbiology* **2005** 12

Rich, R.L., and Myszka, D.G. Survey of the year 2003 commercial optical biosensor literature. *Journal of Molecular Recognition* **2005** 18 1-39.

Riordan, J.R., Rommens, J.M., Kerem, B., Alon, N., Rozmahel, R., Grzelczak, Z. et al. Identification of the cystic fibrosis gene: cloning and characterization of complementary DNA. *Science* **1989** 245 1066-1073.

Ritter, G., Cohen, L.S., Williams, C., Richards, E.C., Old, L.J., and Welt, S. Serological Analysis of Human Anti-Human Antibody Responses in Colon Cancer Patients Treated with Repeated Doses of Humanized Monoclonal Antibody A33. *Cancer Research* **2001** 61 6851-6859.

Rommens, J.M., Iannuzzi, M.C., Kerem, B., Drumm, M.L., Melmer, G., Dean, M. et al. Identification of the cystic fibrosis gene: chromosome walking and jumping. *Science* **1989** 245 1059-1065.

Rouillard, F., Lefebvre-Lacoeuille, C., Fournier, M.-A., and Poirier, D. Chemical Synthesis, 17β-Hydroxysteroid Dehydrogenase Type 1 Inhibitory Activity and Assessment of In Vitro and In Vivo Estrogenic Activities of Estradiol Derivatives. *The Open Enzyme Journal* **2008** 1 61-71

Saadat, M., Truong, P.T., Kader, H.A., Speers, C.H., Berthelet, E., McMurtrie, E., and Olivotto, I.A. Outcomes in patients with primary breast cancer and a subsequent diagnosis of endometrial cancer. *Cancer* **2007** 110 31-37.

Sam, K.M., Bovin, R.P., Tremblay, M.R., Auger, S., and Poirier, D. C16 and C17 derivatives of estradiol as inhibitors of 17 beta-hydroxysteroid dehydrogenase type 1: chemical synthesis and structure-activity relationships. *Drug Design and Discovery* **1998** 15 157-180.

Sawicki, M.W., Erman, M., Puranen, T., Vihko, P., and Ghosh, D. Structure of the ternary complex of human 17β-hydroxysteroid dehydrogenase type 1 with 3-hydroxyestra-1,3,5,7-tetraen-17-one (equilin) and NADP+. *Proceedings of the National Academy of Sciences* **1999** 96 840-845.

Schaasfort, R.B.M., and Tudos, A.J. (2008) *Handbook of Surface Plasmon Resonance*: The Royal Society of Chemistry.

Schuster, D., Nashev, L.G., Kirchmair, J., Laggner, C., Wolber, G., Langer, T., and Odermatt, A. Discovery of Nonsteroidal 17β-Hydroxysteroid Dehydrogenase 1 Inhibitors by Pharmacophore-Based Screening of Virtual Compound Libraries. *Journal of Medicinal Chemistry* **2008** 51 4188-4199.

Schwabe, I., Husen, B., and Einspanier, A. Expression of the estradiol-synthesizing 17β-hydroxysteroid dehydrogenases type 1 and type 7 in the nonhuman primate Callithrix jacchus. *Molecular and Cellular Endocrinology* **2001** 171 187-192.

Scotti, S., Regidor, P.A., Schindler, A.E., and Winterhager, E. Reduced proliferation and cell adhesion in endometriosis. *Molecular Human Reproduction* **2000** 6 610-617.

Siddik, Z.H., and Mehta, K. (2009) *Drug Resistance in Cancer Cells.*

Sillem, M., Hahn, U., Coddington, C.C., Gordon, K., Runnebaum, B., and Hodgen, G.D. Ectopic growth of endometrium depends on its structural integrity and proteolytic activity in the cynomolgus monkey (*Macaca fascicularis*) model of endometriosis. . *Fertility and Sterility* **1996** 66 468-473.

Simpson, E., Rubin, G., Clyne, C., Robertson, K., O'Donnell, L., Davis, S., and Jones, M. Local estrogen biosynthesis in males and females. *Endocrine-Related Cancer* **1999** 6 131-137.
Skindersoe, M.E., Alhede, M., Phipps, R., Yang, L., Jensen, P.O., Rasmussen, T.B. et al. Effects of Antibiotics on Quorum Sensing in Pseudomonas aeruginosa. *Antimicrobial Agents and Chemotherapy* **2008** 52 3648-3663.
Smith, K.M., Bu, Y., and Suga, H. Library Screening for Synthetic Agonists and Antagonists of a Pseudomonas aeruginosa Autoinducer. *Chemistry & Biology* **2003a** 10 563-571.
Smith, K.M., Bu, Y., and Suga, H. Induction and Inhibition of Pseudomonas aeruginosa Quorum Sensing by Synthetic Autoinducer Analogs. *Chemistry & Biology* **2003b** 10 81-89.
Smith, R.S., Harris, S.G., Phipps, R., and Iglewski, B. The Pseudomonas aeruginosa Quorum-Sensing Molecule N-(3-Oxododecanoyl)Homoserine Lactone Contributes to Virulence and Induces Inflammation In Vivo. *Journal of Bacteriology* **2002** 184 1132-1139.
Smuc, T., and Rizner, T.L. Expression of 17β-hydroxysteroid dehydrogenases and other estrogen-metabolizing enzymes in different cancer cell lines. *Chemico-Biological Interactions* **2009** 178 228-233.
Smuc, T., Pucelj, M.R., Sinkovec, J., Husen, B., Thole, H., and Rizner, T.L.n. Expression analysis of the genes involved in estradiol and progesterone action in human ovarian endometriosis. *Gynecological Endocrinology* **2007** 23 105-111.
Spadaro, A., Frotscher, M., and Hartmann, R.W. Optimization of Hydroxybenzothiazoles as Novel Potent and Selective Inhibitors of 17β-HSD1. *Journal of Medicinal Chemistry* **2012a**
Spadaro, A., Negri, M., Marchais-Oberwinkler, S., Bey, E., and Frotscher, M. Hydroxybenzothiazoles as New Nonsteroidal Inhibitors of 17β-Hydroxysteroid Dehydrogenase Type 1 (17β-HSD1). *PLoS ONE* **2012b** 7 e29252.
Stenberg, E., Persson, B.r., Roos, H.k., and Urbaniczky, C. Quantitative determination of surface concentration of protein with surface plasmon resonance using radiolabeled proteins. *Journal of Colloid and Interface Science* **1991** 143 513-526.
Stilley, J., Birt, J., and Sharpe-Timms, K. Cellular and molecular basis for endometriosis-associated infertility. *Cell and Tissue Research* **2012** 1-14.
Stoodley, P., Sauer, K., Davies, D.G., and Costerton, J.W. BIOFILMS AS COMPLEX DIFFERENTIATED COMMUNITIES. *Annual Review of Microbiology* **2002** 56 187-209.
Stutts, M.J., Rossier, B.C., and Boucher, R.C. Cystic Fibrosis Transmembrane Conductance Regulator Inverts Protein Kinase A-mediated Regulation of Epithelial Sodium Channel Single Channel Kinetics. *Journal of Biological Chemistry* **1997** 272 14037-14040.
Stutts, M.J., Canessa, C.M., Olsen, J.C., Hamrick, M., Cohn, J.A., Rossier, B.C., and Boucher, R.C. CFTR as a cAMP-dependent regulator of sodium channels. *Science* **1995** 269 847-850.
Suga, H., and Smith, K.M. Molecular mechanisms of bacterial quorum sensing as a new drug target. *Current Opinion in Chemical Biology* **2003** 7 586-591.
Swanson, S.J., and Mytych, D. (2011) The Use of Surface Plasmon Resonance for the Detection and Characterization of Antibodies. In *Detection and Quantification of Antibodies to Biopharmaceuticals*: John Wiley & Sons, Inc., pp. 193-209.
Swift, S., Downie, J.A., Whitehead, N.A., Barnard, A.M., Salmond, G.P., and Williams, P. Quorum sensing as a population-density-dependent determinant of bacterial physiology. *Advances in microbial physiology* **2001** 45 199-270.
Tramper-Stranders, G.A., Wolfs, T.F.W., Fleer, A., Kimpen, J.L.L., and van der Ent, C.K. Maintenance Azithromycin Treatment in Pediatric Patients With Cystic Fibrosis: Long-Term Outcomes Related to Macrolide Resistance and Pulmonary Function. *The Pediatric Infectious Disease Journal* **2007** 26 8-12 10.1097/1001.inf.0000247109.0000244249.ac.
Urruticoechea, A. The oestrogen-dependent biology of breast cancer. Sensitivity and resistance to aromatase inhibitors revisited: a molecular perspective. *Clinical and Translational Oncology* **2007** 9 752-759.
van Delden, C., and Iglewski, B.H. Cell-to-cell signaling and Pseudomonas aeruginosa infections. *Emerging infectious diseases* **1998** 4 551-560.
Vicker, N., Lawrence, H.R., Allan, G.M., Bubert, C., Smith, A., Tutill, H.J. et al. Focused Libraries of 16-Substituted Estrone Derivatives and Modified E-Ring Steroids: Inhibitors of 17ß-Hydroxysteroid Dehydrogenase Type 1. *ChemMedChem* **2006** 1 464-481.
Voet, D., and Voet, J.G. (1992) *Biochemie*: VCH.
Waldrop, G.L. Smaller Is Better for Antibiotic Discovery. *ACS Chemical Biology* **2009** 4 397-399.
Waters, C.M., and Bassler, B.L. Quorum sensing: cell-to-cell communication in bacteria. *Annual review of cell and developmental biology* **2005** 21 319-346.
WHO, W.H.O. (2002a) Report on Infectious Diseases. In.
WHO, W.H.O. (2002b) The World Health Report. In.
WHO, W.H.O. (2008) The global burden of disease: 2004 update. In.

Wu, H., Song, Z., Givskov, M., Doring, G., Worlitzsch, D., Mathee, K. et al. Pseudomonas aeruginosa mutations in lasI and rhlI quorum sensing systems result in milder chronic lung infection. *Microbiology* **2001** 147 1105-1113.

Wu, L., Einstein, M., Geissler, W.M., Chan, H.K., Elliston, K.O., and Andersson, S. Expression cloning and characterization of human 17 beta-hydroxysteroid dehydrogenase type 2, a microsomal enzyme possessing 20 alpha-hydroxysteroid dehydrogenase activity. *Journal of Biological Chemistry* **1993** 268 12964-12969.

Xiao, G., Déziel, E., He, J., Lépine, F., Lesic, B., Castonguay, M.-H. et al. MvfR, a key Pseudomonas aeruginosa pathogenicity LTTR-class regulatory protein, has dual ligands. *Molecular microbiology* **2006** 62 1689-1699.

Yang, J.Z., Agarwal, S.K., and Foster, W.G. Subchronic Exposure to 2,3,7,8-Tetrachlorodibenzo-p-dioxin Modulates the Pathophysiology of Endometriosis in the Cynomolgus Monkey. *Toxicological Sciences* **2000** 56 374-381.

Yang, L., Rybtke, M.T., Jakobsen, T.H., Hentzer, M., Bjarnsholt, T., Givskov, M., and Tolker-Nielsen, T. Computer-Aided Identification of Recognized Drugs as Pseudomonas aeruginosa Quorum-Sensing Inhibitors. *Antimicrobial Agents and Chemotherapy* **2009** 53 2432-2443.

6 Anhang

6.1 Curriculum Vitae

PERSÖNLICHE DATEN Claudia Henn
Geboren am 18. Mai 1984 in Homburg/Saar

WISSENSCHAFTLICHER WERDEGANG

10/08 – 04/12: Promotion am Helmholtz-Institut für Pharmazeutische Forschung Saarland (HIPS) und Pharmazeutische und Medizinische Chemie Universität des Saarlandes unter Anleitung von Prof. Dr. Rolf W. Hartmann.
„Kommunkationssysteme als Targets zur Überwindung vn Resistenzen tumoraler und bakterieller Erkrankungen: 17β-HSD1-Hemmstoffe und Quorum Sensing Inhibitoren“

01/08 – 09/08: Diplomarbeit in der Bioorganischen Chemie Johannes Gutenberg Universität Mainz unter der Anleitung von Prof. Dr. Horst Kunz
„Ein Weg zur Synthese von Dreikomponenten-Glykopeptidantigenen an Lysyl-lysinderivaten“

AUSBILDUNG

10/03 – 09/08: Studium der Biomedizinischen Chemie an der Johannes Gutenberg Universität Mainz mit dem Abschluss Diplom-Chemikerin (1,6)

08/00 – 03/03: Allgemeine Hochschulreife am staatlichen Heinrich-Heine-Gymnasium Kaiserslautern

6.2 Danksagung

An dieser Stelle möchte ich mich bei allen Personen ganz herzlich bedanken, die zum Gelingen dieser Arbeit beigetragen haben:

Herrn Prof. Dr. Rolf W. Hartmann für die Aufnahme in seinen Arbeitskreis, die interessanten Themen, die tolle Betreuung, für all das was ich durch diese Arbeit lernen konnte, die tollen Möglichkeiten meine Arbeit anzufertigen und vor allem für das stets entgegengebrachte Vertrauen.

Herrn Prof. Dr. Dr. Hans H. Maurer für die Übernahme des Vorsitzes der Prüfungskommission.

Frau Dr. Eva Maria Collnot für die Übernahme des Beisitzes der Prüfungskommission

Dr. Anke Steinbach und Dr. Christina Zimmer für die wissenschaftlichen Diskussionen und die Leitung des PQS-Projektes.

Dr. Martin Frotscher und Dr. Sandrine Marchais-Oberwinkler für die Leitung des HSD-Projektes.

Herrn Dr. Josef Zapp für die Durchführung der NMR-Experimente.

Dr. Stefan Böttcher für die schnelle Hilfe und Unterstützung bei analytischen Komplikationen.

Dem Team des Chemikalienlagers für die reibungslose Zusammenarbeit.

Martina Schwarz, Katrin Schmitt und Corina Przybyla für die tolle Organisation im Sekretariat, die Hilfsbereitschaft und das Finden von Terminen.

Lothar Jager, dem Mann der Technik, für unkomplizierte und schnelle Problemlösung

Christine Maurer, Deborah Montenarh und Benjamin Kirsch für die Zeit während Ihres Forschungspraktikums und die schönen Ergebnisse

Dr. Patricia Kruchten, Dr. Alexander Oster, Ruth Werth, Stefan Hinsberger, Christine Maurer und Michael Zender für die tolle Zusammenarbeit während des EAB-Praktikums und dem ständigen Schokoladennachschub währenddessen.

den jetzigen und ehemaligen Mitstreiter des HSD-Teams

den Mitstreitern des PQS-Teams

den jetzigen und ehemaligen Mitgliedern des Arbeitskreises für die gute Zusammenarbeit und das tolle Arbeitsklima.

Martina Jankowski, Jannine Ludwig, Jeaninne Jung, Laura Schrobildgen, Viktoria Krämer und Simone Amann für die Übernahme der Testung.

Dr. Stefan Boettcher, Dr. Nina Hanke, Martina Jankowski, Benjamin Kirsch, Tobias Klein, Dr. Patricia Kruchten, Sabrina Rau, Dr. Ruth Werth-Brill und Dr. Christina Zimmer für die unzähligen, amüsanten und entspannenden Mittagspausen.

Dr. Christina Zimmer für ihren wissenschaftlichen Beistand, für ihr immer offenes Ohr, ihre Ratschläge in jeglicher Hinsicht, die schnelle HPLC-Hilfe, die Versorgung mit Nervennahrung, die Kaffeepausen, für die tolle Zusammenarbeit und für ihre Freundschaft.

Tobias Klein für die tolle Zusammenarbeit, die wissenschaftlichen und nicht-wissenschaftlichen Diskussionen, die ständige Unterstützung bei dem Erstellen von MOE-Bildchen und sonstigen Software-Problemchen, die täglichen Milchkaffees und Espressi, die Aufheiterung bei schlechter Laune, seine unglaubliche Tiefenentspannung und für seine Freundschaft.

Dr. Alexander Oster für seine Einführung ins HSD-Projekt, die wissenschaftlichen Diskussionen, die entspannte Laborzeit bei der Synthese, seine fortwährende gute Laune, die Begleitung zur „Vienna Summer School of Drug Design“ und für seine Freundschaft.

Sabrina Rau, Dr. Ruth Werth-Brill und Dr. Patricia Kruchten für den wissenschaftlichen Beistand und Diskussionen für offene Ohren, für die Einführung in die biologische Testung und die HPLC-Unterstützung. Vielen Dank für eure Freundschaft.

meinen Freunden für die kleinen Auszeiten.

mein besonderer Dank gilt meinen Eltern, meiner Schwester Caterina und Jens, die immer an mich geglaubt haben, die mich unterstützt haben und die immer für mich da sind und ohne die ich das alles hätte nicht machen können. DANKE!